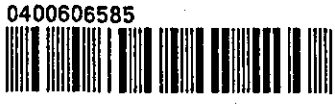

THE APPLICATION OF VIBRATION ANALYSIS TECHNIQUES TO THE DEVELOPMENT OF AN ULTRASONICALLY ASSISTED DIE FORMING PROCESS

by

Margaret Lucas
BSc (Eng), MPhil

A Doctoral Thesis submitted in partial fulfilment of the requirements for the award of Doctor of Philosophy of the Loughborough University of Technology

December 1992

To David Lister

ABSTRACT

One of the requirements for significant cost savings in the manufacture of tinplate cans in the packaging industry, is to achieve a die formed diameter reduction (or neck) on the can, inexpensively and reliably. A novel technique for the formation of a neck on metal canisters, uses the ability of ultrasonic vibration to reduce the apparent friction (and hence forming force) between the die work surface and the material being formed. Ultrasonic forming, although known to be a viable technique, has not been fully exploited due to a lack of understanding of the process. This has resulted in a lack of tool design knowledge and process reliability problems. The aim of the research reported in this thesis, is to investigate the vibration characteristics of ultrasonically excited forming tools with reference to the metal forming process and particularly, from a tool design viewpoint.

Initially, the operating parameters of generator power, hydraulic pressure, die amplitude and frequency are investigated in order to understand the effects of applying an ultrasonic oscillation to the die through the stages of the loading process. In the low ultrasonic frequency range a thick cylindrical die is subject to a number of closely spaced and coupled natural frequencies. These vibration modes must be identified and the die subsequently redesigned, to isolate the tuned operating mode from other problematic modal activity. The design strategy therefore relies on validated predictions of vibration modes in order to tune the required mode to the operating frequency and then effect the necessary design modifications. This is achieved using finite element analysis (FEA) validated by experimental modal analysis (EMA) and supported by software for structural modification. The accuracy of the vibration analysis stage is critical, especially since most instrumentation and sensors are designed for use in the audible range. Conventional modal analysis techniques have been adapted for high frequency measurements by exciting the die with a wide band magnetostrictive transducer and monitoring the generator voltage as an alternative to the forcing function. Consequently, the required design modifications are predicted by estimating "effective mass" terms that allow EMA frequency response function data to simulate measurements collected by measuring the input force.

The solution of the eigenvalue problem by FEA is typically prone to errors at high frequencies. Work is therefore directed towards maximising accuracy to achieve appropriate correlation between calculated and measured modes. The FEA stage of the research assesses alternative modelling techniques and considers the optimum mesh size and analysis strategy within the constraints of solution time.

Improved die geometries are suggested, which produce an isolated operating mode. The designs are based on the predicted effects of structural modifications from FEA calculations, which are supported by EMA data. Finally, the dies are physically modified and retested to validate the design strategy.

ACKNOWLEDGEMENTS

The author would like to acknowledge with gratitude the support and encouragement of Eur Ing Professor Graham Chapman who supervised the research reported in this thesis. The work was undertaken as part of a research project funded by the Science and Engineering Research Council and CMB Technology (formerly Metal Box) plc. Thanks are also due to the other members of the research team, namely Mike Shellabear, Paul Porucznik, Chris Cheers, Vic Roulstone and John Tyrer, for their advice and assistance throughout the duration of the project. The work was carried out in the Department of Mechanical Engineering at Loughborough University of Technology, where the support of the technicians, secretarial staff, drawing office staff and photographic unit has been much appreciated.

Results of the two-dimensional finite element model using ANSYS software (Table 6.1) are reported with the kind permission of Chris Cheers. Results from measurements using electronic speckle pattern interferometry presented in this thesis are reproduced courtesy of Mike Shellabear.

Finally, thanks go to Janet Smith for transforming the author's draft thesis into a final report.

CONTENTS

			Page No
Abstract			i
Acknowledgements			ii
Contents			iii
CHAPTER 1:		BACKGROUND TO RESEARCH	1
	1.1	Introduction	1
	1.2	Metal Forming with an Ultrasonic Assist	2
	1.3	Die Forming of Metal Cans - Dynamic Considerations	6
CHAPTER 2:		INVESTIGATIVE APPROACH TO VIBRATION ANALYSIS	12
	2.1	Combined Analytical Strategy	12
	2.2	Experimental Modal Analysis (EMA)	13
		2.2.1 Introduction	13
		2.2.2 Principles of Modal Analysis	13
		2.2.3 The Fast Fourier Transform (FFT) Analyser	17
		2.2.4 Computer-Aided EMA	19
	2.3	Structural Modification	21
	2.4	The Finite Element Method (FEM)	24
		2.4.1 Introduction	24
		2.4.2 Solution of Finite Element Problems	25
		2.4.3 Dynamic Analysis	29
		2.4.4 PAFEC	31
CHAPTER 3:		DYNAMIC CONSIDERATION OF DIE NECKING PROCESS	35
	3.1	Measuring the Excitation System Parameters	35
	3.2	Analysis of Process Parameters During Forming	36

Page No

3.2.1 Data Acquisition 37
3.2.2 Die Displacement Measurements . . 38
3.2.3 Generator Power Measurements . . 40
3.2.4 Pressure Measurements 41
3.2.5 Conclusions 41
3.3 Die Vibration Under Loaded and Unloaded Conditions 42
3.3.1 Description of Test Rig 43
3.3.2 Pressure Requirement 43
3.3.3 Die Vibration Measurement 44
3.3.4 Die Vibration Results 44
3.3.5 Conclusions 47

CHAPTER 4: VIBRATION ANALYSIS AT ULTRASONIC FREQUENCIES 60
4.1 Requirements for Die Testing 60
4.2 Swept-Sine Modal Testing 61
4.3 Ultrasonic Modal Testing Requirements . . 62
4.4 Acceleration Intensity Method 64
4.4.1 Results 65
4.4.2 Conclusions 66
4.5 Simulating the Excitation Force 67
4.5.1 Experimental Philosophy 67
4.5.2 Sonic Response Characteristics from Beam Analysis 69
4.5.3 Ultrasonic Response from Die Analysis 72
4.5.4 Conclusions 75
4.6 Measuring the Die Response 75

			Page No
CHAPTER	5:	VIBRATION BEHAVIOUR OF ULTRASONIC FORMING DIES	90
	5.1	Introduction	90
	5.2	Experimental Configuration	91
	5.3	Modal Tests on Die with Tubular Mount . .	92
		5.3.1 Frequency Range of Analysis . . .	92
		5.3.2 Measurement Grid	92
		5.3.3 Modal Parameter Estimation	93
		5.3.4 Rotational Coordinates	93
		5.3.5 Die Cylinder Vibration: Pre Curve-Fit Analysis	94
		5.3.6 Curve-Fit Data	97
		5.3.7 Comparison of EMA and ESPI Analysis of the Die	103
		5.3.8 Die Mounting Tail Vibration	104
		5.3.9 Consequence of EMA Findings on Die Design	105
	5.4	Modal Analysis of Alternative Steel Dies . .	105
		5.4.1 EMA of Steel Die 1	105
		5.4.2 EMA of Steel Die 2	106
	5.5	Modal Analysis of a Cracked Aluminium Die	107
	5.6	Conclusions	109
CHAPTER	6:	FINITE ELEMENT MODELLING IN ULTRASONIC DIE DESIGN	128
	6.1	Two-Dimensional FE Modelling of the Die .	128
		6.1.1 2D FE Modelling of 3D Structures .	128
		6.1.2 2D Axiharmonic Die Models	129
	6.2	Three-Dimensional Models of the Die . . .	132
		6.2.1 Introduction	132
		6.2.2 Reduced Analysis in FE Modelling .	133
		6.2.3 Validating the 3D Models	133

Page No

6.3 Modelling a Die Segment Using Cyclic Symmetry 139
6.3.1 Cyclic Symmetry FE Analysis 139
6.3.2 3D Die Models Using Cyclic Symmetry 139
6.4 Conclusions 142

CHAPTER 7: STRUCTURAL MODIFICATION IN THE REDESIGN OF ULTRASONIC DIES . . . 153
7.1 Structural Dynamics Modification (SDM) - Post-Processing EMA Data 153
7.2 Validation of SDM - a Cantilever Beam Study . 156
7.2.1 Investigative Approach 157
7.2.2 Results 157
7.3 Determining a Mass Calibration Factor of SDM from an Uncalibrated Modal Test Data Base 159
7.3.1 Calibrating Mass Addition 159
7.3.2 Evaluating a Mass Subtraction Calibration 162
7.4 Redesign of an Aluminium Forming Die . . 166
7.4.1 SDM Calibrations for a Three-Lobed Die 166
7.4.2 Validating the SDM Analysis 168
7.4.3 Discussion and Conclusions 169

CHAPTER 8: CONCLUSIONS AND RECOMMENDATIONS FOR FURTHER WORK 186
8.1 Conclusions 186
8.2 Further Work 189

Page No

APPENDICES:
A. Ultrasonic Equipment and Process 192
A.1 Introduction 192
A.2 Can Forming Test Rig . . . 192
A.3 Ultrasonic Generators and Transducers 193
B. Thick Cylinder Modes of Vibration . 199
B.1 Mode Classification . . . 199
B.2 Frequency Behaviour of Cylinder Modes 201
C. Sensitivity Trend for Mass Modification 204
D. Publications 207

References 208

CHAPTER 1
BACKGROUND TO RESEARCH

1.1 INTRODUCTION

The research which forms the basis of this thesis arose from novel developments in the packaging industry at CMB Technology (formerly Metal Box plc) to reduce the cost of can manufacture; particularly aerosol and beverage cans. The cost cutting exercise was necessitated by the competition for market share between the highly subsidised Eastern European aluminium can and the more expensive British tin plated steel can.

Aerosol canisters are conventionally produced from tinplate in three parts: cylindrical body, base dome and top cone to fit a standard valve. In contrast the aluminium counterpart is an extruded monobloc container with one end necked down to fit the standard valve (Figure 1.1). A research effort was established at CMB to produce a coneless aerosol by necking down one end of a tinplate welded cylinder to the same shape as the aluminium competitor. The elimination of the cone was estimated to effect material savings of £400K per production line per annum as well as enhance the can's marketability.

The forming of a neck (diameter reduction) on tinplate canisters inexpensively and without damage to the welded side seam or lacquer coating, poses problems. The cylinder is typically less formable than the aluminium can, being harder and thinner (0.2 mm compared to 0.5 mm minimum for aluminium). To achieve the required diameter reduction (for example 45 mm to 25 mm) by die necking, the process must involve several gradual reduction stages, since the forming work that can be done at any one stage is limited by the collapse of the can body. In some cases as many as 16 separate reduction stages are required.

In order to decrease the number of forming operations required to produce a coneless can, researchers at CMB experimented with ultrasonically excited forming dies. Significant reductions in forming force had been achieved in other metal forming processes (such as wire drawing) by the mechanism of friction reduction at the forming surface due to the application of vibration to the tool. Initial work proved that the diameter reduction required to produce a necked tinplate aerosol container could be achieved in a single stage operation utilising an ultrasonically assisted die forming process. Although principally investigated with reference to aerosol manufacture, the process also applies to the forming of beverage cans and other containers where the end closure or valve is of a size that warrants economical container end diameter reduction [1,2,3].

Although demonstrated to be a viable technique, ultrasonic forming and, more especially, its applicability to can production, is little understood. It is therefore the intention, through this research thesis, to investigate the dynamic behaviour of ultrasonically excited tools by reference to the metal forming process parameters and from a tool design viewpoint. In this pursuit, a wide range of vibration topics is encountered; from the characteristics of thick cylinders to the development of suitable measurement techniques for high frequency analysis to the collation of data from several analytical techniques in the validation of vibratory behaviour which is often difficult to interpret.

1.2 METAL FORMING WITH AN ULTRASONIC ASSIST

Firstly, the published work on the nature of ultrasonic aid in metal forming is outlined.

The earliest studies of the effects of ultrasound on the deformation characteristics of metals were conducted in the late 1950s by Blaha and Langenecker [4,5]. Apparent reductions in flow stress during tensile tests on monocrystal specimens were observed due to irradiation with ultrasound (or insonation). This work-softening, which is now known as Blaha's Phenomenon, became the basis for most of the subsequent research into metal insonation

and is illustrated in Figure 1.2. Curve A shows the measured reduction in tensile stress caused by intermittent applications of ultrasound and the return of the stress value to its prior value on cessation of insonation. The lowering of tensile stress by continuous irradiation leads to curve B.

In 1957, Nevill and Brotzen [6] studied the effect of ultrasound on the yield strength of steel wire and similarly noted a reduction in stress. They explained their findings in terms of a mechanism of the alternating acoustic stress superposed on the externally produced stress and further, found that the reduction in stress was directly proportional to the vibration amplitude and independent of frequency in the range they covered (15 to 80 kHz).

Later research by Langenecker [7] calculated the acoustic stress levels due to the application of ultrasound during tensile tests on metals. His calculations supported the superposition theory, agreeing with Nevill and Brotzen. He further postulated that another mechanism of stress reduction was observed when using high-intensity ultrasound that was caused by a heating effect; energy was absorbed preferentially at defect sites, such as dislocations and impurities, which assisted plastic flow.

From this point, the investigations of ultrasonic vibration on materials were broadly separating into two categories in the published literature, namely "volume effects" and "surface effects". Under these headings are grouped the following:

a) Volume effects: The influences of ultrasonics on internal stresses during plastic flow of metal [8-13].

b) Surface effects: The influences of ultrasonics on interfacial friction and other external friction effects [14,15].

Many publications propounded the volume and surface effects of ultrasonically assisted metal deformation. Experimental evidence lent credence to both. For

example, in a series of publications by Winsper, Sansome and their colleagues, the conclusion is drawn that the macroscopic stress superposition theory and microscopic localised temperature effects (causing dislocation movement as well as enhanced friction conditions at the forming surface) all contribute to the force reductions reported in the forming process [16-20].

The relevance of metal insonation to industry is based on the ability to reduce frictional forces between the tool and workpiece in a metal forming process. This led to a new phase in the research effort, concentrating on postulating mechanisms of interfacial friction reduction and assessing their validity in forming operations. Consequently, researchers have attempted to understand the relationship between the activation of vibrations and the resulting reduction in interfacial friction. Fridman [21] showed that when oscillations are applied to a plane surface, the friction between the plane and a slider is considerably reduced. Pohlman and Lehfeldt [8] observed these effects on sliding friction and found that friction reduction was most marked if excitation was parallel to the sliding direction and if the sliding velocity was low.

The mechanisms of friction reduction reported during metal forming are difficult to substantiate but several possibilities have been proposed.

Where a lubricant is employed, the workpiece may be effectively relubricated once every cycle, resulting in improved friction conditions [22]. Another suggestion is that ultrasonic loading is impacting in nature producing the permanent strain associated with such loading. Mitshevich [23] postulated that friction reduction was caused by the periodic reversal of the friction force due to the periodic motion of one surface (the tool) relative to another (the workpiece). If the magnitude of the friction force remains unchanged, its mean value in the direction of sliding is reduced and the reduction is a function of the ratio of oscillatory velocity to sliding velocity. This mechanism is expounded by Nasal and Rymsha [24] to explain tube sinking assisted by axial ultrasonic vibration of the plug. In a similar vein, Kristoffy [14] explains the reduction in force when a die is excited with torsional vibrations by a mechanism of periodic

swinging of the friction vector about the sliding direction. Winsper and Sansome [25] suggest a mechanism for radial drawing die oscillations whereby the induced stresses normal to the wire periodically increase the die pressure, reducing the necessary drawing tension. This is likened to a swaging effect. Papers by Eaves [26] and Rees [27] discuss the significance of the swaging effect where the worked tool is compressed radially to produce an axial extension. Godfrey [28] discovered that low frequency normal oscillations reduced sliding friction when separation of the mating surfaces occurred. Balamuth [29] suggested that surface separation was a mechanism of friction reduction at ultrasonic frequencies and is due to the decrease in the period during which friction forces act.

To summarise, there are three principal mechanisms of forming force reduction proposed in the published literature, which attempt to describe metal deformation assisted by ultrasonic excitation of the forming tool:

1. Friction Vector Reversal

The friction vector effect is caused by the relative motion between the tool and the workpiece surfaces. For the case of axial excitation, if the vibrations cause the tool to move faster than the material being formed, then for part of the cycle the relative velocity of material to tool (and consequently the friction vector) is reversed. For transverse excitation, the line of action of the force swings periodically about the sliding direction of the material, similarly resulting in a reduction of the mean friction force in the direction of motion. This mechanism of friction force reduction also holds for torsionally excited systems.

2. Improved Interfacial Friction Conditions

An effective reduction in the coefficient of friction is caused by periodic separation of the mating surfaces during forming. The two beneficial results are that friction is reduced to zero for part of the cycle and the lubricant film is reestablished every cycle, preventing breakdown at high stress points. Degeneration of vibration energy into heat at the tool/material interface causes a softening of asperities and an associated decrease in surface shear stress attributable to a reduction in the coefficient of friction.

3. Swaging Effect

A radially excited forming tool alternately compresses and releases the workpiece. Since the magnitudes of the three principal stresses are related to the yield stress by the yield criterion, it can be deduced that an increase in the lateral stresses induced by the oscillations must result in a decrease in the axial stress or, in other words, a decrease in the forming force.

These findings support the application of ultrasonics to a die necking operation, where high frequency radial vibration of a cylindrical die is used to reduce interfacial friction at the forming surface. The research is further encouraged by many investigations into metal forming with an ultrasonic assist, in the fields of forging, wire drawing, tube drawing, extrusion and sheet metalworking [30-36].

In conclusion, it can be considered to have been established that the introduction of ultrasonic vibration to a forming process results in beneficial modifications to the operation, which tend to reduce the resistance of the workpiece material to deformation and enhance the finished product. There is still however, some debate as to the precise nature and influences of the causal mechanisms.

1.3 DIE FORMING OF METAL CANS - DYNAMIC CONSIDERATIONS

A study of the published literature may convince interested parties in industry of the viability of employing ultrasound in their metal forming processes, but the proof of its applicability lies with the appropriate design of the tooling and the adaptation of existing production lines to accommodate the ultrasonic generation and excitation equipment. The often posed question "Does it work in practice?" may be reasonably invoked at this stage, since very little work has been reported on the problems of designing reliable forming dies capable of maintaining an operating frequency and necessary vibration amplitude under varying load conditions and with minimum loss of energy to the surrounds.

Some attention was paid to the design of axial mode vibrators in a production environment by Jones in 1968 [35] and more recently by Kariyawasam and Rees [37] and Rippon [27]. Particular consideration was given to acoustic power transmission and mounting design, to minimise vibrational energy attenuation to the support structure. Young el al concentrated on the design of radial mode resonators for forming applications in two papers [38,39], deriving an analytical technique for predicting the resonant frequency of the ring vibrator. Radial resonators were further considered by Biddel in two later publications [40,41]. However, the vibration "problems" common to die design were not identified until the idea of ultrasonically assisted die necking was developed at CMB [42]. Early on in the search for a suitable radial mode die and mounting system, it was realised that the reliability of the tool system was very dependent on the inherent vibration characteristics of the thick cylindrical die.

The problems can be clarified by firstly identifying the prerequisites for an ideal forming die. The ideal resonant system for the ultrasonic necking operation would exhibit the following characteristics:

1. The operating frequency would be chosen to maximise transmitted vibration amplitude from the transducer at a frequency and sound level comfortable for an operating environment.

2. The die would vibrate in a radial mode with maximised uniform radial amplitude at the die bore.

3. The uniform radial mode would be a tuned resonance of the die to match the chosen operating frequency.

4. The die would maintain the tuned vibration mode shape throughout the forming process under the varying loading conditions, i.e. the influence of off-resonance modes of vibration would be negligible such that a resonance tracking facility in the ultrasonic generator would not track the wrong mode.

5. The die geometry would be chosen such that the tuned radial mode is well isolated from the other natural frequencies of the die.

6. The die mounting system would neither depress the tuned vibration amplitude of the die nor transmit vibrational energy to the surrounds.

The operating frequency for production purposes is to be 20 kHz. This low ultrasonic frequency satisfies the requirement for transmitting high amplitude to the forming surface. It is also the frequency used in other industrial processes (such as ultrasonic welding) and therefore allows off-the-shelf purchase of ultrasonic generation equipment. Also, for a high intensity process at 20 kHz reports suggest that ultrasound is safe at greater sound levels than audible noise and therefore development for production is deemed acceptable to operators [43,44,45].

Work into die design and tuning has been carried out at CMB using Finite Element Modelling to predict posible thick cylinder geometries, which exhibit a radial uniform amplitude vibration mode at 20 kHz. It is also necessary to predict all the vibration modes excited around the operating frequency for various die geometries, so that possible influential (or problematic) modes can be identified. Therefore Finite Element Modelling (FEM) is adopted in this thesis to provide information on complete die vibration characteristics. In a non-ideal vibrating system with measurable damping and/or closely spaced modes, tuned frequencies are influenced by the response of off-resonance modes and these problematic modes may be multitudinous, especially if the vibrating system's dynamic characteristics are changing continuously. This is obviously the case for a forming die, where the system is initially freely vibrating, then the can enters the die under axial loading, is formed with ultrasonic assistance and is subsequently knocked out on completion of the diameter reduction (Figure 1.3). For good design practice, it would seem sensible to gain considerable knowledge both of thick cylinder free vibration behaviour and the effects of die loading at its inner diameter.

With these concerns in mind, the thrust of this research programme is to pursue a better understanding of the die necking process with radial ultrasonic excitation, by exploring and developing analytical methods for experimentation and calculation, with the aim of investigating and recommending die design procedure for reliable ultrasonic forming.

Specifically, knowledge is advanced in the design of ultrasonic tooling from the following original research contributions:

1. A modal analysis technique is developed to measure frequency response data from ultrasonic dies, where no measure of force input is possible. This is achieved by identifying a generator electrical signal that can be monitored to represent the forcing function. The relationship is derived from structural modification measurement data and modal sensitivity calculations.

2. A rigorous approach to thick cylinder vibration analysis is proposed that involves multiple estimation techniques to validate vibration parameter data. The approach is shown to enable modal parameter extraction of the coupled, damped, complex and closely spaced modal activity associated with ultrasonic forming dies.

3. The important parameters in die design are identified as amplitude, amplitude uniformity and operational mode isolation. These are optimised by gaining a thorough understanding of thick cylinder vibration behaviour and subsequently effecting die geometry modifications based on mode sensitivities.

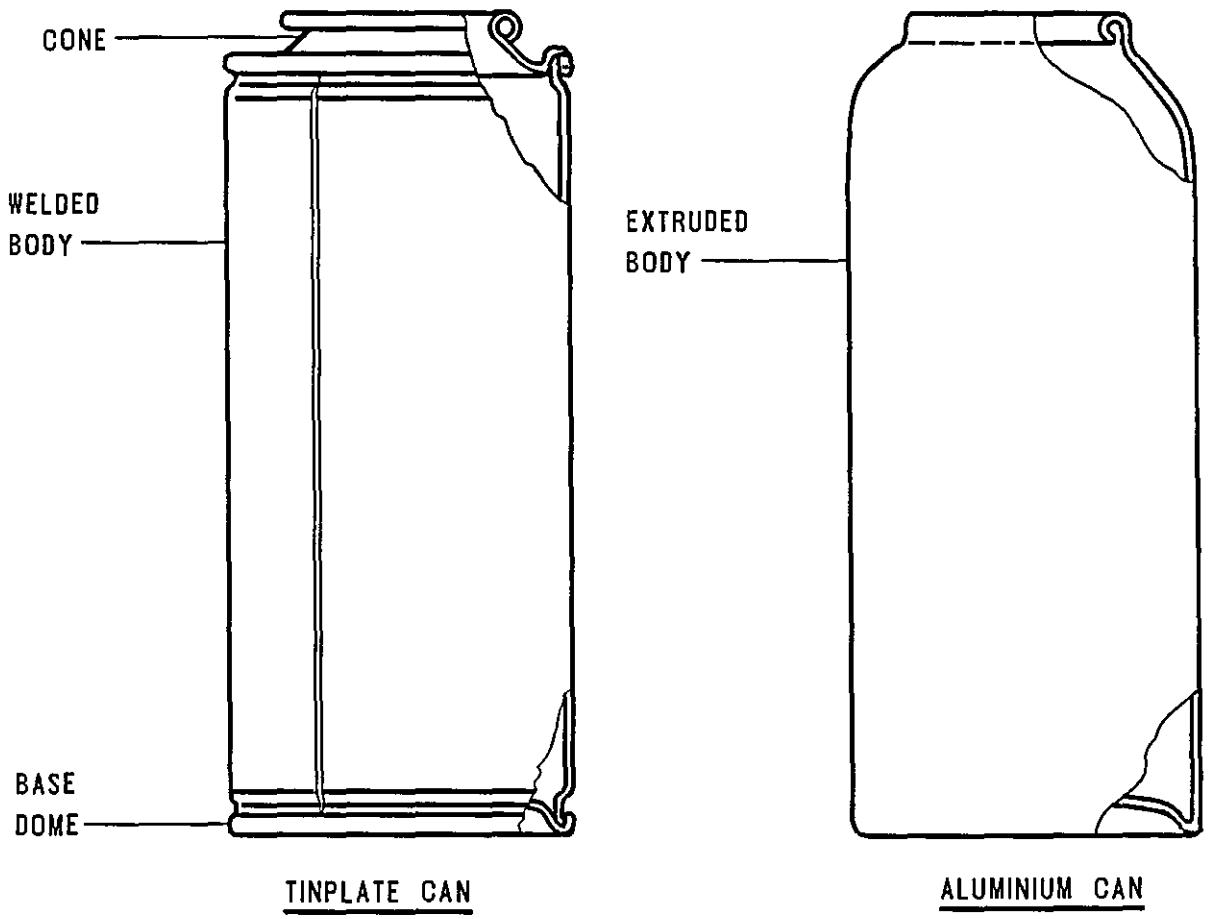

Figure 1.1 : COMPARISON OF CONVENTIONAL AEROSOL CONTAINERS.

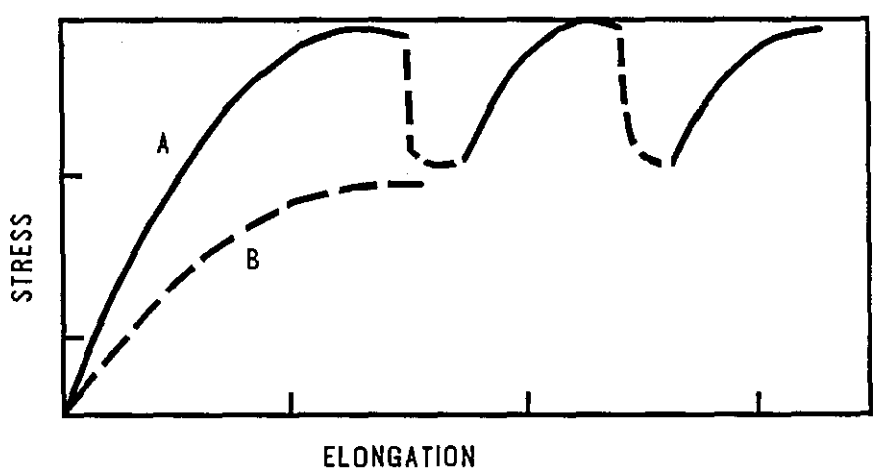

Figure 1.2 : 'BLAHA'S PHENOMENON'
EFFECT OF SUPERIMPOSED ULTRASOUND ON
PERFORMANCE OF METALLIC CRYSTALS.

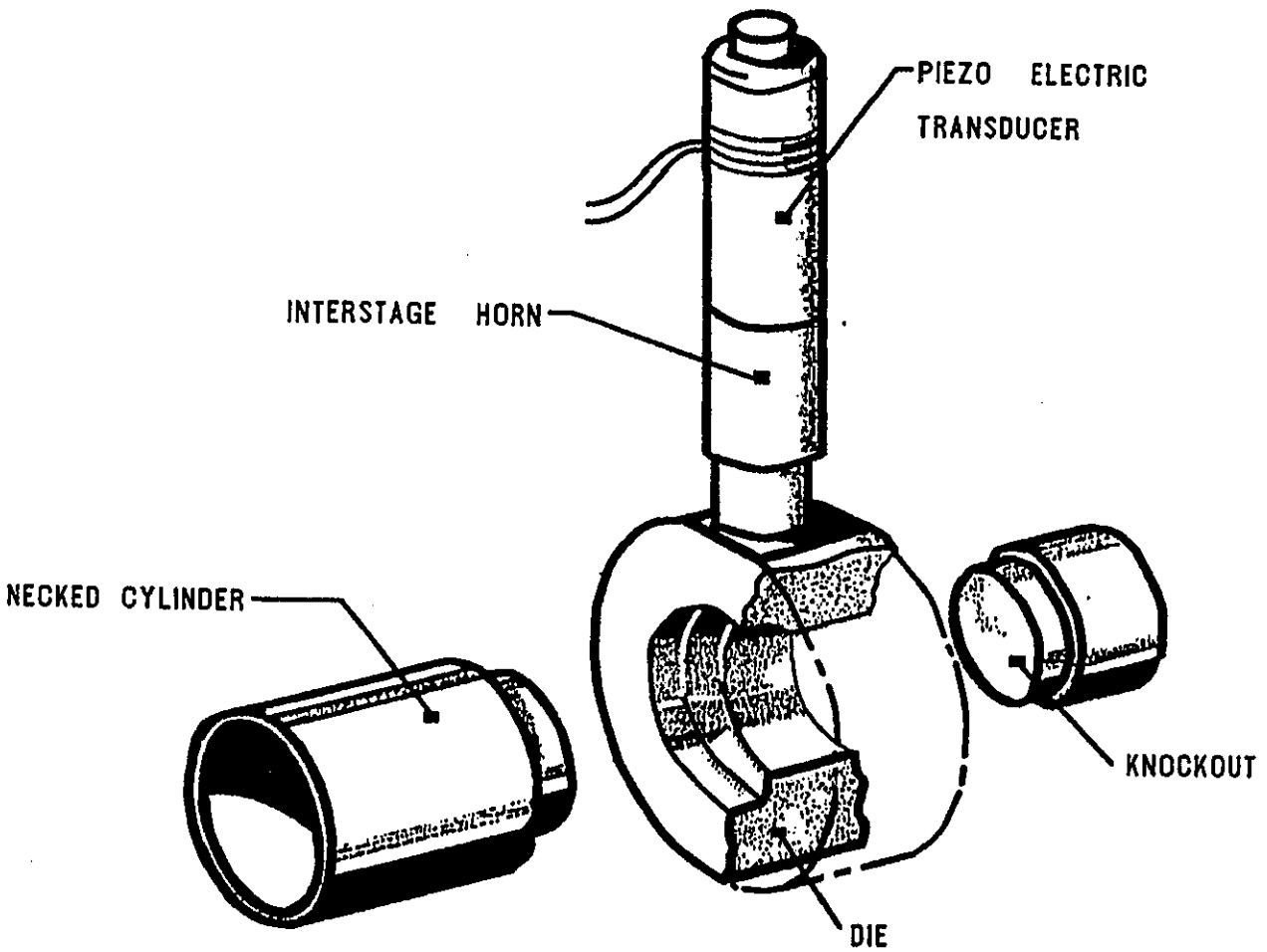

Figure 1.3 PRINCIPLES OF ULTRASONIC DIE NECKING

CHAPTER 2
INVESTIGATIVE APPROACH TO VIBRATION ANALYSIS

2.1 COMBINED ANALYTICAL STRATEGY

Vibration problems in engineering are generally related to resonance phenomena, often due to operational forces exciting unwanted modal responses. This is the case in this study, where the reliability of die design is dependent on the vibratory response at or near the ultrasonic operating frequency. The design philosophy is based on the following closed loop approach:

- A die bolster geometry is calculated to produce a thick cylinder whose fundamental radial modal frequency is 20 kHz.
- The thick cylinder is analysed to determine its vibration characteristics in the low ultrasonic range.
- Physical modifications to achieve effective elimination of unwanted modal behaviour are predicted.
- The die is redesigned to modification predictions and retested for validation of the design procedure.

This approach to die design relies on the accuracy of the vibration analysis stage for extracting a true picture of die characteristics. Further, this picture must constitute a complete dynamic description of the die in such a way that a mathematical dynamic model can be formulated. The next stage of the design can then be accomplished from calculations of effects of structural modifications by manipulation of the experimentally determined mathematical model. The design philosophy therefore relies critically on vibration parameter estimation capability.

As with most vibration analysis problems, other than idealised systems, it is unwise to rely on a single method of vibration parameter estimation. An ability to interpret often complex behaviour correctly, requires a validatory approach to the investigation. The most popular method for studying practical vibration problems involves combining experimentation by Modal Testing with the mathematical approximations of Finite Element Modelling. Employing these methods , it is possible to determine the properties of the normal modes of a structure within a chosen frequency range. This complies with the requirements of the design loop.

Experimental Modal Analysis (EMA) and Finite Element Modelling (FEM) are used extensively throughout this study to investigate and understand die vibration behaviour and to determine the effects of die redesign by Structural Dynamics Modification (SDM).

2.2 EXPERIMENTAL MODAL ANALYSIS (EMA)

2.2.1 Introduction

The analytical development and application of modal analysis has been widely reported. Much of the published material is contained in the IMAC Proceedings [46] which also include extensive bibliographies of EMA publications in other Journals and Proceedings. Many important papers in this field are published in the Journal of Modal Analysis [47]. A wealth of information can be obtained from these sources; some of the most relevant material being referenced individually in this study. Despite the proliferation of EMA, relatively little published work discusses modal identification in structures with complex geometry, high damping or high modal density. No publications on ultrasonic applications of EMA have been found.

2.2.2 Principles of Modal Analysis

Although structures are continuous systems, often their dynamic behaviour can be described by an assemblage of rigid mass, light spring and viscous damper elements. This lumped-parameter mathematical model allows derivation of the

equations of motion, yielding one equation for each degree-of-freedom (DOF) of each mass in the system, in the form

$$[M]\{\ddot{x}\} + [C]\{\dot{x}\} + [K]\{x\} = \{F\}$$

However, [M], [C] and [K] are not directly measurable and therefore the experimentalist must deduce these matrices from measurable quantities. Modal Analysis is the process of defining the dynamic properties of a structure by its modes of vibration which can be measured and related to the equation of motion.

Any free dynamic response can be reduced to a set of discrete modes. The dynamic properties are described by its modal parameters:

1. modal frequency
2. modal damping
3. mode shape

EMA provides a measurement technique which determines these modal parameters in such a way that they can be used to formulate a mathematical dynamic model of the structure. This is achieved by measuring the vibratory response to an excitation force at discrete test locations. The ratio of response to force in the frequency domain is known as a frequency response function (FRF) and FRF acquisition forms the first stage of EMA which is modal testing.

The FRF can take different forms, depending on the response quantity measured. The three common forms are:

1.	Compliance	$\frac{X}{F}$	$\frac{\text{Displacement}}{\text{Force}}$
2.	Mobility	$\frac{V}{F}$	$\frac{\text{Velocity}}{\text{Force}}$
3.	Inertance	$\frac{A}{F}$	$\frac{\text{Acceleration}}{\text{Force}}$

For convenience the frequency response function descriptor $H(\omega)$ is defined here as the ratio of output/input spectra in terms of compliance (displacement/force).

$$X(\omega) = H(\omega).F(\omega)$$

The modal model of a structure is defined in terms of two parameters; pole location (p) and residue (R), by

$$H(\omega) = \frac{R}{j\omega - p} + \frac{R^*}{j\omega - p^*}$$

where p^* and R^* are the complex conjugates of p and R.

Pole location is a complex number. The real part (σ) is the rate at which vibration decays and is related to the modal damping. The imaginary part is the modal frequency or damped natural frequency (ω_r).

$$p = \sigma + j\omega_r$$

where σ is the bandwidth at the half-power points.

Residue indicates mode strength and contains the magnitude level of the resonance curve. It is therefore locally related to the mode shape. The magnitude of a mode with single degree-of-freedom (SDOF) characteristics is approximated by

$$H(\omega_r) \approx \frac{R}{\sigma}$$

For practical structures (i.e. multiple degree-of-freedom (MDOF) systems) FRFs measure the excitation and response between two locations, defined by position and direction. A MDOF modal model describes $H(\omega)$ between measurement DOFs i and j as the sum of the individual modes

$$H_{ij}(\omega) = \sum_{r=1}^{m} \frac{R_{ijr}}{j\omega - p_r} + \frac{R_{ijr}^*}{j\omega - p_r^*}$$

where r is the mode number and m is the number of modes in the model.

Enough FRF measurements must be collected to give a complete set of modal parameters. A complete set is defined by the frequency response matrix (FRM),

$$\begin{bmatrix} H_{11} & H_{12} & \cdots\cdots & H_{1N} \\ H_{21} & H_{22} & \cdots\cdots & H_{2N} \\ \cdot & & & \cdot \\ \cdot & & & \cdot \\ \cdot & & & \cdot \\ H_{N1} & \cdots\cdots & & H_{NN} \end{bmatrix}$$

The FRM is a square matrix where the row number corresponds to the response location and the column number corresponds to the excitation location. Any row or column of the FRM contains sufficient information to compute a complete set of modal parameters.

The modal model relies on linear behaviour such that response is proportional to excitation. This implies that a measured FRF:

a) is independent of excitation type
b) is independent of excitation level
c) satisfies Maxwell's Reciprocity Theorem which states that $H_{ij}(\omega) = H_{ji}(\omega)$.

Mode shape describes the deflected pattern of a structure at its modal frequency. It is a continuous function but is estimated in EMA from a discrete number of measurement DOFs. Spatial resolution requirements are therefore critical.

The modal model of a structure is usually characterised by its normal modes. Normal modes are excited in structures exhibiting light or proportional damping and the modal displacements are real valued. Where damping is localised, complex modes can exist. In this case the modal displacements are complex and can have any phase value. Another complication in the normal mode representation arises from modal coupling. Figure 2.1 illustrates two FRFs. In the first, the modes are lightly damped and well separated and the response in the vicinity of resonance is largely due to a single mode. In the second, the modes are heavily damped and/or densely spaced. The response at a modal frequency is a combination of contributions from all the modes in the frequency band. The effects of coupling on modal parameter estimation are discussed in 2.2.4 [48,49,50,51,52].

2.2.3 The Fast Fourier Transform (FFT) Analyser

A dual channel FFT analyser is used to measure, compute and post process the FRFs which constitute the modal model of a structure. In EMA the FFT analyser is the system front-end (for data acquisition) and is generally linked to a computer equipped with specialist software for modal parameter extraction. The basic functions of the FFT analyser for modal testing are shown in Figure 2.2.

The FRF estimator $H(\omega)$ is achieved in four steps from measurement of the input time signals.

i) Digitised and weighted time signals are transformed using the Fast Fourier Transform algorithm, to the frequency domain, producing complex spectra $F(\omega)$ and $X(\omega)$ of the force and response signals.

ii) In practice, the measured signals will have some random content or signal noise. To reduce the noise floor, signal averaging is used to stabilise the random content and produce a repeatable result. The two autospectra G_{XX} and G_{FF} are then calculated by multiplying each spectrum by its complex conjugate:

$$G_{XX} = \Sigma X^{*}X$$

iii) The cross-spectrum G_{FX} is the complex conjugate of the force spectrum multiplied by the response spectrum:

$$G_{FX} = \Sigma F^{*}X$$

Since the cross-spectrum is complex, it reveals the phase shift between the response and force signals and can be divided into its real and imaginary parts:

$$G_{FX} = C_{FX} + jQ_{FX}$$

where C_{FX} is the coincident spectrum and Q_{FX} is the quadrature spectrum.

iv) The FRF estimator is found from the ratio of the cross- spectrum between X and F to the autospectrum of F:

$$H = \frac{\Sigma F^{*}X}{\Sigma F^{*}F} = \frac{G_{FX}}{G_{FF}}$$

It is assumed that the forcing function f(t) and response signal x(t) are acquired at two separate or coincident measurement DOFs on the structure under analysis.

Of particular relevance to EMA in the low ultrasonic frequency range, is the zoom capability of FFT analysers. This facility enables increased frequency resolution over a selected bandwidth when the baseline resolution is insufficient or contains more spectral information than is required for the analysis. Zoom analysis is performed by oversampling the signal by a factor of m (known as the zoom factor). A digital low-pass filter is employed to pass only the frequency span of interest. During the resampling process only one out of m

samples is kept, thus reducing the sampling frequency without loss of information. This procedure effectively shifts the frequency origin to a new selected centre frequency and concentrates measurement data over a specified frequency range. An added advantage of zoom analysis is the reduction in leakage distortion of the signal since energy smearing occurs within a narrower bandwidth [53,54].

2.2.4 Computer-Aided EMA

Computer-aided modal analysis incorporates the use of dedicated pc based software for post-processing of measured FRF data. In this study, the SMS STAR system software is utilised. The extraction of modal parameters from FRFs relies on the ability to derive the dynamic equation of motion

$$[M]\{\ddot{x}\} + [C]\{\dot{x}\} + [K]\{x\} = 0$$

without explicit knowledge of mass, damping and stiffness distributions within the test structure.

It is known that the equation of motion can be manipulated algebraically to determine a formula for the FRM in terms of the two parameters of pole location and residue, which contain modal parameter information. The values of pole p_r and residue R_{ijr} can therefore be obtained by curve fitting the measured FRF data.

Frequency and damping are global properties and can be estimated by curve fitting any FRF. Although mode shape is also a global property, each individual modal coefficient is a local property, estimated from a particular measurement, and hence a further mathematical process of modal residue sorting is required to determine the mode shapes.

A FRF of a structure is made up of the sum of the resonance contributions of all the individual modes (Figure 2.3). The curve fitting approach to modal parameter estimation depends on the amount of modal damping and mode

separation in the FRF, since these govern the degree of modal coupling and hence the effect of the modal contribution of adjacent modes at a natural frequency (see Figure 2.1). Where there is light damping and low modal density, it is possible to approximate the FRF data in the vicinity of each mode to the response of a SDOF system. This assumes that the modal participation of adjacent modes is negligible. A SDOF curve fitting method is appropriate for such data.

Where there is heavy damping and/or high modal density (ie. heavy coupling), the SDOF assumption is no longer valid and it is necessary to estimate the modal parameters of all the coupled modes simultaneously. A MDOF curve fitting routine is employed for coupled FRFs.

SDOF and MDOF curve fitting routines are based on a rational fraction least squares (RFLS) polynomial algorithm. SDOF curve fitting is limited to data in the vicinity of a single resonance peak and the FRF is mathematically approximated for mode r by the SMS algorithm using:

$$H(j\omega) = \frac{(R2_r\ \sigma_r + R1_r\ \omega_r + j\ R2_r\ \omega)}{(\sigma_r^2 + \omega_r^2 - \omega^2 + 2j\ \sigma_r\ \omega)} + AO + A1(j\omega) + A2(-\omega^2)$$

where A0, A1 and A2 are residual function coefficients.

Residual terms are calculated to compensate for the effects of out-of-band modes on the estimated modal parameters. They are equivalent to the asymptotic behaviour of the mass and stiffness lines of adjacent modes, assuming they are similarly characterised by a SDOF system (Figure 2.4).

The polynomial equation above is fit to the modal test measurements to calculate the modal frequency (ω_r), modal damping (σ_r) and complex residue ($R_r = R1_r + jR2_r$).

The MDOF polynomial method fits a rational fraction polynomial to a measured FRF within a selected frequency band with a defined number of modes. A set of linear equations is solved to give estimates of the polynomial coefficients, which are then processed to produce the modal parameters [55,56].

2.3 STRUCTURAL MODIFICATION

The technique of structural modification uses the data base obtained from a modal test to predict changes in modal properties caused by effecting small, physical modifications to the test structure. Commonly usage is of a comparative nature, whereby a solution to problematic vibration behaviour is calculated from Finite Element modelling and structural modification to predict the optimal redesign of a dynamic structure. Often the solution is intuitive but structural modification calculations can validate a redesign approach or offer the most practical solution. The two methods of combating unwanted vibrations are:

a) attenuate the amplitude at resonance by the addition of damping
b) shift the resonance frequency by altering the mass and/or stiffness of the structure.

Structural modification has its roots in nonlinear mathematical modelling and is based on a matrix perturbation method. It shows how small elemental changes in the mass, stiffness or damping matrix affects the eigensolution.

For simplicity, consider a free undamped system. The spatial model is represented by

$$[M]\{\ddot{x}\} + [K]\{x\} = \{0\}$$

and the solution is determined from the condition

$$\det |[K] - \omega^2 [M]| = 0$$

From this we find the eigenvalues ω_r^2 and, by back substitution, the eigenvectors $\{\psi\}_r$, which reveal the mode shapes.

The orthogonality property states that

$$\{\psi\}^T [M] \{\psi\} = m_r$$

$$\{\psi\}^T [K] \{\psi\} = k_r$$

where m_r and k_r are the generalised mass and stiffness of mode r such that

$$\omega_r^2 = \frac{k_r}{m_r}$$

It is usual to work with mass-normalised eigenvectors $[\phi]$ such that

$$[\phi]^T[M][\phi] = [I]$$

$$[\phi]^T[K][\phi] = [\omega_r^2]$$

and modal coordinates $\{q\}$ such that

$$\{x\} = [\phi]\{q\}$$

The spatial model

$$[M]\{\ddot{x}\} + [K]\{x\} = \{0\}$$

transforms to the modal model

$$[I]\{\ddot{q}\} + [\omega^2]\{q\} = \{0\}$$

If the mass and stiffness of this system is modified such that the differences from the original system are contained in [ΔM] and [ΔK], then the spatial model is

$$[M + \Delta M]\{\ddot{x}\} + [K + \Delta K]\{x\} = \{0\}$$

and the modal model, using the original system transformation, is

$$([I] + [\phi]^T[\Delta M][\phi])\{\ddot{q}\} + ([\omega^2] + [\phi]^T[\Delta K][\phi])\{q\} = \{0\}$$

The new mass and stiffness matrices [M´] and [K´] constituting the structural modification are

$$[M'] = [I] + [\phi]^T[\Delta M][\phi]$$

$$[K'] = [\omega^2] + [\phi]^T[\Delta K][\phi]$$

The new system of equations of motion can therefore be defined using the modal data of the original unmodified system.

The validity of the results of a structural modification analysis must be viewed with reference to its inherent limitations. Firstly, erroneous predictions will be caused by modal truncation; i.e. where there is insufficient information in the data base to fully describe the dynamic behaviour of the structure. Also the method only allows lumped parameters (mass, spring and damper elements) to be applied and these may only be added to or removed from locations which were measurement DOFs in the original modal test. In practice any added mass or spring element will affect structural response in rotational and translational DOFs [57,58,59].

2.4 THE FINITE ELEMENT METHOD (FEM)

2.4.1 Introduction

The Finite Element method stems from the fundamental mathematical technique of approximating continuous functions using polynomials. The basic idea is to find the solution of a complicated problem by discretising the region of interest and replacing the large problem with a series of smaller ones.

Although the name "Finite Element method" is fairly recent, the technique was introduced centuries ago by the early mathematicians to determine an approximation of pi. Two polygons were used to describe an upper and lower bound of the circumference of a circle. By increasing the number of sides (or finite elements) on the polygon a closer approximation to a circle was obtained [60].

Modern use of FEM was developed mainly by structural design engineers as a practical method for solving elasticity problems. This was of a semi-analytic nature, largely in aircraft design in the 1940s.

Since then engineers and mathematicians have worked separately to develop the method. Engineers have concentrated on application to all areas of structural design while mathematicians efforts were directed towards interpretation of FEM in terms of well known variational and weighted residual methods [61].

With the arrival of high speed computers, the means of performing the large number of calculations was obtained and the diversity of the method was universally recognised. Consequently the theory has expanded to accommodate the solution of many varied and complex engineering problems in areas of structural and continuum mechanics.

2.4.2 Solution of Finite Element Problems

The application of FEM to an engineering problem can be viewed as a series of steps:

a) The region of interest is divided into distinct elements over which the main variables are interpolated. The variables are identified with nodal points which lie along the periphery of the element or, in some cases, within the element.

b) For each element certain characteristics are evaluated. A displacement function defines the state of movement within an element. From energy theorems a stiffness matrix can be derived relating nodal forces to nodal displacements.

c) The stiffness matrix and load vector for each element is then assembled to produce the global stiffness and global load vector. These define the overall characteristics of the region of interest.

d) The global stiffness matrix and load vector give a system of simultaneous equations which may be solved for the unknown nodal variables.

The accuracy of the solution is dependent on the choice of displacement function. It is usually a simple polynomial with coefficients determined by the nodal displacement parameters. It can also be given in terms of shape functions. An appropriate displacement function will satisfy the following conditions:

i) The function and its first derivative must be continuous over the element.

ii) The function should allow for rigid body translation or rotation without straining the element.

iii) The function should allow for uniform strain within the element.

iv) The function should allow for internal compatibility as well as compatibility of strain or displacement along adjacent element boundaries.

Typically triangular or quadrilateral elements are used in FEM. As a simple example consider two triangular elements with node points at their vertices (Figure 2.5(a)). If the two elements are joined at two node points then a displaced shape conforming to the above conditions is shown in Figure 2.5(b).

Having chosen a suitable trial function, the displacements at any point within the element are derived by the matrix equation

$$\{U\} = [P]\{\alpha\}$$

where $\{\alpha\}$ is the column vector of the coefficients of the displacement function. For nodal displacement $\{U_e\}$ the matrix equation is

$$\{U_e\} = [A]\{\alpha\}$$

The displacements at any point within the element can be expressed in terms of the nodal displacements of the element by

$$\{U\} = [P][A]^{-1}\{U_e\}$$

At any point in the finite region the strains are given by

$$\{\varepsilon\} = [B]\{\alpha\}$$

The relationship between the strains and nodal displacements is

$$\{\varepsilon\} = [B][A]^{-1} \{U_e\}$$

In this case $[B][A]^{-1}$ is called the element strain matrix. If the stress-strain relationship is given by

$$\{\sigma\} = [D]\{\varepsilon\}$$

then stress is related to nodal displacement by

$$\{\sigma\} = [D][B][A]^{-1} \{U_e\}$$

[D] is an elasticity matrix incorporating the material properties required to relate the stress and strain values in the element. [A], [B], [P] and [D] are matrices of an appropriate order for the system under analysis.

The forces acting on the element are described as nodal forces $\{F_e\}$ and are related to the nodal displacements by

$$\{F_e\} = [S_e]\{U_e\}$$

$[S_e]$ is the element stiffness matrix and the product $[S_e]\{U_e\}$ is the list of generalised forces acting on the element.

The stiffness matrix of an element is determined using the principle of virtual work. A virtual displacement $\{\overline{U}\}$ is imposed onto the nodal displacement $\{U_e\}$. The resulting virtual strains will be $\{\overline{\varepsilon}\}$ and the virtual strain energy is

$$[SE] = \int_v \{\overline{\varepsilon}\}^T \{\sigma\}\, dV$$

From the equation relating strain and nodal displacements, the virtual strain in terms of virtual displacement is

$$\{\bar{\varepsilon}\} = [B][A]^{-1} \{\bar{U}\}$$

which may be substituted into the equation for virtual strain energy to give

$$[SE] = \int_v [[B][A]^{-1} \{\bar{U}\}]^T [D][B][A]^{-1} \{U_e\} \, dV$$

In general this simplifies to

$$[SE] = \{\bar{U}\}^T [A]^{-T} \int_v [B]^T [D][B] \, dV \, [A]^{-1} \{U_e\}$$

The external work done on the element by the nodal forces $\{F_e\}$ is given by

$$\{W_e\} = \{\bar{U}\}^T \{F_e\}$$

In terms of nodal displacements this becomes

$$\{W_e\} = \{\bar{U}\}^T [S_e]\{U_e\}$$

By the principle of virtual work, the work done is equated to the strain energy

$$[SE] = \{\bar{U}\}^T [S_e]\{U_e\} = \{\bar{U}\}^T [A]^{-T} \int_v [B]^T [D][B] \, dV \, [A]^{-1}\{U_e\}$$

which can be rearranged to obtain the element stiffness matrix

$$[S_e] = [A]^{-T} \int_v [B]^T [D][B] \, dV \, [A]^{-1}$$

Once the stiffness matrix for each element is determined, the matrices are assembled to produce an overall system stiffness matrix $[S_s]$. The element matrices in local axes are transformed into a global stiffness matrix in a global

coordinate system. At this point the boundary conditions are incorporated into the problem and the system equations for the entire region are solved to obtain the nodal displacements. From these primary unknowns values of stress or strain at any point in the region can be calculated.

2.4.3 Dynamic Analysis

In a dynamic analysis displacements, velocities and strains are all time dependent.

The displacement is again given by

$$\{U_e\} = [A]\{\alpha\}$$

and

$$\{U\} = [P][A]^{-1} \{U_e\}$$

where {U} is the time dependent displacement field.

Differentiating this equation with respect to time gives the velocity field

$$\dot{\{U\}} = [P][A]^{-1} \dot{\{U_e\}}$$

where $\dot{\{U_e\}}$ is the vector of nodal velocities.

To derive the dynamic equations of motion the Lagrange equation is used

$$\frac{d}{dt}\left\{\frac{\delta L}{\delta \dot{U}}\right\} - \left\{\frac{\delta L}{\delta U}\right\} = \left\{\frac{\delta R}{\delta \dot{U}}\right\} = \{0\}$$

In a dynamic analysis the kinetic energy as well as the strain energy must be considered. In this case, the Lagrangian (L) is given by

$$L = KE - SE$$

R is the dissipation function which is proportional to the relative velocities and dependent on the damping coefficient.

The system equations of motion are

$$[KE] = \{\dot{U}_s\}^T [M_s]\{\dot{U}_s\}$$

$$[SE] = \{U_s\}^T [S_s]\{U_s\} - \{U_s\} \{F_s\}$$

$$[R] = \{\dot{U}_s\}^T [C_s]\{\dot{U}_s\}$$

where $[M_s]$ is the master mass matrix
$[S_s]$ is the master stiffness matrix
$[C_s]$ is the master damping matrix
$\{F_s\}$ is the total load vector

By substituting these equations into the Lagrange equation the dynamic equations of motion for the system are derived

$$[M_s]\{\ddot{U}_s\} + [C_s]\{\dot{U}_s\} + [S_s]\{U_s\} = \{F_s\}$$

or if damping is neglected

$$[M_s]\{\ddot{U}_s\} + [S_s]\{U_s\} = \{F_s\}$$

It is assumed that all displacements in the system vary sinusoidally with time at frequency ω, such that

$$\{\ddot{U}_s\} = -\omega^2 \{U_s\}$$

By substitution, the two equations above give

$$([S_s] - \omega^2 [M_s]) \{U_s\} = \{F_s\}$$

where $\{F_s\}$ is a list of all the harmonically varying forces applied to the system.

The natural frequencies are calculated by determining the frequencies at which the system will vibrate without any external forces being applied, i.e. when $\{F_s\} = \{0\}$. The natural frequencies are found when the square matrix

$$[S_s] - \omega^2 [M_s]$$

has a zero determinant [62, 63].

2.4.4 PAFEC

The viability of FEM has led to the development of computer packages to cope with the increasing complexity of mesh generation and calculations. The package used in this study is called PAFEC (Program for Automatic Finite Element Calculations).

The PAFEC software consists of ten computer programs called Phases; the phases required for a solution depending on the type of problem. For a dynamic analysis to calculate natural frequencies and mode shapes, four phases are needed; namely 1,4,6 and 7. These four programs are executed sequentially to perform an analysis and their individual functions are

PHASE 1 (READ):
The data file is read and placed into backing store

PHASE 4 (PRE-SOLUTION HOUSEKEEPING):
The DOFs of the problem are numbered and constrained according to the input constraints

PHASE 6 (ELEMENTS):
The stiffness and mass matrices of all the elements are derived and stored

PHASE 7 (SOLUTION):

The system equations are solved for the primary unknowns.

The input data in PAFEC is organised into modules describing the structure's dimensions, element mesh, material properties, boundary conditions and excitation/loading specification. An interactive graphics facility called PIGS is used for mesh generation and creation of the data file. The standard layout procedure for preparation of data files is described in the PAFEC manual [64]. A control module precedes the input data. The control statements guide the FE job through the various optional paths and define the output information required along with the primary unknowns.

PAFEC calculations are performed in this study to provide predictions of die dynamic behaviour and for comparison with experimentally determined behaviour estimations.

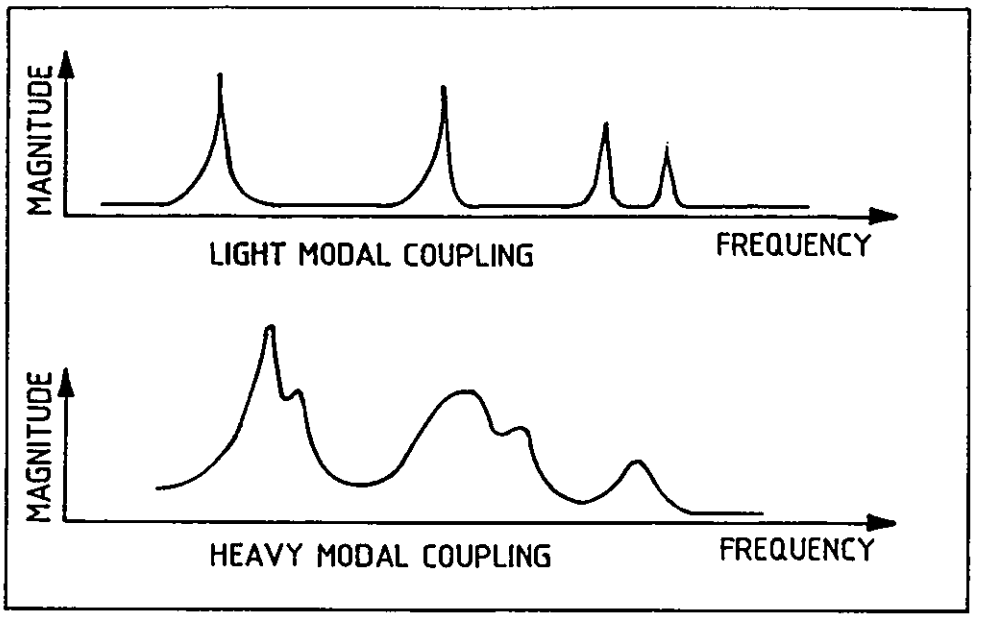

Figure 2.1 Modal Coupling

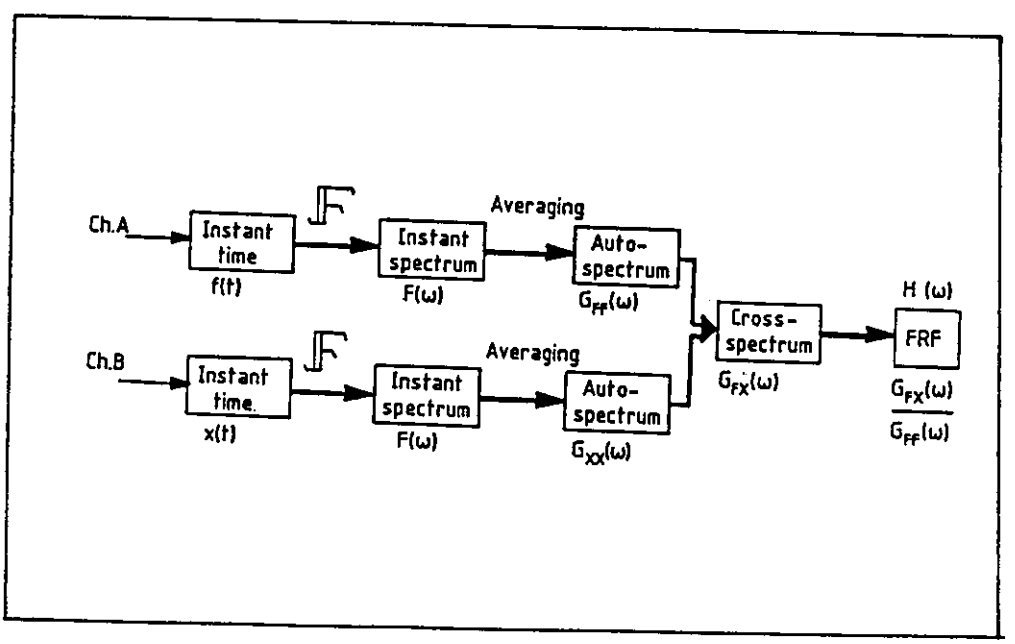

Figure 2.2 Functions of FFT Analyser in EMA

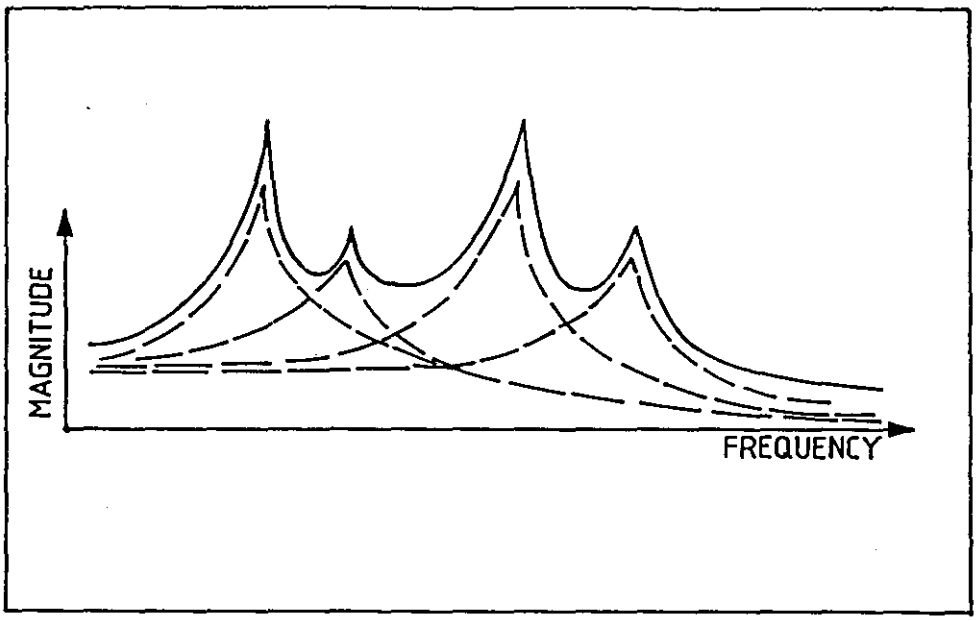

Figure 2.3 Modal Participation in a MDOF FRF

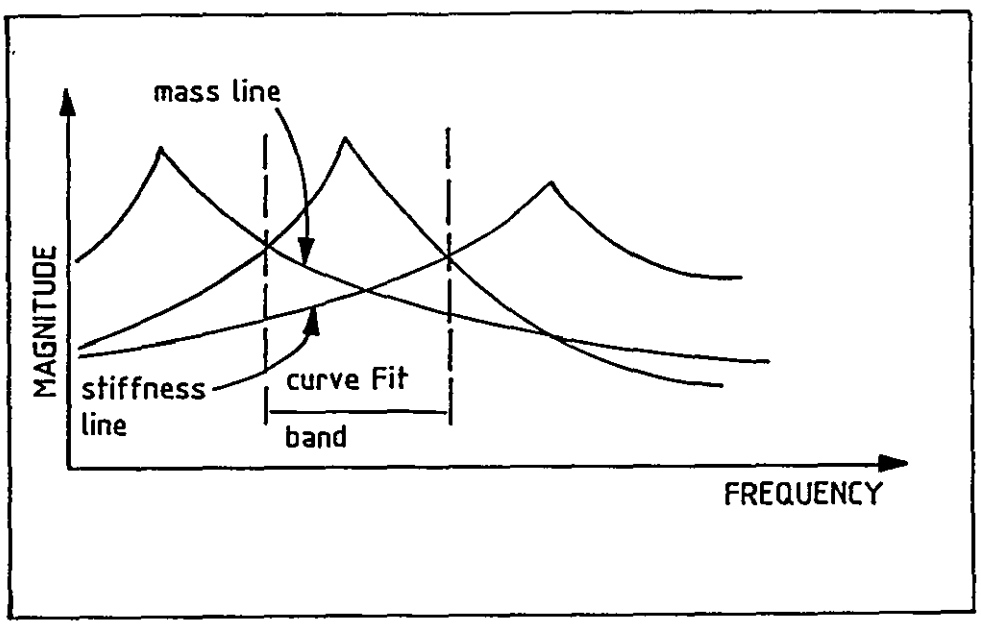

Figure 2.4 Effects of out-of-band modes

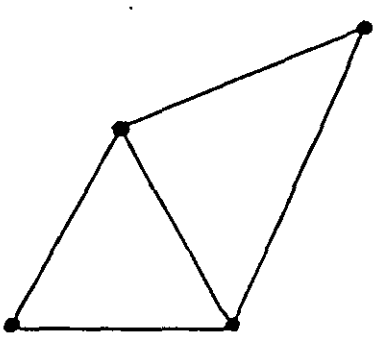

a) Triangular elements

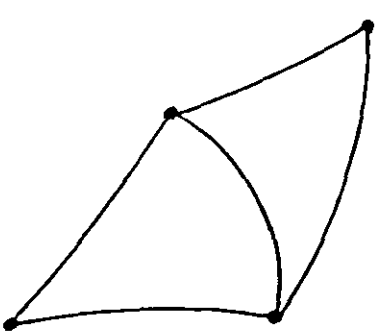

b) Displaced shape of elements

Figure 2.5 Finite Elements Conforming to Displacement Function Conditions

CHAPTER 3
DYNAMIC CONSIDERATION OF DIE NECKING PROCESS

3.1 MEASURING THE EXCITATION SYSTEM PARAMETERS

Previous to this study, resonant modes of vibration of forming dies were measured at CMB by sprinkling powder on the die face and recording dispersion patterns at excitation frequencies around the operating frequency. This simple technique relies on the principle that fine powder particles scattered on a vibrating surface will tend to settle in nonvibrating regions, such that the dispersed powder displays a mode shape indicated by its nodal lines. Although the resulting information was useful for checking that a die was tuned to vibrate in the correct mode at 20 kHz, little knowledge could be gained concerning the wider vibration behaviour of the die and the interpretation of more complex mode shapes. Further, no measurements had been performed to investigate changes in die dynamic characteristics throughout the forming process.

This meant that although thick cylinder die designs inherently exhibit a density of modes around the required tuned frequency (Appendix B), it was not known what modes these were, whether they interfered with die necking reliability and how they were affected by the variation in die loading during forming.

The main questions inviting consideration were:

i) Are modes close to the tuned resonant mode necessarily detrimental to successful die forming?

ii) Is the generating equipment transmitting amplitude effectively and maintaining the desired vibration mode during the forming period?

iii) What are the implications of continual die loading and unloading to die design criteria?

To obtain answers to these questions, insight is required into the actual vibration behaviour of a forming die in its loaded and unloaded state. To this end an experimental study was initiated in which two paths of investigation were followed.

1. Various operating parameters (input power, hydraulic pressure, die vibration amplitude) were measured and analysed over the forming period using two different ultrasonic generators.

2. An experimental rig consisting of a die statically loaded with a part-formed can under hydraulic pressure was designed so that die vibratory response under simulated forming conditions could be compared with those measured without loading.

This experimental investigation was conceived as an initial knowledge gathering exercise to look at some of the fundamental process parameters in terms of ultrasonic effects.

3.2 ANALYSIS OF PROCESS PARAMETERS DURING FORMING

The first series of experiments, as outlined above, involved monitoring three process parameters:

i) Die oscillation magnitude
ii) Ultrasonic generator power
iii) Inlet hydraulic pressure.

Measurements were conducted on a die necking test rig consisting of an ultrasonic head that would constitute one of the ultrasonic necking stages of the proposed aerosol container production machine. This test rig, illustrating the principles of die necking, is described in Appendix A.

For each of the three parameters above, four experimental configurations were examined. For each measurement, the test rig's hydraulic and pneumatic processes of ram motion and knockout are activated so that this motion alone defines one of the configurations. The four configurations are:

a) Ultrasonic excitation during can forming
b) No ultrasonic excitation during can forming
c) Ultrasonic excitation with no can forming
d) No ultrasonic excitation and no can forming

Measurements of die oscillation amplitude were noted for all four test conditions and were checked for repeatability. The power from the ultrasonic generator was monitored for test configurations a) and c) and the ram inlet hydraulic pressure was measured for all four test conditions.

Two ultrasonic power generators were employed separately in order to record any differences in the ultrasonic amplitude transmitted to the die during the necking operation and to measure the generator power in each case. The two generators, one supplied by Kerry Ultrasonics and the other by Telsonic, are described in Appendix A.

3.2.1 Data Acquisition

Measurements of the process parameters were aquired as time traces using a dual channel FFT analyser. Because the ultrasonic forming stage is known to take less than half a second, the analyser was operated in its extended memory mode so that measurements could be displayed in two traces; one a compressed time representation, the other an expanded block of the time history. By introducing some overlap of the time blocks, it was possible to perform a reasonably detailed analysis of the amplitude and frequency content of the monitored signals at steps throughout the ultrasonic switch on period. The process steps represented by time blocks of data could be identified in terms of position along the can profile from knowledge of the can geometry. The can profile and dimensions are illustrated in Figure 3.1.

3.2.2 Die Displacement Measurements

Radial displacement amplitude of the die outer diameter is measured by a noncontacting transducer which is a modified inductive proximity probe. The probe is adapted for ultrasonic measurements by using a carrier frequency of several MegaHertz; well in excess of the low ultrasonic range of interest. Electronic filters are included to reject all low frequency signals. This allows the probe to be held in a non-ideal mounting device without adversely affecting the accuracy of the readings. The probe is connected through an amplitude meter to the FFT analyser so the time traces can be calibrated and absolute readings obtained.

Kerry Generator:

Figures 3.2 to 3.4 are the time histories in compressed time of the die displacement for test configurations a), c) and d) respectively. Figure 3.5 repeats configuration a) for a lower inlet hydraulic pressure. Inspection of the die response reveals a period of ultrasonic amplitude build-up, after which the die circumference attains a vibration amplitude of 18.6 µm pk/pk. When there is no can being loaded (Figure 3.3) die amplitude settles to a value of 18 µm pk/pk for the duration of the ultrasonic period. When a can is necked with ultrasonic assistance at the working hydraulic pressure of 100 psi (Figure 3.2), there is a marked dip in die amplitude which occurs at the onset of forming ie. at the point where the can leaves its parallel path in the die pellet. The minimum amplitude is 16.5 µm during necking. Amplitude is regained to 17.8 µm at the point of inflection then dips again slightly for the remainder of the forming period. A reduction in hydraulic ram pressure to 30 psi lessens the effect of forming on die response (Figure 3.5) but consequently reduces the reliability of the necking operation.

The changes in vibration amplitude during ultrasonic forming are due to alteration of the modal damping characteristics when the die is under different loading states. As the can enters the die and the material leaves its parallel path, the can will hug the die pellet contours due to the elastic springback experienced in this type of plastic deformation. After reaching the point of

inflection, it is suspected that the can will tend to hug the plunger contours and the loading effect of the can on the die is reduced. More energy is therefore dissipated when forming is incipient. It is expected that the stiffening of the die structure due to loading will affect the resonant frequency but this should be compensated for in terms of maintaining amplitude by the automatic frequency control which locks on to resonance.

These deductions are supported by a frequency analysis of the die displacement. It is clear from Figure 3.4 that there is frequency content due to the system's response to the hydraulic and pneumatic processes. This is observed as a 250 Hz component superimposed on the forming measurement signals. The four spectra of particular interest to understanding die behaviour are shown in Figures 3.6-3.9. The zoom capability of the FFT analyser permits close inspection within a narrow band around the operating frequency. Figures 3.6 and 3.7 indicate the frequency content in the time block when the ultrasonics is switched on (Figure 3.7 is displayed with increased gain). Figure 3.8 represents the time block when forming commences and Figure 3.9 is the spectrum 0.02 seconds later.

When the ultrasonics is switched on, the amplitude build-up period excites several frequencies as well as the tuned die radial mode frequency. The 21.4 kHz peak is the most dominant but frequencies at 18.4, 19.7, 22.9 and 24.3 kHz are also detected. This is the first indication of the die natural frequencies proximate to the tuned resonance, as it responds to the transient switch-on of the ultrasonic excitation. The operating frequency at this stage is 19.9 kHz. When forming begins this frequency changes; the generator locking on to the altered frequency at 20.1 kHz and then 20.05 kHz. This changeover is clear from examination of Figures 3.8 and 3.9.

Telsonic Generator.

Measurements of die displacement with the transducer driven by the Telsonic generator, are presented in Figures 3.10-3.14. Figure 3.10 is a time history of ultrasonic necking measured over 1.12 seconds and points out some of the

process stages. Figures 3.11-3.14 represent the response to the four test conditions a) to d) respectively.

Figure 3.11 demonstrates the difference in die performance using the Telsonic system. There is a sharp dip in amplitude during the forming period. The time trace reveals that the loss in amplitude occurs at the point where forming commences, reaches a minimum value of 6 µm pk/pk and subsequently regains amplitude while the can is still advancing through the first curve of the neck profile. However, the maximum die vibration amplitude is higher in this case; being 22.5 µm pk/pk. From the measurement of die vibration with no can present (Figure 3.13), the radial amplitude of the die circumference is uniformly at the same level as the maximum amplitude during can forming; namely 22.5 µm pk/pk.

The response to the Telsonic generator driving the excitation system also differs in that the ultrasonic build-up period is barely discernible (less than 0.01s). The frequency spectra at ultrasonic switch-on do not exhibit frequencies other than the tuned operational modal frequency. This single monitored mode is initially at 19.9 kHz, increases when forming begins to 20.15 kHz, then settles to 20.05 kHz for the remainder of the ultrasonic period.

3.2.3 Generator Power Measurements

The power from the ultrasonic generator was measured for test configurations a) and c) using the Kerry system (Figures 3.15 and 3.16) and for test configuration a) using the Telsonic system (Figure 3.17).

Kerry Generator:

Figure 3.15 illustrates the measured power requirement with no can forming. The power builds up over 0.12 seconds then decreases gradually for the rest of the stroke. When the can forming operation is introduced, the power requirement changes. Figure 3.16 shows that the power is a minimum at the point when the can enters the die then increases over the forming period.

Telsonic Generator:

Figure 3.17 illustrates the power measured for an ultrasonically assisted necking operation using the Telsonic generator. There is a small peak in the power signal at the point when forming starts and then a sharp dip which corresponds to the vibration amplitude drop-off measured previously. Power amplitude then increases over the forming period.

3.2.4 Pressure Measurements

Kerry Generator:

The inlet hydraulic pressure was measured for test configurations a) to d) (Figures 3.18-3.21). There is a slight increase in pressure detected when forming begins, with or without ultrasonic excitation of the die. More revealing information is obtained from frequency analysis of the pressure signal. Because the pressure build-up period after ultrasonic inception is observed in four time blocks of analyser extended memory, the frequency spectra reveal many vibration peaks being excited in the low ultrasonic range (Figures 3.22-3.24). The frequencies of the spectral peaks are consistent with those detected in the die displacement signal, indicating that system resonances are being excited by the transient switch-on of the ultrasonics for this particular generator. These measurements therefore serve to confirm that the die tuned operating mode is not well isolated from the influence of other modes of vibration.

3.2.5 Conclusions

The conclusion from this analysis is that the measured forming parameters change over the forming period. The three observations of most significance to the reliability of the necking process are:

1. The existence of die natural frequencies close to the operating frequency could lead to difficulties in maintaining the tuned resonant mode without influence from other modes of vibration.

2. An increase in damping due to the altered dynamic state of the die during forming increases the likelihood of modal coupling, which results in a superposition of the effects of closely spaced modes.

3. The operating frequency changes during the necking process as the excitation system tries to maintain maximum die amplitude by locking-on to a resonant condition. With high modal density around the operating frequency, there is a danger of locking-on to the wrong mode of vibration.

Maintaining the tuned mode of the die is critical to successful ultrasonic die forming as it is essential to excite a uniform radial amplitude at the forming surface. Interference from the response contribution of another mode leads to amplitude variations and possibly nodal points on the forming surface. This would result in failure of the can neck. It is suspected that the phenomenon of "mode-switching" threatens the reliability of ultrasonic forming and that culpability lies with the three contributory factors described above.

3.3 DIE VIBRATION UNDER LOADED AND UNLOADED CONDITIONS

The problem of mode-switching (resulting in process failure) is the phenomenon relevant to the die loading investigation. The implication of mode-switching is that if there exist modes with natural frequencies close to the operating frequency, one of these modes could be excited in preference to the tuned mode by nature of its preferential modal characteristics. This phenomenon occurs due to high modal density around the operating frequency and is exacerbated by the changing dynamic behaviour of the die during the forming process.

Mode-switching is considered portentous by reason of the findings from the previous analysis of forming parameters. In order to draw firm conclusions regarding the existence of close, problematic modes, an investigation is

conducted into the differences between die vibration behaviour under loaded and unloaded conditions.

3.3.1 Description of Test Rig

A test rig was designed to investigate modal behaviour of a die within a narrow bandwidth around the operating frequency, for two of the process stages:

1. Die unloaded (free vibration)
2. Die loaded with can and plunger under hydraulic pressure

On the forming test rig, die characteristics change continuously during can necking, making sequential capture of die response data at particular stages of the process extremely difficult. The philosophy of the experimentation was therefore based on static loading of the die with a preformed can and plunger under realistic hydraulic pressure conditions. This simulates the die state at the point in the forming cycle where the die is fully loaded.

The test rig is shown in Figure 3.25. Loading the die involves applying hydraulic pressure in an axial sense through the back of the die, forcing the preformed can and plunger into the die pellet. Pressure is applied until the operational value is reached. At this point the ultrasonics is switched on and the die vibration response is measured. On completion, the ultrasonics is switched off, pressure is released and a back pressure is applied to free the plunger and can from the die.

3.3.2 Pressure Requirement

Information obtained on the forming rig at CMB revealed that between 1 and 2 kN of force is used to hold the plunger in the die. The hydraulic test rig therefore required 2 kN capability to simulate the load experienced by the die in a real forming operation. The test rig is rated at 1000 psi (the inside piston being one square inch and the maximum pressure being limited by the switch). This allows a possible 5 kN load. A pressure of 400 psi was used for the loaded die measurements.

3.3.3 Die Vibration Measurement

Accelerometers were used to measure surface acceleration at points around the die. After signal conditioning, the measurements are captured using an FFT analyser. The zoom mode of the analyser allows signal acquisition in a narrow frequency band. The chosen bandwidth for this study was 19.25 kHz to 21.75 kHz so that detail of vibratory activity in the vicinity of the operating frequency could be inspected.

The die vibration characteristics are displayed as frequency response functions (FRFs) containing amplitude and phase information. The development of the ultrasonic vibration measurement technique employed, is described in Chapter 4.

It was intimated by the previous study of forming parameters that damping was a varying parameter during forming. Therefore the modal damping is determined for the loaded and unloaded die. Modal damping is estimated from the logarithmic decrement (δ), which can be calculated from an FRF measurement using the formula:

$$\delta = \frac{\pi \Delta f}{f_n}$$

where f_n is the natural frequency and $\Delta f = f_2 - f_1$ is the difference between the half-power frequencies above and below resonance (i.e. the frequencies at which peak amplitude is reduced by 3 dB or by a factor of $\sqrt{2}$) [65,66]. The damping factor is found from the logarithmic decrement by:

$$\xi = \frac{\delta}{2\pi} = \frac{\Delta f}{2 f_n}$$

3.3.4 Die Vibration Results

The changes in die vibration behaviour caused by loading the die with can and plunger can be observed and quantified by overlaying the FRFs from the loaded die measurements on top of those from the unloaded die

measurements. Figure 3.26(a,b) and 3.27(a,b) present the resulting traces in this manner. Figure 3.26 shows FRFs of radial measurements at two positions on the die circumference and Figure 3.27 shows two die face FRFs measured in an axial sense.

The resulting FRFs illustrate that several natural frequencies are present in the narrow analysis band around the operating frequency (all within 10% of the operating frequency). However, two natural frequencies of the die dominate the radial response. One is known to be the frequency to which the die was tuned at the design stage (i.e. the fundamental radial mode R0 at a nominal 20 kHz). The other dominant response is expected to be either the first or third radial harmonic, R1 or R3, which tend to occur close to the fundamental mode in thick cylinders (Appendix B). Whichever mode it is, the responsiveness indicates that this is likely to be the most problematic mode since its radial response contribution to the tuned mode will restrict the ability to excite a uniform amplitude of vibration at the die bore during forming.

Participation of off-resonance modes on the tuned R0 mode will be severe under conditions of high modal density and/or heavy damping. The resulting modal coupling seen in the measured FRFs means that one mode cannot be excited to the exclusion of the others in close proximity, which defeats the purpose of designing a die to display pure modal behaviour. Modal participation by approximately equally dominant modes, such as the two radial modes prominent in the analysis band, therefore causes concern for the reliability of the die tuning procedure. It also explains the occurrence of mode-switching encountered in necking trials, because the results show that the modal participation problem is worsened by loading the die.

It is observed that the natural frequency of the fundamental mode increases measurably when the die is loaded. In fact the R0 mode increases by over 100 Hz. The close dominant mode, on the other hand, appears to maintain its natural frequency at 20.8 kHz, thus reducing the mode separation from 4% to 3.5%. Also, there is considerable loss in radial vibration amplitude for both

dominant modes (with no corresponding loss in axial amplitude). This implies that more power is required during forming to maintain amplitude, which was borne out by power measurements taken on the forming rig. To assess how these two modes are affected individually, the amplitude and phase at each resonance was plotted at 30° intervals around the die circumference. Figure 3.28 (a,b) show that while the R0 mode loses approximately two thirds of its unloaded radial amplitude, the other mode (now revealed to be the R3 mode) loses approximately one half of its peak unloaded amplitude. This means that under loaded conditions the R3 mode dominates the spectrum.

The other aspect of die behaviour likely to influence modal participation of R3 in R0 is the modal damping. The measured damping values, determined from the logarithmic decrement, are presented in Table 3.1. From the radial measurements, the damping value associated with the R0 mode increases by 120% under loading and the damping in the R3 mode increases by 147%. This causes the R0 and R3 modes to be more closely coupled by spreading the response over a wider frequency band, and adversely affecting the ability to excite R0 in isolation.

RADIAL MEASUREMENTS			
ξ (%) Die unloaded		ξ (%) Die loaded	
RO	R3	RO	R3
0.15	0.40	0.33	0.99
AXIAL MEASUREMENTS			
ξ (%) Die unloaded		ξ (%) Die loaded	
RO	R3	RO	R3
0.19	0.43	0.25	0.43

TABLE 3.1: COMPARISON OF DAMPING VALUES

3.3.5 Conclusions

Measurements from the test rig experimental investigation have provided further understanding of the problems associated with ultrasonic forming.

When the die is loaded with can and plunger during the ultrasonic process, the innate dynamic characteristics of the vibrating system change such that the natural frequencies of the two close radial modes R0 and R3, exist in close proximity, with the R3 mode becoming the preferred mode and dominating the group of modal frequencies around the tuned fundamental mode. The increased modal coupling, resulting from changes in relative peak response amplitude between the modes and increased modal damping, leads to modal participation of off-resonance modes, incurring detrimental penalties on the uniformity of the R0 amplitude. The inability to excite the R0 mode as a pure mode and the threat of mode-switching during operation are serious die design problems that require tackling. These initial experimental investigations point to the necessity for a rigorous approach to die vibration analysis to advance the understanding of thick cylinder vibration behaviour with a view to a die redesign strategy which separates undesirable modes from the operating mode.

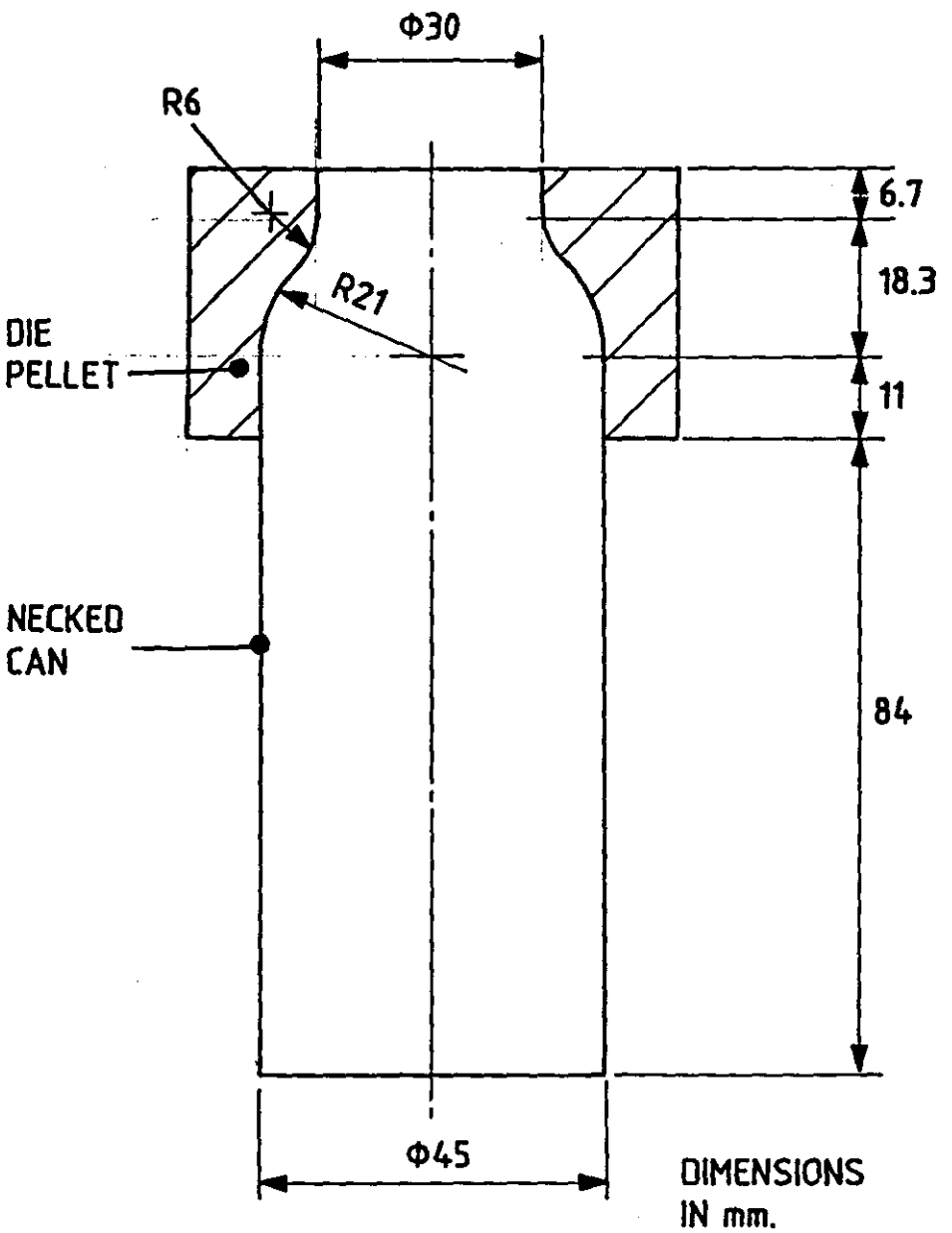

Figure 3.1 NECKED CAN PROFILE

Measurements using Kerry Generator of Die Displacement

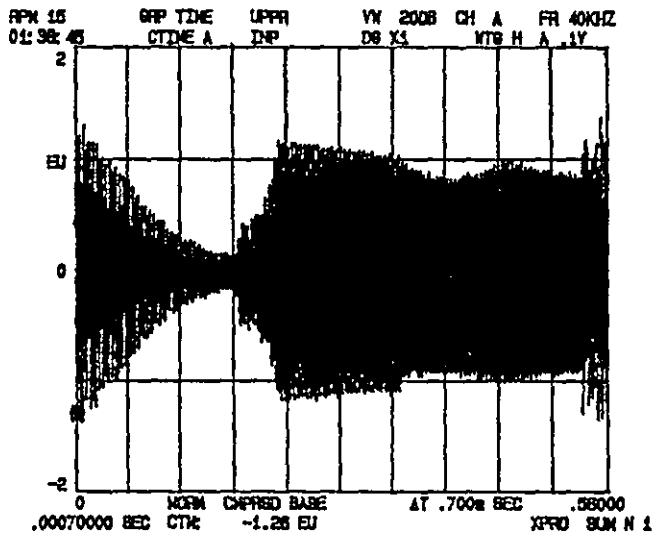

Figure 3.2 Ultrasonics, can

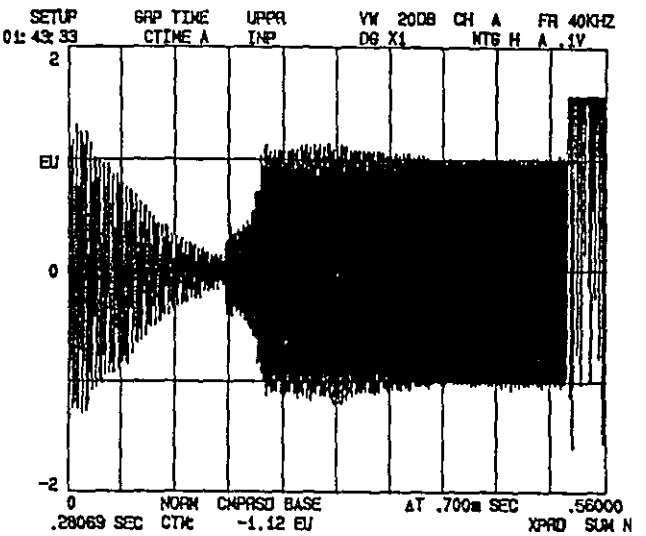

Figure 3.3 Ultrasonics, no can

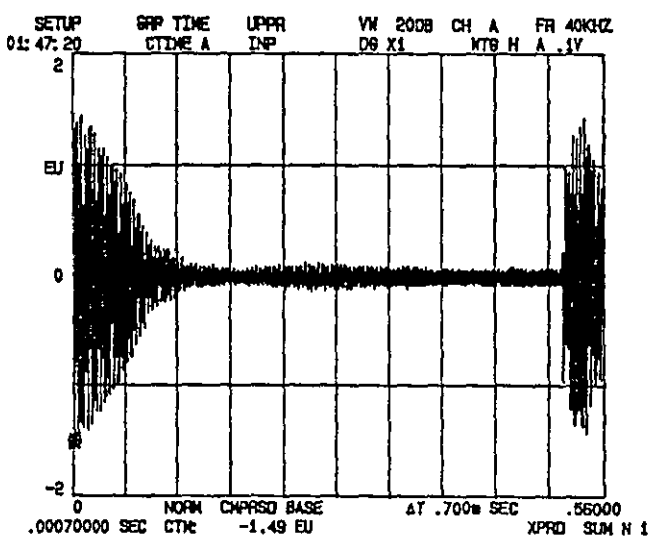

Figure 3.4 No ultrasonics, no can

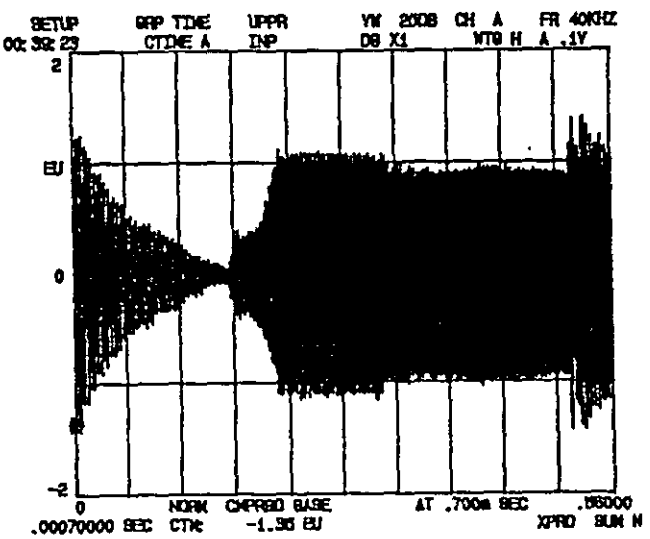

Figure 3.5 Ultrasonic forming, low pressure

Measurements Using Kerry Generator of Die Displacement Frequency Content

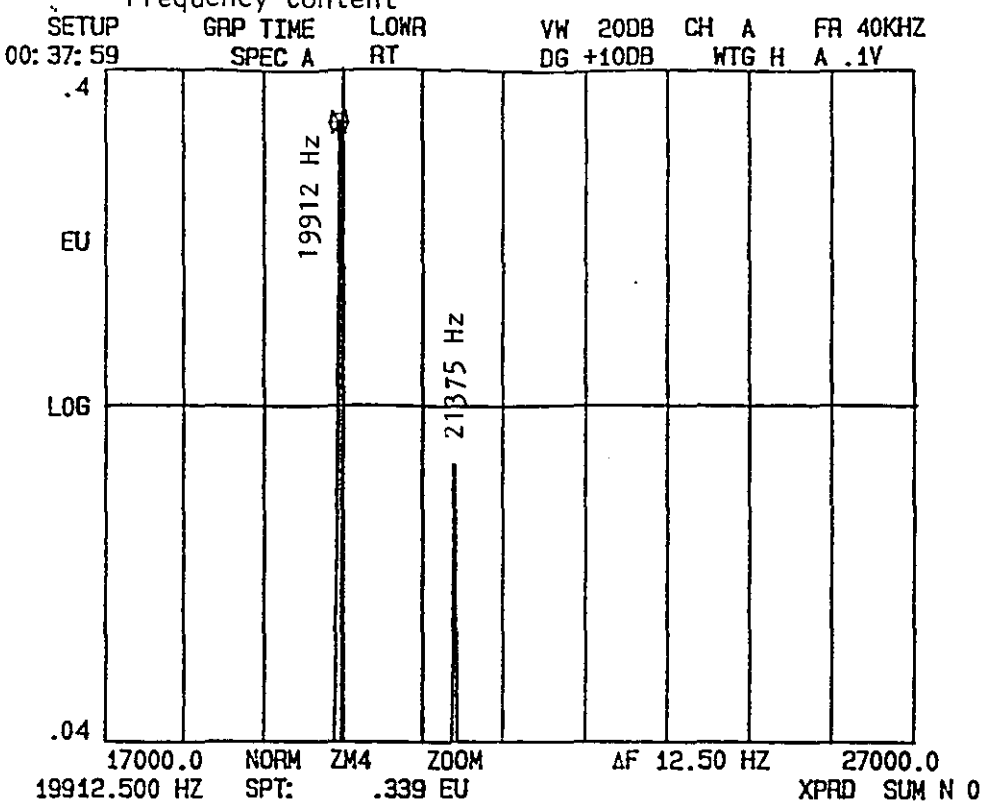

Figure 3.6 At Ultrasonic Switch On

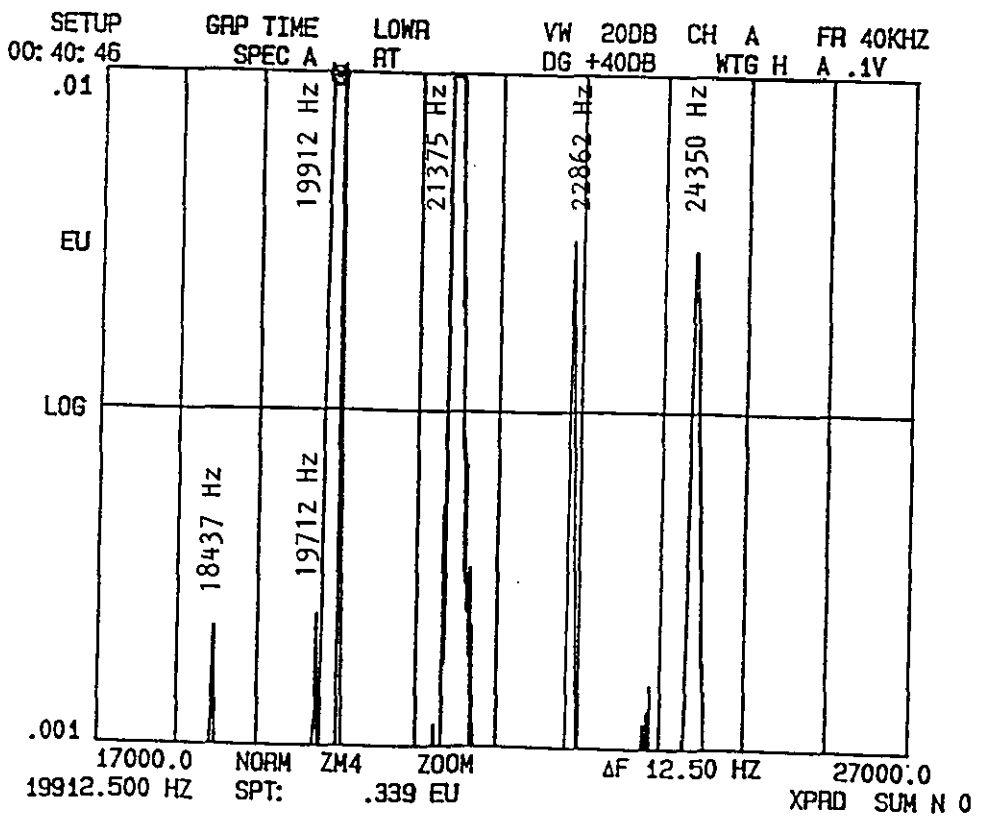

Figure 3.7 At Ultrasonic Switch On (Increased Gain)

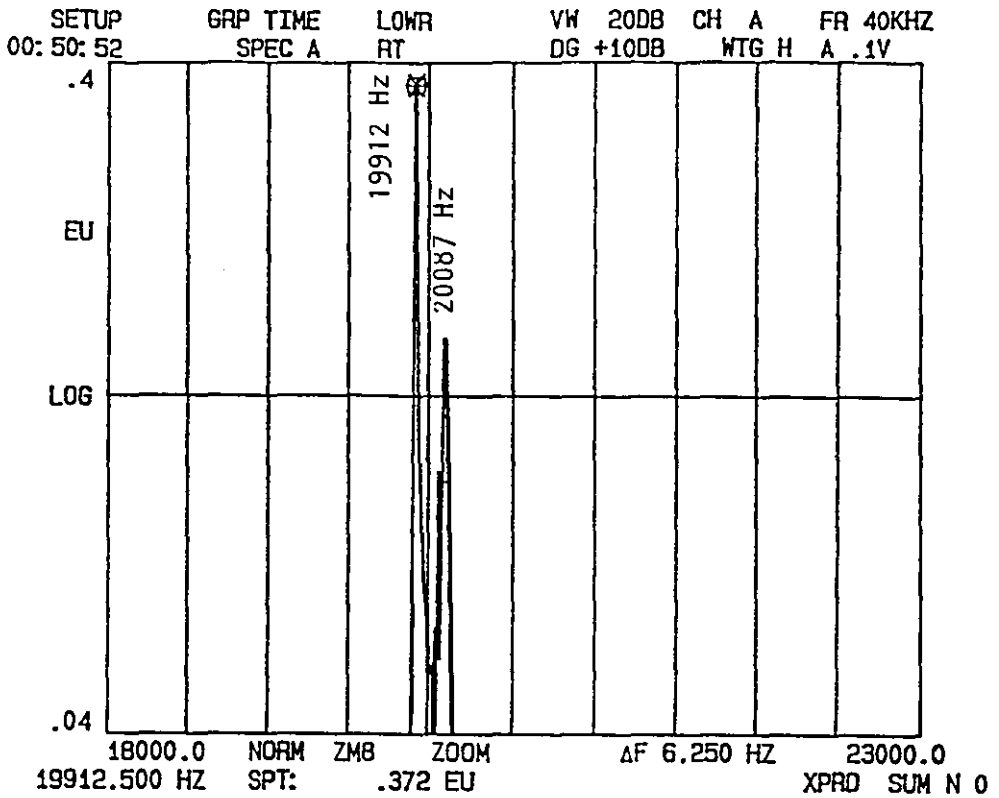

Figure 3.8 At Commencement of Forming

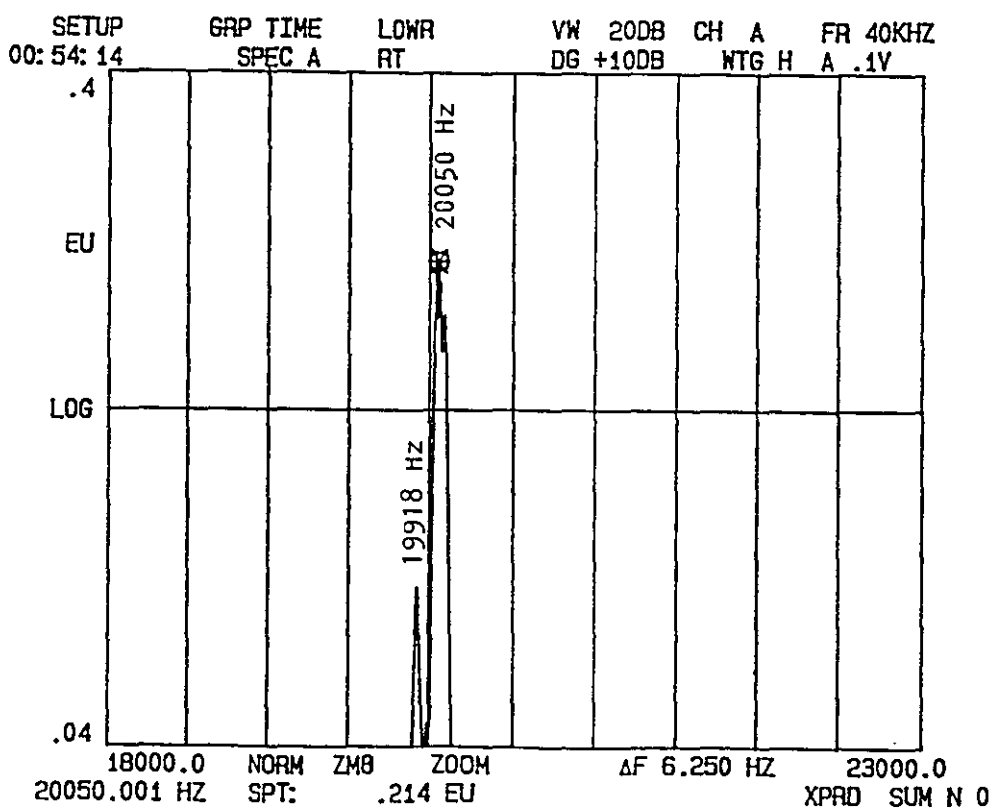

Figure 3.9 0.02 Seconds after Commencement of Forming

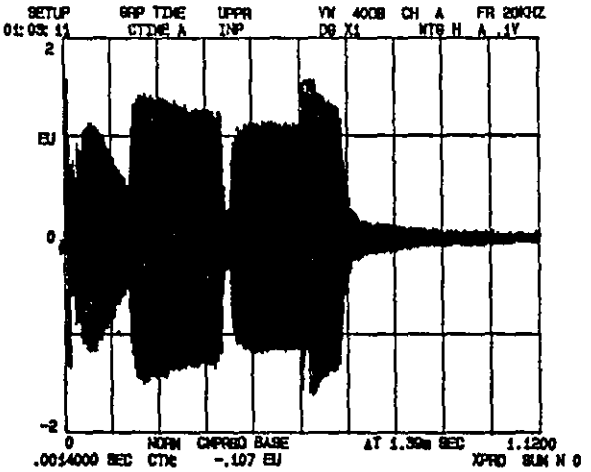

Figure 3.10 Extended Time History.Ultrasonics, can

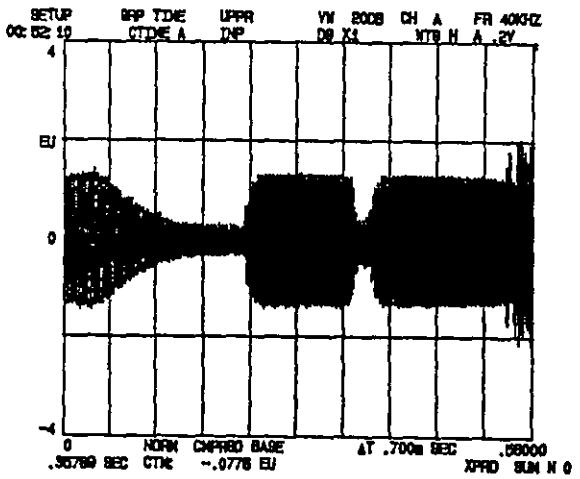

Figure 3.11 Ultrasonics, can

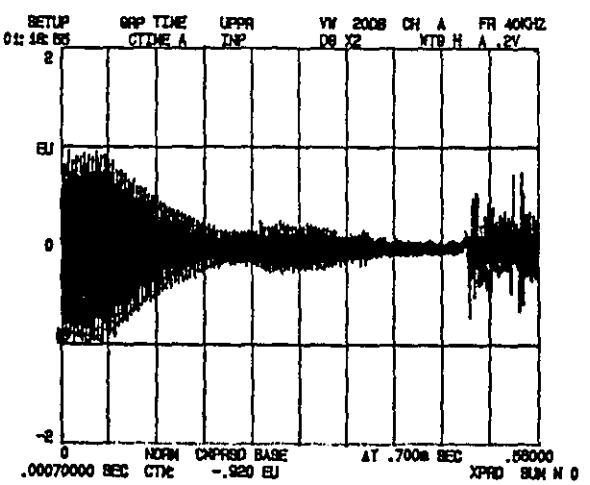

Figure 3.12 No Ultrasonics, can

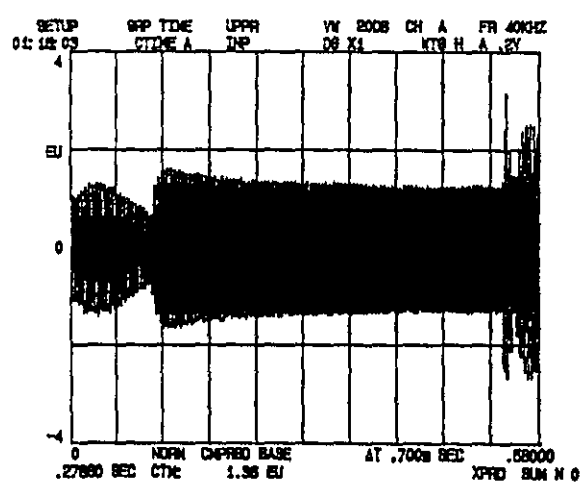

Figure 3.13 Ultrasonics, no can

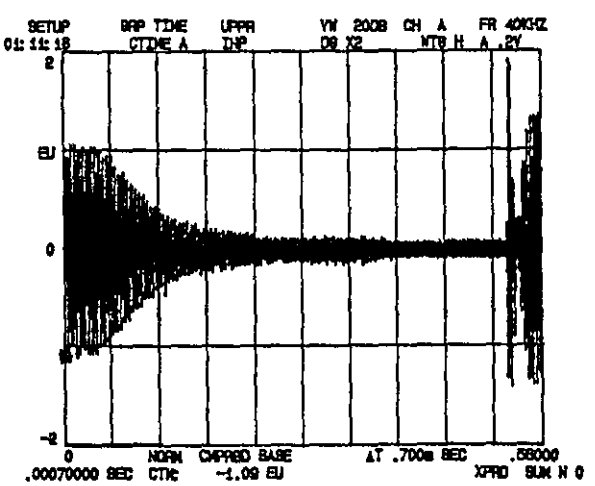

Figure 3.14 No ultrasonics, no can

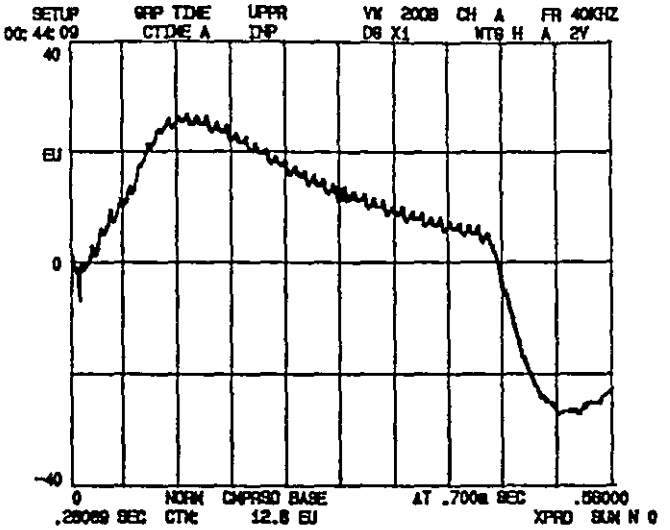

Figure 3.15 Kerry Generator Power, Ultrasonics, No Can

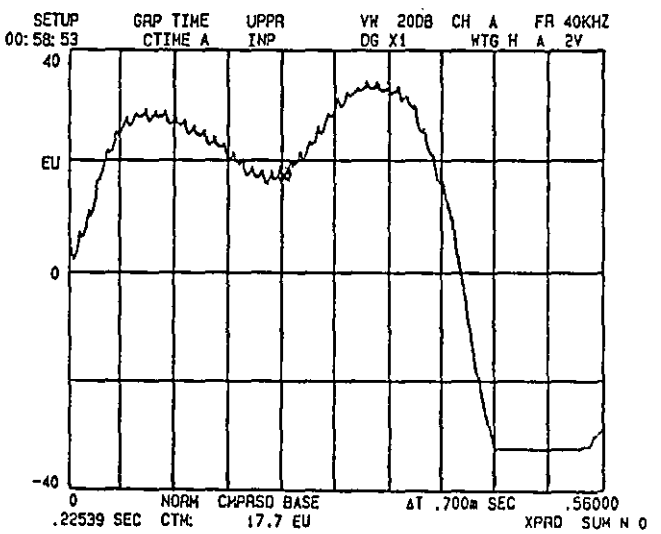

Figure 3.16 Kerry Generator Power Ultrasonics, Can

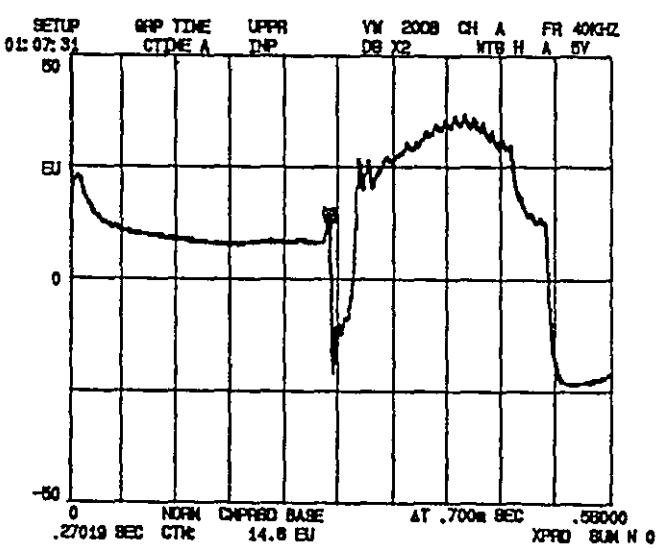

Figure 3.17 Telsonic Generator Power, Ultrasonics, Can

Inlet Ram Hydraulic Pressure Measurements, Ultrasonic Power from Kerry Generator

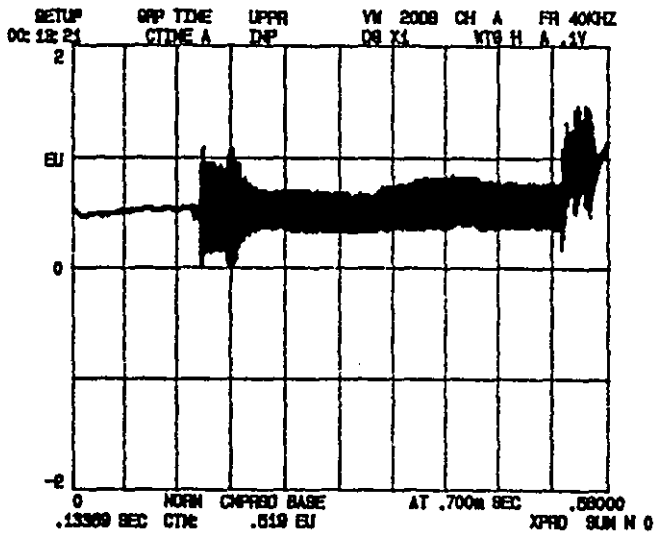

Figure 3.18 Ultrasonics, Can

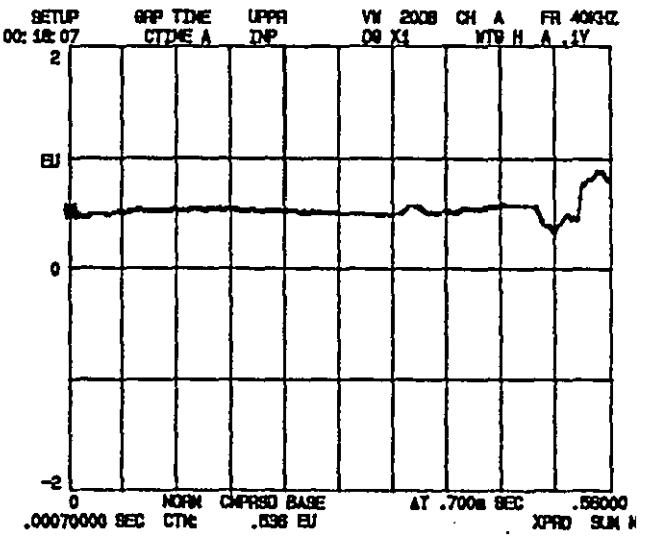

Figure 3.19 No Ultrasonics, Can

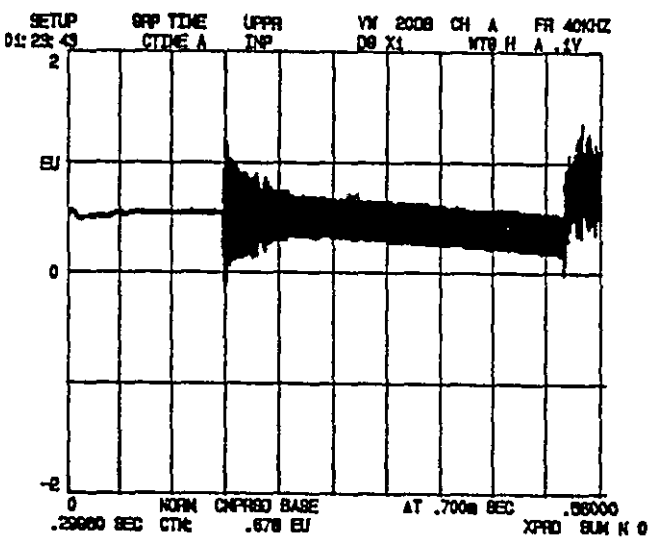

Figure 3.20 Ultrasonics, No Can

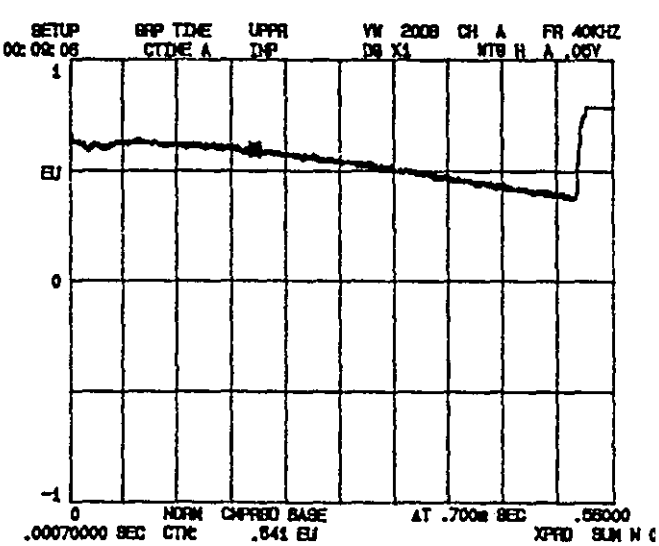

Figure 3.21 No Ultrasonics, No Can

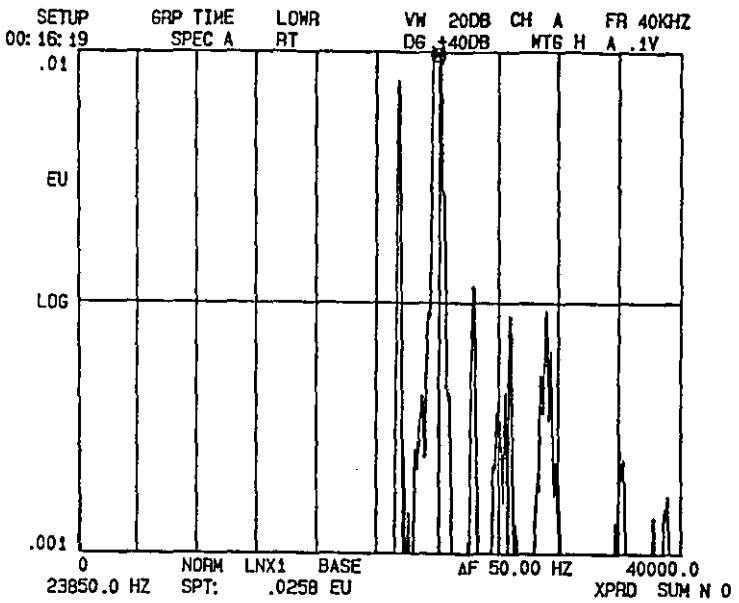

Figure 3.22

At Ultrasonic Switch on
0-40 kHz

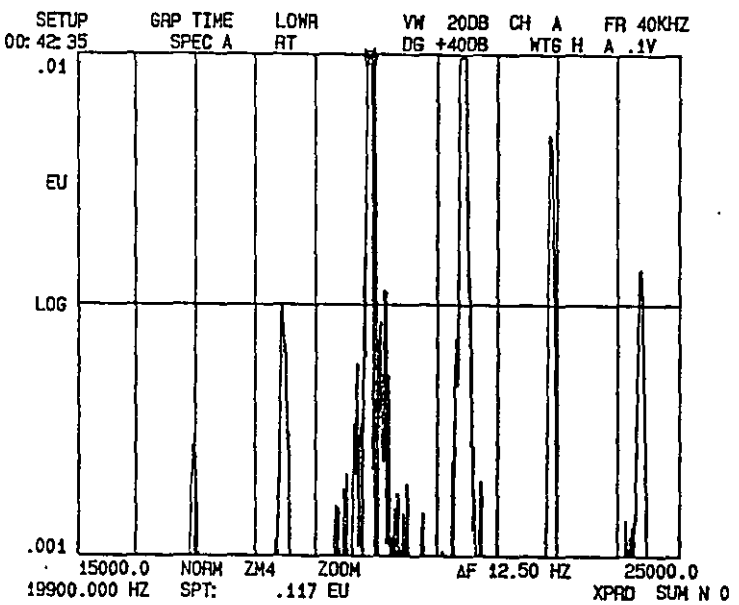

Figure 3.23

Time Block After Ultra-
sonic Switch On
15-25 kHz

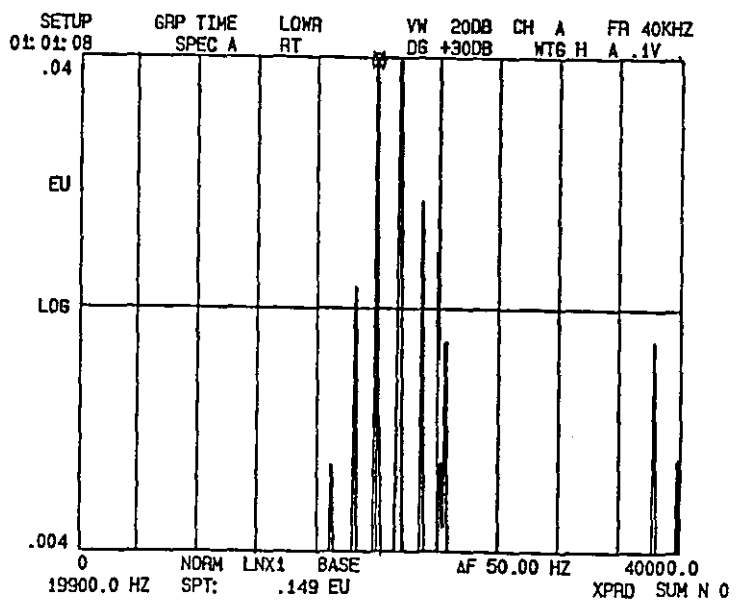

Figure 3.24

Two Time Blocks After
Ultrasonic Switch on
0-40 kHz

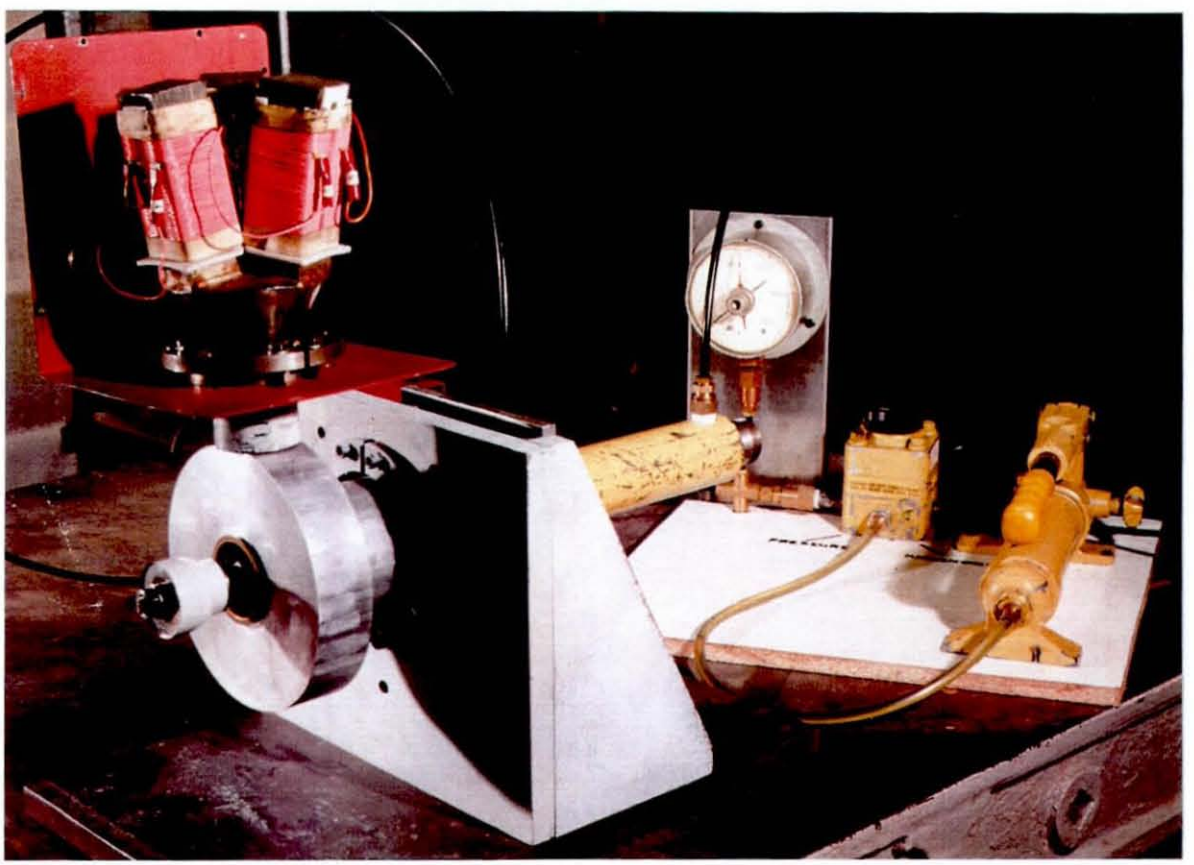

Figure 3.25 Die Loading Test Rig

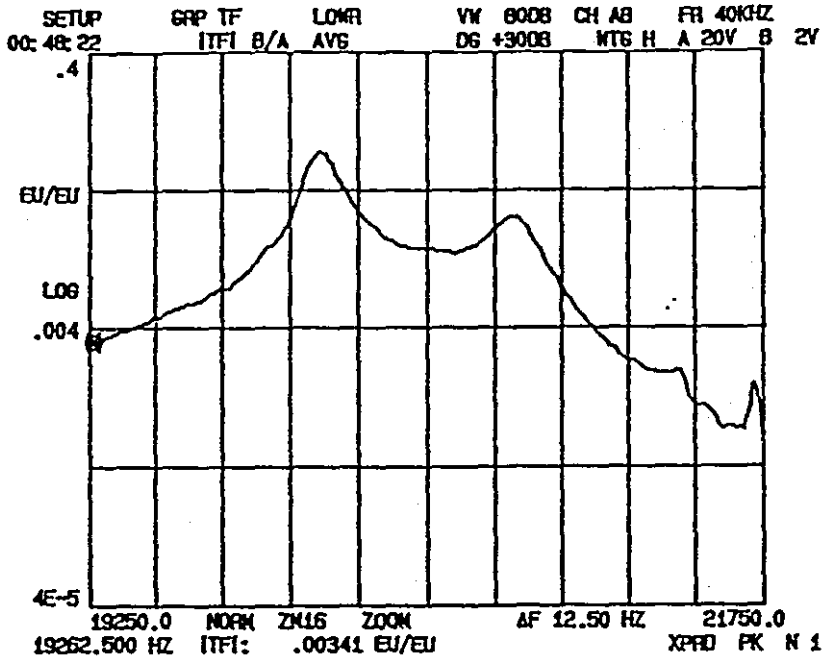
SETUP
00: 48: 22
GRP TF
ITFI B/A
LOWR
AVG
VW 800B
DG +300B
CH AB
MTG H
FR 40KHZ
A 20V B 2V
.4
EU/EU
LOG
.004
4E-5
19250.0
NORM ZM16 ZOOM
AF 12.50 HZ
21750.0
19262.500 HZ ITFI: .00341 EU/EU
XPRD PK N 1

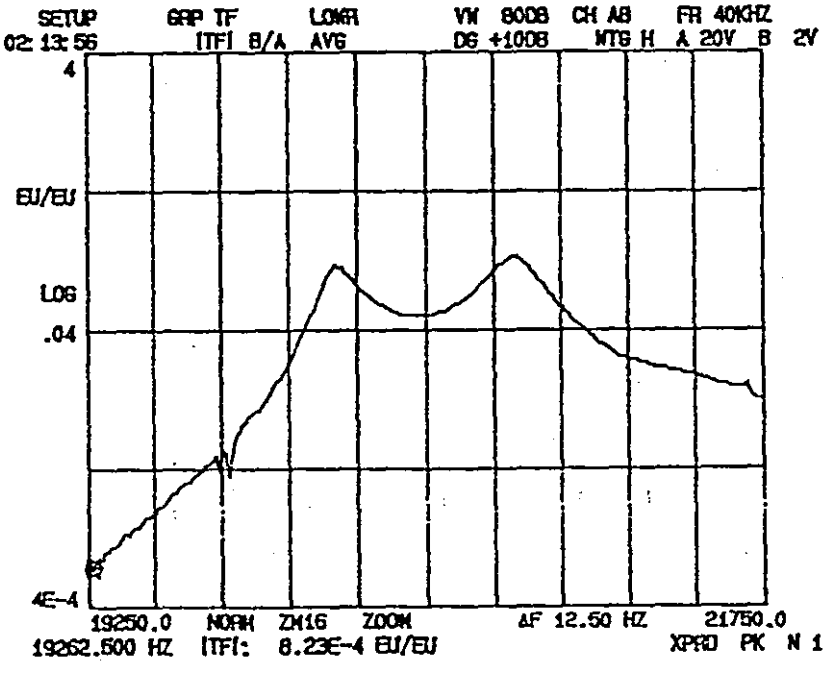
SETUP
02: 13: 56
GRP TF
ITFI B/A
LOWR
AVG
VW 800B
DG +100B
CH AB
MTG H
FR 40KHZ
A 20V B 2V
4
EU/EU
LOG
.04
4E-4
19250.0
NORM ZM16 ZOOM
AF 12.50 HZ
21750.0
19262.500 HZ ITFI: 8.23E-4 EU/EU
XPRD PK N 1

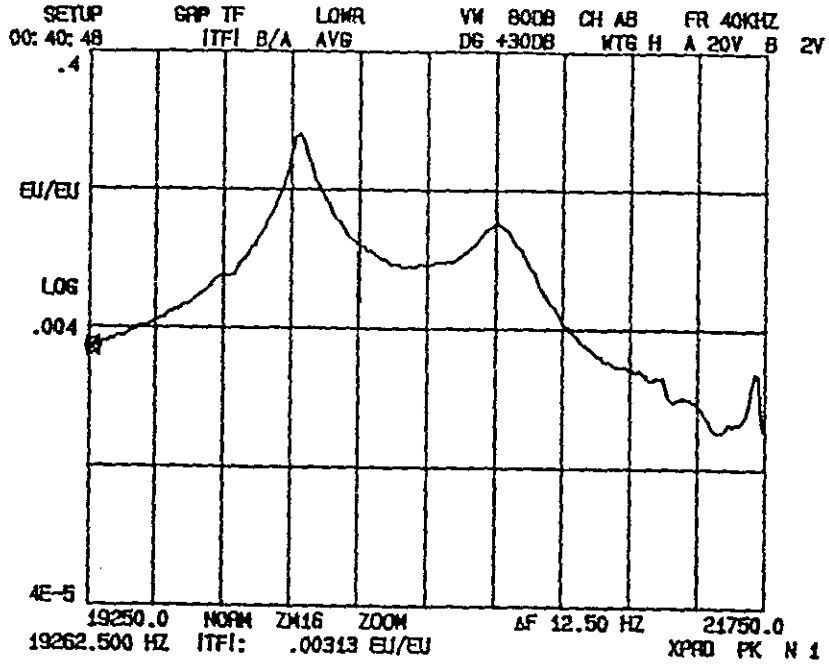

(a) FRF at measurement DOF No 13

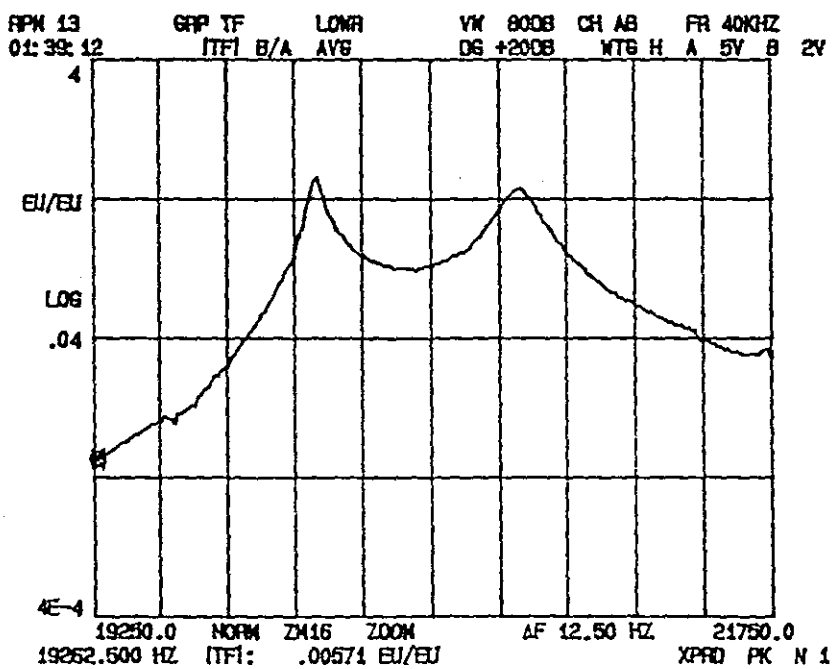

(b) FRF at measurement DOF No 16

Figure 3.26: Unloaded Die

Overlay: Die Loaded with Can

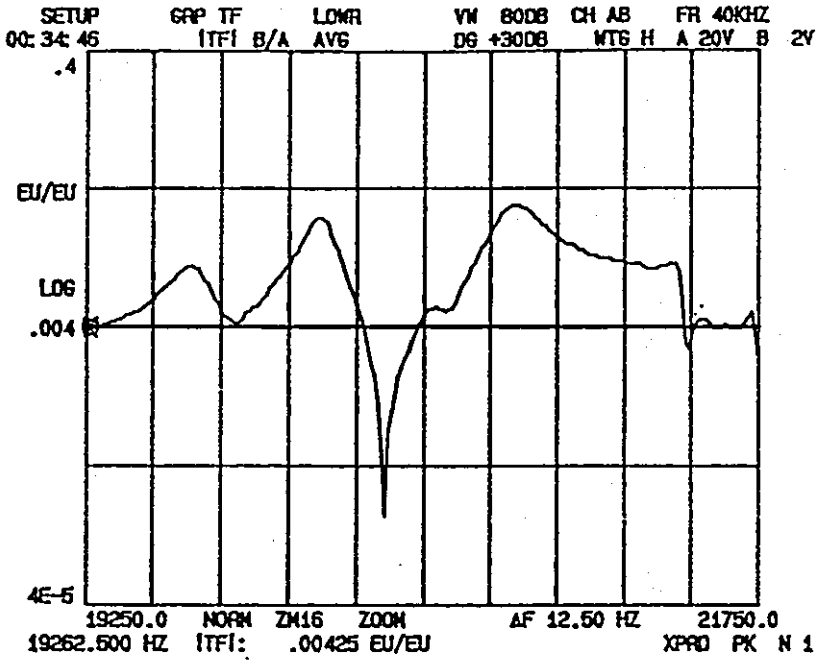
SETUP
00: 34: 46
GRP TF
ITFI B/A
LOWR
AVG
VW 800B
DG +300B
CH AB
MTG H
FR 40KHZ
A 20V B 2V
.4
EU/EU
LOG
.004
4E-5
19250.0
NORM
ZM16
ZOOM
AF 12.50 HZ
21750.0
19262.500 HZ
ITFI: .00425 EU/EU
XPRD PK N 1

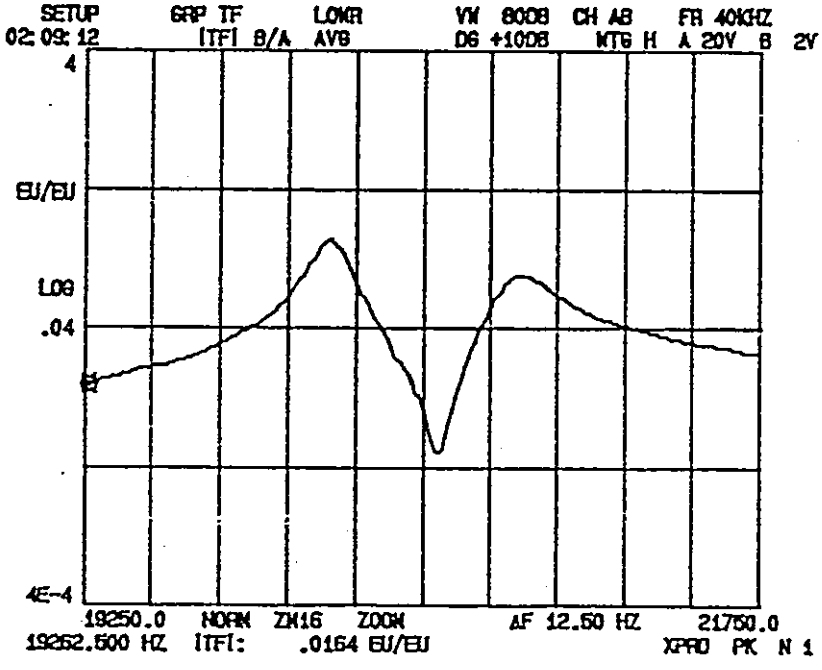
SETUP
02: 09: 12
GRP TF
ITFI B/A
LOWR
AVG
VW 800B
DG +100B
CH AB
MTG H
FR 40KHZ
A 20V B 2V
4
EU/EU
LOG
.04
4E-4
19250.0
NORM
ZM16
ZOOM
AF 12.50 HZ
21750.0
19262.500 HZ
ITFI: .0164 EU/EU
XPRD PK N 1

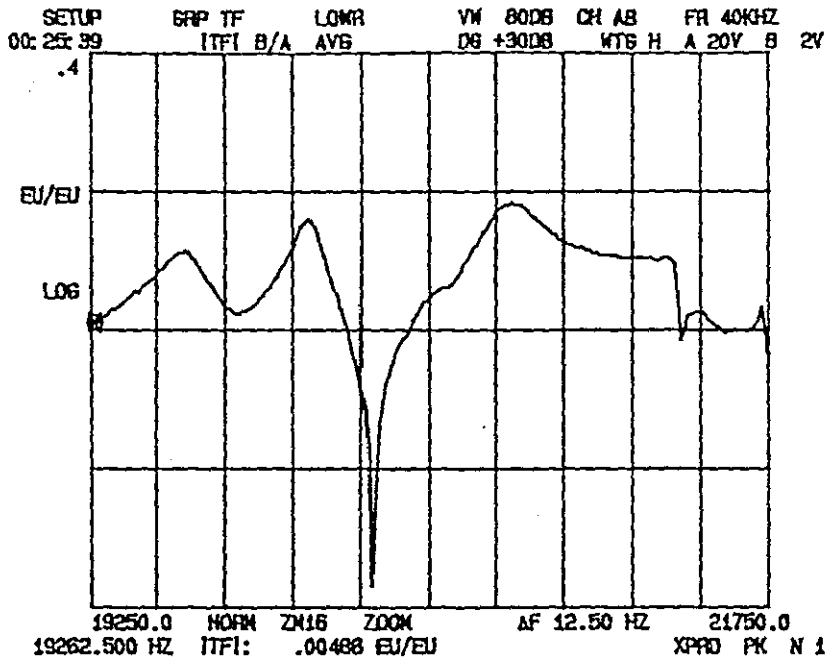

(a) FRF at Axial Measurement DOF No 2

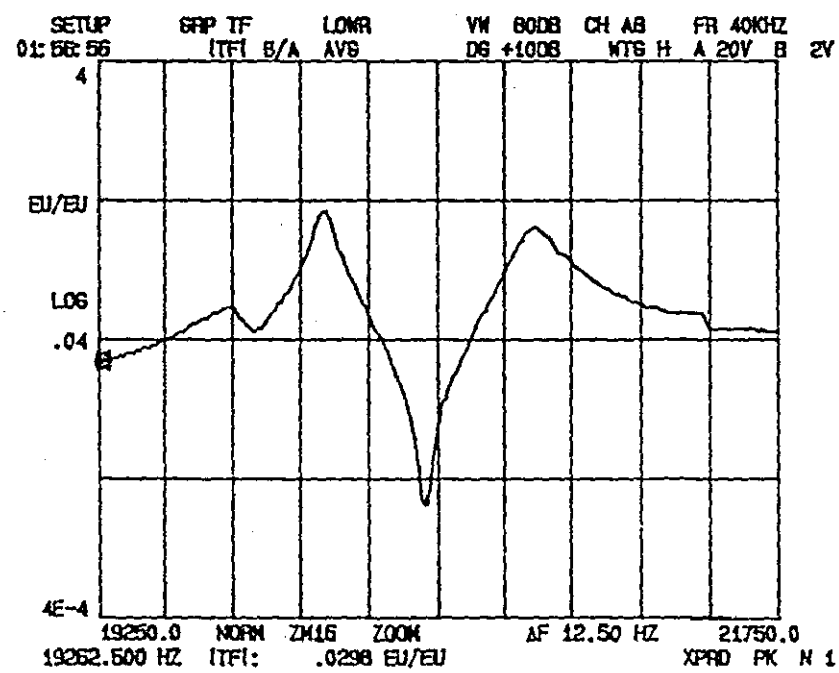

(b) FRF at Axial Measurement DOF No 4

Figure 3.27: Unloaded Die

Overlay: Die Loaded with Can

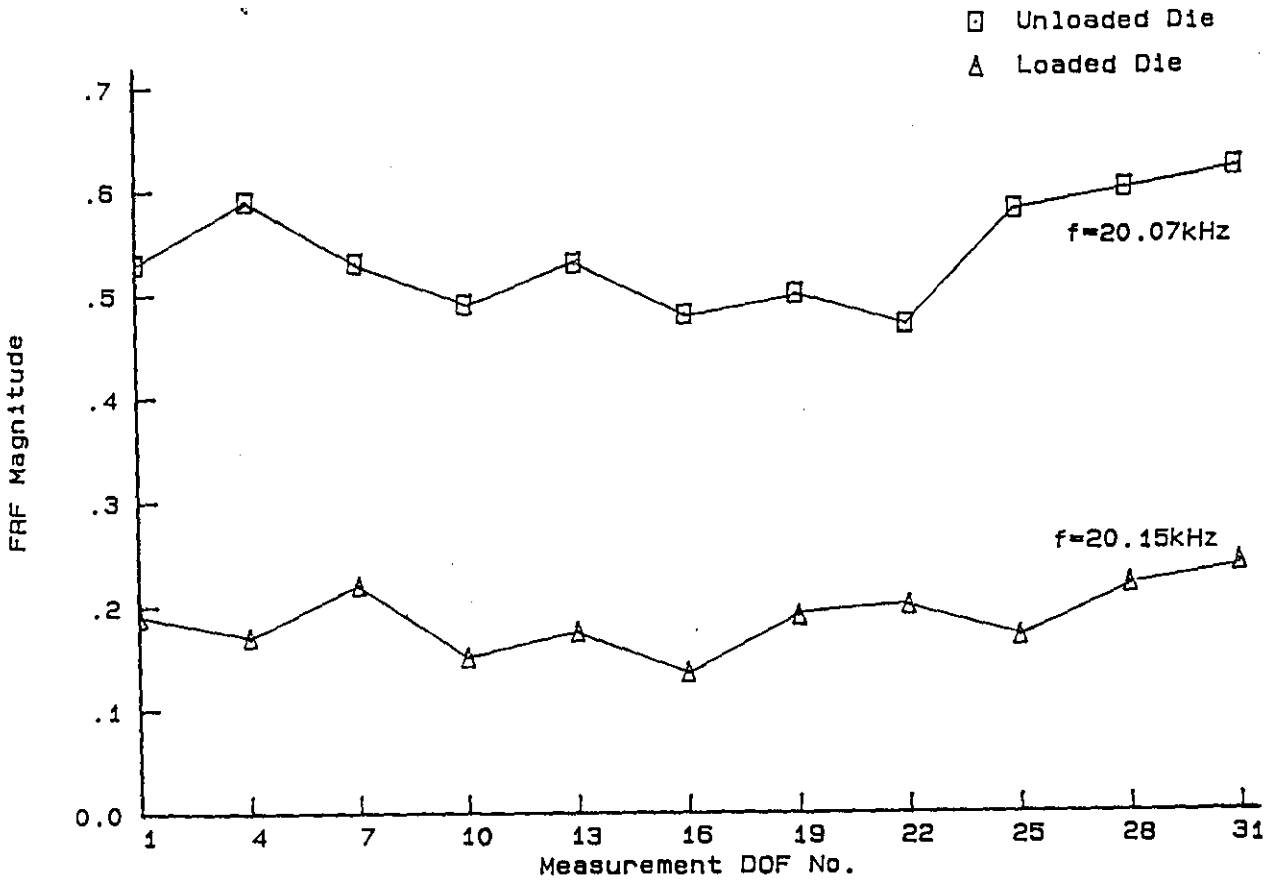

(a) Effect on R0 Mode of Loading Die with Can

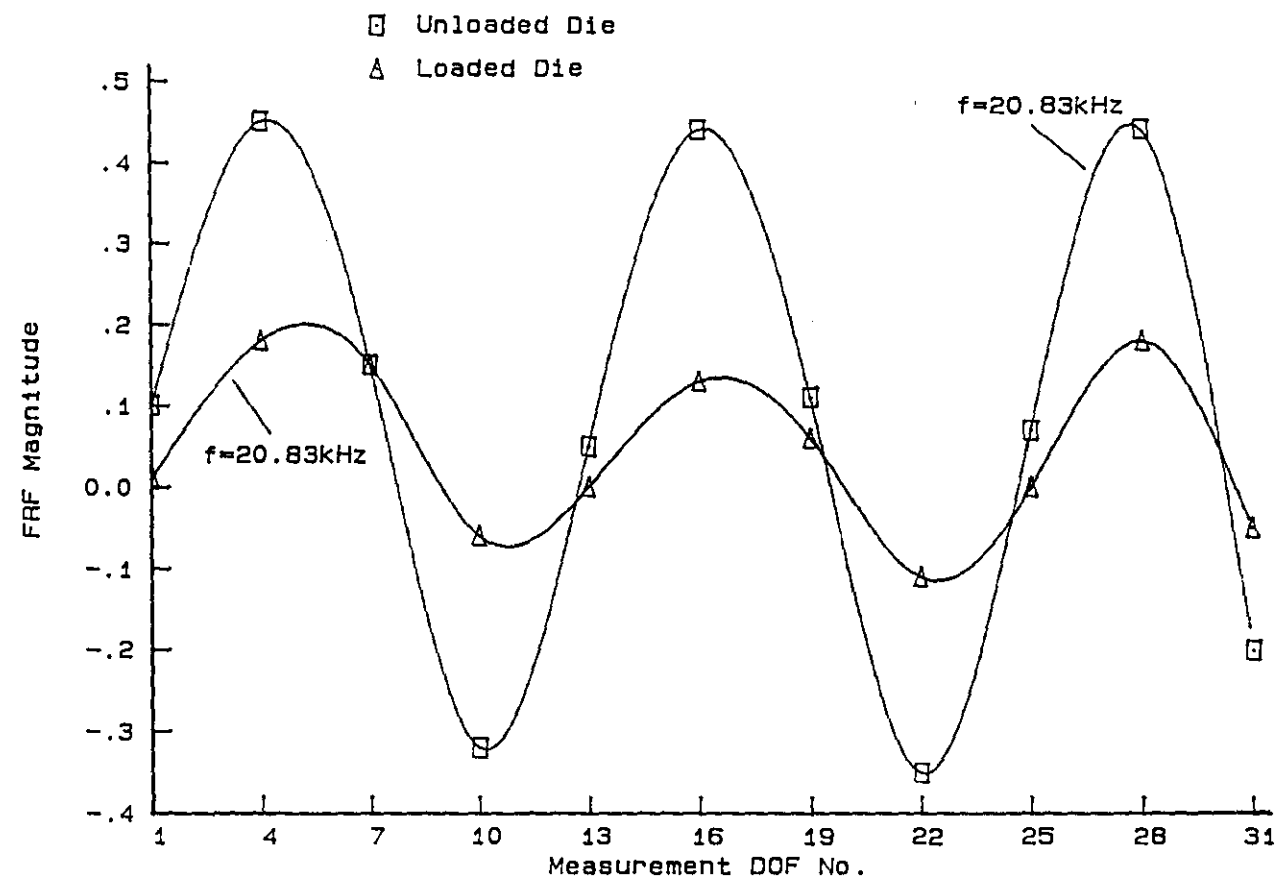

Figure 3.28 (b) Effect on R3 Mode of Loading Die with Can

CHAPTER 4
VIBRATION ANALYSIS AT ULTRASONIC FREQUENCIES

4.1 REQUIREMENTS FOR DIE TESTING

The inherent vibration behaviour of forming dies is to be investigated in order to identify and analyse problems associated with resonance phenomena. A thorough knowledge of die problematic modal behaviour is essential to the development of a redesign strategy.

The requirement of such an investigation is the extraction by measurement of the vibration parameters which constitute a complete dynamic description of the die and which are subsequently sufficient for formulating a mathematical dynamic model. The measured dynamic characteristics of the die enable identification of closely spaced modes and their coupling effects. The mathematical model is required for data reduction purposes and to simulate alterations in die behaviour due to physical modifications (die redesign). Experimental modal analysis (EMA) is a well-known technique for describing, understanding and modelling structural vibration and appears to satisfy the objectives of this study. EMA is described in Chapter 2.

The most generally used modal method is Frequency Response Function (FRF) testing supported by a dual channel FFT analyser. The FRF is a measure of the ratio of the fourier transform of the output (response) and the fourier transform of the input (forcing function). The excitation of the structure is typically measured by a force transducer and the response by an accelerometer. Measured signals are directed to the FFT analyser for data acquisition and signal digitising and postprocessing. Conventional Modal Analysis performs well in determining modal parameters of structures and sub-structural components in the sonic frequency range. Adaptation of this technique to the low ultrasonic band has not previously been reported and poses measurement difficulties due to the excitation system and availability of suitable transducers and instrumentation.

4.2 SWEPT-SINE MODAL TESTING

Signature measurement from the die in the frequency domain is restricted to a swept-sine analysis in this study, due to the single frequency excitation limitation of ultrasonic exciters. Conventional sonic tests commonly use electrodynamic shakers to excite the test structure with the sine sweep controlled by a power oscillator and the forcing function measured at the shaker contact point on the structure.

A sinusoidally varying input force applied to a structure will produce an oscillatory output motion at the same frequency. If these two measured signals are acquired as an FRF then the output amplitude will be multiplied by $|H(\omega)|$ and the phase between input and output will be shifted by $< H(\omega)$. Ideally, the FRF describes the dynamic properties of a system independent of the excitation signal type. In reality the quality of the FRF is affected by the excitation function, mainly due to the digital processing.

Slow sine-sweep is the traditional method of frequency response measurement and involves the oscillation frequency being varied slowly but continuously through the range of interest. The sweep rate is critical; an excessive rate will produce distortions in the FRF due to missed information. There is usually a compromise between length of measurement time and measurement quality, but a simple quality check can be performed by adopting a sweep-up followed by a sweep-down test procedure. It is important to beware of the phenomenon of leakage (or smearing of energy throughout the frequency domain). This is associated with swept-sine testing because the FFT time records are finite, whereas a single line spectrum can only be produced if the sine wave exists from minus infinity to plus infinity. Leakage is reduced but not eliminated by windowing. One significant advantage of swept-sine measurement is the lack of noise contamination in the FRF compared with other excitation functions. Generally the signal to noise ratio is very high for this technique.

4.3 ULTRASONIC MODAL TESTING REQUIREMENTS

The die is excited by a magnetostrictive ultrasonic transducer and horn powered by a Techno-Form Sonics ultrasonic generator (Appendix A). Although the transducer is designed to a working frequency of 20 kHz (i.e. transducer and horn are half wavelength), magnetostrictive transducers can be detuned without significant loss of amplitude at the horn/die interface. The excitation frequency range is limited by the generator capability which allows an analysis band of 13-28 kHz.

The die is held so that the unconstrained (free) vibration behaviour of the die can be measured. This can be achieved in two ways. In both cases the die is suspended at the horn antinode through a threaded mounting stud. Then either the horn can be held at a mounting flange at its nodal circumference or the die tail can be held at its nodal mounting flange. Both configurations minimally restrain the die whilst allowing fixure to the surrounds. The die test rig was devised with these two configurations in mind, so that the die could be mounted in its operational fashion (held at the tail) or in an alternative arrangement that permits unrestrained tail vibration behaviour to be studied (i.e. at the horn node). The test rig and experimental set up for die vibration analysis are discussed further in Chapter 5 (see Figure 5.3).

The measurement system for die analysis required careful consideration since conventional sensors and their associated electronics are almost invariably designed with linear characteristics in the audible range only. The vibration analysis concentrated on using accelerometers to detect motion. To reduce the effects of mass loading, light-weight subminiature accelerometers were selected, with a high mounted resonant frequency and a flat response to beyond 30 kHz. The output signals were conditioned through modified high gain charge amplifiers capable of a linear output characteristic to above 26 kHz. An eddy current ultrasonic displacement probe was also utilised for vibration deformation measurement.

The dual channel FFT analyser, for signal acquisition and display, has a frequency range of 0-40 kHz. Most importantly for this study, it has the capability to perform swept-sine testing within a preset frequency band. Zoom processing is used to obtain higher resolution in the vicinity of resonant response and in the range of interest to the analysis. It is a technique in which the lower and upper frequency limits are selectable over fixed bandwidths. This facility allows densely spaced modes to be more closely inspected by concentrating measurement points over a narrower bandwidth. Another advantage for swept-sine testing is that distortion of the FRF due to leakage is reduced because energy smearing is within a narrower frequency range.

Data collected by the analyser is down-loaded through an IEEE interface to a personal computer for data post-processing and modal parameter extraction. The pc is equipped with SMS STAR structural dynamics analysis software. The primary function of the software is the determination of the eigenvalues and eigenvectors from the measurement data by curve fitting the FRFs. The resulting mathematical representation of the experimental model can subsequently be used to predict the effects on the modal parameters of physical alterations to the measured structure; a technique known as structural dynamics modification (SDM).

To complete the analysis requirements it is necessary to monitor the input force from the ultrasonic exciter to the die. Conventional load cells were found to be unsuitable for this task and therefore alternative force transducers for high frequency measurement were considered. Ultrasonic excitation systems cannot be readily adapted to monitor transmission line forces, as interruption of the system geometry with measurement sensors detunes the system and introduces problems of amplitude transmission to the die. Firstly insertion of a modified piezo-disk between the die and the horn was attempted. This upset the system tuning and the brittle nature of the ceramic presented insurmountable vibration transmission problems. Later attempts to insert a thin piezo-film at the interface also failed because the requirement for a positive

connection between the horn and die conflicted with the degree of flexibility needed in the force sensitive film.

Finally, attention was turned to the possibility of monitoring an electrical signal, representative of the excitation system forcing function. This investigation is described in Section 4.5. Meanwhile it was decided to look into the feasibility of conducting die vibration analysis without measuring the excitation force.

4.4 ACCELERATION INTENSITY METHOD

The method used to investigate the modal behaviour of the die at ultrasonic frequencies is loosely based on a surface intensity technique. By this method the motion of a structure is described by sound pressure level which is measured by two microphones to construct an intensity map of the relative level between pairs of points on the structure's surface. Mapping surface intensity involves determination of the mean square sound pressure and the phase difference of the sound field between the two microphones. Measurements are acquired using a dual channel FFT analyser [67, 68].

A similar description of surface acceleration can be achieved using two accelerometers to determine the relative motion between different points on the die surface. The operational deflection shape of a structure at a particular frequency can be obtained and represents the response of a structure to unknown but real forces. The deflection shape measured at the natural frequencies of the structure are its normal modes. Acceleration level is measured as is the phase difference between each pair of acceleration signals. In this way the die mode shapes (or relative response patterns) within the analysis band can be mapped out over the vibrating surface. One of the two accelerometers is positioned at a reference point, chosen close to the excitation injection point to maximise its response content. The other accelerometer is moved around a grid of measurement positions on the die surface. For each grid point the two response signals are measured by the swept-sine method under steady state conditions and fed to the two channels of the FFT analyser.

A frequency range of 16-26 kHz constituted the zoom analysis band. The natural frequencies and corresponding mode shapes of the die were determined by the following procedure:

First an estimate of the natural frequency values was made from the positions of the response spectral peaks in the acceleration signals. A frequency response function between the roving accelerometer signal and the reference signal is then displayed. At each natural frequency estimate, the magnitude and phase of the FRF is recorded. Since the FRF is effectively the ratio of two acceleration signals, the phase value at any die natural frequency must be either 0° (the reference point and grid point are moving in-phase) or 180° (the reference point and grid point are moving out-of-phase). Therefore the frequencies closest to the original estimates that give a phase value of 0° or 180° are assumed to be the actual die natural frequencies. Finally the FRF magnitude at each natural frequency is plotted over the grid of die surface measurement positions to extract the mode shapes.

4.4.1 Results

The reference acceleration spectrum is shown in Figure 4.1. Five modes of vibration were identified by the acceleration intensity method. These are presented in Table 4.1. The mode classification is explained in Appendix B.

Mode	Frequency (kHz)
R1	16.75
T1	17.50
T4	19.54
RO	20.08
R3	20.81

TABLE 4.1: DIE MODES BY SURFACE ACCELERATION MEASUREMENT

4.4.2 Conclusions

The acceleration intensity technique is a practical method of obtaining vibration information of a structure in the absence of a measure of the excitation force. It is possible to determine die natural frequencies and mode shapes but the technique is limited in its ability to extract modal information. The main drawbacks are:

1. The number of natural frequencies detected is dependent on the number excited at the reference position and the quality and quantity of the information relies on a good choice of reference position. The driving point measurement, which would be the ideal reference point, is unobtainable.

2. Not all the spectral peaks in the reference signal could be classified as recognisable modes. If peaks were consistently sharp or dominant in the spectrum at each grid point then it was possible to map the mode shape successfully. Weak, coupled or damped modes proved impossible to identify.

3. The FRF magnitudes plotted as mode shapes are relative acceleration levels between the pair of measurements for each grid point. No knowledge of absolute amplitudes is obtained.

4. There is no accurate way of estimating the modal damping using this method.

5. It is not possible to postprocess the measured data to obtain a mathematical dynamic model of the die utilising the EMA software algorithms.

For these reasons this technique has limitations regarding this study. However, the results have indicated the presence of modes close to the working mode and have identified some of the mode shapes successfully. It is concluded that

the measurement of acceleration intensity is more appropriate for analysing lightly damped structures with low modal density.

4.5 SIMULATING THE EXCITATION FORCE

4.5.1 Experimental Philosophy

For progress to be made, it was necessary to identify a signal which displayed the characteristics of the forcing function and was representative of the force input to the die. Attention was therefore turned to monitoring electrical input quantities.

It is known that some mechanical variable (depending on the transducer) at the horn of a magnetic-flux type electroacoustic transducer, is continuously in-phase with the voltage supplied by the generator, even under varying acoustic loads [69]. This suggests that the voltage supplied to the transducer coils from the ultrasonic generator may be a representation of the forcing function at the die/horn interface. On this basis an experimental programme was initiated, to validate voltage signal measurement as a force substitute, in terms of a modal analysis survey of the die. This involved comparison of conventional acceleration/force FRF content with the information contained in acceleration/voltage FRF measurements. The validation process takes advantage of certain similarities between magnetostrictive transducers and electrodynamic (moving coil) transducers, which are both subgroups of the same transducer type, i.e. magnetic flux type reversible transducers.

Magnetostrictive transducers produce vibrations as a result of an applied alternating field. If a rod is magnetised and a coil wrapped round it, and the rod is lengthened or shortened by tension or compression, a voltage will be induced in the coil. When the rod returns to its original position, a voltage of opposite polarity is induced. Conversely if an a.c. voltage is applied to the coil, the rod will vibrate at the voltage frequency. The equivalent circuit for a magnetostrictive transducer was derived by Butterworth and Smith [70] and is shown in a simplified version in Figure 4.2. Z_e is the clamped electrical

impedance and Z_T is the motional impedance, representing the mechanical properties of the loaded transducer. The current through the motional arm I_M, is proportional to the oscillatory amplitude at the drive end of the transducer and vibrational resonance occurs when I_M reaches maximum value with respect to frequency.

The electrodynamic (or electromagnetic) shaker also produces vibrations as the result of an applied alternating field. The supplied input signal is converted to an alternating magnetic field in which is placed a coil attached to the exciter table (the drive face), Figure 4.3. The motion is produced by a current passing through the coil in the magnetic field. The moving coil oscillator is designed to display linear behaviour. Magnetostrictive oscillators will maintain linearity (of flux intensity and strain) when used at low power, which is a satisfactory experimental constraint. For both magnetostrictive and electrodynamic exciters, the frequency and amplitude of excitation are controlled independently. Another common feature is that the electrical impedance of these devices varies with amplitude of motion of the moving component. This results in impedance mismatch between the exciter and the excited structure, which will be detected in the force signal at the driving point.

The similarities between these two magnetic-flux type transducers aid comparison of conventional EMA with the ultrasonic version of EMA that represents the forcing function by a voltage signal. Typical force signal features can be identified and explained and subsequently matched to the characteristics of the monitored voltage signal, for validation of the ultrasonic vibration analysis.

The experimental validation programme involves comparison of a conventional sonic swept-sine modal survey by acceleration/force FRF measurement with an ultrasonic swept-sine modal survey by acceleration/voltage FRF measurement. For the former, a simple cantilever beam is the test object. It is excited at its free end by an electrodynamic shaker (Figure 4.4). Vibration is transmitted to the structure unidirectionally by means of a slim stinger of high axial stiffness

but low transverse and rotational stiffnesses (thus permitting directional control of excitation while allowing freedom from constraint in the other five degrees-of-freedom). The force at the drive point is monitored by a load cell attached to the beam via a threaded stud. A roving accelerometer measures the beam vibration response and both signals are acquired by an FFT analyser for FRF analysis.

The ultrasonic test was conducted on a thick cylinder with a magnetostrictive transducer providing the excitation. The experimental apparatus is identical to the acceleration intensity investigation described previously. In this case the voltage supplied to the transducer coils represents the force signal measurement and one accelerometer monitors the cylinder response at grid points. Signal postprocessing is consistent with the sonic analysis.

4.5.2 Sonic Response Characteristics from Beam Analysis

Three sets of results depicting the frequency response of the cantilever beam in various display modes, from three different measurement points, are presented in Figures 4.5-4.7. The common features of a frequency response function can be determined in these results by direct observation of each measurement. This is achieved by considering the following five items:

i) Driving point measurement
ii) Cross-point measurement
iii) Single degree-of-freedom behaviour
iv) Effects of modal coupling
v) Exciter characteristics (impedance mismatch)

i) Driving point measurement (Figure 4.5):

A driving point FRF is a measurement of force and acceleration response at the same physical location, which is the excitation injection point. As the acceleration response of the structure is in the direction of forcing at this point, the modes of vibration will all be in-phase with each other. The peak

responses in the imaginary part of the FRF all have positive amplitude if the force and acceleration are measured in the same direction, or all have negative amplitude if excitation is in the opposite direction to acceleration measurement. The real part of the FRF passes through zero in the same sense at each natural frequency. The Nyquist circles therefore all lie along the imaginary axis within the same two quadrants in the Argand plane. In log magnitude format, distinct antiresonances occur between every natural frequency. When adjacent modes are in-phase with each other at a measurement point, the mass and stiffness lines of the two modes intersect and ideally the individual single degree-of-freedom systems sum to zero. In reality this results in near zero magnitude at an antiresonance. The phase information is also indicative of driving point response. The phase angle of the FRF leads through resonance and lags through antiresonance.

ii) Cross-point measurements (Figures 4.6,4.7):

A cross-point FRF is a measurement of force at the excitation point and acceleration at any chosen position on the structure other than the driving point. These FRFs display modes that are in-phase or out-of-phase with the driving point measurement depending on the position of the accelerometer in relation to the individual mode shapes. In log magnitude format, if two adjacent modes are out-of-phase with each other, the intersecting mass and stiffness lines will not cancel. Instead of a sharp antiresonance, a smooth curve joins the modal peaks.

iii) Single degree-of-freedom (SDOF) behaviour:

The FRFs from beam swept-sine tests, approximate to SDOF behaviour in the vicinity of each resonance. If a resonance is due primarily to a single mode, the effects of off-resonance modes being minimal, then the FRF resonance characteristics are:

a) Magnitude of the frequency response is a maximum
b) Imaginary part of the FRF peaks
c) Real part of the FRF is zero
d) Response lags input by 90°

e) Nyquist circle is distinct and lies along the imaginary axis, passing through the origin in the complex plane.

iv) Effects of modal coupling:

Although the beam FRFs display SDOF behaviour near many of its modes, it is clear that for some modes SDOF approximation is not adequate. At these natural frequencies the phase shift through resonance is not 180°, the real part is nonzero and the Nyquist circle is not centred on the imaginary axis.

For lightly damped structures, the normal modes are easily excited and proportional damping can be assumed, even though modes of vibration are generally complex. This is because the non-proportional coupling effects are usually negligible. A problem arises when modes are closely spaced. Such modes appear complex but in fact can be regarded as normal modes. The non-SDOF characteristics are generally due to the effects of modal coupling between adjacent modes, where off-resonance mode behaviour participates in the response around the natural frequency. Modal coupling can be observed by its distortion of the Nyquist circles in the complex plane. The difference between complex behaviour and coupling of closely spaced modes is illustrated in Figure 4.8 [71].

v) Exciter characteristics:

The phenomenon of impedance mismatch in swept-sine testing was mentioned in Section 4.5.1 and is a factor influencing FRFs where excitation is provided by magnetic-flux type transducers. Its presence can be detected in the force spectrum which is measured at the driving point on the beam. The force and acceleration spectra from a beam test are presented in Figure 4.9. Impedance mismatch exists between the beam and the shaker and is due to the electrical impedance of the exciter coil varying with amplitude of motion. At a resonance, the apparent mass of the beam is small and therefore very little force is required to produce a large response. If we assume that at resonance the beam behaves like a SDOF oscillator, then the measured force by the load cell

is the difference between the force generated by the exciter and the true applied force given by:

$$F_T = F_E - F_A \qquad \text{(Figure 4.10)}$$

where F_T is the force vector measured from moving exciter table and stinger

F_E is the force vector generated by the exciter

F_A is the force vector applied to the beam.

Since F_A is small, a small dip in the force spectrum is measured by the load cell in the vicinity of resonance. The drop in force level in the test spectrum at resonance is clear from Figure 4.9. The force dips in this case are not severe enough to risk susceptibility to noise contamination but demonstrate a recognisable feature of force signal measurement using magnetic-flux type transducers.

4.5.3 Ultrasonic Response from Die Analysis

In the ultrasonic tests the FRF is a measure of the acceleration response and input voltage, such that an "effective inertance" $\ddot{X}/V$ substitutes for the conventional $\ddot{X}/F$ function. The viability of using the voltage supplied to the magnetostrictive exciter as a driving point force representation can be judged by comparing the characteristics of the ultrasonic measurements with the sonic counterparts considered in 4.5.2 i) to v).

i) Driving point measurement (Figure 4.11):

A driving point measurement is obtained by attaching an accelerometer on the die flat, which provides the horn/die interface. The horn operates in a longitudinal mode so that excitation amplitude is nearly uniform over the horn end face. Excitation is therefore not a point source, which has two advantages:

a) All modes of interest to this investigation can be excited. The problem of forcing at a modal node does not arise.

b) The area of the die flat where the exciter is mounted will move in-phase with the forcing function. An accelerometer mounted on the flat will measure the in-phase motion even though it is not positioned at the true injection point.

Inspection of the driving point measurement (Figure 4.11) reveals FRF behaviour that distinguishes the force referenced FRF from the voltage referenced FRF. The FRF log magnitude illustrates the expected antiresonance trough between consecutive natural frequencies that indicates in-phase motion of the modes. The phase information however is not consistent with point inertance measurement. There is a phase shift of 180° through resonance but the phase angle is 0° at the natural frequency rather than 90°. The phase change is from +90° to -90° through resonance rather than 180° to 0°. This 90° phase difference between force and voltage results in FRF characteristics that are consistent with point mobility measurements, where input force and velocity response are monitored at the excitation position (i.e. $\dot{X}/F$). The point mobility FRF similarity is also observed in the alternative displays of the point measurement. The phase difference between mobility and inertance results in peak amplitudes in the real part of the FRF and zero valued imaginary part at resonance and this is seen in the measurements. The real part peaks all have negative values, which supports the mobility analogy. The Nyquist circles all lie along the real axis within the same two quadrants in the Argand plane.

ii) Cross-point measurements (Figures 4.12, 4.13):

Comparison of Figures 4.11 and 4.12 illustrates the expected differences in driving point and cross-point measurement FRFs. From the cross-point measurements, typical mobility characteristics are observed. The FRFs display modes that can be in-phase or out-of-phase with each other. The log magnitude shows mass and stiffness line cancelation (antiresonance) between adjacent modes that are in-phase and smooth curves between out- of-phase adjacent modes.

iii) SDOF behaviour:

The SDOF assumption presupposes the following conditions at resonance for mobility measurements:

a) Magnitude of the frequency response is a maximum
b) Real part of the FRF peaks with a positive or negative value
c) Imaginary part of the FRF is zero
d) Response is in-phase with the input
e) Nyquist circle is distinct and lies along the real axis, passing through the origin.

These five conditions are in the main, confirmed by inspection of the acceleration/voltage FRF measurements from the die.

iv) Effects of modal coupling:

As with the beam measurements, the die FRFs appear to exhibit mainly SDOF behaviour with some rotation of the Nyquist circle due to modal complexity. Essentially the response consists of the normal modes but with modal coupling detected. Coupling of closely spaced modes is more pronounced in the die analysis and the distortion of the Nyquist circles is particularly clear in Figure 4.13. The effects of modal coupling are observed as two loops between modal responses in the complex plane, which further confirms the mobility-type features of the ultrasonic measurements.

v) Exciter characteristics (Figure 4.14):

The frequency spectrum of the supply voltage typifies a force spectrum from a swept-sine test using a magnetic-flux type transducer. As with the force signal measured at the driving point on the beam, the voltage signal dips in the vicinity of resonance; a result of impedance mismatch between the die and the magnetostrictive exciter. This is given more clarity by displaying the signals on a linear scale (Figure 4.14(b)). This evidence reinforces the belief that the voltage signal is a viable representation of the forcing function at the die/horn

interface and could be successfully adopted as a force reference substitute in ultrasonic modal analysis.

4.5.4 Conclusions

After attempting first to measure the force applied to the die and then to measure several electrical signals without success, a monitoring signal satisfying the requirements of modal testing was found. The voltage supplied to the coils of the magnetostrictive exciter was strong enough to provide meaningful, relatively noise free measurements after transforming down to meet the loading restrictions of the FFT analyser. The effectiveness of the voltage reference in FRF testing was carefully assessed by comparison with well-known, conventional sonic modal test results. The findings showed that an acceleration/voltage FRF in the ultrasonic analysis was consistently 90° out-of-phase with an acceleration/force FRF and was in essence, a mobility measurement. However, since acceleration is being measured and not velocity, the FRF magnitude will be a factor of ω greater than a real measurement of die mobility. At high frequencies this factor is important in the identification of weak modes of vibration, which tend to be lost in the noise floor of velocity and displacement measurements.

The monitoring of the voltage signal allows measurement of uncalibrated driving point and cross-point mobility-type FRFs such that signal postprocessing for modal parameter extraction can be achieved. This experimental approach, to conduct EMA at ultrasonic frequencies, is deemed to be successful and suitable for simulating the excitation force.

4.6 MEASURING THE DIE RESPONSE

To complete the pursuit of an ultrasonic modal analysis procedure, the type of response measurement is considered. The die vibratory motion can be measured as a surface deformation or a surface acceleration. An adapted proximity probe is employed in the former and an accelerometer in the latter. As the displacement probe is an inductive device, it is non-contacting, which

offers the immediate advantage of avoiding mass loading of the die. Accelerometers, on the other hand, are contact transducers but mass loading effects are minimised by choosing subminiature piezoelectric devices. Attachment of the accelerometer to the die surface for each measurement location required considerable care to ensure that a strong bond was achieved, capable of withstanding the large surface accelerations associated with high frequency vibration. The drawback of the laborious acceleration measurement (due to the repeated bonding and cleaning of the accelerometer) must be balanced against the advantage provided by the geometric size of the accelerometer, which permits measurement locations unobtainable using the proximity probe.

The deciding factor in choosing displacement or acceleration measurement is the quality and quantity of information obtainable from the response data. Figure 4.15(a) and (b) present cross-point FRFs measured at the same position on the die by means of the displacement and acceleration transducers respectively.

As a consequence of the low amplitudes associated with high frequency modes measured at low ultrasonic power levels, only detection of the two most dominant natural frequencies was achieved by displacement measurement. Weak modal activity was lost in the noise floor and the signal to noise ratio was generally poor. The effects of noise contamination resulting in poor signal quality, can be seen in Figure 4.15(a) as disturbance of the smooth FRF curve at either end of the zoom range.

In the acceleration response FRF five modes are detected. At ultrasonic frequencies the ω^2 multiplying factor from measuring acceleration rather than displacement is significant in that weak modes can induce enough surface acceleration to be detected in the FRF measurement. This avoids the necessity of several excitation injection sites in identifying all modes of vibration. The mass loading effect of accelerometers appears to be negligible

since the natural frequencies of the two dominant modes agree for both displacement and acceleration measurement.

It is concluded that despite the temporal advantages of displacement monitoring, modal analysis of the ultrasonic forming die is best accomplished by FRF data acquisition of voltage and acceleration signals.

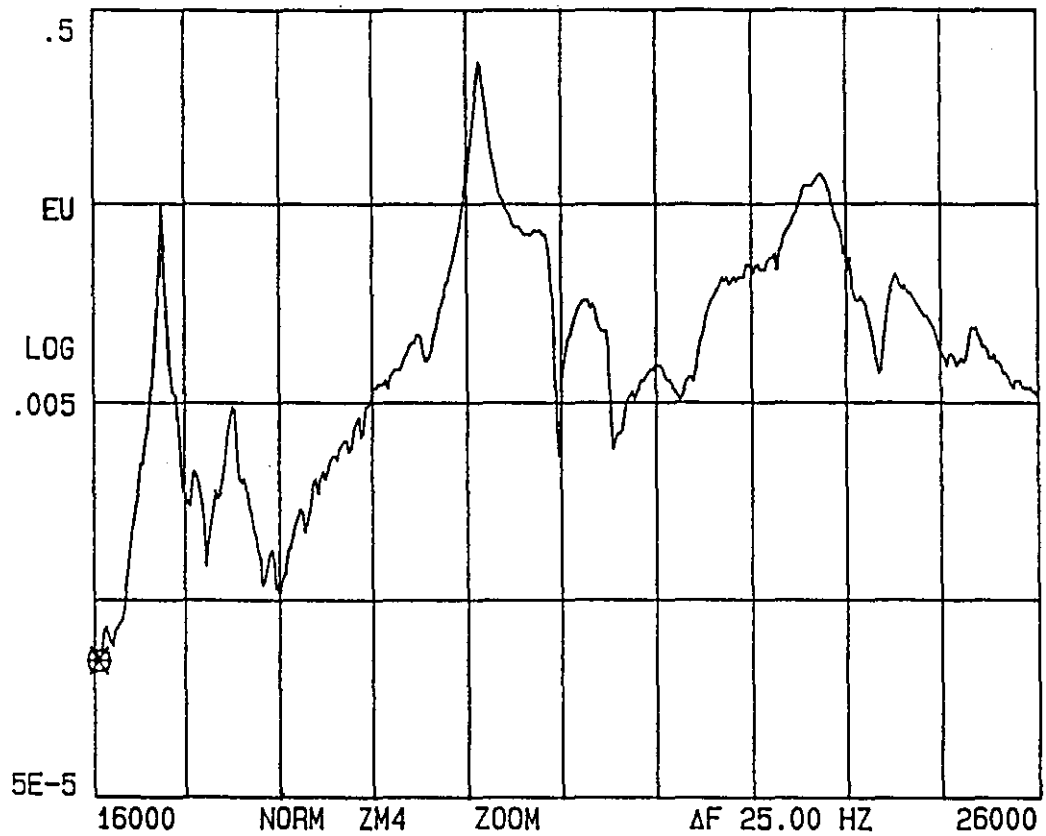

FIGURE 4.1 REFERENCE ACCELERATION SPECTRUM

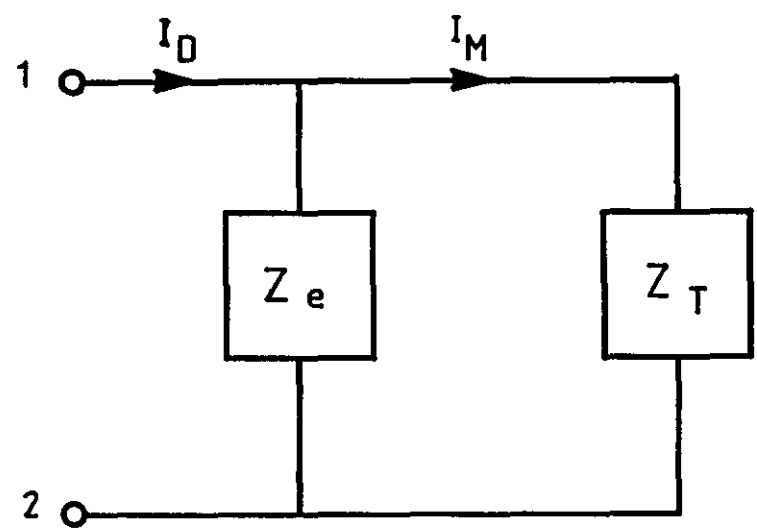

Figure 4.2 SIMPLIFIED EQUIVALENT CIRCUIT FOR MAGNETOSTRICTIVE TRANSDUCER

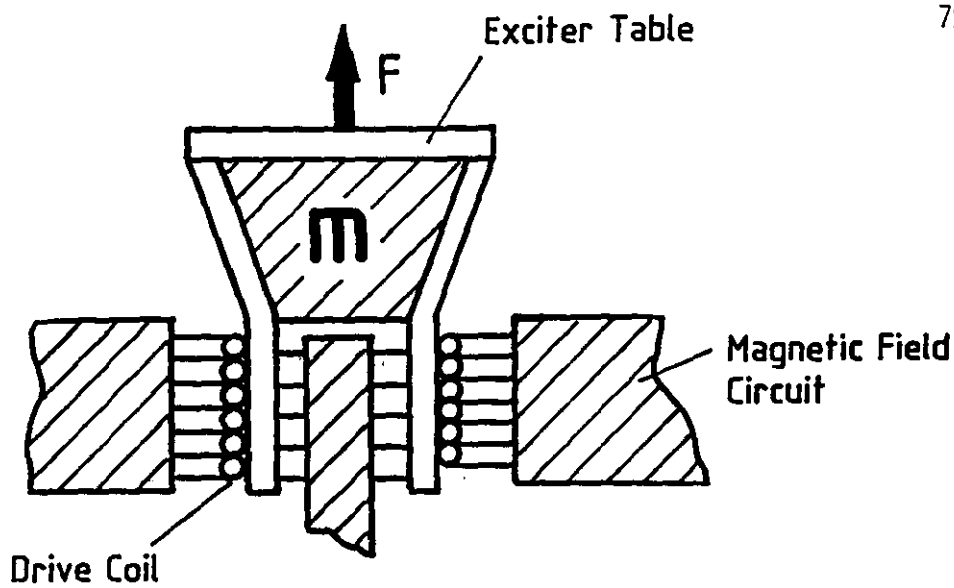

$F = BIL$ F = force
B = magnetic flux density
L = coil length

$F = ma$ m = exciter mass
a = exciter table acceleration

Figure 4.3 ELECTRODYNAMIC SHAKER

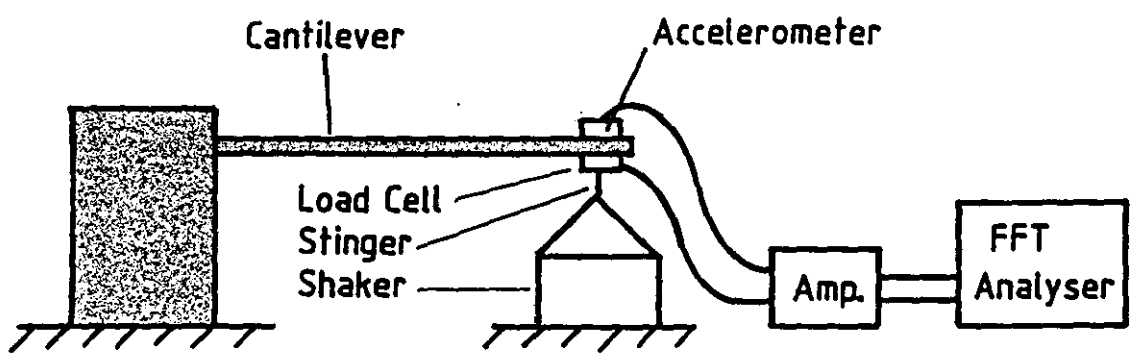

Figure 4.4 CONVENTIONAL SONIC MODAL TEST

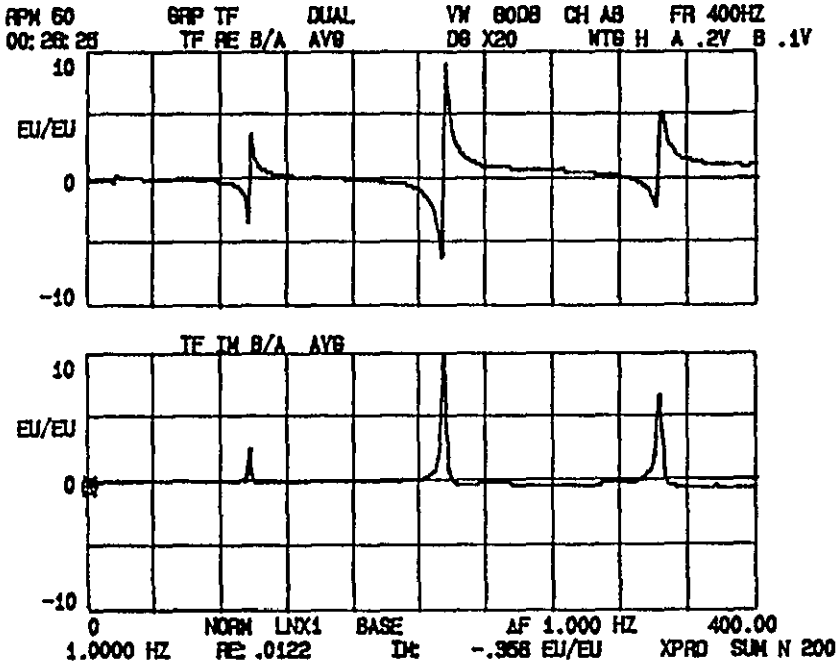

a) Real and Imaginary Parts

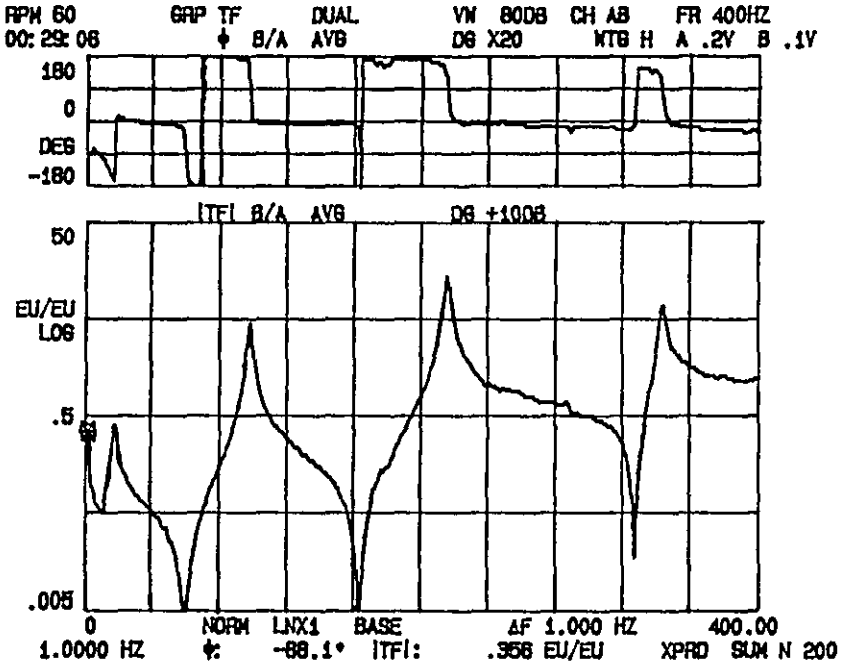

b) Magnitude and Phase

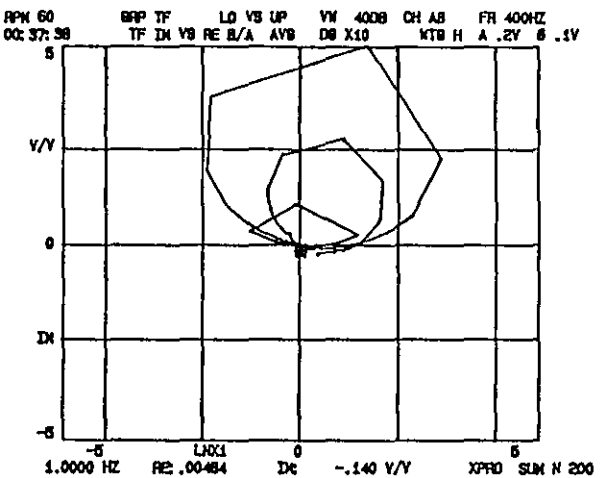

c) Nyquist Circles

FIGURE 4.5 DRIVING POINT FRF FROM BEAM MEASUREMENT

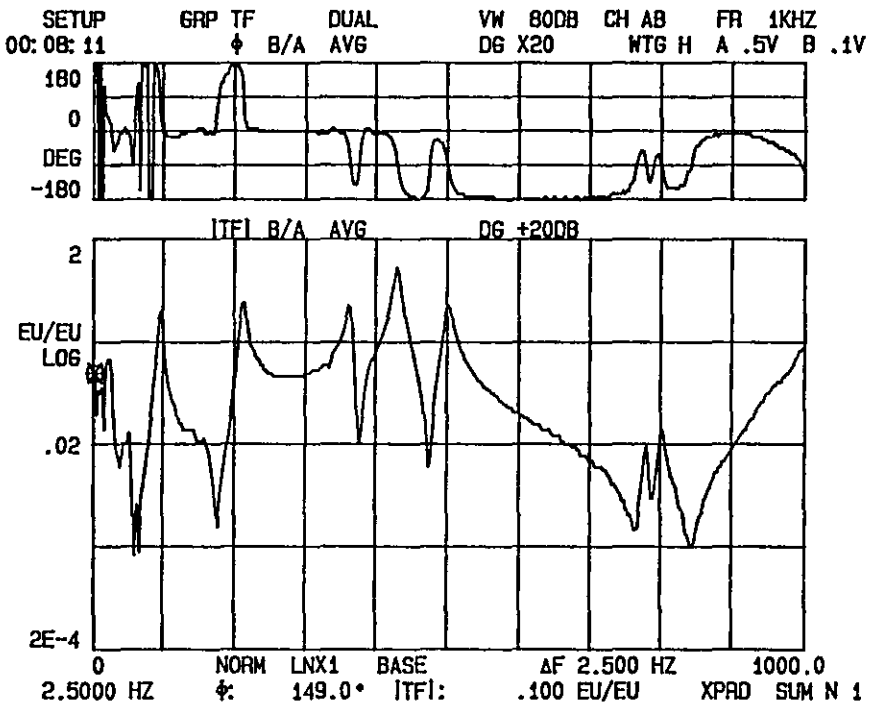

a) Magnitude and Phase

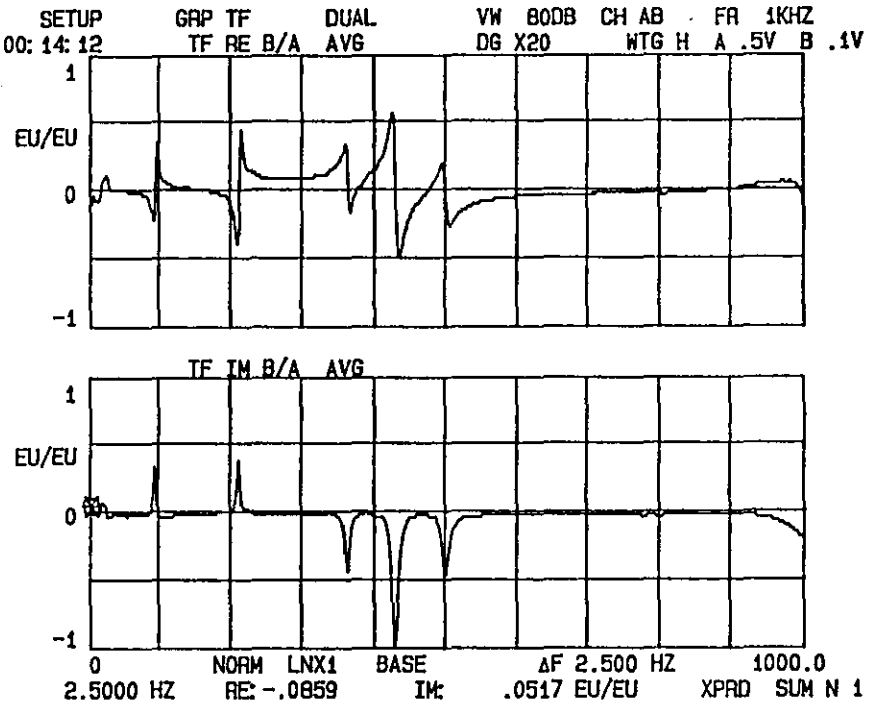

b) Real and Imaginary Parts

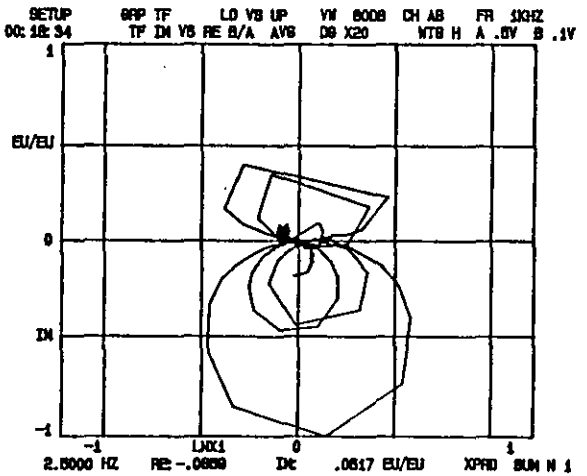

c) Nyquist Circles

FIGURE 4.6 CROSS-POINT FRF FROM BEAM MEASUREMENT

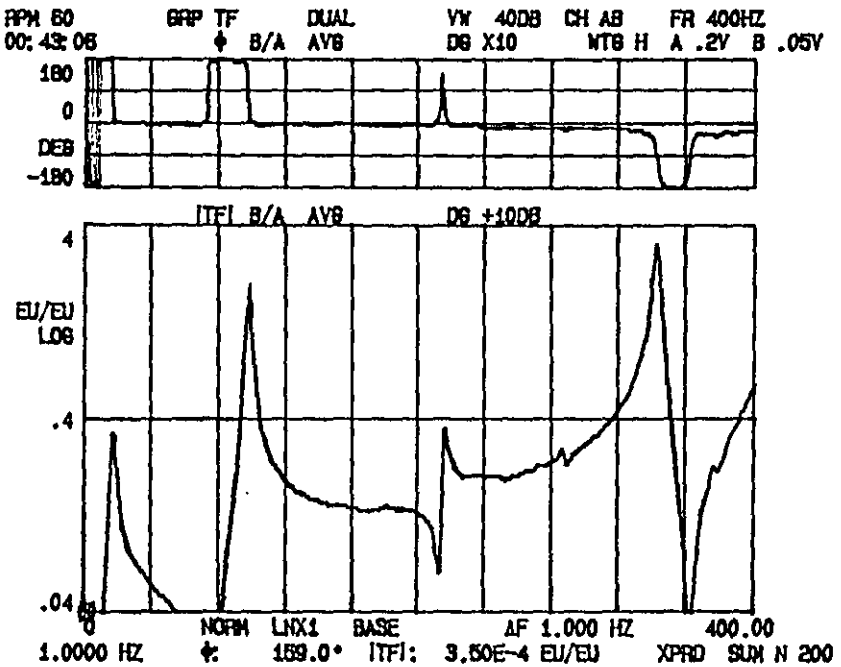

a) Magnitude and Phase

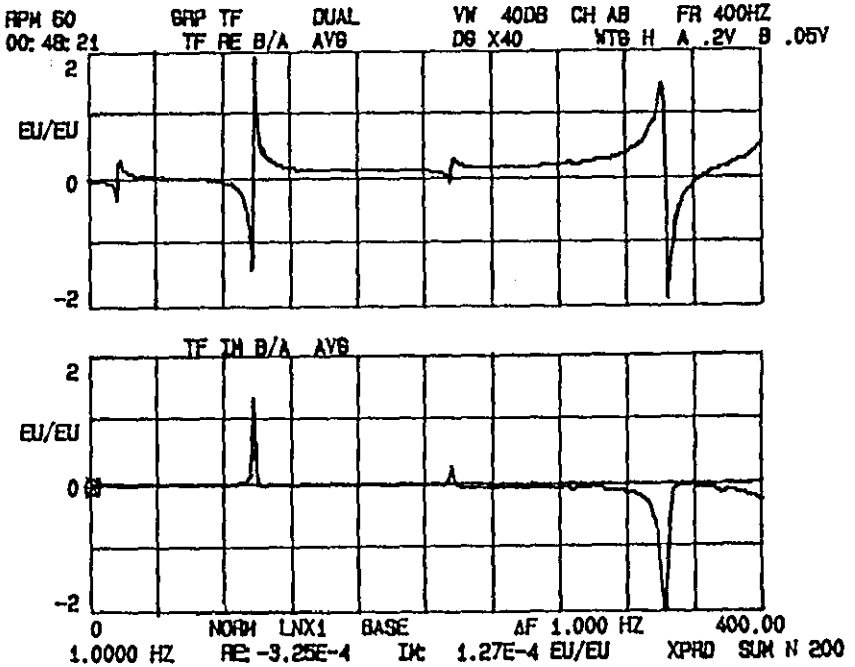

b) Real and Imaginary Parts

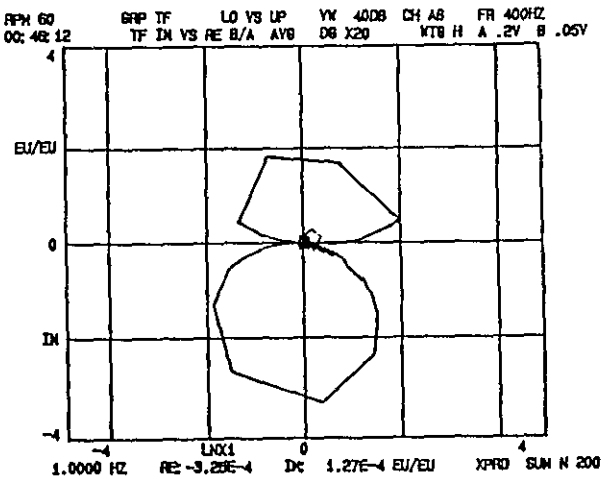

c) Nyquist Circles

FIGURE 4.7 CROSS-POINT FRF FROM BEAM MEASUREMENT

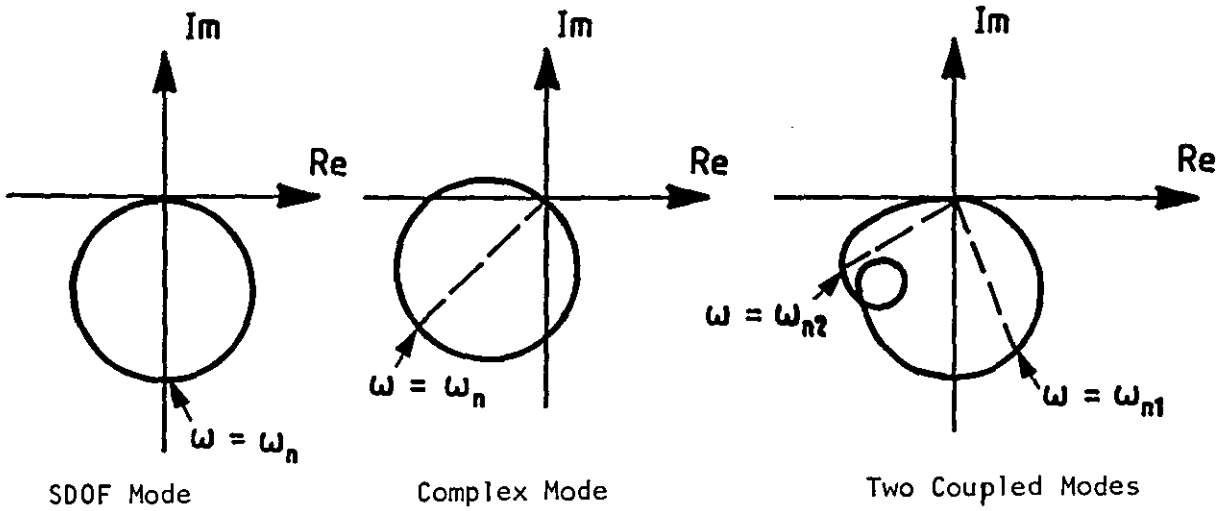

Figure 4.8 INERTANCE MEASUREMENT

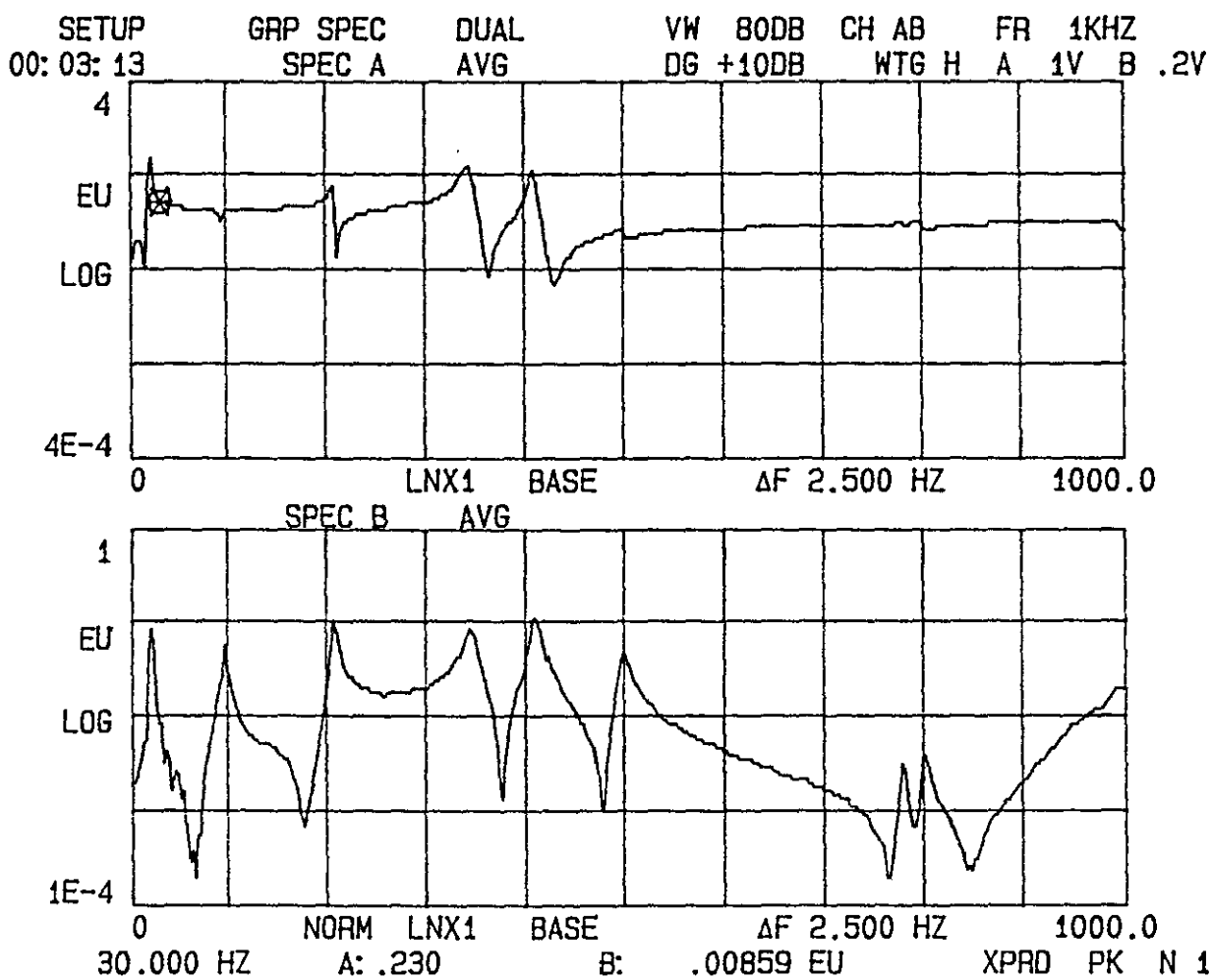

FIGURE 4.9 FORCE SPECTRUM (TOP) AND ACCELERATION SPECTRUM FROM BEAM MEASUREMENT

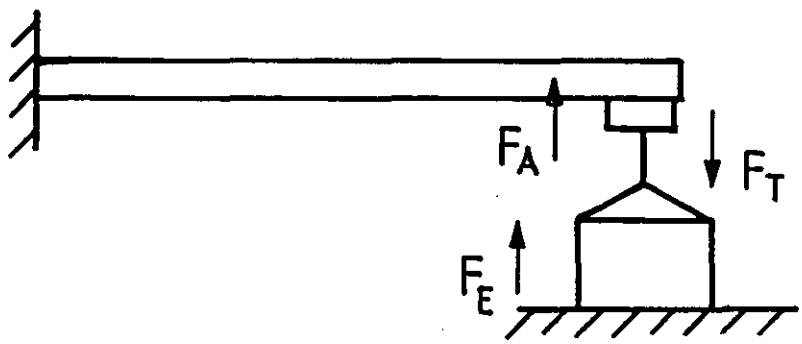

Figure 4.10 FORCES GENERATED AND TRANSMITTED BY SHAKER

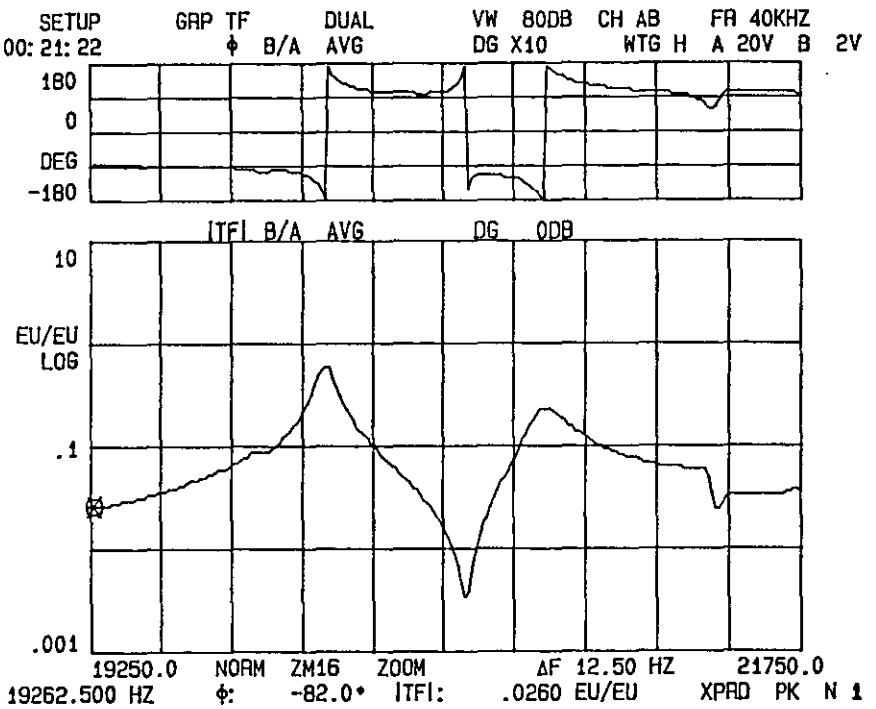

a) Magnitude and Phase

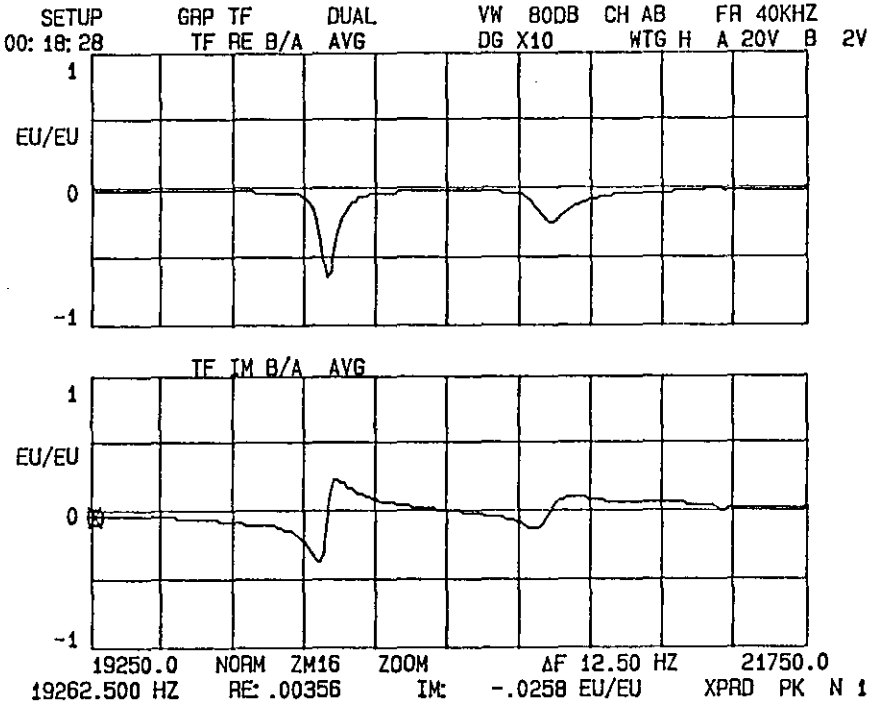

b) Real and Imaginary Parts

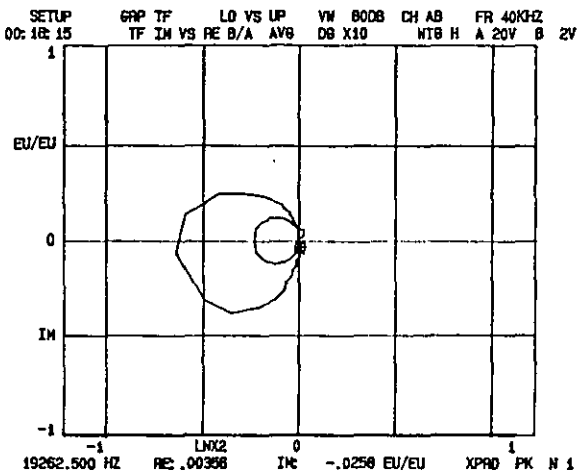

c) Nyquist Circles

FIGURE 4.11 DRIVING POINT FRF FROM DIF MEASUREMENT

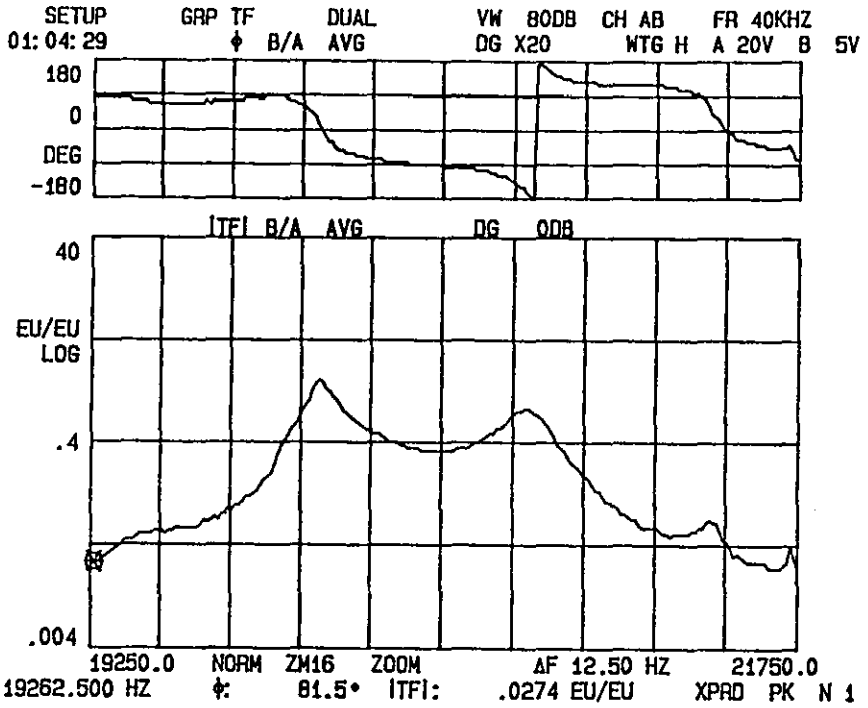

a) Magnitude and Phase

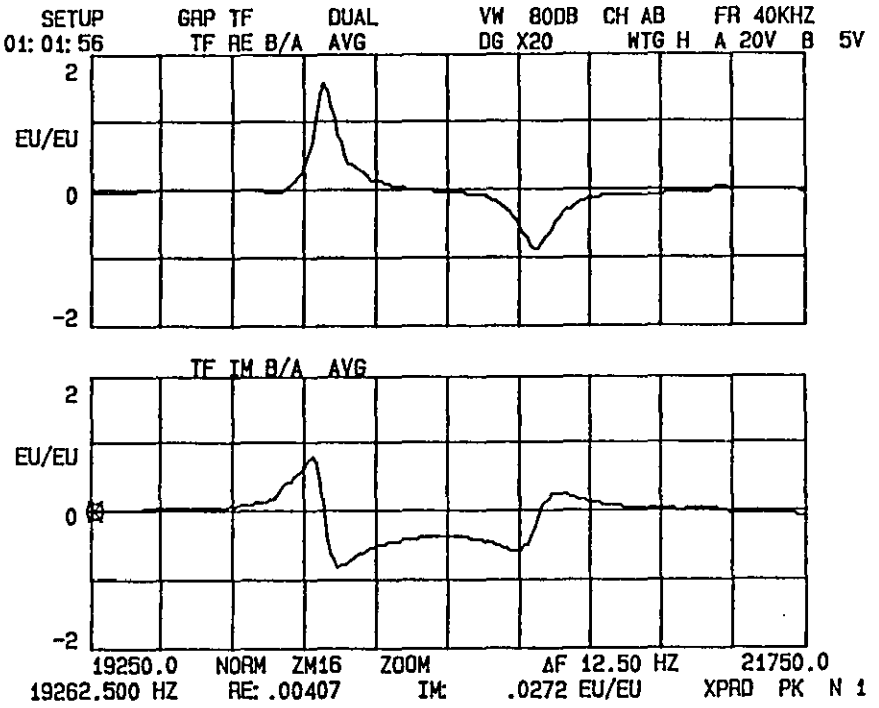

b) Real and Imaginary Parts

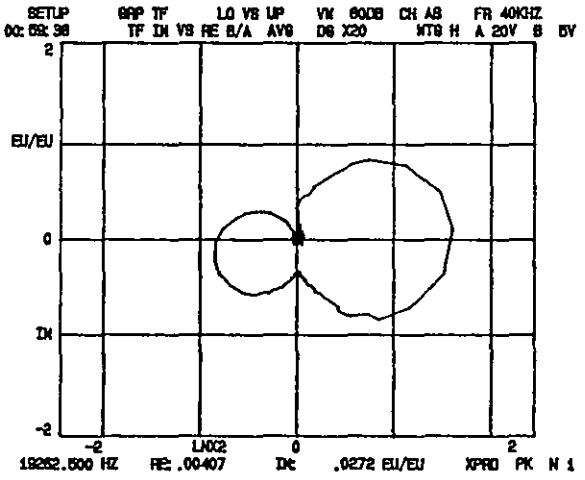

c) Nyquist Circles

FIGURE 4.12 CROSS-POINT FRF FROM DIF MEASUREMENT

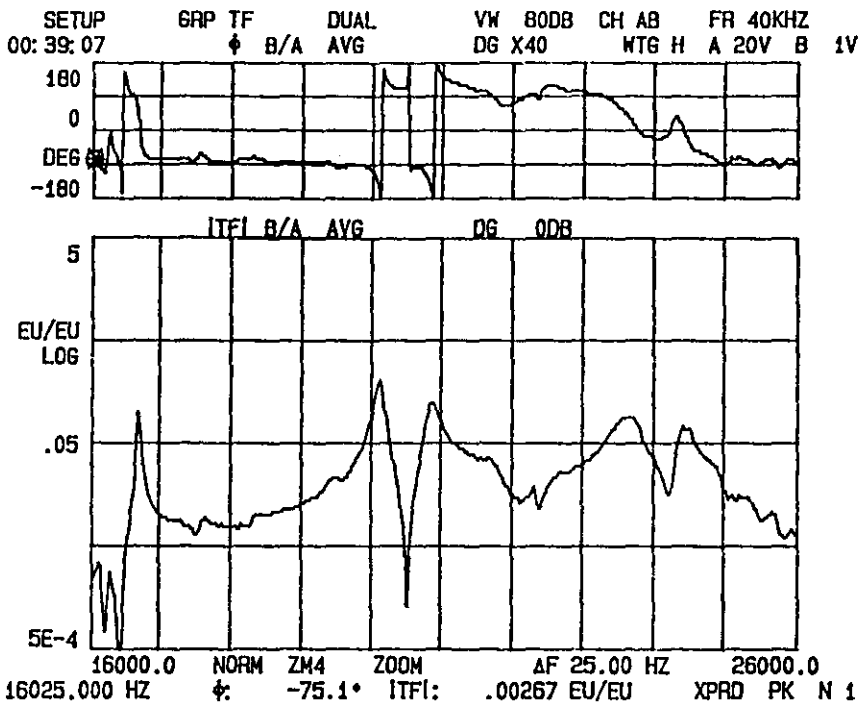

a) Magnitude and Phase

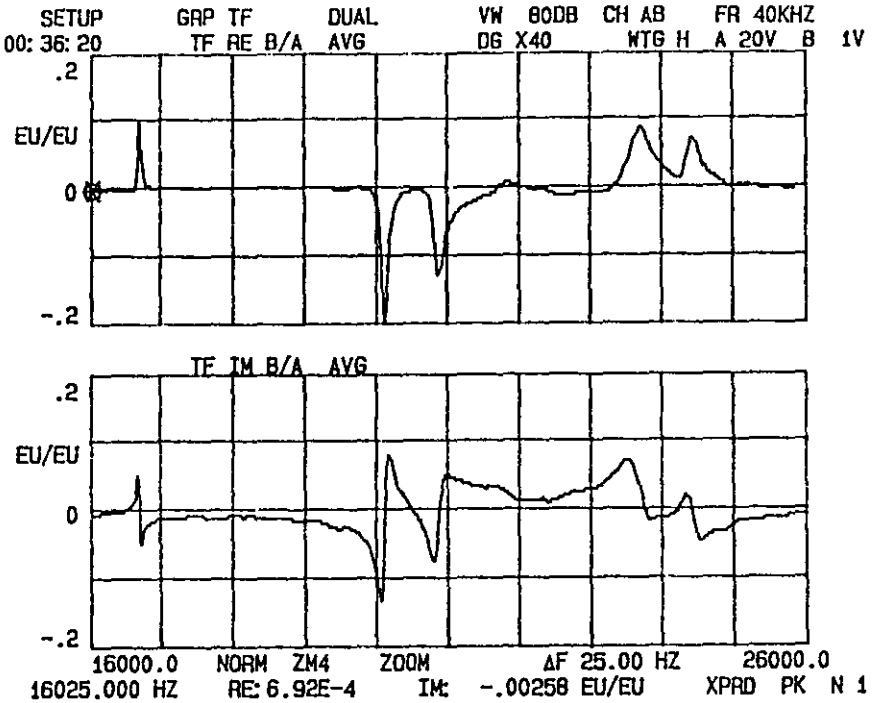

b) Real and Imaginary Parts

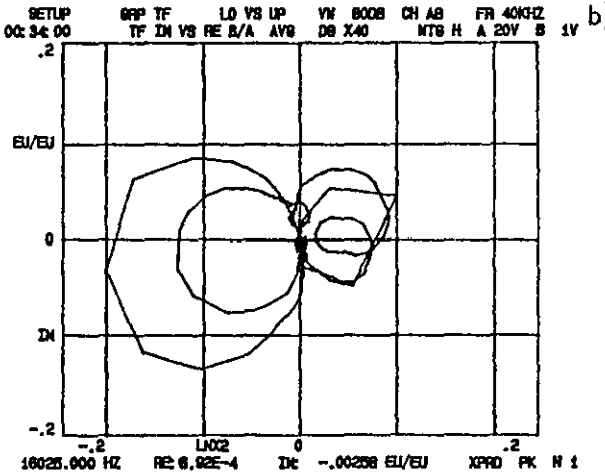

c) Nyquist Circles

FIGURE 4.13 CROSS-POINT FRF FROM DIE MEASUREMENT DISPLAYING MODAL COUPLING

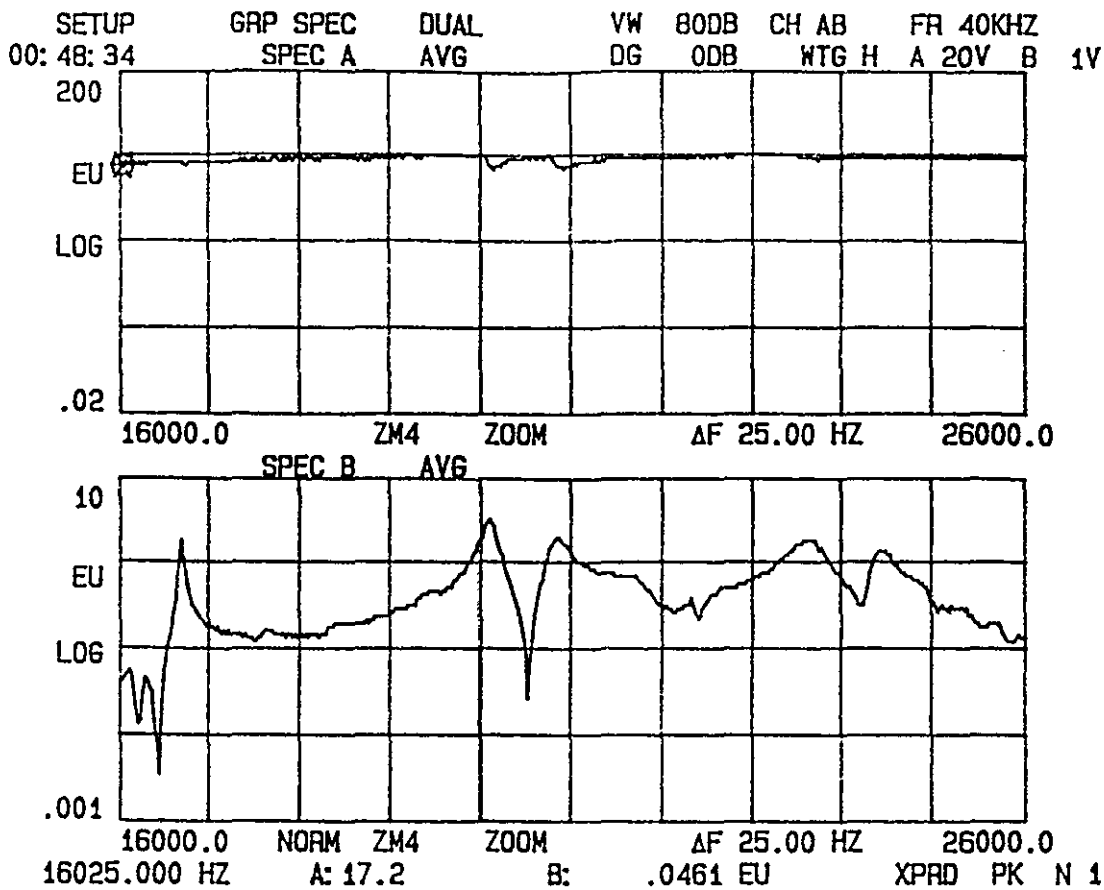

a) Logarithmic Display

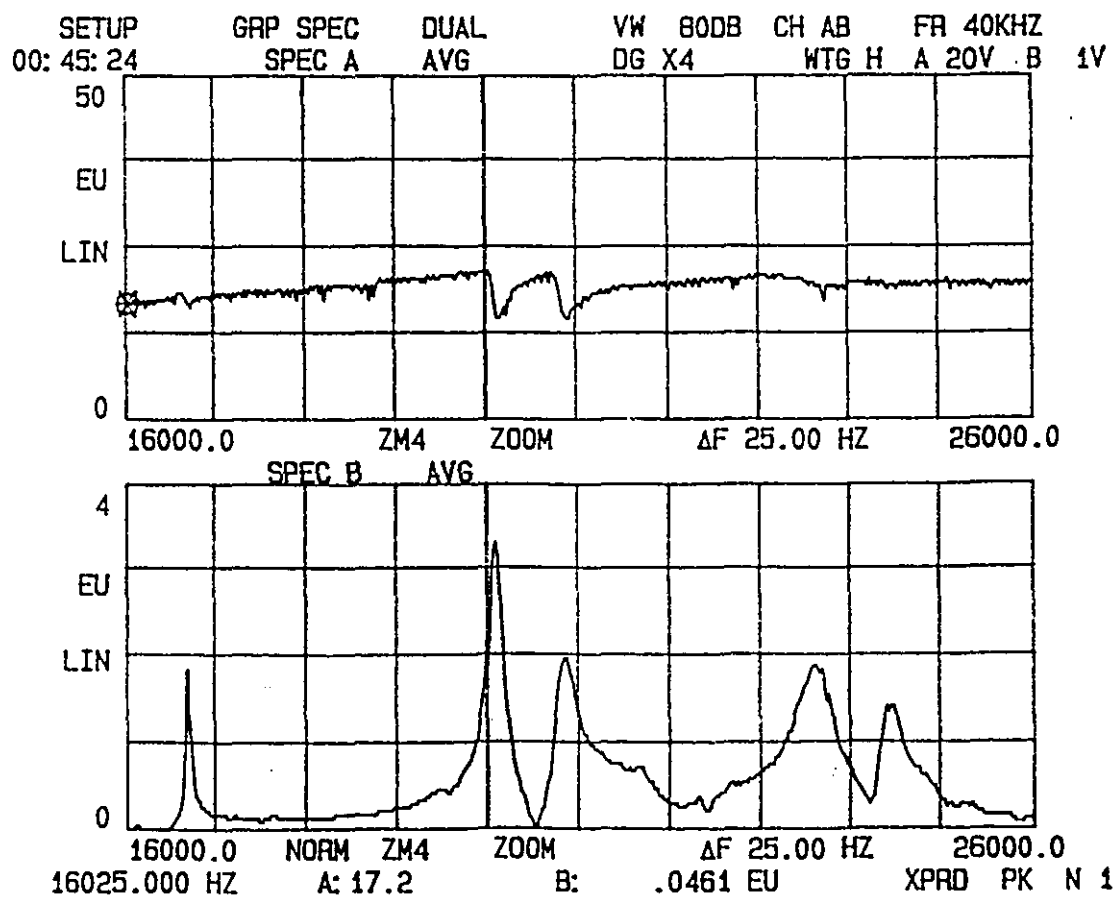

b) Linear Display

FIGURE 4.14 VOLTAGE AND ACCELERATION SPECTRA SHOWING EXCITER CHARACTERISTICS

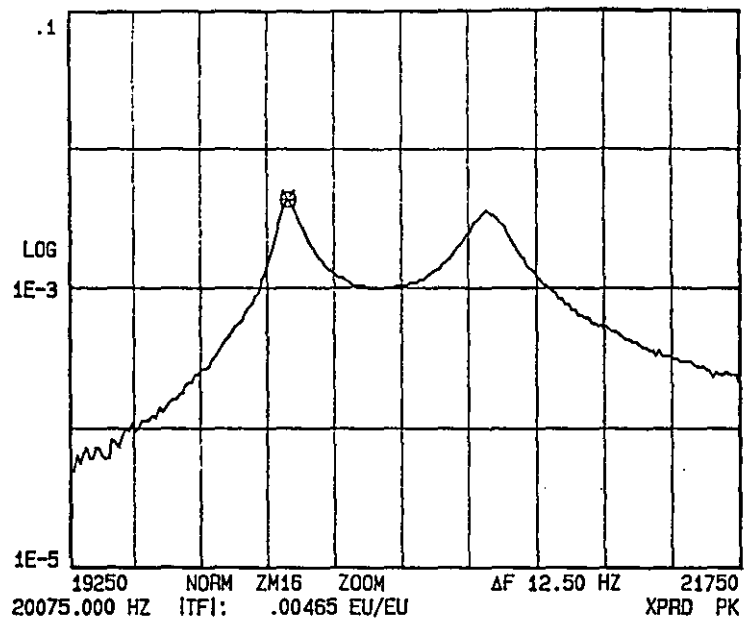

a) Spectrum Measured by Displacement Probe

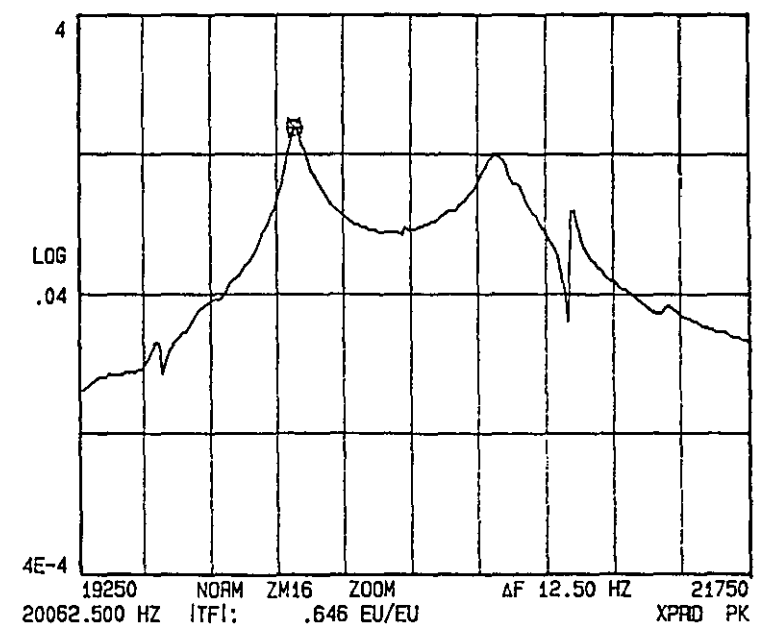

b) Spectrum Measured by an Accelerometer

FIGURE 4.15 DIE RESPONSE MEASUREMENT SPECTRA

CHAPTER 5
VIBRATION BEHAVIOUR OF ULTRASONIC FORMING DIES

5.1 INTRODUCTION

This chapter constitutes the experimental analysis stage in the design of ultrasonic forming dies. The objective is to determine the modal parameters and infer their effects on die operation. Remembering the subsequent design stage of structural modification, information must be obtained on both:

a) modes close to and at the operating frequency, and
b) die behaviour away from the operating frequency that may influence a die redesign strategy.

Die vibration analysis cannot merely be confined to a narrow band around the working mode. For the die forming operation, radial behaviour is critical and isolation of the fundamental radial mode is a particular aim of this study. However, any mode or mode combination that exhibits a component of radial motion in the response can either (i) participate in the fundamental mode if the corresponding frequencies are close, or (ii) be shifted close to the fundamental mode by a structural modification even though the frequencies were initially well-separated. Hence it is essential to understand volume vibration and identify all the modes in the low ultrasonic range. Modal tests are conducted for radial and axial motion over several different frequency bands, with emphasis on radial response near 20 kHz.

Three dies are analysed so that the validity of the design philosophy can be verified at a later stage. The first is an aluminium die with tubular mounting tail and ferro-titanit nickro pellet (Appendix A2). This is the most current die design undergoing trials and its problematic behaviour is the root of this study. Consequently, the analysis concentrates on this particular die and its redesign.

The other two dies are one piece steel cylinders, manufactured early on in the ultrasonic forming project and used in initial process trials. These dies are similarly analysed to confirm the effectiveness of EMA in determining thick cylinder modal characteristics and to extend the design validation to alternative die cylinder geometries.

The results from a fourth die are also presented. This particular aluminium die developed a crack in trials, that severely altered its vibration behaviour. It is included briefly in this study to show the catastrophic effects of poor die design.

Photographs of the four dies under test, are presented in Figure 5.1.

5.2 EXPERIMENTAL CONFIGURATION

A line diagram schematic and photograph of the set-up for EMA of the dies is shown in Figure 5.2. FRFs from die surface measurements are obtained from voltage and acceleration signals, which are directed to the two channels of an FFT analyser. Gathered data is stored on disk for subsequent down-loading to an IBM pc for curve fitting and modal parameter estimation.

A test rig was designed for die vibration analysis (Figure 5.3). The rig was fabricated from steel plate to provide a table-top mounting structure for the die. The semi-circular mounting adaptor on the back-plate allows the die to be mounted either at the tail mounting flange or at the transducer horn nodal flange, so the die could be tested as an effectively freely vibrating system. Electrical signal monitoring is achieved by attaching the input cable connecter and measurement signal BNC connection to a thin plate bolted on to the nodal flange on the horn. The electrical component required to measure the voltage supplied to the transducer coils, was also attached to this plate. The voltage signal could not be measured directly, so is reduced through a 10 MHz, 10:1 attenuator before being fed to the analyser. All the vibration tests were conducted on a vibration isolated table.

5.3 MODAL TESTS ON DIE WITH TUBULAR MOUNT

5.3.1 Frequency Range of Analysis

It is known that the response of a structure at any frequency is affected by all its modes of vibration. In a vibration analysis the influence of out-of-range modes is often small and can either be ignored or approximated to a constant value. It is also possible for an out-of-range mode to have a significant or even dominating effect on measured vibration, so choice of the analysis range must be prudent. Three frequency ranges are included in the experimentation:

1. 19250-21750 Hz: for detailed analysis around the operating mode (Figure 5.4)
2. 16000-26000 Hz: for thick cylinder vibration study and die redesign stage (Figure 5.5)
3. 13000-28000 Hz: for nondetailed analysis of out-of-range- of-interest modes and to check validity of range 2.

It is obvious that there is significant off-resonance mode participation as expected in structures with close modal spacing. A common feature of the FRFs is grouping of modes. The die response roughly subdivides into groups of modes, the one surrounding the operating frequency being of particular interest. The two groups on either side are also important for obtaining a wider understanding of thick cylinder behaviour and for acquiring sufficient data for structural modification analysis. The influence of neighbouring mode groups on each other will be largely overshadowed by the modal coupling within each group.

5.3.2 Measurement Grid

The measurement locations are chosen to generate sufficient data for determination of higher radial harmonics, axial variation and die face out-of-plane motion. To ensure correct identification of all possible modes in the frequency range without a surfeit of measurements, the test grid consisted of 31 radial positions x 3 face positions x 3 axial positions for high resolution

tests, and lower numbered variations. The most used grids are displayed in Figures 5.6 and 5.7.

5.3.3 Modal Parameter Estimation

The modal parameters (natural frequency, modal damping, mode shape) are determined from the gathered data by signal postprocessing techniques. Parameter estimation is verified by a multiple method approach. Firstly, the coincident response (or real part) of the FRF is loaded into the waterfall display feature of the FFT analyser thus plotting the modes as a series of deformations of straight lines representing die circumferences. This method is commonly known as coincident peak picking (conventional modal tests of acceleration response are processed by quadrature peak picking). A damping estimate is calculated from the half-power frequencies of the resonance response. Secondly, the FRFs are curve fitted individually by a SDOF polynomial curve fitting algorithm from which the modal frequency, modal damping and complex residue are obtained. Residual function constants are estimated by the algorithm, to compensate for the effects of out-of-band modes. Finally, parameter estimation of close modes is achieved by using a MDOF polynomial curve-fitting algorithm. If the accuracy of the SDOF assumption is in question for any mode, both SDOF and MDOF approximations are employed (see Chapter 2).

5.3.4 Rotational Coordinates

The use of unidirectional accelerometers for vibration analysis of cylinders allows radial and axial motion to be measured but does not account for hoop (rotational) motion. R, A and T type modes are identifiable from the measurement data, but modes exciting mainly in-plane motion of the die face (F and D modes) are not easily detected and impossible to identify. (For mode nomenclature, see Appendix B).

Only the fundamental modes F0, D0 and FD0 are wholly undetectable. The first harmonics D1 and FD1, are in fact the same modes as R1 and T1 respectively and therefore present no difficulty. The higher harmonics are

detectable but can be falsely categorised because only the radial and axial components of the response are measured.

One way of assisting modal data interpretation is to predict the natural frequencies at which these modes occur, theoretically. The use of Finite Element modelling for this purpose is discussed in Chapter 6. Assistance with rotational behaviour analysis was also available from a study of thick cylinder volume vibrations using a laser speckle technique, by Shellabear and Tyrer [72,73] at Loughborough University. The thick cylinder vibration results from Electronic Speckle Pattern Interferometry (ESPI) measurements have been published in a PhD Thesis [74] and are presented in this study to validate EMA and FEM results. Rather than discuss the ESPI measurements here in terms of fringe analysis, they are presented in this thesis as representations of frequency response spectra, based on the maximum in-plane and maximum out-of-plane amplitude measurements over the frequency range. Thus a comparison with the frequency response from modal tests can be made.

5.3.5 Die Cylinder Vibration Behaviour: Pre-Curve Fit Analysis

A typical radial acceleration spectrum (Figure 5.8) is measured on a die edge circumference in the 16-26 kHz frequency range. There are several response maxima, most likely excited by mode shapes with largely radial vibratory motion. The circumferential radial contribution of these modes is examined by coincident peak picking in a waterfall display of the FRFs. The results are shown in Figure 5.9. Six modes are detected with enough radial amplitude to recognise their mode order.

Radial and Torsional modes (R,T) can be distinguished by comparing an edge circumference FRF with a central circumference FRF. The radial responses of two such FRFs have peaks indicated in the edge circumference measurement (Figure 5.10) which are not observed in the central circumference measurement (Figure 5.11). It is therefore estimated that these are T-type modes.

Axial measurements on the die face also aid distinction between R and T modes. Figure 5.12(a,b) show a radial and axial direction FRF respectively, measured at the same grid position at a die edge circumference. The two dominant radial peaks are considerably reduced in amplitude in the axial measurement (a feature of R-type modes), whereas the radially weak mode at 19.8kHz maintains amplitude in both radial and axial directions (a feature of T-type modes). From this approach to modal identification, a first estimate of the vibration characteristics of the die is produced (Table 5.1). Damping values are calculated from the half-power frequencies. Accuracy in using this method of modal parameter estimation is restricted to analysis of strong, lightly damped and well-separated modes.

Mode Type	Harmonic Number	Frequency (Hz)	Damping (%)
T	-	16650	0.11
R	1	16800	0.08
T	-	18100	-
T	-	19800	-
R	0	20075	0.15
R	3	20825	0.40
R	3	21475	0.05
R	4	23725	0.73
R	4	24500	0.76

TABLE 5.1: MODAL PARAMETER ESTIMATES FROM MEASURED FRFs

From Table 5.1 it appears that more than one frequency is found for the same mode. In particular two R3 and two R4 modes are detected. Mode pairs (or dual resonances) are two natural frequencies of different values associated with two phase displaced modes of the same mode shape. The frequency separation is dependent on the amount of asymmetry in the structure and the frequencies tend to coincide for perfectly symmetrical structures. The relative

strength of the two modes also depends on structural asymmetry and on the position of excitation. For cylinder vibration with circumferential wave numbers, the mode pairs are one-quarter wavelength phase displaced [75]. In the study of thick cylinder vibration modes one of the mode pair is often dominant with the other being barely detectable [76]. The natural frequency of a particular wave number is usually associated with the stronger mode of the pair, normally the so- called symmetric mode (i.e. symmetric about an axis through the driving point in the direction of excitation). In the case of die vibration, excitation is not limited to a point source, but is transmitted over the area of the horn face. This increases the possibility of exciting the antisymmetric (or quarter wavelength rotated) mode and for the pair to consist of two responsive modes. The phenomenon of dual resonance is a further complication in both determining modal parameters and eliminating unwanted modal behaviour.

Before computer-aided modal analysis is initiated, the FRFs are inspected so that behaviour due to heavy modal coupling or nonclassical damping can be detected. This information allows anticipation of non-SDOF characteristics in the vicinity of a resonance, which influences the choice of curve-fitting procedure by indicating invalidations of the SDOF assumption.

The effects of complex and coupled modal behaviour are epitomised by the four Nyquist plots of die FRFs in Figure 5.13. Three modes are excited in close proximity. The die response depends on the measurement position and can produce contradictory evidence of mode participation characteristics:

a) indicates the presence of two lightly damped, well-separated normal modes, with circles emanating from the origin and near symmetrical about the real axis. The assumption that each mode is mainly characterised by SDOF behaviour would seem reasonable.

b) shows that an FRF measured 40° further round the die circumference gives different information of the modes. This Nyquist representation depicts three coupled modes. The two measured in a) are out-of-phase

at this grid point and the coupling effect is seen as a discontinuity in the circles. The coupling with the in-phase mode results in a loop interruption of the corresponding circles. The Nyquist plot indicates the presence of a weak coupled mode at 19.8 kHz, whose response is dominated by the mode at 20.07 kHz. The SDOF assumption is not valid for this mode and there is now doubt as to its validity in identification of the other two modes.

c) is measured in the axial sense on the die face and depicts heavy coupling between the modes at 19.80 kHZ and 20.07 kHz. Both of these modes are dominant in the axial FRF. The mode at 20.07 kHz is rotated about the real axis in the Argand plane (a feature of complex modes), whereas the other two modes lie along the real axis symmetrically. Also, the mode at 20.82 kHz is an isolated, lightly damped normal mode to which the SDOF assumption is only attributable in this measurement.

d) is also an axial measurement from the die face but in this Nyquist plot there is no SDOF modal behaviour near resonance. The three modes now appear as closely coupled modes whose modal characteristics could only realistically be described in terms of mode combinations.

Modal coupling is a feature of die vibration and is not only confined to the near-operating frequency range. Figure 5.14 depicts coupling between two in-phase higher modes with positive real values (at 23.72 and 24.50 kHz). The study of Nyquist representations of measured data directs attention to the criticality of simplifying assumptions in the extraction of modal parameters from FRFs.

5.3.6 Curve-Fit Data

The second method of modal parameter estimation relies on a software based technique which generates data from mathematical curve-fit approximations of the measured FRFs. The curve-fitting algorithms assume that:

i) a structure's dynamic behaviour is fully described by the properties of its individual modes

ii) the modes are normal modes and exhibit proportional damping.

The choice of curve fit is then dependent on whether modal coupling is perceived as being light or heavy in the vicinity of resonance.

The curve-fitting stage of the modal analysis survey must produce a mathematical description of the die vibration parameters, so that modes may be properly identified and the resulting model may be manipulated to predict the effects of physical modifications to the die. This stage does however allow enormous scope for error, especially for non-classical behaviour analysis. A procedure was therefore adopted, to develop confidence in the results, which involved employing SDOF and MDOF curve-fitting routines and fitting both the FRF log magnitude and real part displays. The credibility of modal information was based on two criteria:

a) the curve fit produces a smooth mode shape with believable damping values in comparison with other curve fit attempts

b) the natural frequencies and mode shapes are comparable and understandable in relation to the findings of alternative analysis methods (i.e. waterfall plots, FEM and ESPI).

Frequency and damping values from curve-fitting are presented in Tables 5.2-5.6. Table 5.2(a,b) are the results from curve-fitting the three modes dominating the 19.25-21.75kHz frequency range. In (a) the FRF is fitted using three SDOF fit bands whereas in (b) a 3DOF polynomial is matched to the FRF log magnitude. The values in both cases are similar and comparable with previous information. However, the two strong modes (found to be the R0 and R3 modes, Figure 5.15) are estimated to be pure harmonics by (a) but with modal coupling by (b). The SDOF assumption is valid despite the proximity of the modes since the normal modes are successfully determined. The MDOF behaviour is also valid because modal participation between the two modes is

expected due to their proximity. This seeming anomaly arises because such die modes are "near normal" with the amount of modal coupling predicted depending on the width of the fit band. The validity of both fit assumptions is due to die modal coupling being characterised by modal density rather than heavy damping.

Mode	Frequency (Hz)	Damping (%)
1	20.079K	156.661m
2	20.807K	437.187m
3	21.461K	86.400m

TABLE 5.2(a): SDOF CURVE FIT OF FRF LOG. MAGNITUDE

Mode	Frequency (Hz)	Damping (%)
1	20.040K	208.661m
2	20.752K	461.730m
3	21.544K	48.302m

TABLE 5.2(b): 3DOF CURVE FIT OF FRF LOG. MAGNITUDE

Tables 5.3(a,b) are the frequency and damping results of all modes in the 19.25-21.75 kHz range. Table 5.3(a) is from fitted log magnitude displays of the FRFs and (b) is from fitted real parts. The discrepancies are as follows:

1. A distinct mode is observed just below and closely coupled to the R0 mode. Another indistinct mode appears in some of the FRFs at almost the same frequency as the R0 mode and is only detected when the R0 resonance peak is sharp (i.e. when the R3 amplitude is small and the lower mode has no measurable amplitude). A reasonable explanation is that a mode pair exists just below the operating frequency and that the weaker of the pair is coincident with R0. An attempt to identify the mode pair using a 3DOF curve fit produced the results of modes 1,2 and 3 in Table (a). Modes 1 and 2 are entirely spurious; the frequency of

the lower mode is inconsistent with the data from the waterfall plots and neither mode is discernible. Only the R0 mode is identified in the fit band. When the real part is fitted, only the lower of the unidentified mode pair ever excites enough amplitude to be analysed. A 2DOF curve-fit results in modes 1 and 2 in Table (b). A fourth harmonic T-type mode is found at 19.7kHz, which is supported by previous waterfall plot findings. The possibility that the mode coincident with R0 is also a T4, and the two modes are a T4 pair, seems likely but could not be corroborated by any curve-fitting method. From the consistency of R0 estimations, the effect on the response at resonance of the coincident weak mode is assumed negligible.

2. The R3 mode and those modes coupled with it, are undesirable. The two modes at 20.8 and 21.4kHz are identified as an R3 pair (Figure 5.16), the dominant one being the symmetric mode and the weaker one being the antisymmetric mode. Another weak mode is detected at a frequency between the mode pair. A 3 DOF fit gives modes 4, 5 and 6 in Table (a) and a 2 DOF fit around one of the pair leads to mode 4 and 5 in Table (b). In both cases it was impossible to classify the mode since the symmetric R3 mode dominated its response.

3. The antisymmetric mode of the R3 pair is closely coupled with its pair, but is itself a sharply defined peak (i.e. very lightly damped). Only SDOF curve-fitting produces credible damping value estimations. The damping value in Table 5.2(a) is more realistic than those in Table 5.3(a,b).

Mode	Frequency (Hz)	Damping (%)
1	19.523K	296.708m
2	19.909K	82.482m
3	20.073K	154.664m
4	20.845K	279.813m
5	21.097K	290.222m
6	21.414K	105.818m

TABLE 5.3(a): CURVE FIT OF FRF LOG. MAGNITUDE

Mode	Frequency (Hz)	Damping (%)
1	19.737K	106.676m
2	20.065K	143.478m
3	20.811K	329.712m
4	21.035K	336.043m
5	21.438K	16.020m

TABLE 5.3(b): CURVE FIT OF FRF REAL PART

Tables 5.4(a,b) are the frequency and damping results from the 16-26 kHz analysis. Table (a) comprises curve-fit estimations of the FRF log magnitudes and (b) are estimations from the real parts of the FRFs. The log magnitude displays indicated two close modes at around 24 kHz whereas the real part displays depicted three close modes, the central one being weaker and more heavily damped than the two either side. All three are closely coupled and were identified by a 3 DOF curve-fit of the real part of the FRFs. Modes at 23.7 and 24.6 kHz were identified as an R4 mode pair and the mode at 24.0 kHz was found to be a second order mode of unknown type. Also from this analysis the R1 mode was discovered at 16.7 kHz and another weak mode of indeterminate type was detected at 25.2 kHz.

Mode	Frequency (Hz)	Damping (%)
1	16.724K	76.684m
2	20.103K	198.933m
3	20.829K	483.816m
4	21.467K	474.301m
5	23.732K	661.636m
6	24.467K	395.322m
7	25.223K	464.462m

TABLE 5.4(a): CURVE FIT OF FRF LOG. MAGNITUDE

Mode	Frequency (Hz)	Damping (%)
1	16.750K	56.763m
2	20.103K	230.059m
3	20.881K	386.960m
4	21.490K	101.897m
5	23.693K	63.195m
6	23.958K	1.134m
7	24.459K	545.707m
8	25.205K	349.049m

TABLE 5.4(b): CURVE FIT OF FRF REAL PART

Table 5.5 presents the frequency and damping values resulting from axial FRF measurements on the die face. The phase information from mode shapes on the die face supported the radial information in distinguishing T and R-type modes. From face measurements it was possible to define the mode at 20.0 kHz (coincident with the R0 mode) as a torsional mode, which further suggests that it may be the antisymmetric mode of the T4 pair. Its damping value was estimable from axial FRFs and is very light in comparison to the R0 mode damping.

Mode	Frequency (Hz)	Damping (%)
1	19.735K	23.745m
2	20.023K	12.000m
3	20.059K	160.301m
4	20.808K	429.186m
5	21.434K	20.073m

TABLE 5.5: CURVE FIT OF AXIAL FRF MEASUREMENTS

The weak modes which were detected but not identified in the radial measurements, were not observed in axial FRFs. This indicates that they could be modes exciting mainly rotational deformation (i.e. F or D-type modes). It is not possible to verify the existence of this class of modes without supportive evidence from another analysis technique.

Finally the dominant out-of-range (i.e. outside 16-26 kHz) modes were curve-fitted to give a more complete picture of die vibration. Three lower modes were identified and are listed, along with all the best estimates of frequency and damping values from the curve-fitting stage of the investigation, in Table 5.6.

Mode Type	Harmonic Number	Frequency (Hz)	Damping (m%)
R	2	13600	128
T	3	14200	175
T	3	15100	404
T	1	16600	110
R	1	16800	76
T	4	19735	107
T	-	20023	12
R	0	20076	157
R	3	20825	437
R	3	21461	86
R	4	23693	660
-	-	23958	1134
R	4	24459	546
-	-	25223	464

TABLE 5.6: DIE MODAL PARAMETERS FROM CURVE-FITTING MEASURED FREQUENCY RESPONSE FUNCTIONS

5.3.7 Comparison of EMA and ESPI Analysis of the Die

Confirmation of the validity of the ultrasonic approach to EMA can be drawn from a comparison with results obtained using a laser speckle pattern vibration analysis technique (ESPI) which was referred to in section 5.3.4. A graphical portrayal of die response in the frequency domain from ESPI measurements of the die face is presented in Figure 5.17.

The ability of the optical method to measure in-plane die face motion and out-of-plane motion, allows detection of F and D type modes as well as R and T modes. Out-of-plane ESPI measurements give further confirmation of T-type behaviour.

The difference between the ESPI and EMA results is significant in the 23.5-24.5 kHz frequency range. A D2 mode pair is identified in this region by the ESPI analysis, whereas an R4 pair surrounding an unidentifiable mode is detected by EMA. This discrepancy is a peculiarity of vibration measurement systems, and arises due to the high modal density in this frequency range. The most likely explanation is that coupled R4 and D2 mode combinations are excited at near coincident frequencies. Since no face rotation is measured by EMA the R4 modes are dominant, although the radial motion contribution from the stronger of the D2 mode pair is detected because its natural frequency is at the antiresonance between the R4 pair (since heavy coupling exists, the term "antiresonance" is used loosely here). ESPI, on the other hand, measures modes of vibration from studying the motion of the die face. If in this narrow frequency band, face rotational amplitude exceeds any pure radial deformation, the hoop-type modes will be detected to the exclusion of the radial modes. Perceived modal strength is therefore dependent on the measurement technique employed in the analysis. However, since radial die behaviour is critical to die performance, the EMA results are of particular relevance to the die design process.

5.3.8 Die Mounting Tail Vibration

Analysis of the die mounting tail aimed to ensure that the mounting system was tuned to be compliant at the die operating frequency, such that die radial response was not impaired by the method used to fix it to the surrounds. A waterfall display of FRFs measured around the tail circumference close to the die, illustrated the presence of a zero order radial mode at 20125 Hz (Figure 5.18). This was confirmed by out-of-plane ESPI measurement of a side view of the die and mounting tail. The zero order mode was found at 20100 Hz but with a response bandwidth from 19980 Hz to 20150 Hz, within which this mode could be detected. A representation of the ESPI fringe pattern is depicted in Figure 5.19. The fringes (representing contours of equal vibration amplitude) are presented as hatched and cross-hatched regions, with the nodal lines being observed as white regions. Normally the pattern would be viewed as dark and bright speckled fringes respectively. The tail response is identified as the

required tuned mode with a nodal line between the die and mounting flange, and with the mounting flange also being nodal.

5.3.9 Consequence of EMA Findings on Die Design

The modal analysis survey of the die extracted the die modal parameters which will be used in the die redesign stage to effect structural modifications. The most obvious requirement for an improved die is the separation of the R3 mode from the R0 mode, while maintaining R0 at the operating frequency. In achieving this mode separation it is also essential not to induce frequency shifts in the other modes (especially R1 and R4) such that they are consequently excited close to 20 kHz. These two criteria are the primary concerns because the radial normal modes are the most dominant and influential in the frequency range. However the T modes, in particular T4, could be problematic if the stronger of the mode pair became coincident with R0 (due to a design change or an operational load alteration). The participation of the T mode in the mode combination could result in enough mode distortion to reduce the effective amplitude of the tuned system. Because of this, all modes close to R0 are viewed as potential operational influencers. Ideally, isolation of the R0 mode at 20 kHz, within a bandwidth of 10% above and below, is the optimum die design aim.

5.4 MODAL ANALYSIS OF ALTERNATIVE STEEL DIES

The same analysis procedure for obtaining verifiable modal parameters, was conducted on two alternative one piece steel dies.

5.4.1 EMA of Steel Die 1

Figure 5.20 shows two of the measured FRFs, in log magnitude and phase display format. Within the 16-26 kHz range three peaks dominate the die response. These are identified initially from waterfall plots around the die circumference grid (Figure 5.21) as:

Mode R1 at 19375 Hz
Mode R0 at 20075 Hz
Mode R3 at 22550 Hz.

Having instituted curve-fitting, the modal parameters of the die were determined to give a more complete description of die behaviour, and to formulate a mathematical model for future processing. The final set of best fit estimates of frequencies, damping values and mode shapes are presented in Table 5.7. The die response from ESPI analysis is illustrated in Figure 5.22 and good agreement with EMA results is achieved.

Mode	Frequency (Hz)	Damping (m%)
T1	18235	298
R1	19038	283
R1	19363	112
R0	20067	75
T4	20656	1013
R3	22440	815
R3	23877	22

TABLE 5.7: MODAL PARAMETERS OF STEEL DIE 1

As was true with the aluminium die, the thick cylinder feature of closely spaced and coupled modes characterises the response of the steel die. However the modes appear in a different order and in this case the R1 mode particularly interferes with die performance requirements. The success of this die as an ultrasonic forming tool demands the separation of the R1 and R0 modes, maintaining R0 at 20 kHz and avoiding shifting the strong R3, T4 or T1 modes close to R0.

5.4.2 EMA of Steel Die 2

Figure 5.23 shows two of the FRFs in log magnitude and phase display format, measured on the second steel die. The 17-27 kHz frequency range was more appropriate to this study. The modes identified from waterfall plots of die circumference FRFs were:

Mode R1 at 18675 Hz
Mode R1 at 19175 Hz
Mode R0 at 19875 Hz
Mode R3 at 20950 Hz.

The best estimates of modal parameters from curve-fitting the FRFs are presented in Table 5.8. This die typifies a poor design. The density of strong modes around the operating frequency and the high modal density within the measured frequency range leaves little scope for isolating the R0 mode by design modifications. The R1 and R3 modes both seriously influence die amplitude during forming and any die structural modification would have to effect a diverging frequency shift on these two modes whilst maintaining R0 at 20 kHz.

Mode	Frequency (Hz)	Damping (m%)
T1	18607	68
R1	18716	434
R1	19177	159
R0	19872	112
R3	20862	199
R3	22492	959
T3	23571	94
T3	24683	350
T4	26062	185

TABLE 5.8: MODAL PARAMETERS OF STEEL DIE 2

5.5 MODAL ANALYSIS OF A CRACKED ALUMINIUM DIE

During forming trials of the original cylindrical dies manufactured in the early stages of the ultrasonic forming project, one of the two piece aluminium dies developed a lengthwise through-thickness crack at the interference fit between the bolster and pellet. It was decided to investigate the vibration behaviour of this die as it provided an opportunity to discover the effects on thick cylinder modal properties of this type of flaw.

A modal survey of this die was conducted employing the same test and analysis procedure as with the previously analysed dies. The FRFs were gathered from the measurement grid and a typical FRF is displayed in Figure 5.24. Resonance peaks with corresponding phase shifts through resonance, the expected high modal density and strongly coupled behaviour are observed in the response magnitude display. The distinct peaks are clearly seen in the real part of the FRF and the good circular approximations of the Nyquist representations illustrate the loops associated with modal coupling and slight off-axis rotation indicative of complex modal behaviour. The determination of the frequency and damping parameters was therefore straightforward.

The identification of mode shapes was not straightforward. Figure 5.25 is a waterfall plot of radial FRFs measured at 20° intervals around a die edge circumference. Within the measured frequency range, only higher order modes exist. No R0 mode is detected and there is no continuous harmonic wave shape in the measured radial modes. The occurrence of distorted versions of high order cylinder mode shapes is confirmed by curve-fitting the modal test data. The results are presented in Table 5.9, with some of the modes classified as their nearest representations of pure cylinder modes. ESPI analysis supported the EMA evidence and the findings from these measurements are included in Table 5.9.

Mode	Frequency (Hz)	
	EMA	ESPI
T1	17537	17330
T4	18375	18250
R3	19304	19200
R4	20125	20210
R4	22156	22160
R5	24910	24930

TABLE 5.9: MODAL FREQUENCIES OF CRACKED ALUMINIUM DIE

The results from this study indicate two major effects of a crack at the inner radius of a thick cylinder:

*The EMA and ESPI results are subject to measurement tolerances, especially bandwidth and thermal effects.

1. The cracked die essentially behaves like a thick cylinder with the frequencies of the radial harmonic modes lowered. The discontinuity in the cylindrical shape of the die, caused by the crack, effectively increases the mean diameter of the cylinder. Radial modes of a cylinder can be viewed as ring modes and, since the modal frequency is inversely proportional to its mean radius [77], the modal frequencies are consequently reduced.

2. The presence of a crack which is able to open and close during vibration, alters the strain pattern due to resonance, causing distortion of mode shapes. The die assumes the form of a distorted cylinder whose thickness varies around the circumference; being a minimum at the crack location.

The development of a crack in a die leads to failure of the ultrasonic forming process. Structural fatigue is a problem associated with high frequency vibration and these results highlight the importance of choosing fatigue resistant and flawless materials for die manufacture.

The results of this analysis are also useful for providing a method for monitoring die health. Forming process reliability problems can be linked to the presence of a crack by measuring the radial mode frequencies, so that the institution of remedial action can occur before die failure.

5.6 CONCLUSIONS

A rigorous method for the extraction of modal parameters of ultrasonic forming dies is proposed, that provides accurate and reliable information of die vibration characteristics. Frequency response function data is collected from the die within appropriate frequency bands, over measurement grids that satisfy spatial resolution requirements. An initial estimation of modal frequencies and mode shapes is achieved from a waterfall display of the coincident peaks of the FRFs. Nyquist circles are analysed to detect modal coupling and this

knowledge conditions the FRF curve-fitting stage by supporting or invalidating the SDOF modal behaviour approximations. Both SDOF and MDOF curve-fitting routines are subsequently adopted to determine the modal parameters. Finally the results of ESPI measurements are compared with EMA data to confirm die vibration behaviour and to provide information on rotational coordinate motion. The curve-fitted FRFs make up the modal test data base that will be used to investigate die redesign.

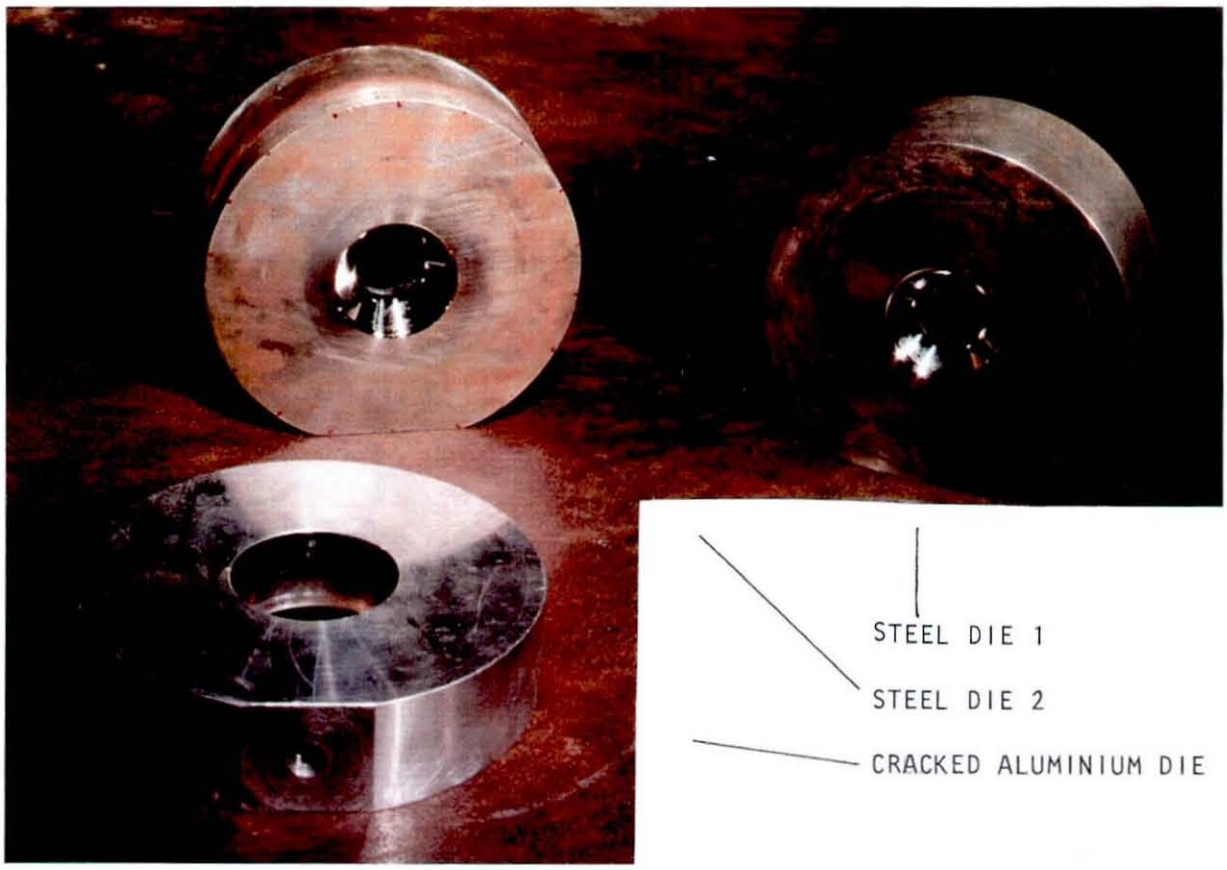

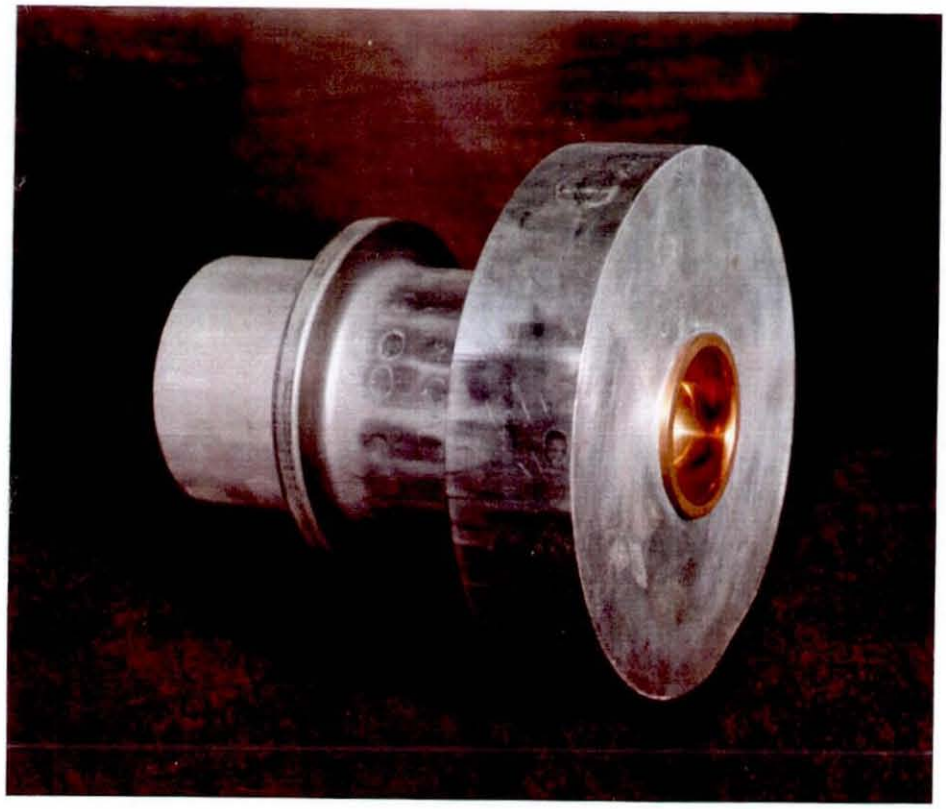

ALUMINIUM DIE WITH TUBULAR MOUNTING TAIL

Figure 5.1 Four Ultrasonic Forming Dies

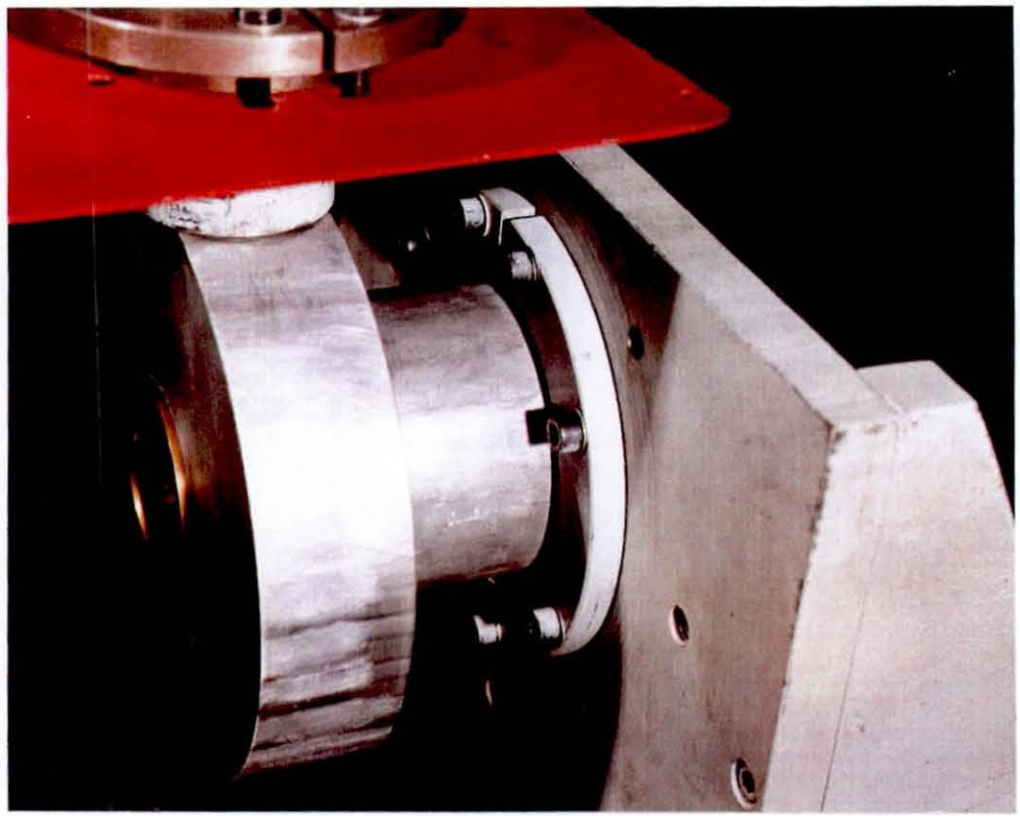

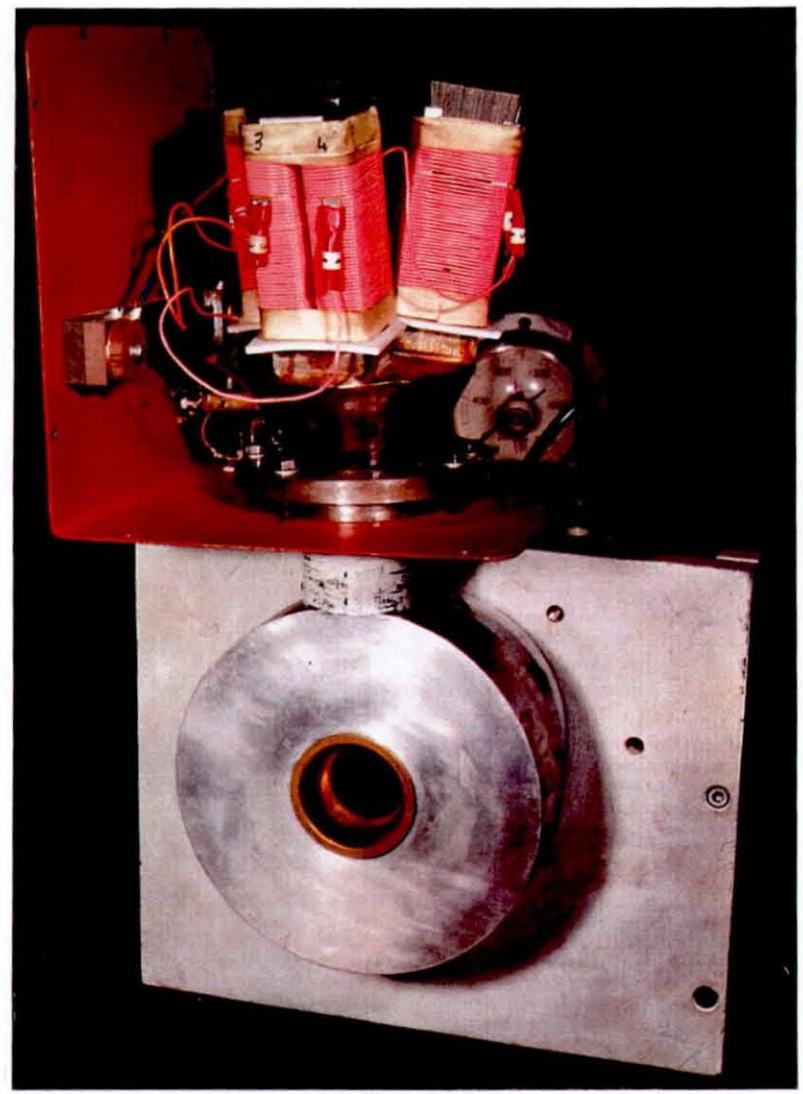

Figure 5.3 Test Rig for Mounting Dies

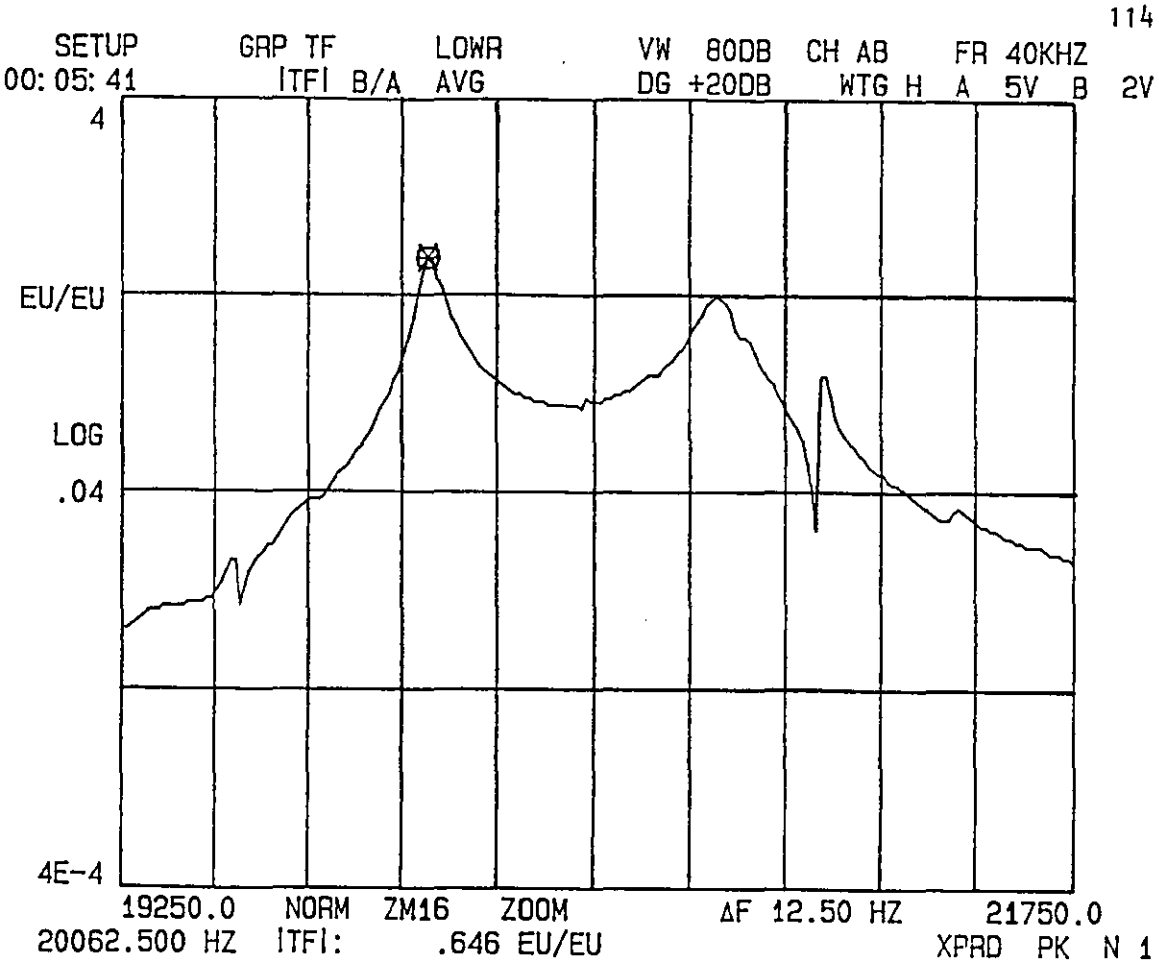

Figure 5.4 Narrow Band Frequency Range

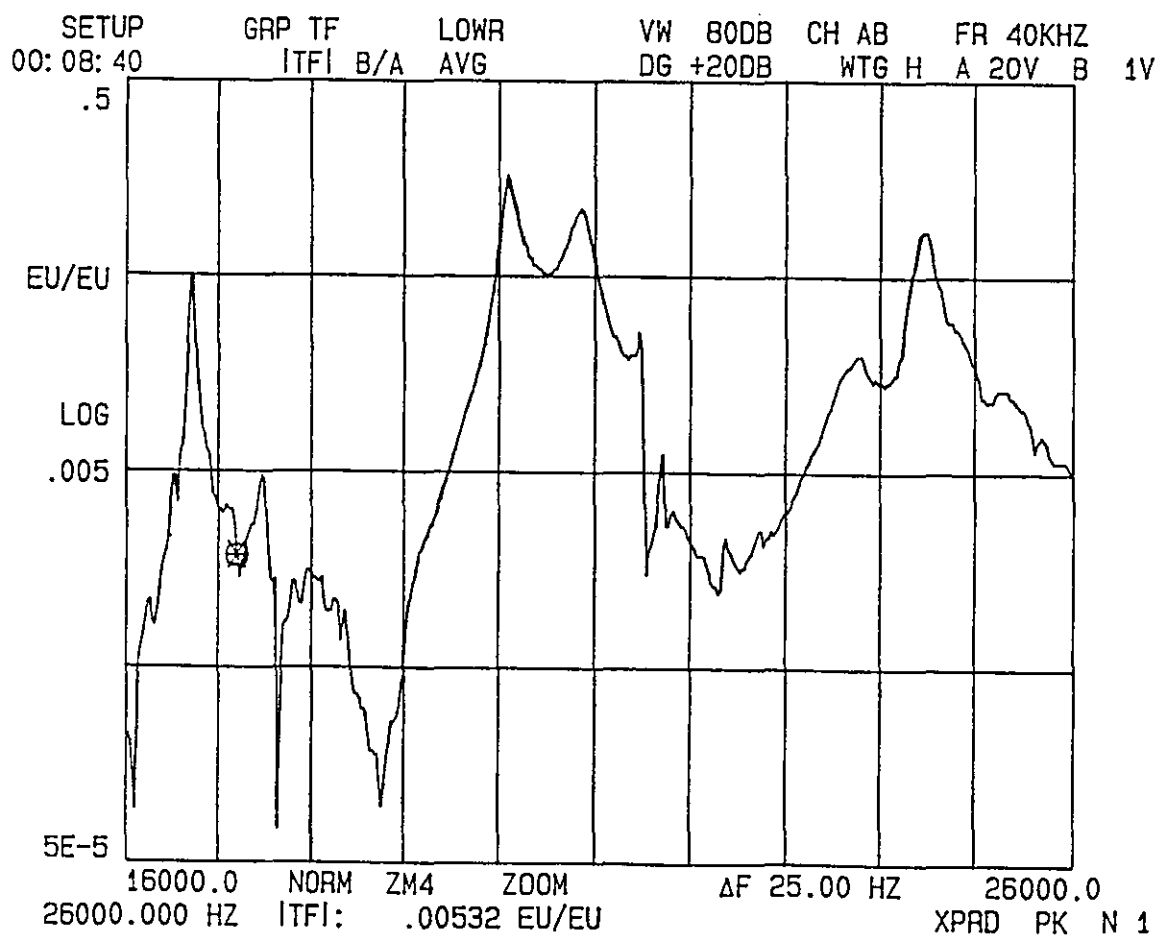

Figure 5.5 Frequency Range for EMA of Die

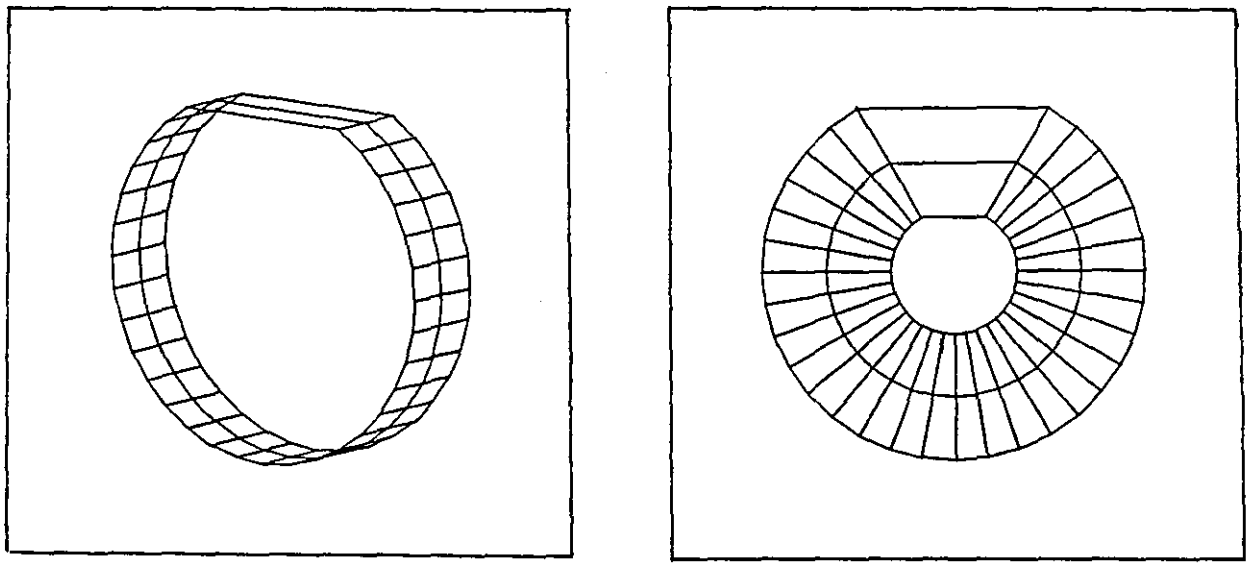

Figure 5.6 Radial and Axial Measurement Positions

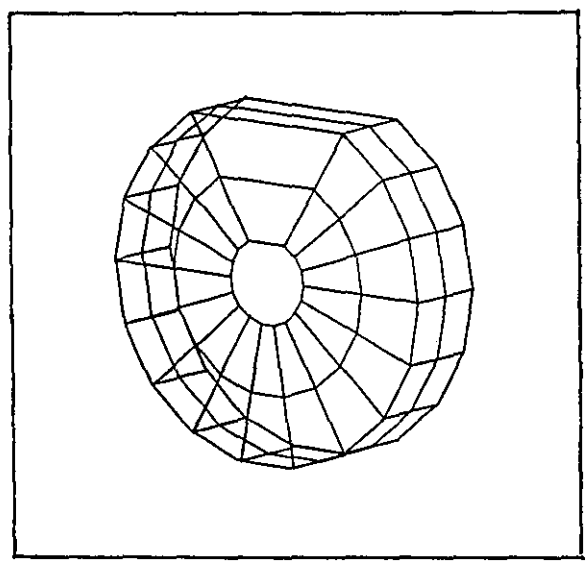

Figure 5.7 Die Measurement Grid

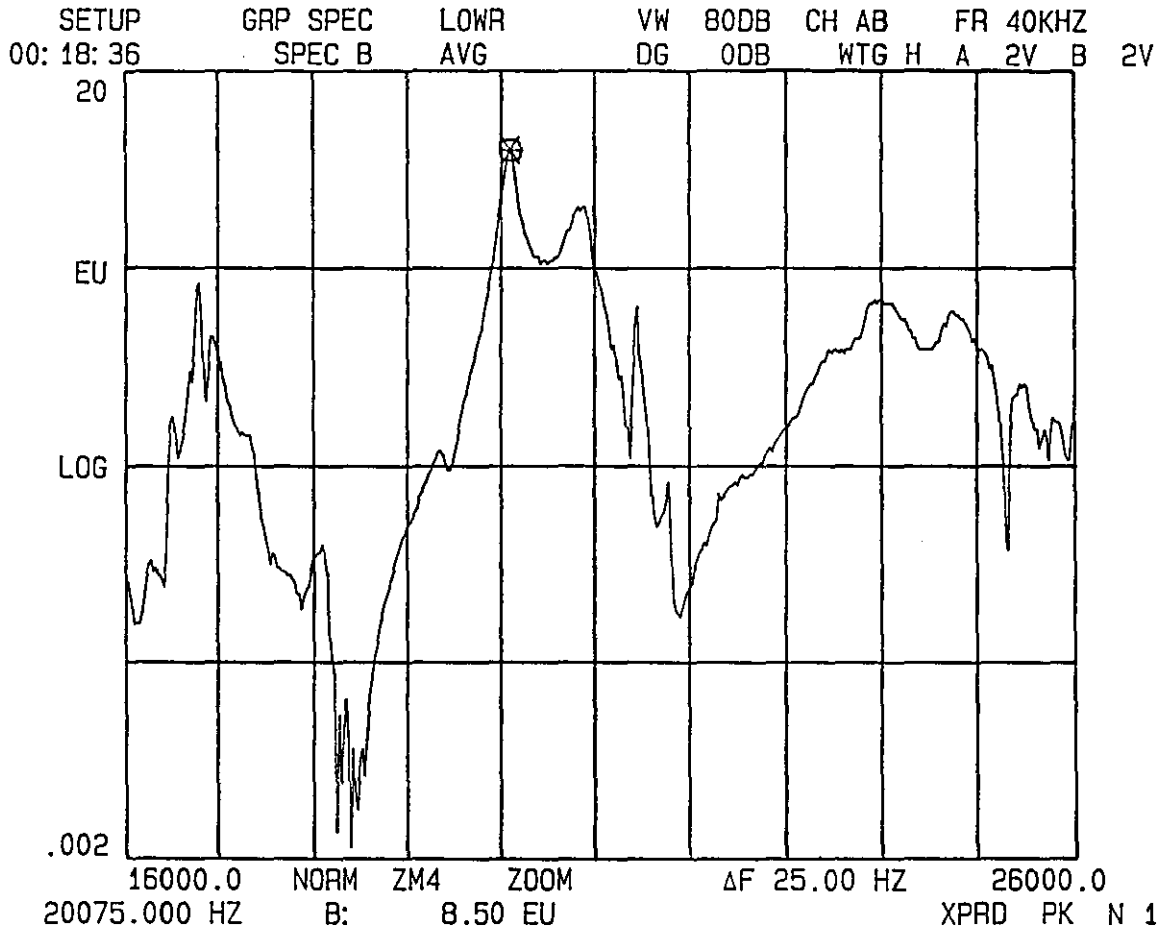

Figure 5.8 Die Edge Circumference Radial Acceleration Spectrum

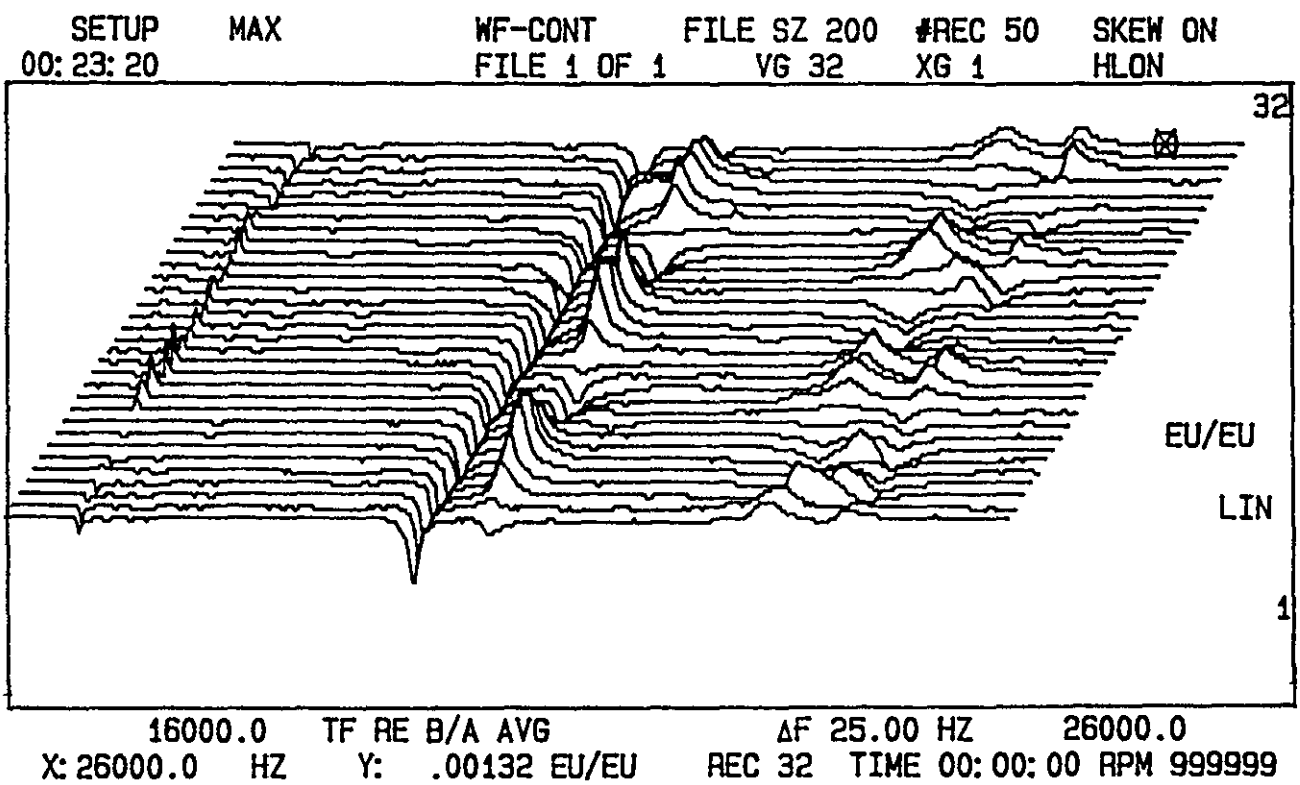

Figure 5.9 Waterfall Plot of Die Circumference Radial Response

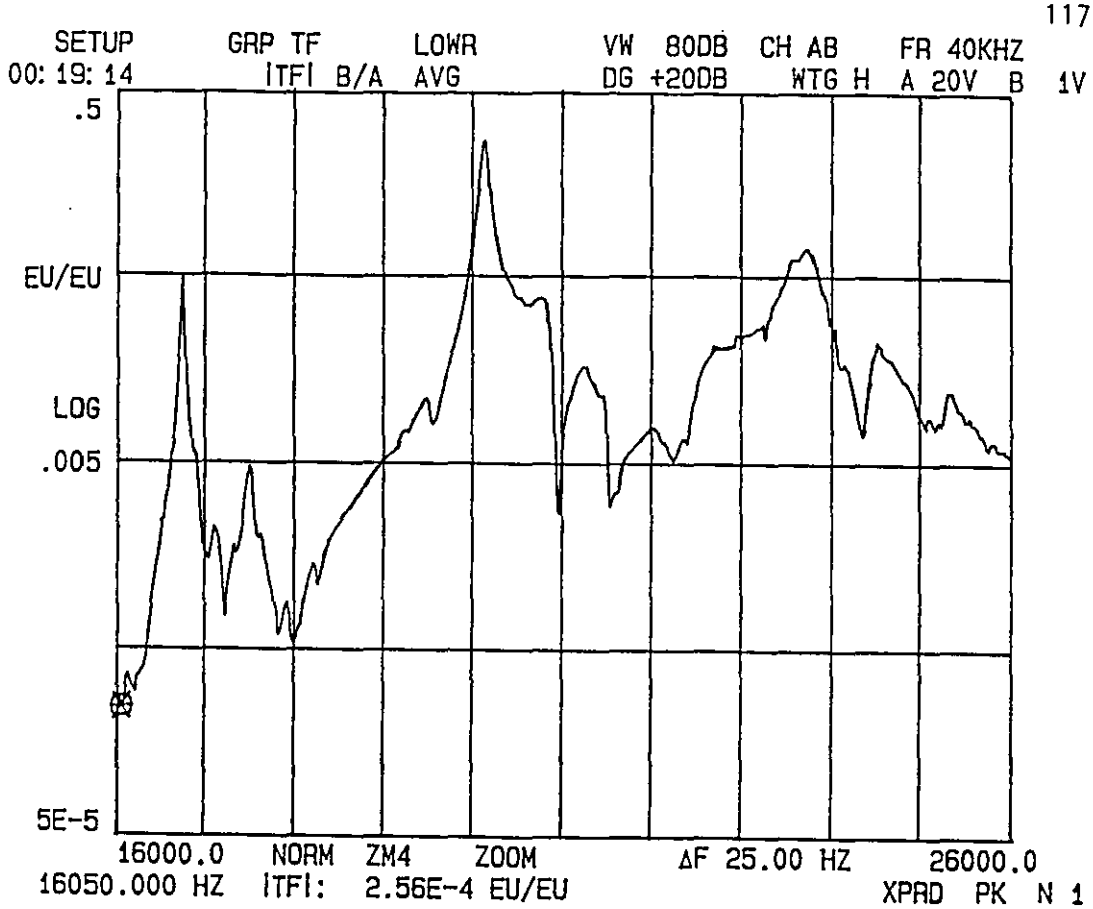

Figure 5.10 Edge Circumference FRF

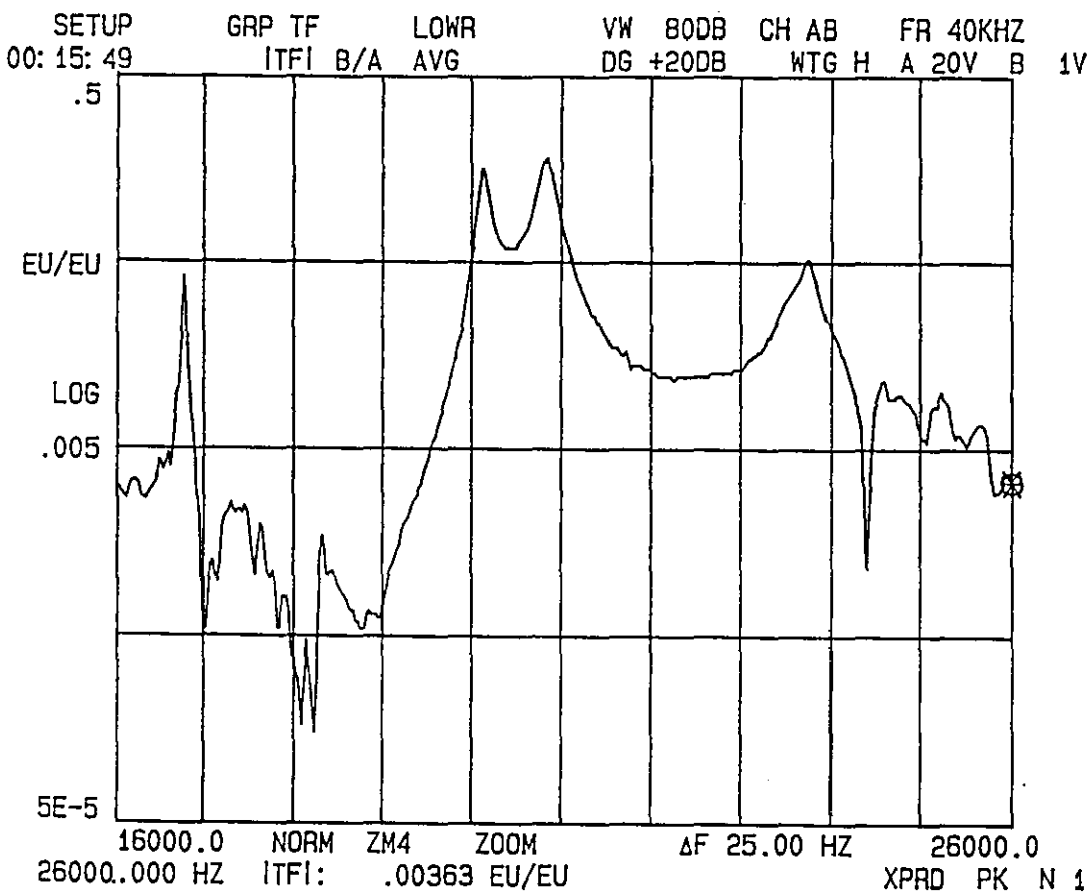

Figure 5.11 Central Circumference FRF

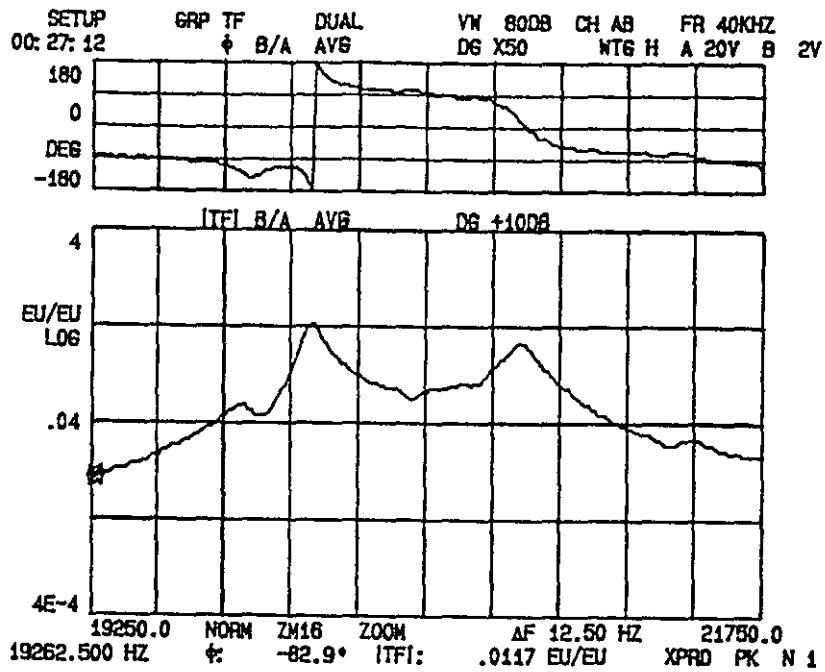

a) Radially Measured FRF

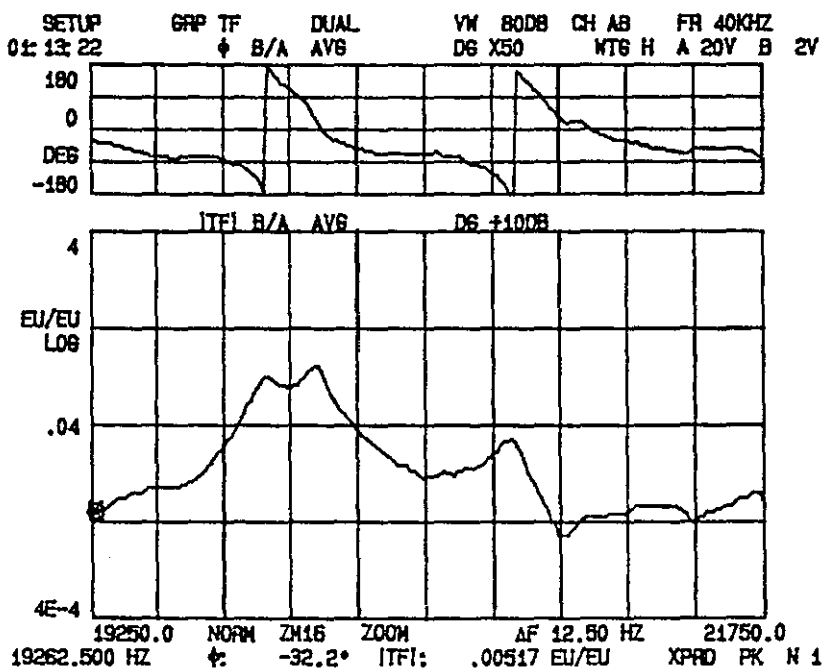

b) Axially Measured FRF

Figure 5.12 Radial and Axial Vibration at the Same Measurement Position

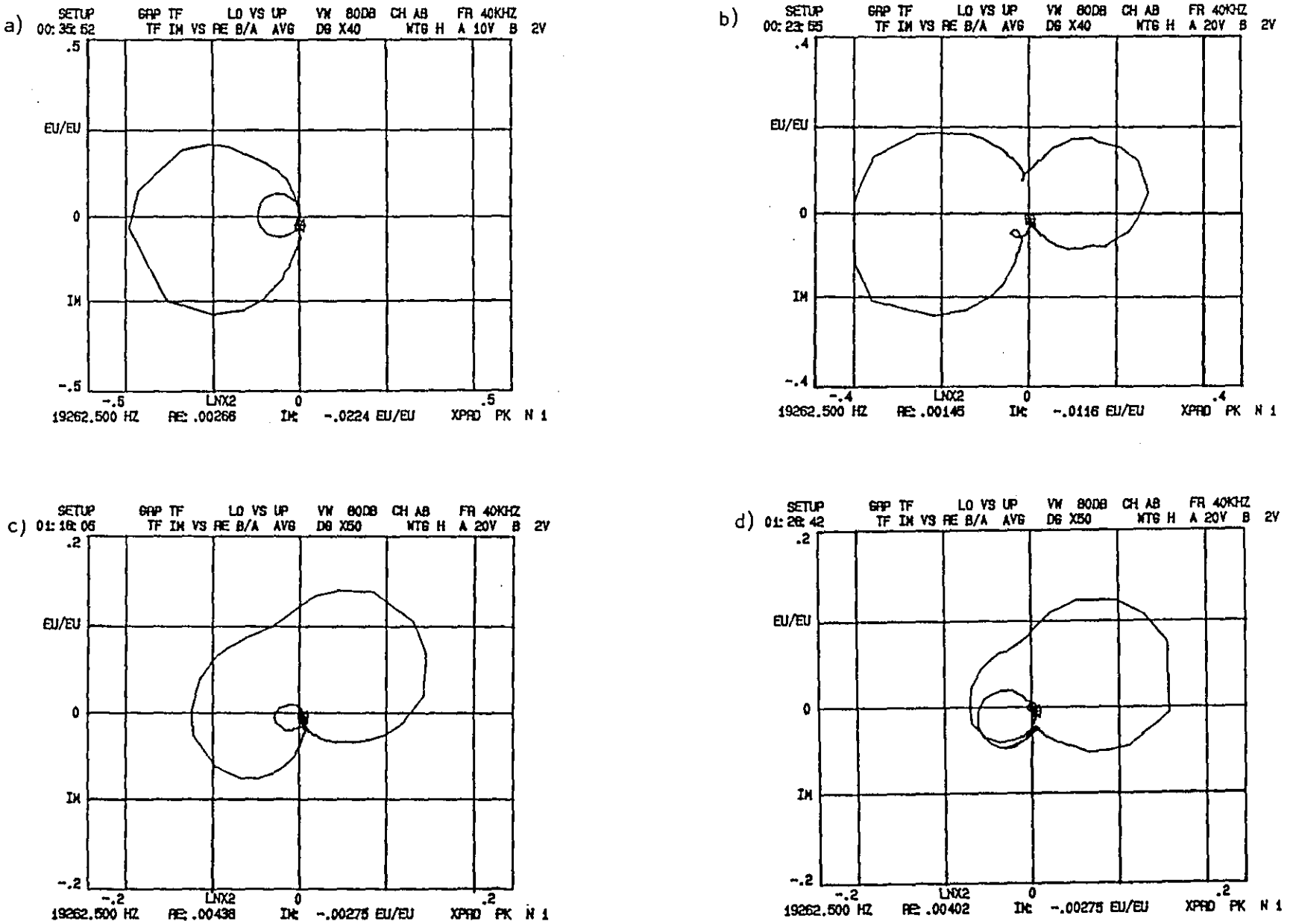

Figure 5.13 Nyquist Circle Plots of Die FRF Measurements

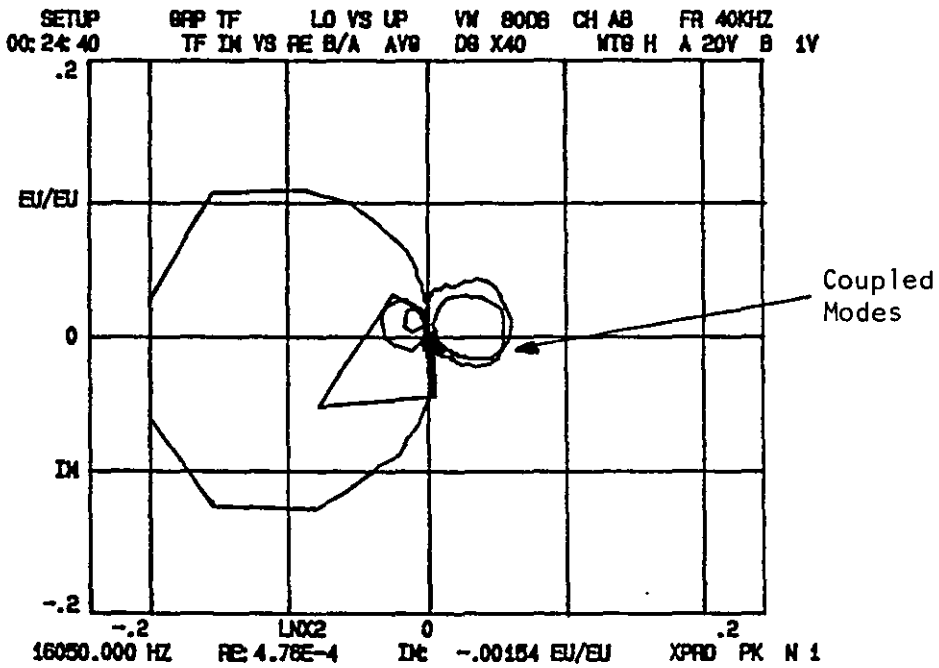

Figure 5.14 Nyquist Circles Showing Coupling Between Two Modes

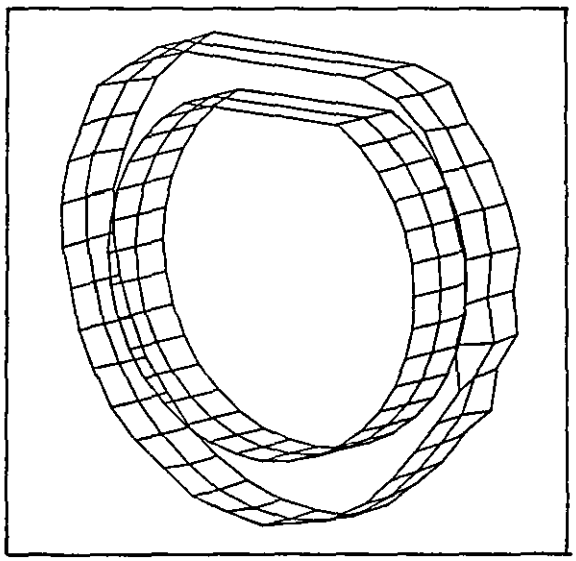

a) R0 Mode

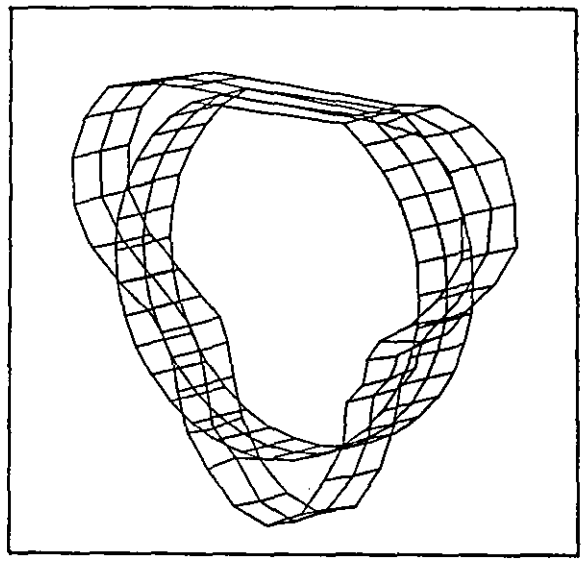

b) R3 Mode

Figure 5.15 Two Radial Modes from Circumference FRF Measurements

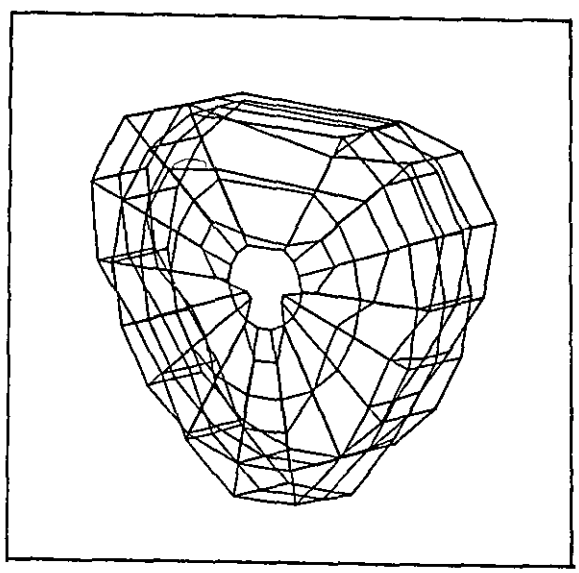

a) Symmetric Mode

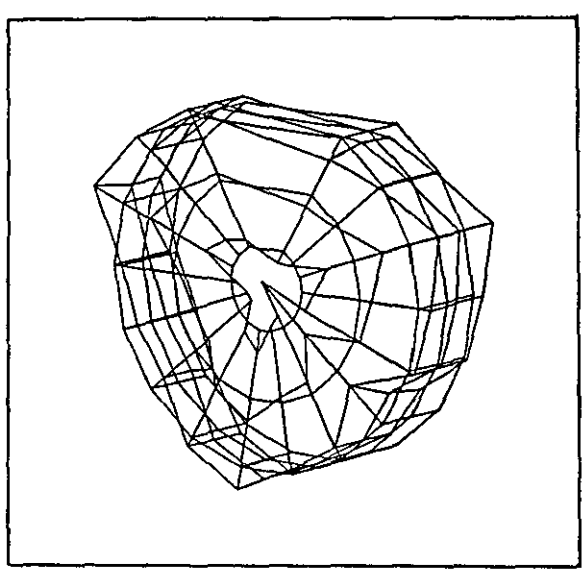

b) Antisymmetric Mode

Figure 5.16 R3 Mode Pair

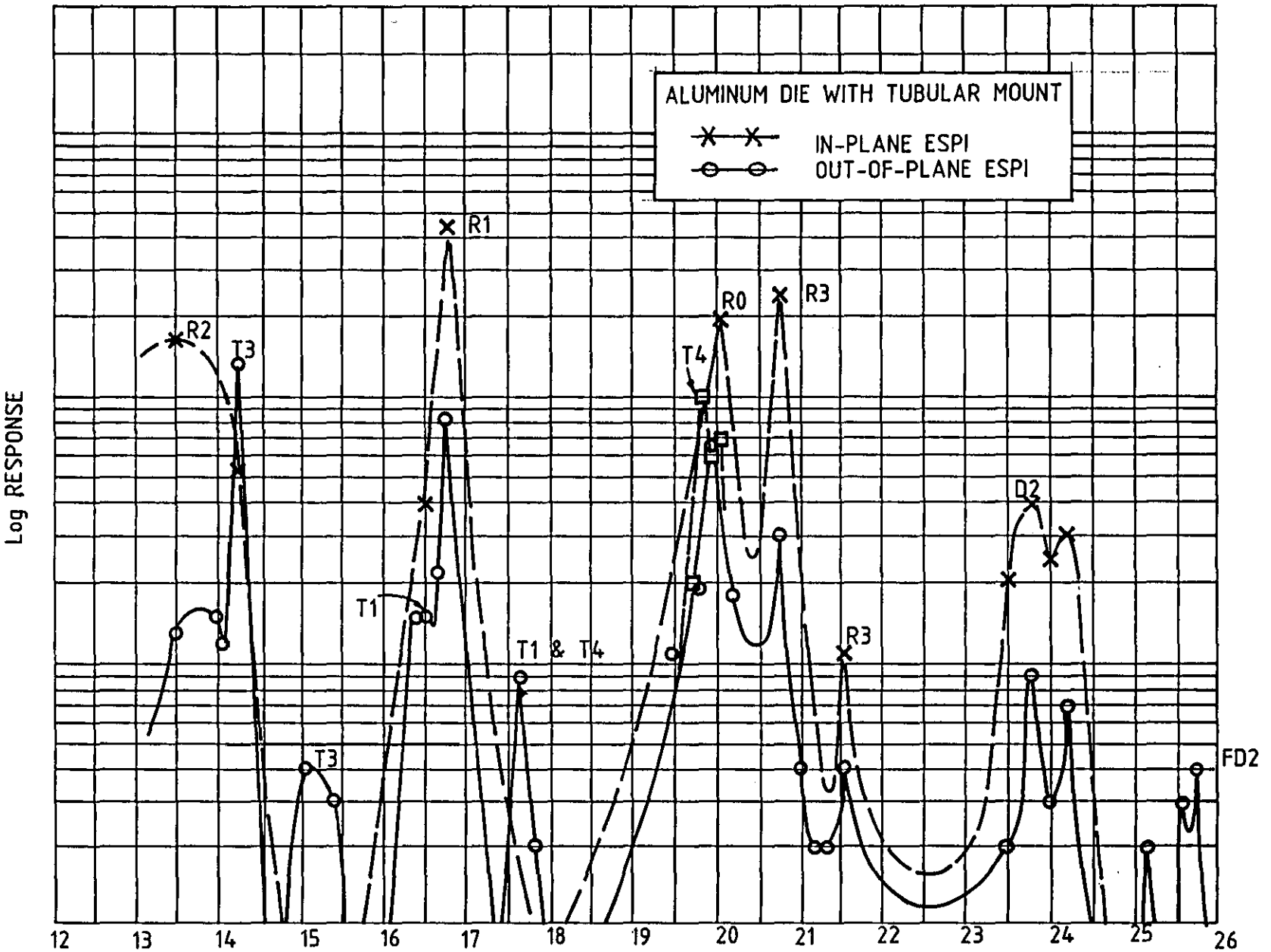
ALUMINUM DIE WITH TUBULAR MOUNT
IN-PLANE ESPI
OUT-OF-PLANE ESPI
Log RESPONSE
R1
R2
T3
R0
R3
T4
D2
T1
T1 & T4
R3
T3
FD2
12
13
14
15
16
17
18
19
20
21
22
23
24
25
26
FREQUENCY, kHz

Figure 5.17

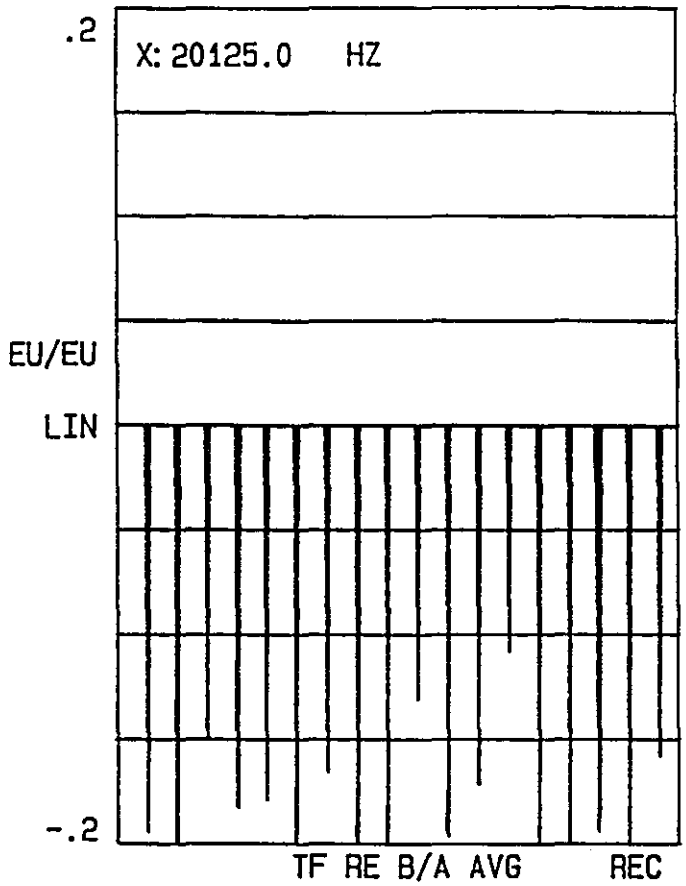

Figure 5.18 Radial Response of Die Mounting Tail Circumference

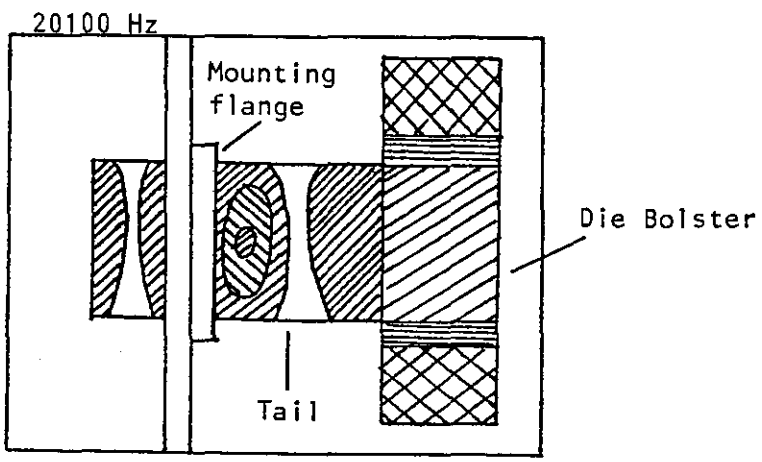

Figure 5.19 Side View of Die and Mounting Tail Showing ESPI Fringe Pattern

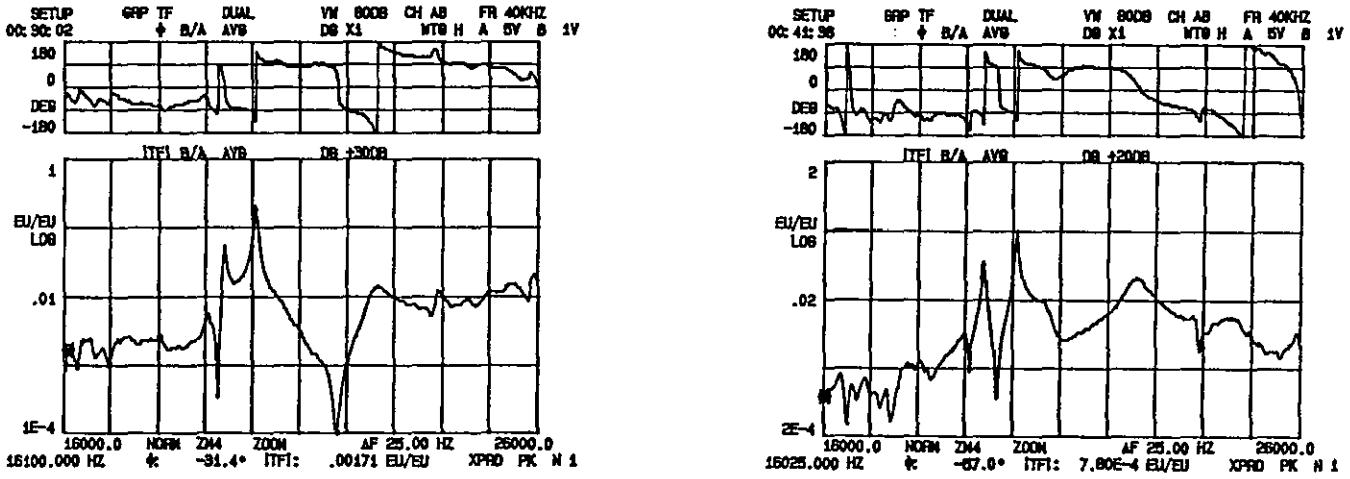

Figure 5.20 Two Radial FRFs Measured on Steel Die 1

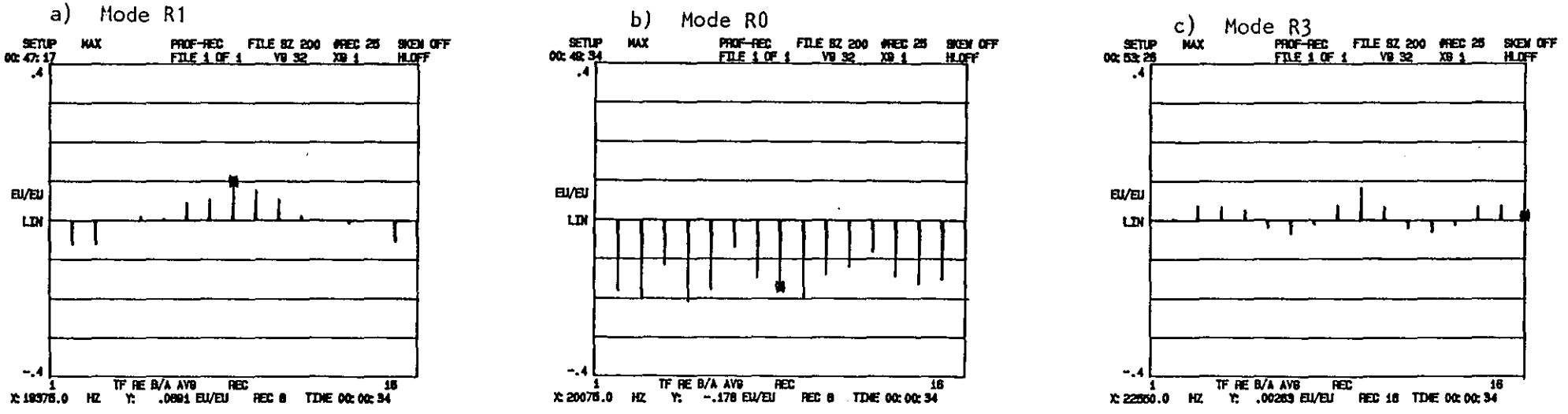

Figure 5.21 Three Radial Modes of Steel Die 1 Identified from Waterfall Analysis

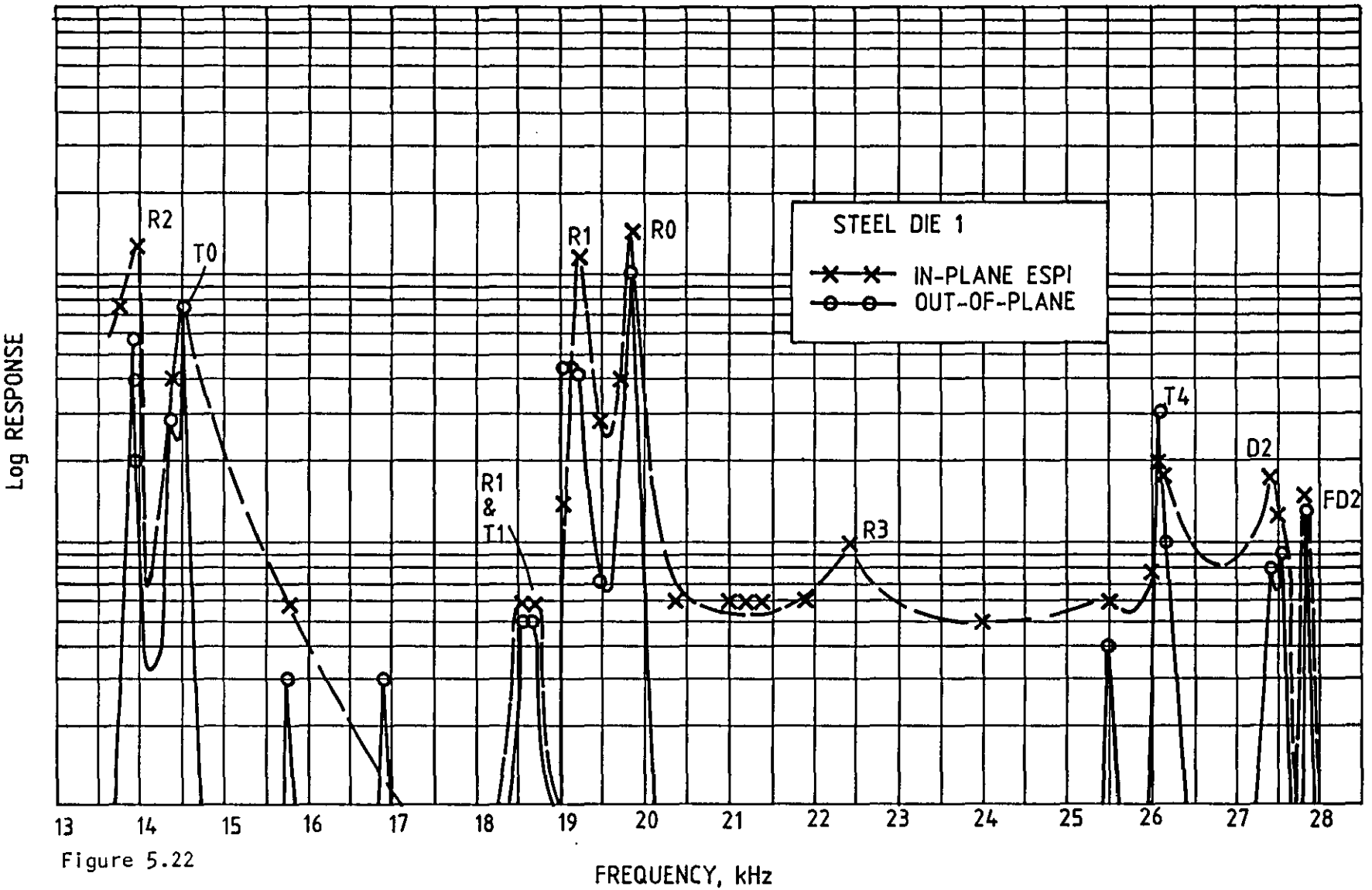
STEEL DIE 1
IN-PLANE ESPI
OUT-OF-PLANE
R2
T0
R1
R0
R1
&
T1
R3
T4
D2
FD2
Log RESPONSE
13
14
15
16
17
18
19
20
21
22
23
24
25
26
27
28
FREQUENCY, kHz

Figure 5.22

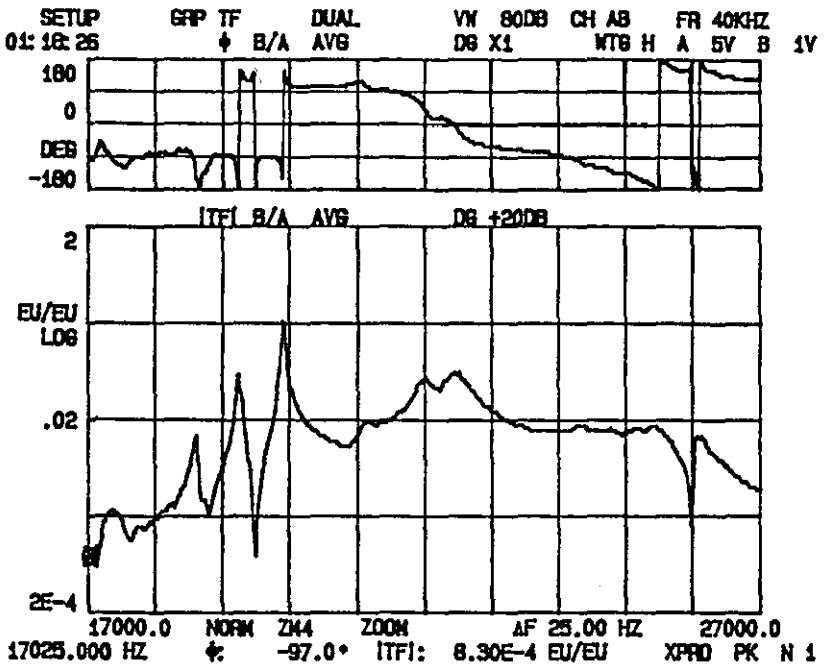

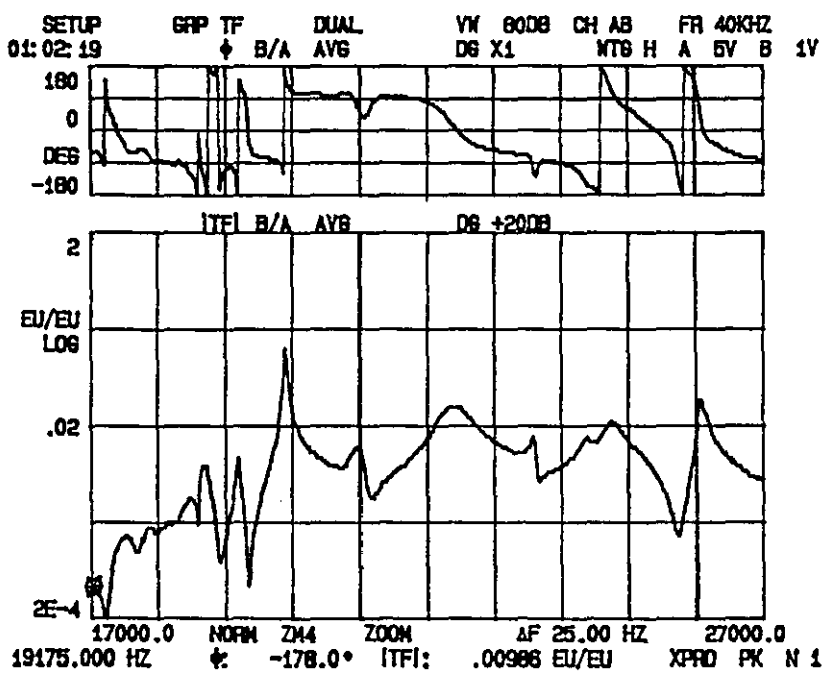

Figure 5.23 Two Radial FRFs Measured on Steel Die 2

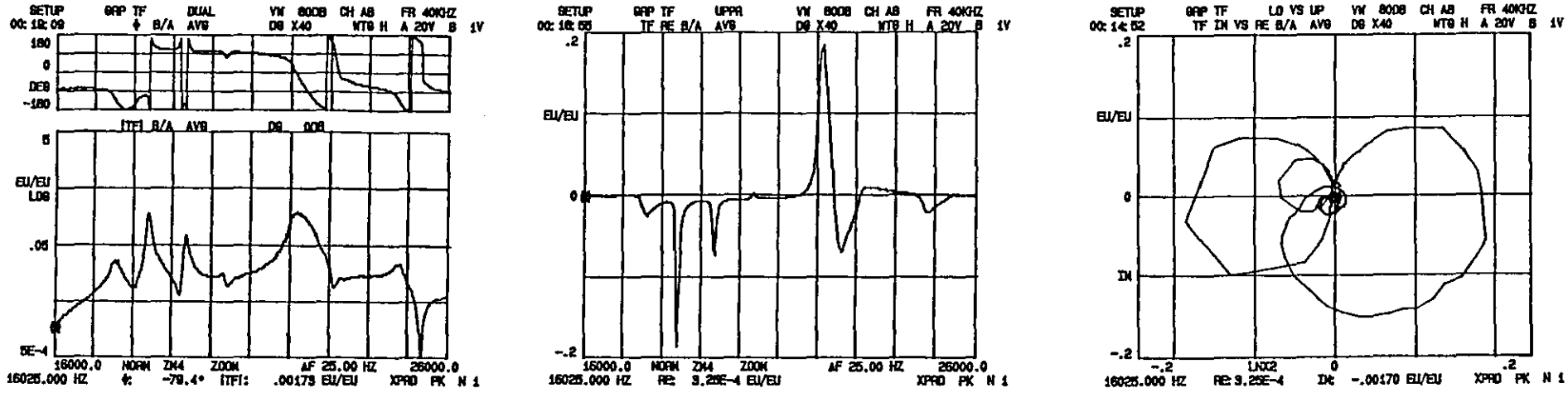

Figure 5.24 Radial FRF Measured on Cracked Aluminium Die

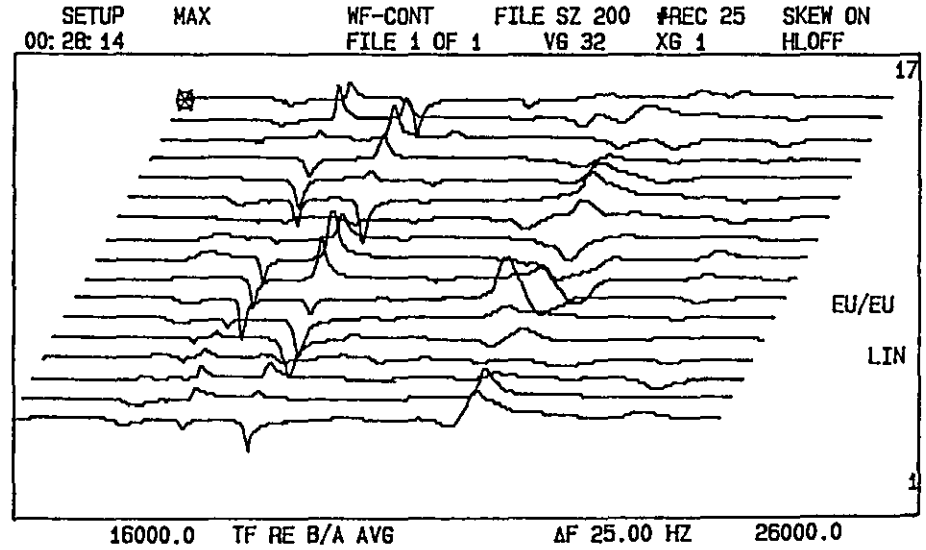

Figure 5.25 Waterfall Display of Circumference Vibration from Cracked Aluminium Die

CHAPTER 6
FINITE ELEMENT MODELLING IN ULTRASONIC DIE DESIGN

6.1 TWO-DIMENSIONAL FE MODELLING OF THE DIE

6.1.1 2D FE Modelling of 3D Structures

In some static FE analyses the situation arises where the structure being modelled and the applied load have a common axis of symmetry. In these cases a cross-section of the structure can be meshed using two-dimensional elements as an alternative to three-dimensional modelling. This is known as axisymmetric analysis. For a dynamic analysis, the structure may be axisymmetric but the mode shapes (calculated from nodal displacements) vary around the circumference of the structure. Solids of revolution can be modelled by a 2D element mesh of a single generator plane with the variation in radial, axial and tangential components of displacement, describing the mode shape, being expressed using Fourier series. This modelling procedure is known as axiharmonic analysis.

The symmetry of the forming dies makes two dimensional FE modelling an option for predicting die modes. The main advantage of this approach is that the FE model can be more finely meshed since 2D calculations require significantly less computer time than the corresponding 3D model calculations, due to the vastly reduced number of DOFs involved. The modes of the die are determined for each selected harmonic number. This technique is valid (i) for designing radial mode dies tuned to a 20 kHz frequency, (ii) for comparisons between die vibration predictions and measurements and (iii) to assess the capability of FE modelling in determining accurately the vibration state of the die. The disadvantage of this modelling technique is that the reliance on an axis of symmetry rules out the possibility of analysing alternative die geometries. It is therefore necessary to employ 3D modelling for die redesign calculations.

6.1.2 2D Axiharmonic Die Models

Much of the initial 2D FE modelling was carried out at Metal Box by Cheers [78] using the ANSYS suite of software. This work investigated the effects of increasing the number of elements and the number of selected master degrees of freedom in the FE mesh, on the tendency of the calculated die natural frequencies to a single value for each mode. From the findings of this study it was possible to estimate the required number of master DOFs and mesh density for the die model using the PAFEC software.

The reasons for conducting a 2D analysis of the die in this investigation were: (a) to compare the FE modal frequencies predicted using PAFEC with those from modal analysis estimations and (b) to calculate the effects of the die tail on the vibration modes of the die bolster.

The component parts of the die are meshed to produce a realistic representation of the forming tool. The aluminium bolster and mounting tail and ferro-titanit nickro pellet constitute the complete model as illustrated in its meshed form in Figure 6.1(a). The tail, incorporating a mounting flange, is designed to be a compliant member at the operating frequency. It is required in order to maintain tool alignment and accommodate axial thrust during forming. The effect of the mounting tail on the modal characteristics of the die can be estimated by comparing the calculated natural frequencies of the complete die model ((a) in a free-free state and (b) with the mounting flange representatively restrained), with the natural frequencies of the die bolster alone as calculated by Cheers [79] using ANSYS software.

The resulting modal frequencies are presented in Table 6.1. The penultimate column of figures is the result for a 2D model of the die with the mounting tail shortened, such that the clamping flange is positioned at the half-wave nodal circumference of the tuned mode of the tail (Figure 6.1(b)). This models a possible alternative to the current tuned tail design, which offers savings in material. The frequencies are calculated for free vibration. The right hand column of figures is the EMA estimates of die modal frequencies as reported in Chapter 5.

Mode	Estimated Natural Frequencies (Hz)				
	Free Die (PAFEC)	Clamped Flange (PAFEC)	Die Bolster (ANSYS) [78]	Short Tail (PAFEC)	(EMA)
T2	6503	-	6115	6160	-
TO	9422	9283	9634	9153	-
R2	12040	12124	11910	12133	13600
T3	12520	14325	12864	14224	14200
R1	16542	17758	16703	16111	16800
T1	17191	18400	17106	17082	16600
T4	19494	19944	19532	20139	19735
RO	20022	20000	19995	20205	20076
R3	20917	20733	21423	20860	20825
D2	25091	27081	24237	26232	24220*
FD2	27518	27506	26856	-	25770*
R4	27825	29963	28204	29424	24459

* ESPI results by Shellabear

TABLE 6.1: DIE MODAL FREQUENCIES FROM 2D FE MODELLING

The results from the PAFEC model of the original die (LH column) are all within 3% of the values predicted by Cheers [78] using ANSYS, except the T2 mode which has a 5% discrepancy. This magnitude of error is consistent with those expected due to differences in the algorithms adopted by the two software companies [80]. The effect of the tail on the die modal frequencies can be assumed to be negligible. The thick cylinder bolster dominates the vibration behaviour of the die as a whole and the thin tubular mounting tail responds at the bolster frequencies in flexural modes with axial wave number increasing with increasing frequency.

The effect on die vibration of clamping the tail nodal flange can be determined by comparing the first and second column of values in Table 6.1. By comparison with the right hand column, these FE models can be validated. The EMA studies were performed with the die held at its mounting flange and the clamped flange FE model was restrained to represent the in-situ die vibration condition.

The first observation is that restraining the die at its mounting flange does not produce a consistent stiffening of the structure for all modes. At the operating frequency the tail responds in its tuned radial mode to maintain the tuned frequency of the bolster. At other die modal frequencies the tail behaves in a similar manner; becoming compliant due to coupling of bolster and tail modes at die modal frequencies. Where the die must act to overcome resistance to resonance in the die tail, the tail restraints lead to an increase in modal frequencies.

Comparison of calculated frequencies with those obtained experimentally shows some inconsistencies in the magnitude of the errors involved. Modes T3, T4, R0 and R3 are all calculated well within 1% of the measured frequency values. R1 and T1 are 5.4% and 9.7% lower than the calculated frequencies but are much closer (1.5% and 3.4%) to the calculated free vibration frequencies. For these two modes the FE model imposes more restraint than is actually experienced by the die under clamped conditions. The R2 mode on the other hand is less restrained in the model than on the test rig. The differences between calculated and measured frequencies are mainly due to difficulties in modelling the restraints of the clamp on the mounting flange. In experiments the flange is situated in a clamping ring with a series of bolts holding the flange in the ring onto the back plate of the test rig. The imposed restraint is therefore not truly axisymmetric. Some freedom will exist in this set-up and the effect on modal frequencies will depend on the amount of coupling between the bolster and tail in each mode.

The R4 mode is significantly separated from its predicted frequency. However the ESPI and EMA investigations showed that the R4 mode was excited at the same frequency as the D2 mode which means that making a direct comparison of frequency values for this particular mode is not meaningful. It is possible that the R4 mode is also excited outside the measurement range.

The design of the tubular tail was considered in the light of the FE model of the clamped die. It was observed that the part of the tail behind the flange was not

responsive at any of the die modes once restraints were imposed on the flange. Further, the length of the tail in front of the flange had been designed to be tuned to a tail mode exhibiting uniform radial amplitude and one axial wavelength so that the tail would be compliant at 20 kHz and the die could be mounted at a nodal circumference. Since the clamping restraints were acting to reduce the effective length of the tail, a new mounting system was designed using 2D FE modelling which positioned the flange at the half-wavelength nodal circumference and eliminated the portion of the tail behind the flange. The calculated frequency values for this alternative design (presented in Table 6.1) do not differ significantly from the original die design. The modes, as expected, generally exhibit lower order axial wave numbers for the tail and the die modal frequencies tend to be slightly higher. The shortened mounting tail does not however lead to improved mode separation around the operating frequency and therefore does not assist in the solution of the problematic die vibration behaviour.

2D axiharmonic FE modelling is an accurate means of predicting the vibration behaviour of an ultrasonic forming die. Errors are introduced by slight inaccuracies in representing the restraints imposed by clamping devices. The important modal frequencies at and close to the operating frequency are calculated to within 0.7% of measured values, which validates the model for die design purposes. 2D FE modelling can successfully be adopted to predict the modes of a die of a given cylinder geometry and can produce information of close modal frequencies that are likely to reduce the efficiency of the die during the forming process.

6.2 THREE-DIMENSIONAL MODELS OF THE DIE

6.2.1 Introduction

A programme of three dimensional modelling of ultrasonic forming dies was initiated in order to produce validated FE approximations of die vibration characteristics that could subsequently be modified to investigate the effects of alternative die geometries on the modal frequencies close to the operating

mode. Having determined from 2D analysis that the tubular mounting tail does not alter the die bolster frequencies significantly, 3D analysis was restricted to thick cylinder modelling since more complex models were prohibitive in terms of solution time.

6.2.2 Reduced Analysis in FE Modelling

In dynamic analysis the natural frequencies are determined from a symmetric real eigenvalue problem rather than from evaluating the determinant of the matrix equation of motion. Extracting the eigenvalues from a system with a large number of degrees of freedom is prohibitively expensive in computer time and therefore a process of eigenvalue economisation is required to reduce the analysis time. This is achieved by choosing master DOFs at which the primary variable will be calculated. The master degrees of freedom (mDOFs) are selected automatically using PAFEC by determining those DOFs which have an appreciable inertia effect on the structure. Most DOFs have very little effect on the terms in the mass matrix. The stiffness matrix, on the other hand, is obtained by differentiation of displacements and a large number of DOFs is necessary to prevent inaccuracies. Once the number of mDOFs has been decided the generalised displacements vector can be partitioned into master DOFs and slave DOFs. The slave DOFs are then reduced out by neglecting the inertia terms in the partitioned equation.

6.2.3 Validating the 3D Models

The first stage in the validation process was to determine the required mesh density and number of master DOFs in a reduced analysis that would produce accurate mode predictions. Numerous 3D models of a tested die cylinder were created, of varying element size and number of masters. The dependence of modal frequencies tending to a single value for each mode, on the two parameters of number of elements and number of master DOFs, was analysed. Typical results from this study, illustrating the resulting choice of master freedoms and mesh, are presented in Figures 6.2 and 6.3.

The lowest number of elements model (32 elements) is used to illustrate the tendency to an accurate modal frequency prediction as the number of masters is increased (Figure 6.2). In general, if higher frequency modes are to be predicted, more masters are required to calculate modal frequencies accurately. The asymptotic frequency values are the most accurate predictions obtainable from a 32 element model of the die. For this particular model, the modal frequencies were all within 1% of the associated asymptotic value using 200 master DOFs. It was not expected that such a coarse mesh would produce results that were comparable with experimentally determined modal frequencies and therefore similar studies were performed for more densely meshed models. The process was repeated for three other models of increasing mesh density. A similar pattern emerged in each case. It was found that 300 masters was sufficient to predict the asymptotic frequency value of any of the modes of the most finely meshed model (108 elements), to within 1% error.

Figure 6.3 illustrates the effect on modal frequency of the number of elements in the FE mesh in a reduced analysis using 300 masters. The asymptotic frequency values are reached to within 1% error using 90 elements in the mesh. It is observed that the order of the modes changes through the range of mesh size and that the curvature of the modal frequency versus number of elements variation, is mode shape dependent. As would be expected, due to the circumferential wave order, the higher harmonic number modes are more sensitive to increased mesh size. The lower harmonic modes (for example, R0 and T0) are less dependent on mesh density and the resulting curves are gentler in the figure. As with 2D FE die modelling, too coarse a mesh will restrict die movement (an effective stiffening) and result in the modal frequencies being overestimated.

From this analysis, it was determined that an element mesh consisting of 108 3D elements and 300 master degrees-of-freedom constituted an accurate model of the die for modal frequency predictions up to the fourth order radial and torsional modes. The results from this model are compared with the EMA estimations of modal frequencies in Table 6.2.

Mode	Estimated Natural Frequencies (Hz)	
	3D FE Model 108 Elements 300 mDOFs	EMA
T2	5290	-
TO	9023	-
R2	8845	13600
T3	11897	14200
T1	14038	16600
RO	16481	20076
R1	17410	16800
T4	18936	19735
R3	19722	20825
D2	24099	24220*

* ESPI results by Shellabear

TABLE 6.2: 3D DIE FE MODEL MODAL FREQUENCIES

Although the mesh and masters combination has been shown to produce accurate results for mode prediction, it is clear from Table 6.2 that the model does not compare well with the measured frequencies. The R2 mode is deviant by 34.5% from the measured value. The difference reduces to 17.9% for R0 and to 0.5% for D2. Generally, the frequencies are underestimated by this model which would indicate that the die is in fact stiffer to radial movement than has been modelled.

The 3D FE models have so far all been based on the geometry of the die bolster and have neglected the ferro-titanit nickro pellet. EMA and ESPI estimations have shown that the die responds in known cylinder modes of vibration at its natural frequencies, despite the irregular, non-cylindrical profile of its inside surface. The effect on modal frequencies of the pellet has not been considered and is the main cause of discrepancies between the two sets of data in Table 6.2. Radially responsive thick cylinder natural frequencies are largely dependent on the mean radius (i.e. 1/2[IR+OR]) of the cylinder. Thick cylinder modal behaviour is analogous to beam vibration. If the cylinder is unwrapped, it can be thought of as a beam of length equal to the circumference

at the mean radius of the cylinder. The modal frequencies of a beam decrease with increasing length and similarly, the modal frequencies of a cylinder decrease with increasing mean circumference, or mean radius. The FE model needs to be improved to take account of pellet effects.

The second simplification of the die is to model it as an aluminium cylinder, rather than taking into account the material of the inner pellet. Since the thick cylinder simplification is being adopted for reasons of solution time, the strategy of including only the bolster material could be validated by refining the FE model specifically to match the experimental results. This can be achieved by determining an effective inner radius that produces FE predictions of natural frequencies that are supported by experimental evidence. This requires that the simplification to an aluminium cylinder only affects this effective inner radius value.

A study was carried out to determine the relationship between the die's inside radius (which affects the mean radius) and its modal frequencies, for an aluminium cylinder model. The results are presented in Figure 6.4.

The figure depicts the first five radial mode frequencies varying with inner radius of the die. The lower order modes show a linear relationship between these two parameters, with the R0 and R2 modes being significantly affected by inner radius. The R2 mode follows the beam analogy of linear frequency reduction with increasing mean circumference. The R0 and R1 modes do not fit this analogy (see Appendix B). The R0 mode however, follows a similar trend to R2; its modal frequency being directly dependent on the thickness of the cylinder and therefore dependent on the inner radius. Increasing cylinder thickness and increasing stiffness are synonymous for the R0 mode because die straining in this mode is either entirely in tension or entirely in compression at any part of its vibration cycle. The R1 mode is unaffected by the inner radius. In this mode, the die is entirely in shear and therefore perceives no stiffening effect from a decreasing inner radius value.

The higher modes (R3 and R4) natural frequencies also decrease with increasing inner radius but the variation is gradual and non-linear. The curves produced for these two modes are parallel in Figure 6.4, which suggests that R3 and R4 are very similarly affected by the inner radius value. The regression of the curves for the R3 and R4 modes is consistent with the beam analogy but the non-linearity of the curves suggests a breakdown of the beam analogy which is probably due to the thickness of the die cylinder. The effective length of a beam (ie. its harmonic half wavelength) is very short in comparison to its actual length at high harmonics. For the case of the die, the effective length is a fraction of the mean circumference and will not only be very short in comparison to this dimension, but will be short in comparison to the die thickness at the third and fourth harmonics. It is therefore unrealistic to turn to beam vibration theory to understand the geometry dependency of high harmonics.

The aluminium cylinder geometry that closely matches the measured modal frequencies of the complete die, is found from Figure 6.4 to have an inner radius of 18 mm. The actual mean radius of the die inner pellet is 19.7 mm (representing a 45 mm to 25 mm diameter necking operation). The estimate of 18 mm is consistent with expected discrepancies due to the simplification of the die to an aluminium cylinder and in particular with the increased stiffening influence of the actual die pellet material. An FE model of the die with an inner radius of 18 mm was meshed using 108 elements and 300 master DOFs. The calculated modal frequencies are listed and compared with EMA estimations in Table 6.3. The corresponding mode shapes are represented by their boundary motion (for ease of visualisation) in Figure 6.5.

Mode	Estimated Natural Frequencies (Hz)		
	Refined 3D Model	EMA	% Error
T2	5606	-	-
TO	9562	-	-
R2	13141	13600	-3.3
T3	13945	14200	-1.8
T1	16561	16600	-0.2
R1	17424	16800	+3.7
T4	19155	19735	-2.9
RO	20069	20076	0.0
R3	21368	20825	+2.6
D2	25490	24220*	+5.2
FD2	26643	25770*	+3.3
R4	27989	24459	-

* ESPI results by Shellabear

TABLE 6.3: REFINED 3D FE MODE PREDICTIONS

It can be observed from Table 6.3 that the refined, simplified 3D model produces validated estimations of the die modal frequencies. The comparison shown in Figure 6.6 provides further evidence of good correlation between calculated and measured values. A linear fit of predicted frequencies plotted against measured frequencies produces a line of gradient 0.97 and a predicted correlation coefficient of 0.997. All calculated results are within 4% of EMA estimations (except D2) and have 0% and 2.6% discrepancy for the R0 and R3 modes respectively. The effective inner radius of the cylinder was chosen with emphasis on obtaining minimum possible error between the calculated and measured results for these two modes. Close proximity of R0 and R3 modes is known to cause mode switching in ultrasonic die operation. Accurate prediction of their frequencies is critical since mode separation will form the basis of a die redesign effort. This refined FE model will be modified to predict the effects of geometry alterations on R0 and R3 mode separation. Accurate FE predictions of the non-problematic modes is also important to this work because it is essential to ensure that a modification that separates R0 and R3

does not lead to the prediction of another of the die modes being excited close to the operating frequency.

6.3 MODELLING A DIE SEGMENT USING CYCLIC SYMMETRY

6.3.1 Cyclic Symmetry FE Analysis

The die bolster cylinder can be analysed using the method of cyclic symmetry in FE modelling. The FE mesh models a segment of the structure formed by pure rotation. The eigenvalue calculations are performed by first determining the vectors of segment interface displacements in the radial, circumferential and axial directions. The stiffness matrix and mass matrix are the same for each segment and can be partitioned such that the terms relating to the two interfaces of the segment are separated. If there are n identical segments describing the structure then there will be n distinct eigenvalue problems. The advantages of this procedure are a considerable reduction in solution time, improved numerical conditioning and the elimination of unrequired computations by specifying only the harmonics of interest [81]. As with other FE analysis methods, a reduced number of DOFs is used by selecting masters, chosen from both interface and internal freedoms. Cyclic symmetry analysis could not be used for die redesign, except if a modification retained a repeated segment, but could be adopted to construct models that incorporate the die pellet material since the resulting additional computing time is not prohibitive.

6.3.2 3D Die Models using Cyclic Symmetry

One twelfth (or 30° segment) of the die is modelled. The rule governing cyclic symmetry analysis is that there must be a sufficient number of segments to display at least a quarter of the circumferential harmonic wave in order to calculate a particular mode [63]. The actual segment which is meshed, describes the circumferential distance between an adjacent node and antinode of the third harmonic wave. This means that the first and second harmonics can be calculated by multiple segments and also enables the third harmonic and higher to be calculated. This is represented pictorially in Figure 6.7.

The following two FE die models are presented from this work:

1. 9 3D brick elements modelling a 30° segment of the aluminium die bolster, with 35 mDOFs.

2. 12 3D brick elements modelling a 30° segment of the aluminium die (9 elements) and ferro-titanit nickro pellet (3 elements), with 50 mDOFs. The die pellet is simplified to a cylinder of inner radius 19.7 mm.

In both cases the number of elements used in the mesh and the chosen number of masters were selected by the same method as in section 6.3.3. The asymptotic frequency value for each mode was calculated within 1% error for the mesh size and masters combinations given in 1 and 2 above.

The aim is to compare FE model 1 with the 3D model of the whole die bolster to determine whether there is any significant improvement in frequency prediction using cyclic symmetry analysis. The results from FE model 2 are compared with both the experimentally obtained modal frequencies and with those from the 3D model of the whole die (i.e. those presented in Table 6.3).

The results from these models are recorded in Table 6.4 and compared with experimental data in Figure 6.8. The modes from the second FE model are presented in Figure 6.9.

Mode	Calculated Natural Frequencies (Hz)		
	Cyclic Symmetry Model 1	Full Structure Die Bolster	% Difference
T2	5322	5290	-0.6
TO	9051	9023	-0.3
R2	8830	8845	0.2
T3	12010	11897	-0.9
T1	14495	14038	-3.1
RO	16495	16481	-0.1
R1	17410	17410	0.0
T4	19114	18936	-0.9
R3	19111	19722	3.2
D2	24421	24099	-1.3
FD2	25609	-	-
R4	28118	-	-

TABLE 6.4: COMPARISON OF MODAL FREQUENCIES USING TWO MODELLING TECHNIQUES

Mode	Estimated Natural Frequencies (Hz)		
	Cyclic Symmetry Model 2	Full Structure Bolster + Pellet	EMA
T2	5842	5606	-
T0	9547	9562	-
R2	11598	13141	13600
T3	12228	13945	14200
T1	16431	16561	16600
R1	16875	17424	16800
T4	18923	19155	19375
RO	20142	20069	20076
R3	21398	21368	20825
D2	24120	25490	24220*
FD2	26312	26643	25770*
R4	28466	27989	24459

* ESPI results by Shellabear

TABLE 6.5: CYCLIC SYMMETRY MODEL COMPARED WITH FULL STRUCTURE AND EXPERIMENTAL MODELS

There is negligible difference between the die bolster frequencies predicted by cyclic symmetry and by modelling the whole structure (Table 6.4). It can be concluded that for models containing similar simplifications and the same material properties, the advantage of adopting this modelling technique is the considerable reduction in solution time and no improvement in accuracy can be expected. From this statement, it would be expected that noticeable improvements would result from the die bolster and pellet model, since in this case the pellet material is included in the model and a realistic value for the mean inner radius is used. Contradictory to this, the cyclic symmetry model does not correlate as well with measured frequency values as the simplified full structure model (Table 6.5). This is clearly observed by the increased data scatter in Figure 6.8 as compared with Figure 6.6. The reduced accuracy is entirely due to two erroneously calculated modal frequencies associated with the R2 and T3 modes, which are similarly in error on comparison with the full structure FE model. It is difficult to find an explanation for these two anomalies, especially since both higher and lower radial and torsional modes have been accurately predicted. It is possible that the profiled inner pellet influences some of the modal frequencies in such a way that it is unrealistic to simplify this element of the die to a cylinder. This does not account for the discrepancies being confined to two adjacent modes. The advantage of the full structure model is that model refinement can be performed selectively, to ensure that frequencies correlate well with measurement data in all modes.

6.4 CONCLUSIONS

1. Two-dimensional axiharmonic analysis can successfully predict die modal frequencies. This technique can be employed to design radial mode forming dies tuned to 20 kHz and to estimate the frequencies of modes close to the tuned R0 mode. The FE models cannot be adapted to predict the effects of design modifications unless the axis of symmetry is retained in a redesigned die.

2. Cyclic symmetry analysis in general produces accurate predictions of die modal frequencies. The solution time is greatly reduced from conventional 3D analysis but difficulties can arise in refining out anomalous erroneous modes. The models cannot be utilised for design modifications to the die unless the repeated segment is retained by the alteration.

3. Modelling the die using 3D brick elements can produce accurate validated mode predictions, providing care is taken to maximise accuracy by considering the choice of mesh size and number of master degrees-of-freedom. Simplifications to the die geometry can be compensated for by a process of selective model refinements that allow the model to be matched directly with experimentally determined mode estimations. The final refined FE model can subsequently be modified to calculate the effects of geometry modifications, with the advantage that confidence has been gained in the realism of the base model.

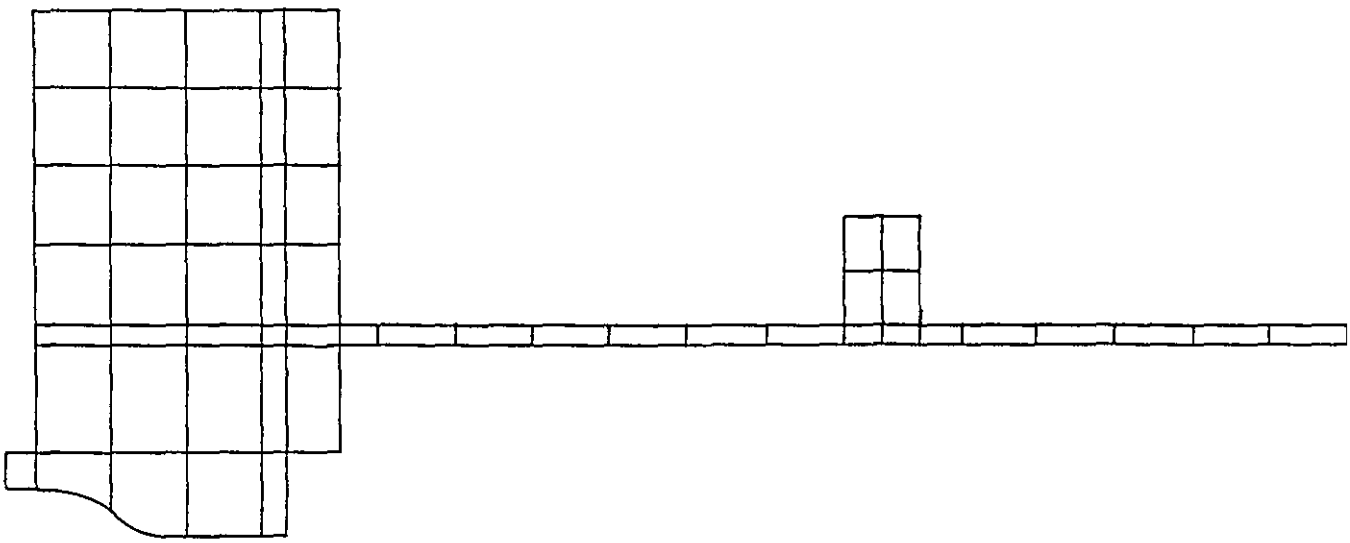

Figure 6.1a) 2D Axiharmonic FE Model of Die and Mounting Tail

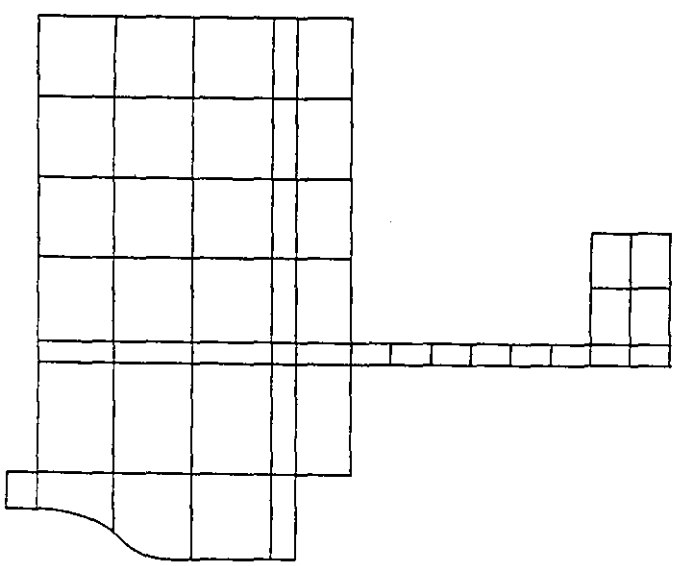

Figure 6.1b) 2D Model of Die with Shortened Tuned Mounting Tail

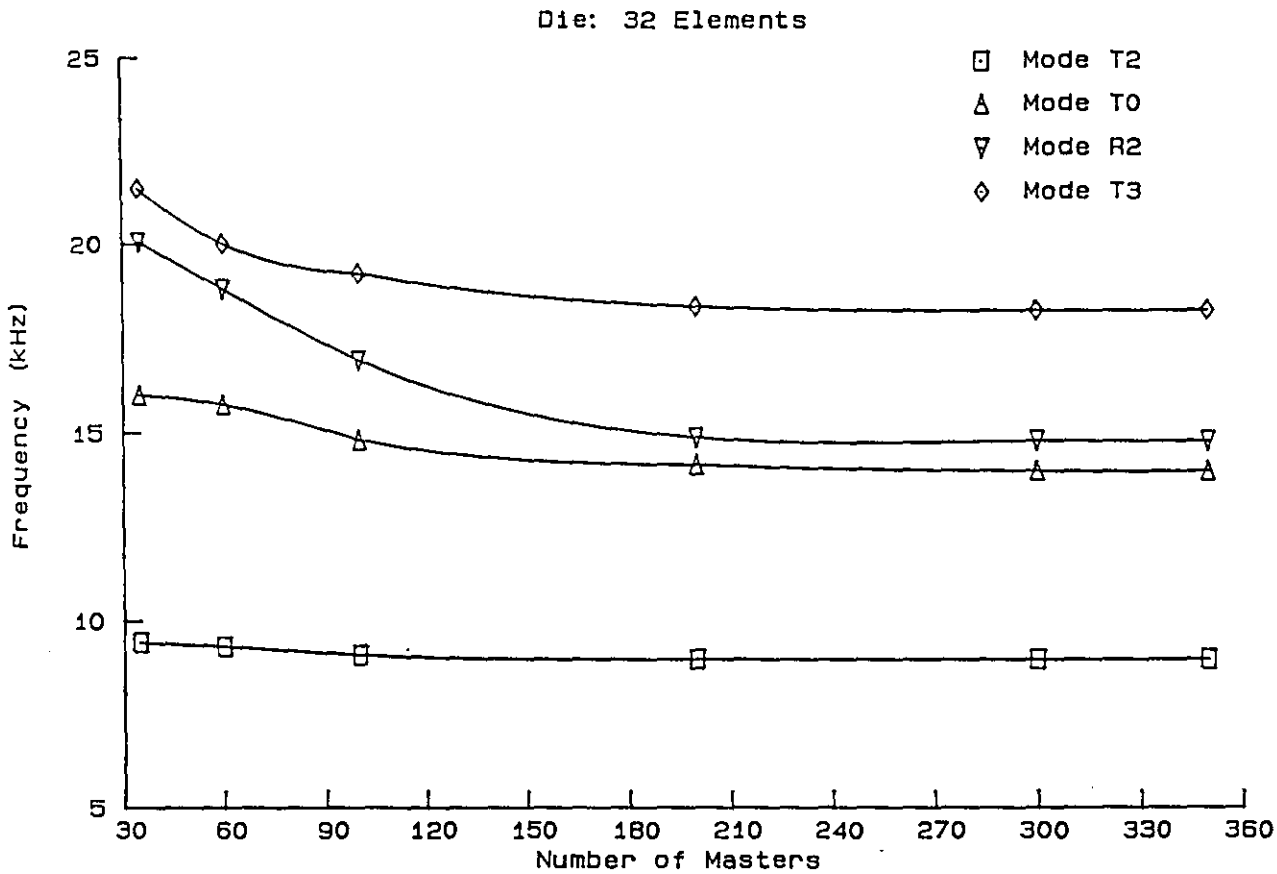

Figure 6.2 (a) Effect of Number of MDOFs on Calculated Frequency

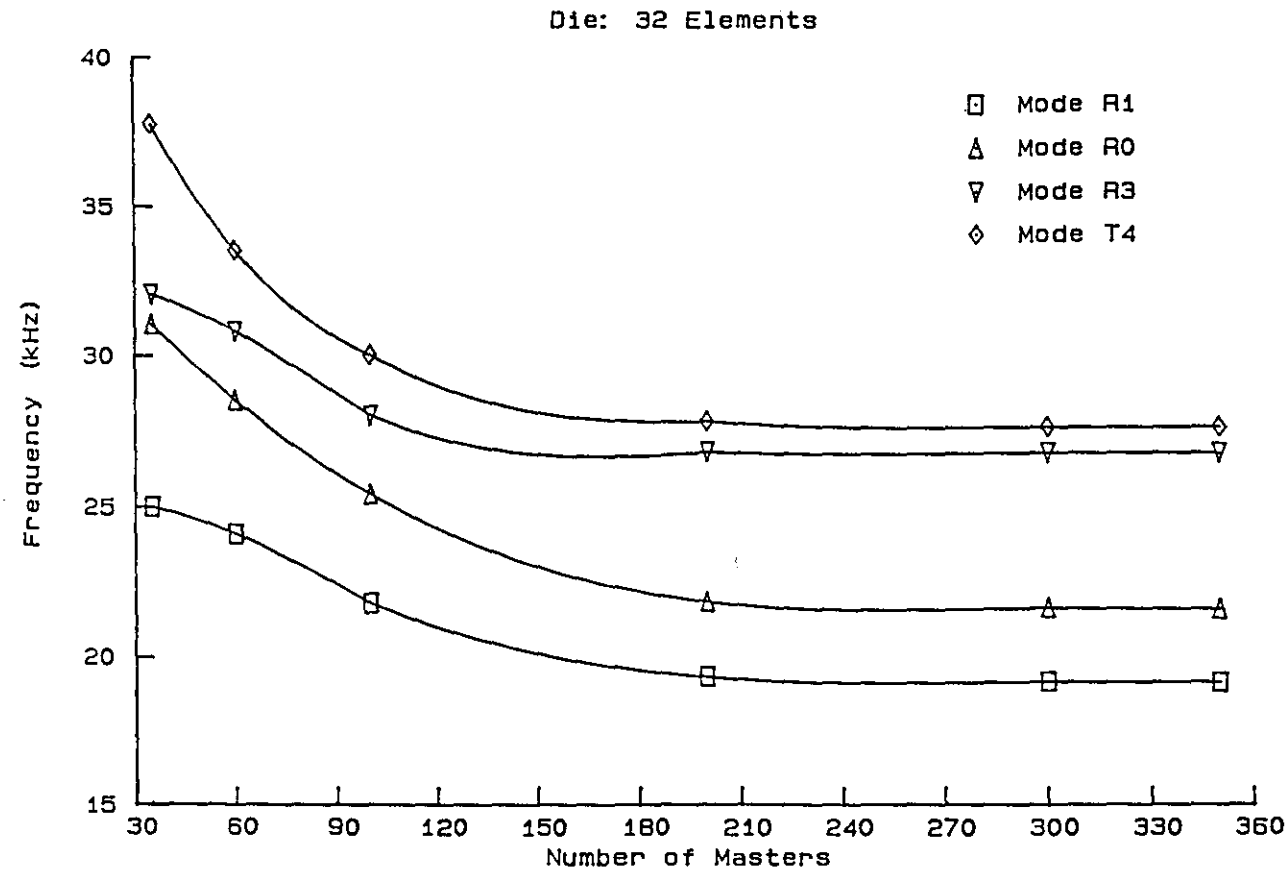

Figure 6.2 (b) Effect of Number of MDOFs on Calculated Frequency

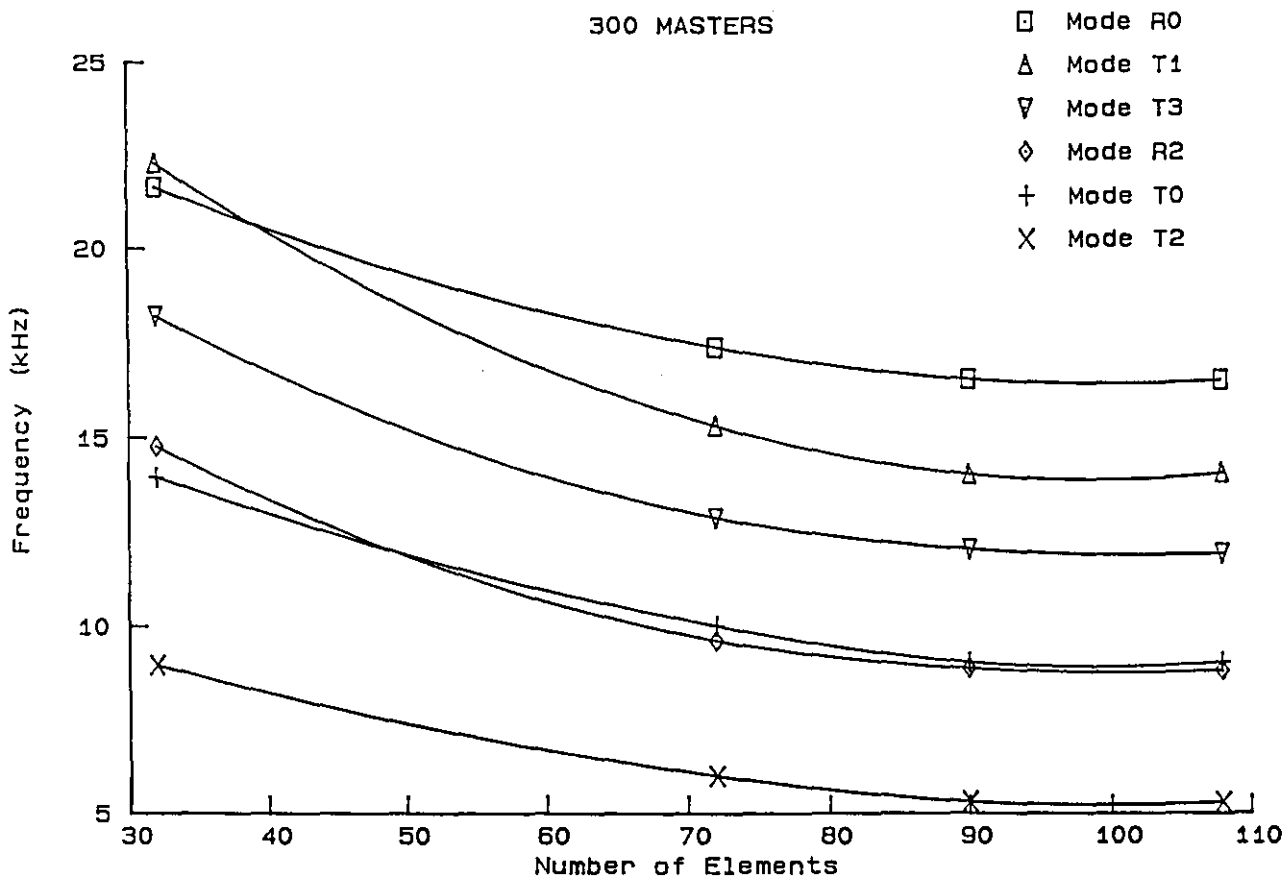

Figure 6.3 Effect of Mesh Density on Calculated Frequency

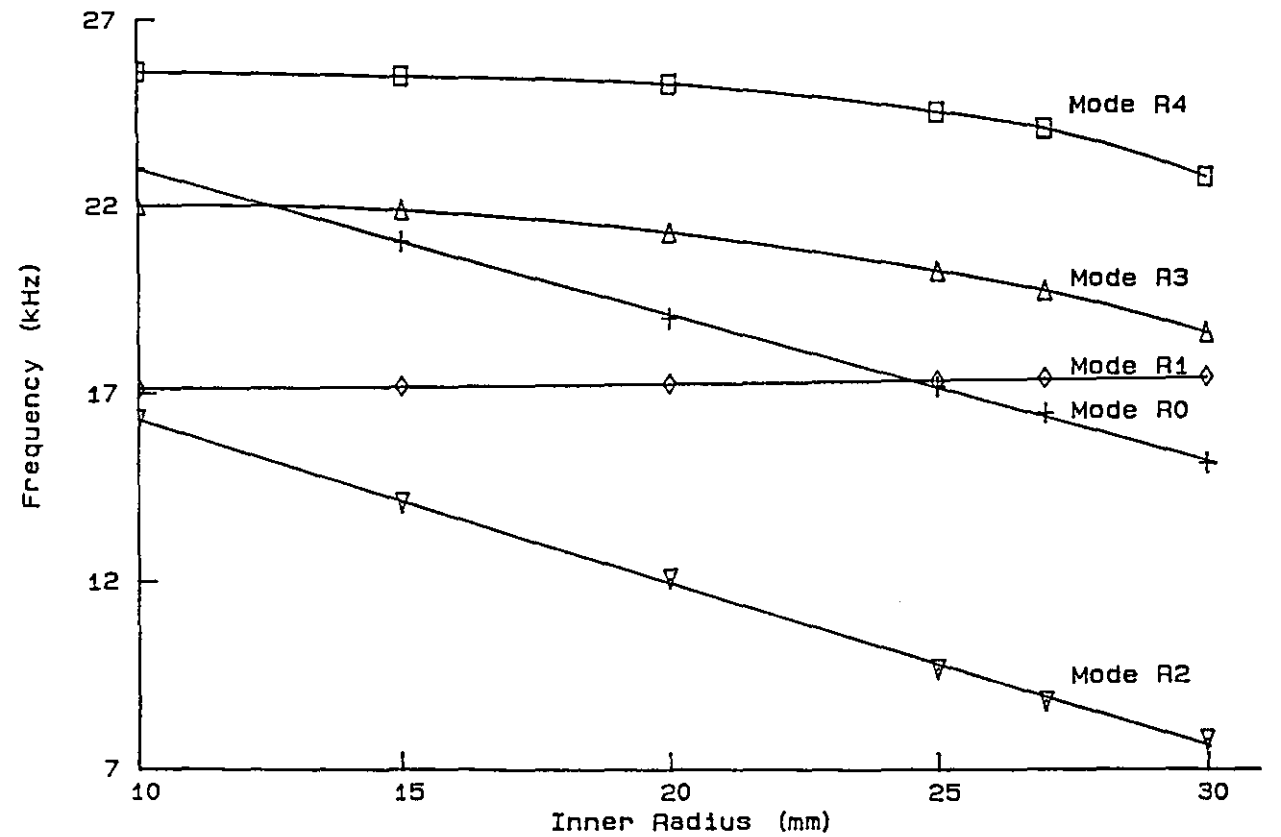

Figure 6.4 Inner Radius Effect on Calculated Frequencies

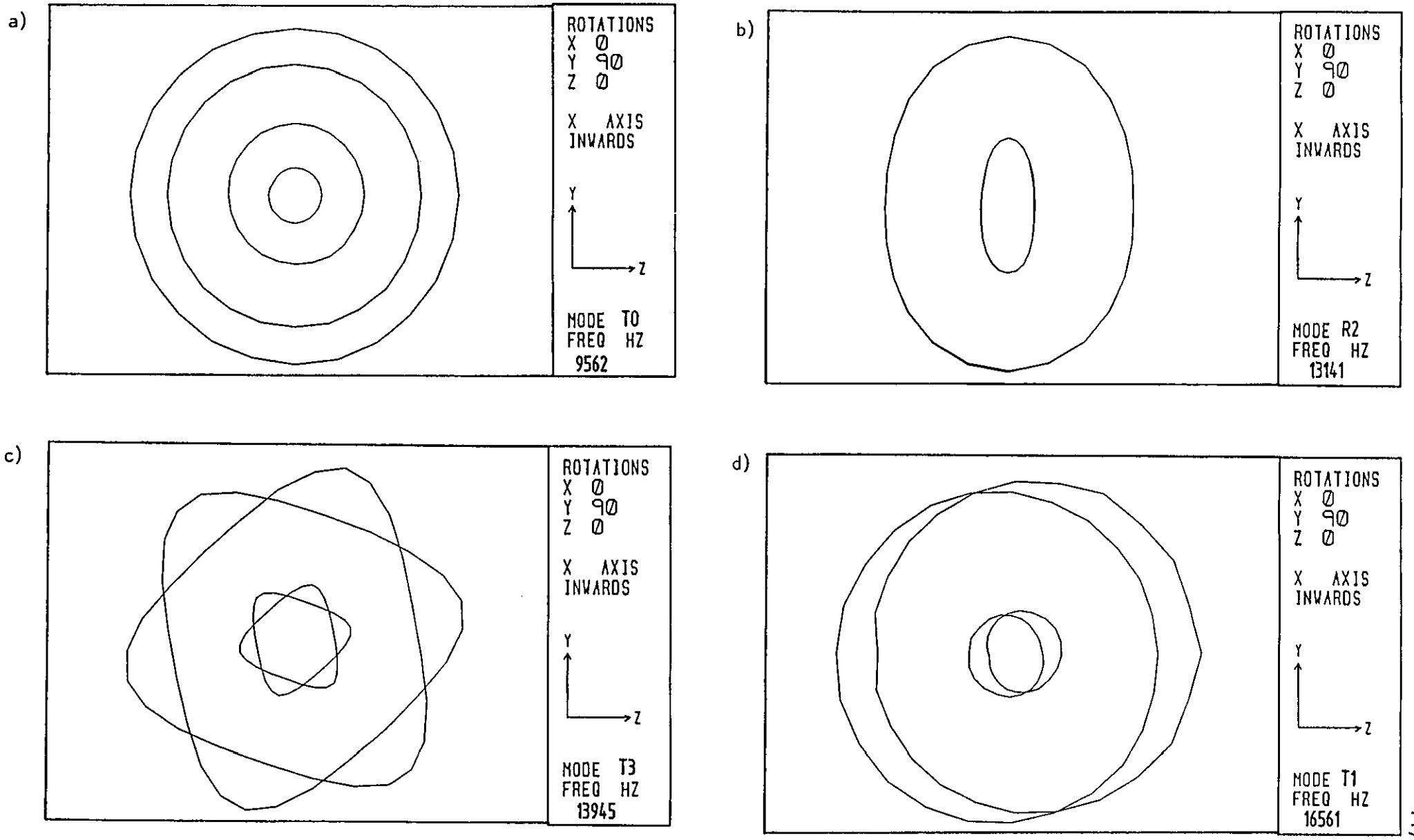

Figure 6.5 Modal Frequencies by FE Calculations

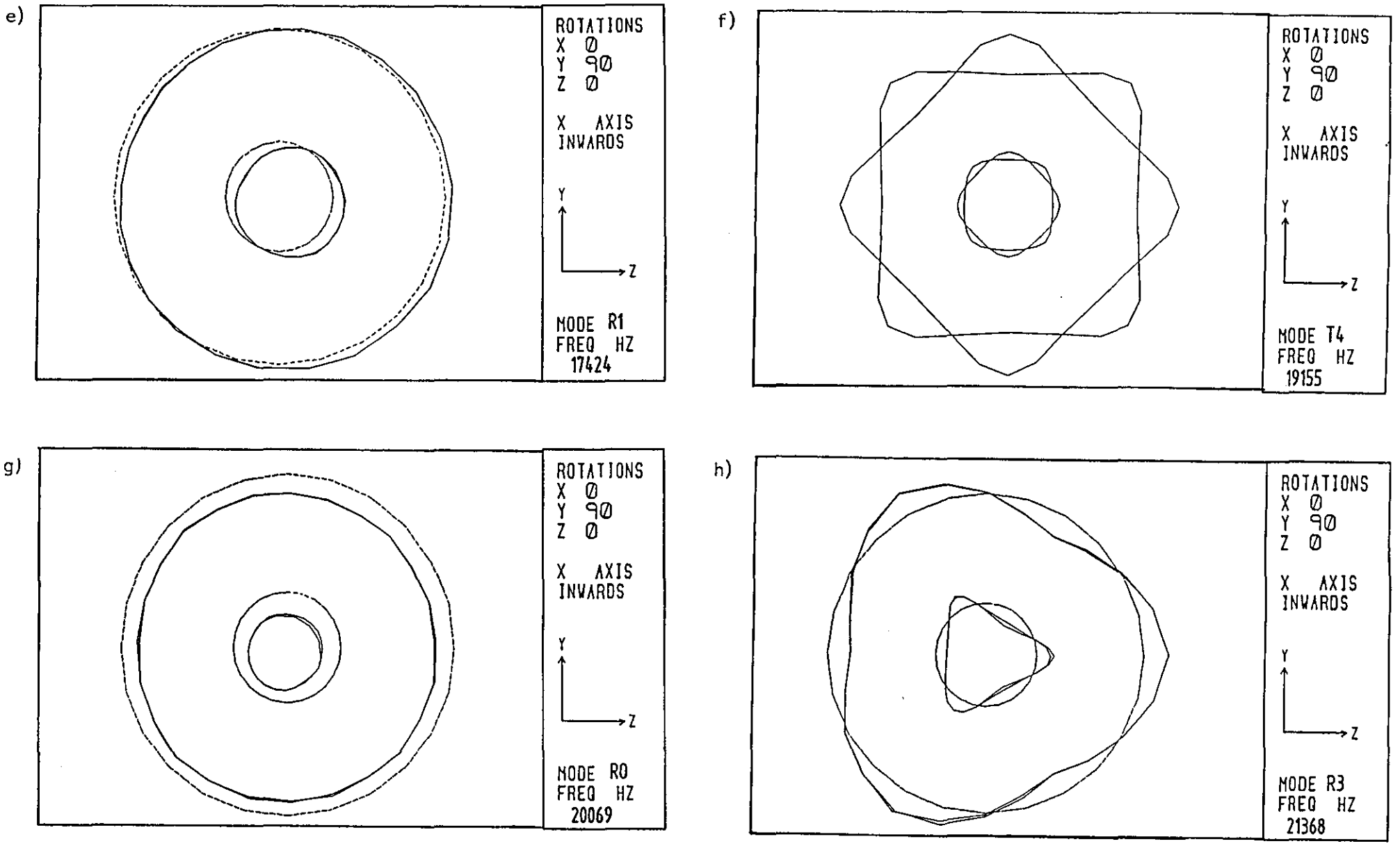

Figure 6.5 Modal Frequencies by FE Calculations

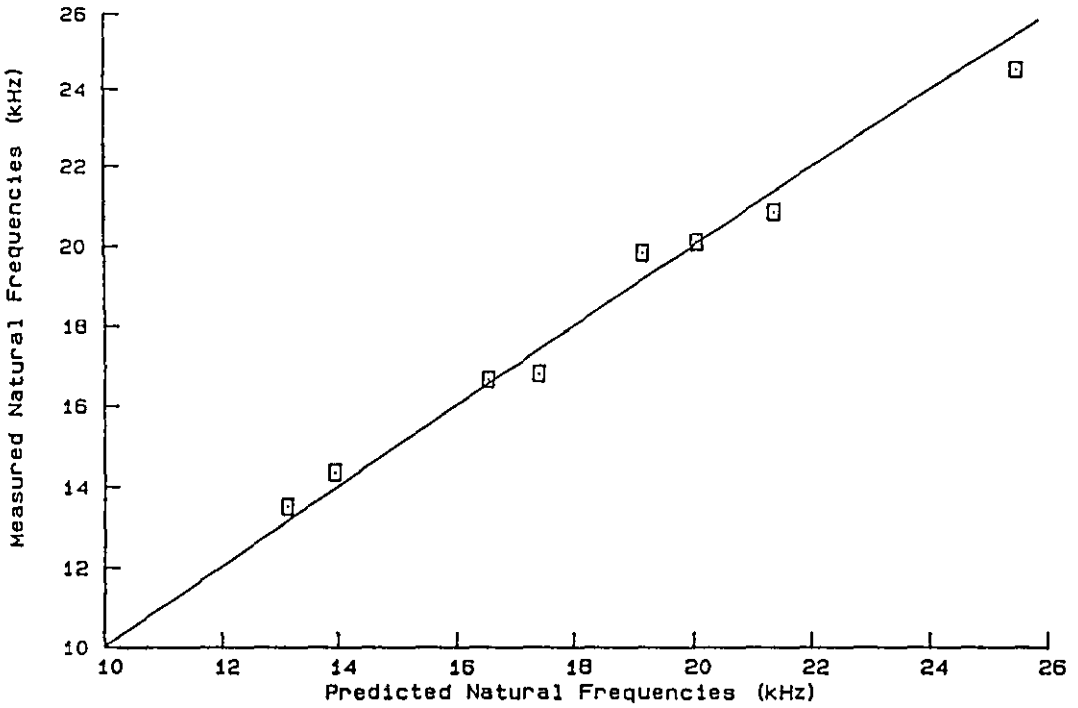

Figure 6.6 Comparing Measured and Predicted Data

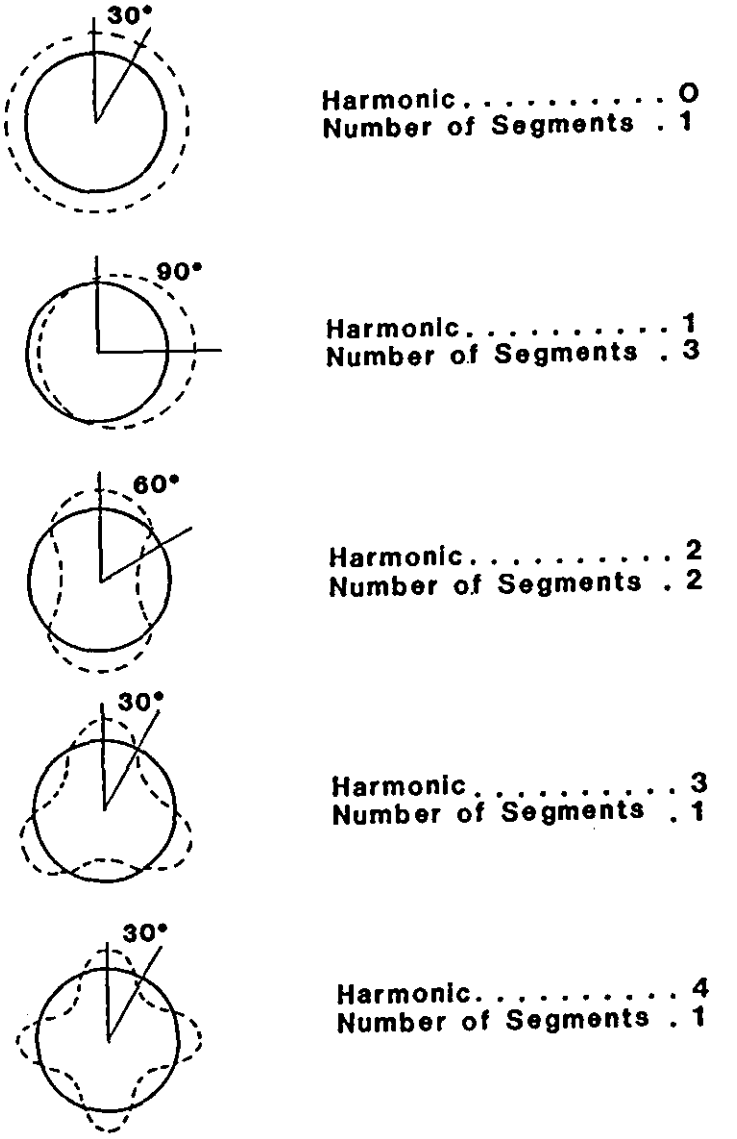

Figure 6.7 Mode Calculations by Modelling a 30° Die Segment

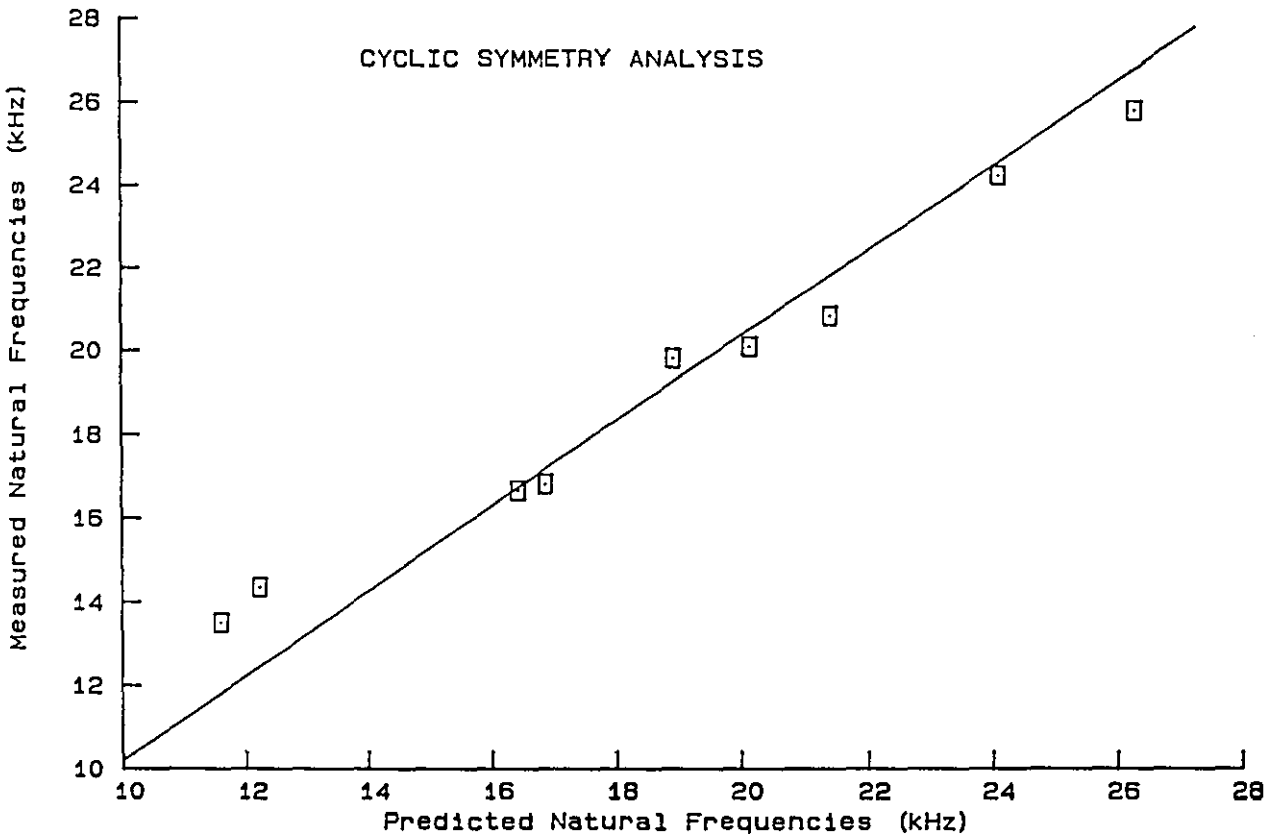

Figure 6.8 Comparison of Measured and Calculated Frequencies

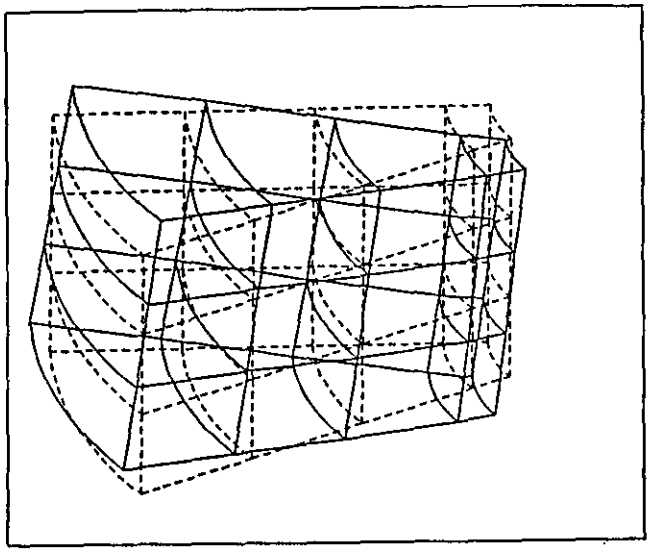

a) Mode: T0
Frequency: 9547 Hz

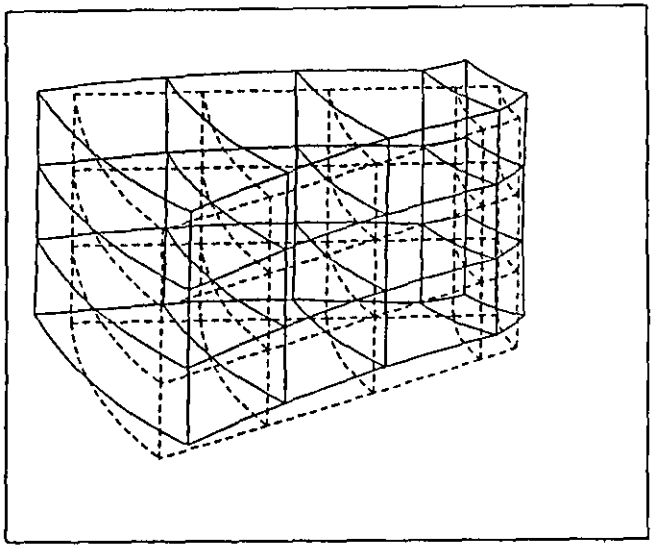

b) Mode: R2
Frequency: 11598 Hz

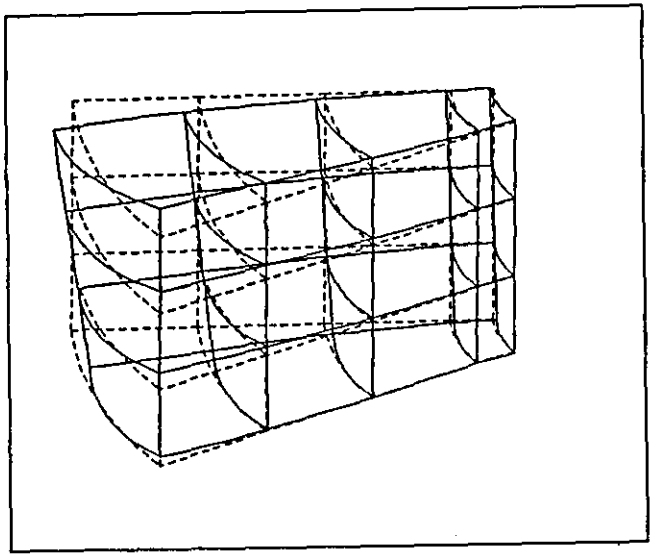

c) Mode: T3
Frequency: 12228 Hz

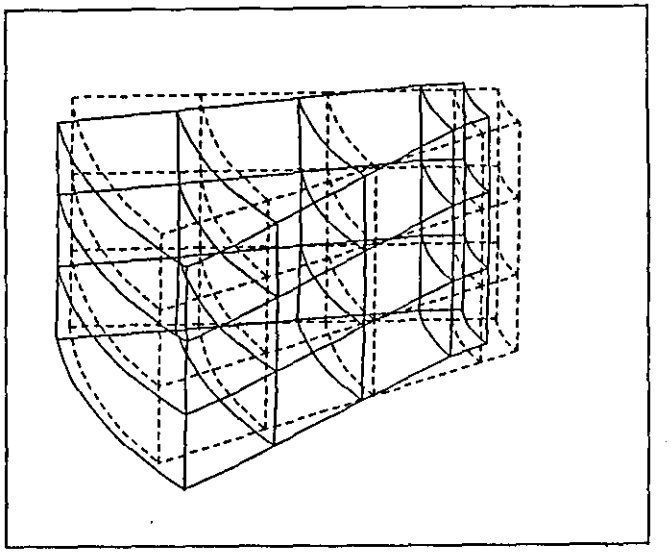

d) Mode: T1
Frequency: 16431 Hz

Figure 6.9 Cyclic Symmetry FE Model of Die Segment

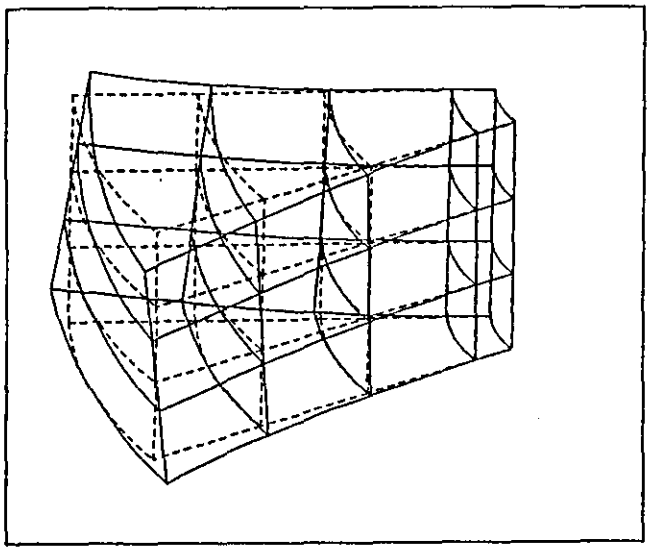

e) Mode: T4
Frequency: 18923 Hz

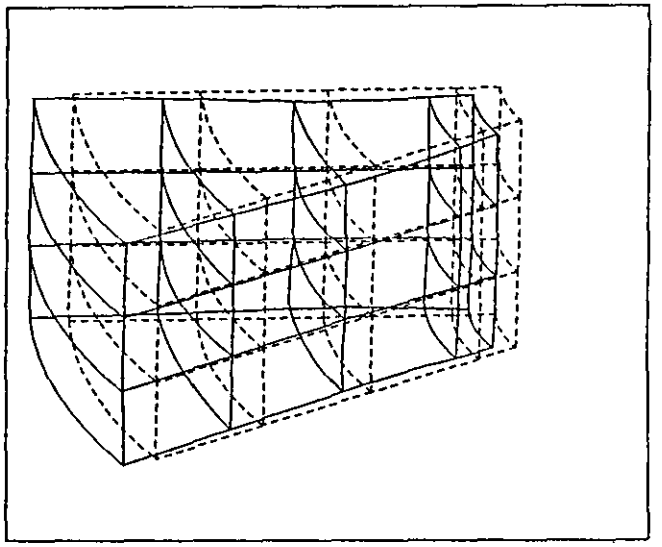

f) Mode: R0
Frequency: 20142 Hz

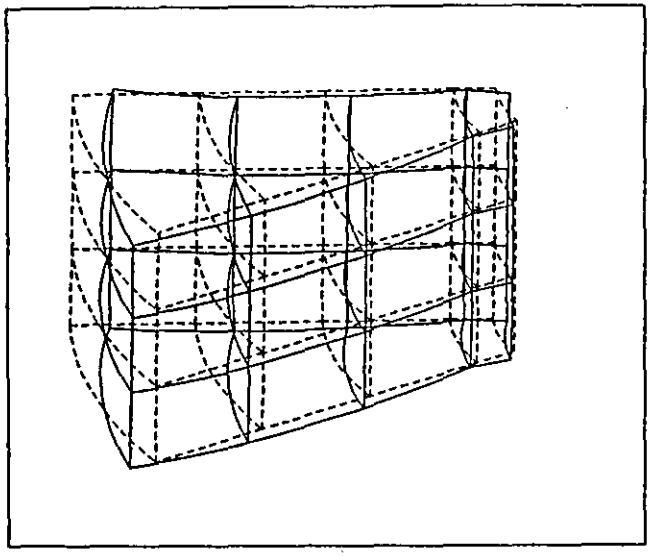

g) Mode: R3
Frequency: 21398 Hz

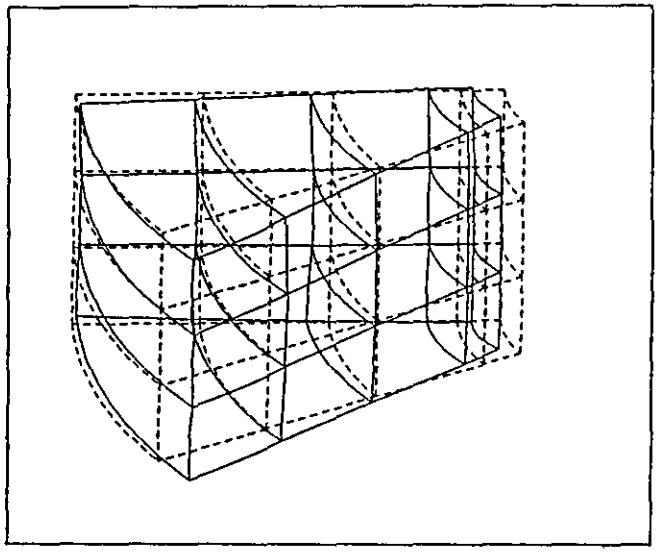

h) Mode: D2
Frequency: 24120 Hz

Figure 6.9 Cyclic Symmetry FE Model of Die Segment

CHAPTER 7
STRUCTURAL MODIFICATION IN THE REDESIGN OF ULTRASONIC DIES

7.1 STRUCTURAL DYNAMICS MODIFICATION (SDM) - POST-PROCESSING EMA DATA

The main purpose of ultrasonic die vibration study, is to improve die design by gathering knowledge of cylindrical die dynamic characteristics and subsequently effecting changes to die behaviour by isolation of the tuned R0 mode from unwanted modal influences, through physical modification of the die. Success in using SDM presupposes that an accurate formulation of a mathematical model of the die modal parameters was achieved from the two prerequisite stages of modal test and curve-fitting. Confidence in the die models has been attained by a rigorous approach to the experimentation and by verification of modal parameter estimations from comparison with FEM and ESPI results.

It is important at this point to discuss some of the limitations of SDM in redesign predictions. Firstly, since the technique is based on matrix perturbation, it is only possible to modify by a known value of mass, stiffness or damping at a measurement DOF, (i.e. at a grid point in a measurement direction from which data has been acquired and processed). In reality, a physical modification to a structure incurs some alteration of all three of these parameters, although in many cases the effect of one parameter is overriding.

The possibilities for design modification of an ultrasonic die are restricted to geometrical alterations of the die bolster. Since the inside diameter profile of the die is predefined by the forming requirements, it was decided to consider departing from the cylindrical shape of the die by modifying its outside diameter. Such an alteration is essentially a mass addition or subtraction modification approach to redesign and therefore this study concentrates on investigating the mass parameter in relation to mode separation.

The limitation of SDM to mass modifications at measurement DOFs has three consequences:

i) An alteration to the die geometry must be approximated by a distributed mass modification over the appropriate range of grid points. This is rendered more accurate if there is a large number of grid points available.

ii) Frequency shifting of F and D type modes is not feasible because no rotational DOFs were measured. Radial information however, is abundant and it is the radial influence of close modes that impairs die performance. It is clear that the EMA stage was geared towards die radial behaviour modification.

iii) Any mass modification of the outside diameter of the die will also result in an altered stiffness state. It is hoped that if die shape changes are chosen with care, the mass effect will dominate frequency behaviour of the unwanted modes. In addition, it is the frequency behaviour trends due to mass subtraction that are more useful to design considerations than absolute values. The purpose of the analysis is to search for an improved die shape which can be validated by Finite Element calculations, rather than attempt to achieve a greater degree of accuracy by predicting mass and stiffness relationships for every modification.

The second limitation in the use of SDM for die redesign is its reliance on a measure of excitation force in the modal testing stage. The mass, stiffness and damping matrix values of the mathematical representation relate the die response to the ultrasonic input voltage and not directly to the forcing function at the driving point. In Chapter 3 it was shown that the voltage and force are related by a known phase value and unknown magnitude value. Since the magnitude relationship was not evaluated, the modal model of the die represents a model formulated from an uncalibrated modal test (i.e. one where

the measured force and response signals are not referenced to the input voltages of the FFT analyser). The consequences of this limitation are twofold:

i) The modal parameter estimations are unaffected; frequency, damping and mode shape can all be determined from an uncalibrated modal test. The amplitude values describing the mode shapes however, are not directly related to actual structural deformation magnitudes at resonance.

ii) A new eigensolution can be calculated by a mass matrix perturbation to predict the resulting modal frequencies. However, it is not possible to relate the mass modification directly to a physical mass value when the measurement system is uncalibrated. This limitation is severe. Even if an accurate relationship between mass modification and frequency shift is not sought, it is still essential that mass modifications for trend predictions are near representations of real mass values. Alternatively, a method of relating real mass values to the effective masses used in SDM calculations must be found. This may be achieved by matching experimentally obtained mass/frequency trends with those from SDM predictions.

These errors in structural modification due to an uncalibrated modal test are resolved by relating actual mass to effective mass values by a scaling factor. This involves direct comparison between the experimentally determined frequency shift due to a physical modification of mass m_E, with the amount of mass m_T required in the theoretical analysis to achieve an equivalent frequency shift by SDM estimation. It is therefore not necessary to determine a direct relationship between measured voltage levels and the input forcing function in order to utilise the EMA data base for die redesign by SDM. A general explanation of uncalibrated test system errors is presented in a paper by Deel and Luk [59]:

> *"If the true response magnitudes are all scaled by a factor r, then all physical mass, stiffness and damping coefficients are scaled*

by 1/r. This amounts to using a non-standard system of units having magnitudes r times larger than the standard units, and so a given mass modification will be calculated as having the same effect as the equivalent modification scaled by the factor r on a valid modal data base. Thus, a specified 1kg mass modification will be calculated as if rkg had been specified."

This chapter presents the approach to system calibration by the use of scaling factors required for ultrasonic die redesign by mass modification of the die circumference. Design trends describing frequency effects of mass subtraction are determined by Sensitivity Analysis such that measurement DOFs can be ranked in order of their influence on modal frequency. In support of this work, the validated 3D finite element model of the die is modified in line with the SDM findings and the new modal frequencies are predicted. Finally, the die redesign recommendations for geometry alterations are instituted and validated by Modal Analysis.

7.2 VALIDATION OF SDM - A CANTILEVER BEAM STUDY

A preliminary SDM exercise was undertaken so that the effectiveness of the computer algorithm in predicting mass modification effects on modal frequencies could be assessed for a simple structure by comparison with experimental modifications. The secondary aim was concerned with validating the idea that a physical addition of material, in the form of a lumped mass, to such a structure has largely a mass addition effect in dynamic terms. A cantilever beam was adopted as the test structure because beam bending modes are analogous to radial ring modes of vibration and therefore success of the validation would inspire confidence in the SDM study of die models. In this case the modal tests were well-calibrated so that mass values assigned at beam measurement DOFs were directly comparable with real masses attached to the beam. Part of this study was carried out in collaboration with a final year project student [82].

7.2.1 Investigative Approach

A diagram of the experimental layout is presented in Figure 7.1. An electrodynamic shaker is driven by a broadband noise source generated in the FFT analyser. A load cell monitors the input force at the driving point on the beam and the vibratory response is measured by a roving accelerometer. A unigain piezoelectric accelerometer is attached to the beam by a layer of beeswax. Force and acceleration signals are processed as FRFs by the dual channel analyser and transferred to the pc for curve-fitting and modal parameter extraction.

The mass modification study takes two routes:

1. The effect on the first two modal frequencies, of sequential mass increases at a measurement DOF, are measured and calculated.

2. A single mass value is traversed along the beam grid, to determine the sensitivity of each measurement DOF to a mass modification.

The SDM algorithm limitation of point-mass addition is approximated experimentally by situating the mass on a small platform with a blunted conical base, thus allowing mass blocks to be attached to the beam over a small contact area. The measurement grid simplifies the beam to a line constituting 18 measurement positions.

7.2.2 Results

From modal tests, the first two transverse bending modes were found at 123 Hz and 786 Hz (Figure 7.2).

Figures 7.3 and 7.4 plot the measured frequency changes, due to a mass addition positioned at sequential grid positions on the beam, for the first and second mode respectively. Figures 7.5 and 7.6 plot the corresponding results of modifications calculated by the SDM algorithm (and based on beam modal test data). Both sets of results can be compared in Figures 7.7 and 7.8.

For both modes of vibration the variation in frequency between SDM predictions and test modification results is a maximum at the antinodes. The difference increases with mass, producing a variance of within 1% per 100 grams for both modes. The SDM predictions are consistently higher than the test frequencies, which is contrary to expectation, if there is a stiffening contribution from the added mass. Since both sets of results are estimated from the same original modal data base, there is no physical reason for these discrepancies and it can be assumed that the cause is associated with the matrix perturbation technique. The errors involved are sufficiently small to validate the use of SDM for mass modification calculations.

Of greater interest are the results which indicate the linear range for mass modification of the beam. Since structural redesign by mass modification generally assumes that mass alterations are small in comparison with the mass of the structure, it is useful to determine the mass value at which linearity breaks down (see Appendix C).

Figure 7.9(a) compares frequency estimations by SDM and modal test for mass addition at the antinode of mode 1. Figure 7.9(b) similarly compares these estimations at the antinode of mode 2. In both cases linearity holds in the test analysis to approximately a 0.6 kg modification. At this mass value, frequency decay is no longer linear but becomes asymptotic. The SDM results retain linearity over the test range.

These results show that for a linear cantilever with well separated, lightly damped normal modes, SDM predictions of frequency behaviour are meaningful for physical mass modifications at an antinode of up to 20% of the total mass of the original structure. From this study, it was deemed reasonable that redesign of the forming dies by mass alteration could be adequately calculated by SDM with assumed linearity, if the modifications were well within this limit.

7.3 DETERMINING A MASS CALIBRATION FACTOR FOR SDM FROM AN UNCALIBRATED MODAL TEST DATA BASE

7.3.1 Calibrating a Mass Addition

A similar study programme to that performed on the cantilever beam was carried out using the EMA data base as the starting point. Firstly, the EMA data base from the original die modal tests was used along with the SDM software algorithm to predict the modal frequency shifts due to mass additions at selected measurement DOFs. All modifications of the die are concentrated on its outer circumference as this is intuitively the most sensitive region in terms of radial mode frequency shifting. The mass values input for frequency estimations are at this stage merely numbers bearing no relationship with real masses, but are entered so that the mass versus frequency trend can be identified. Subsequently, block masses were added to the die at selected measurement DOFs to analyse physical mass modifications of the die outer circumference. For each mass addition the die was retested to determine the modal frequencies from FRF measurements of acceleration and voltage signals (as described in Chapter 5). The two sets of results are then compared to determine a relationship between "real" mass and "theoretical" mass. This allows a mass calibration factor to be found such that the SDM estimated frequencies become meaningful.

An initial requirement of this study is to identify the linear range for mass additions in SDM. The incomplete Taylor Series expansion used in the matrix perturbation assumes mass alterations that are small in comparison to the mass of the structure. The limitations were found for the cantilever beam and must be similarly determined for the die. Since a mass calibration factor is required to give meaning to the SDM mass values, the linearity limitation could have severe implications on the possible safe range of use for this technique.

A measurement DOF is selected to analyse the added mass versus frequency trends for three radial modes of vibration; namely the R0, R1 and R3 modes.

It has been shown that these three modes are most likely to couple strongly and interfere with die performance (see Chapter 5). The modification position is an antinode of the R3 mode and close to the antinode of the R1 mode (the R0 mode is entirely antinodal). The position is chosen to maximise sensitivity to structural modification so that the limit of mass modification in SDM calculations can be determined. Sensitivity analysis is used for two purposes. Firstly, the sensitivity of a modal frequency to a known mass addition at a particular DOF can be considered. The sensitivity is then defined as the initial slope of the curve showing the rate at which the natural frequency approaches the anti-resonance of the FRF. Secondly, the sensitivity of the measurement points on the structure can be considered. The achievable frequency shift of a mode due to a mass addition is dependent on the position of the measurement DOF in the harmonic wave. This type of sensitivity analysis is also known as "degree-of-freedom ranking". In this study, the mode sensitivities are calculated and the DOFs are ranked intuitively for mass modification effects.

The modal frequency dependencies on mass modification are presented in Figures 7.10, 7.11 and 7.12 for the R1, R0 and R3 modes respectively. The linear range, indication the mode sensitivities, was identified for each curve and replotted for smaller mass increments. The effective theoretical mass sensitivity (S_T) of each mode was then derived from the slope of the linear graph and found to be:

$$S_T\,(R1) = 0.20\ Hz/g$$
$$S_T\,(R0) = 0.22\ Hz/g$$
$$S_T\,(R3) = 18.4\ Hz/g$$

The mass modification effects on these three modes, from physical mass additions to the die at the same measurement DOF, are plotted in Figures 7.13, 7.14 and 7.15. The sensitivities are similarly determined from the initial slope of the mass versus modal frequency curves and are found to be:

$$S_E\ (R1) = 0.68\ Hz/g$$
$$S_E\ (R0) = 0.93\ Hz/g$$
$$S_E\ (R3) = 19.8\ Hz/g$$

From these sensitivities, the estimations of the calibration factor required for the modal test mass modification terms are:

Estimated Calibration Factor (r)	
Mode	$r=S_E/S_T$
R1	3.33
R0	4.23
R3	1.08

The scaling factor r required to produce equivalent values of mass modification on the EMA data base has been estimated to be between 1 and 5. For the three radial modes the predictions of r have been to a similar order of magnitude but the results do not lead to a direct relationship being determined between the magnitude of the measured voltage signal and the magnitude of the forcing function input to the die. The possible sources of inaccuracy in this attempt to obtain a value for r, are numerous. It is not realistically practicable to physically simulate a purely mass modification at a point and in a well defined measurement axis on the die. The base diameter of the mass blocks which were fixed to the die was 10 mm, which was more representative of a distributed mass addition. The mass covered only one measurement grid point and was therefore not distributed in the theoretical model. The stiffness contribution of added mass has been ignored, which becomes an invalid simplification for the larger mass additions, where the added material significantly distorts the shape of the die, effectively increasing its thickness over a part of the structure. The directionality of added mass cannot be physically controlled in line with the theoretical model. Although radial effects are dominant, the lumped mass experimental approach will affect motion in all degrees-of-freedom. Further, the modal data base model assumes SDOF

vibration characteristics in the vicinity of each mode. Additional damping from the physical modifications can exacerbate modal coupling rendering the SDOF approximation less valid. In the experimentally determined curves (Figures 7.13 to 7.15) the data scatter provides an additional source of error in estimating the initial slope from the three graphs.

On the plus side, the calibration estimations provide ballpark figures for considering actual die design modifications. For the three radial modes, the modal frequency regression trends are very similar on comparing experimental and theoretical mass addition curves. One result which is extremely helpful for die redesign, is the high sensitivity of the R3 mode to a mass modification compared to the R0 and R1 modes. This indicates that the desired mode separation (involving isolating the R0 mode at 20kHz and shifting the R3 mode to a higher frequency without bringing the R1 mode too close to R0) should be a feasible proposition with careful choice of modification. The sensitivity of the R3 mode is over 19 times that of the R0 or R1 modes and more reliable data was therefore obtained from the analysis of the R3 mode. Consequently, the calibration factor is approximated to unity at this stage of the work and it is assumed that the voltage signal measured during modal testing was equal in magnitude to the forcing function applied to the die. This is a first approximation and will be refined by evidence gathered from further modification studies.

7.3.2 Evaluating a Mass Subtraction Calibration

The initial mass calibration factor estimation and the effectiveness of SDM predictions are to be assessed by attempting to redesign a die cylinder. In order to test the design approach, the EMA data base of the steel die, which is presented in Chapter 5.4.1, will be used as the basis of the SDM analysis. The modal frequencies in this case were R1 at 19363 Hz, R0 at 20067 Hz, T4 at 20656 Hz and R3 at 22440 Hz. Rather than trying to achieve R0 mode isolation, the prediction of frequency shifts in all four of the modes is attempted, as this will give a stronger indication of the validity of the SDM mass subtraction simulation. To achieve this aim the following strategy is adopted:

1. Calculate the frequency sensitivity to mass subtraction of the outer circumference measurement DOFs for the R1 and R3 modes.

2. Choose an alternative die geometry and estimate the new modal frequencies by approximating the physical alterations to mass subtraction modifications.

3. Modify the steel cylinder and retest the die to measure the modal frequencies and mode shapes of the radial response.

4. Evaluate the design process in terms of the success in predicting modal frequencies by mass modification.

This stage of the work attempts to prove the redesign approach by considering a practical example that will lend confidence to the redesign of the actual aluminium forming die.

The R1 and R3 mode sensitivities at three radial measurement DOFs on the die are illustrated in Figure 7.16. The chosen DOFs represent measurement grid points closest to a node, an antinode and an intermediate position on the harmonic wave in each case. As expected, the modal frequencies are most influenced by mass subtraction at an antinode of the radial mode. From the sensitivity graphs, the most effective design alternative for achieving increases in the radial mode frequencies would appear to be a modification involving removal of mass from the die at a position diametrically opposite to the excitation input, which is an antinode of both the R1 and R3 modes. This modification is not chosen however, because it is anticipated that for the particular case of the R1 mode, physical removal of die material from an antinode could have a greater stiffness reduction effect than a mass subtraction effect, the possible outcome being a reduction in the R1 modal frequency. The evidence that invalidates this type of geometry alteration adequately simulating a mass modification in the R1 mode, comes from two sources; firstly from the resulting frequency behaviour due to die inner radius variation predicted by

FEM (Figure 6.4) and secondly from 2D plane stress FE models which calculated the effects of size, position and number of flats on the natural frequencies of forming dies [42]. In Figure 6.4 (and discussed in Chapter 6.3.3) the R1 frequency was unaffected by the geometry alteration, the mass and stiffness effects effectively cancelled each other out. In the work done by Cheers [42], both R1 frequency increases and decreases were reported, depending on the configuration analysed. The anomalous nature of the R1 mode which causes these phenomena is discussed in Appendix B.

The die is modified to produce two flats 180° apart, machined on the outside surface and which include angles of 40°, as shown below. The SDM analysis simulates this process by distributing the mass subtractions over the measurement DOFs lying within the machined area. A known mass of material is removed from either side of the cylinder and the results of the modal test for the radial mode frequencies are compared with the SDM predictions.

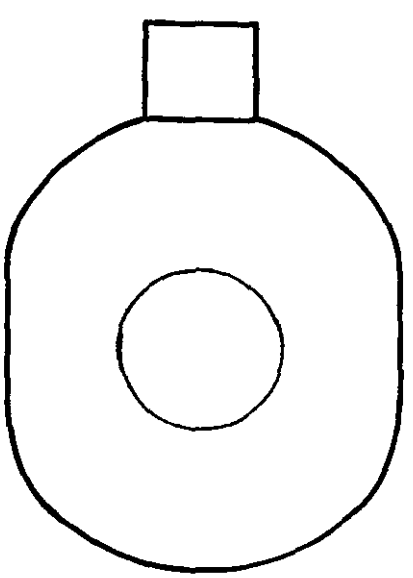

2-Lobed Die

The calculated mode sensitivities to mass subtraction are presented in Figure 7.17. The modal frequencies predicted by SDM for removal of mass at measurement DOFs representing the machined flats, are reported in Table 7.1 along with the EMA measured die frequencies for the original and modified cylinder.

Modal Frequencies (Hz)			
Mode	SDM	EMA	
	Lobed Die	Lobed die	Original Die
R1	19433	19570	19363
R0	20316	20165	20067
T4	20940	21075	20656
R3	24519	24690	22440

TABLE 7.1: ESTIMATED NATURAL FREQUENCIES OF A 2-LOBED STEEL CYLINDER

Values of calibration factor can only be estimated if it is assumed that the experimental mass subtraction versus frequency curves follow the same linear trends as the SDM sensitivity curves. Although this assumption has not been validated for mass subtraction events, linearity could reasonably be expected in this mass range (from 0-1.8% of the total original cylinder mass). Some support for this assumption can be gained from the very similar trends between experimental and theoretical curves obtained in the mass addition study. Based on a linearity assumption, the sensitivity values and calibration factor estimations are given in Table 7.2.

Mode	S_E (Hz/g)	S_T (Hz/g)	$r=S_E/S_T$
R1	1.59	0.54	2.94
R0	0.75	1.92	0.39
T4	3.22	2.19	1.47
R3	17.31	15.99	1.08

TABLE 7.2: MASS SUBTRACTION SENSITIVITIES AND CALIBRATION FACTOR ESTIMATIONS

The results from the mass subtraction effects compare well with the mass addition analysis, especially for the R3 mode which predicts the same scaling factor of 1.08 for uncalibrated modal data in both studies. Further evidence that there is approximately a one to one relationship between measured voltage levels and the magnitude of the excitation, is provided by the recorded behaviour of the T4 mode to a structural modification. The T4 and R3 modes can both be thought of as belonging to the family of thick cylinder modes that are analogous to beam flexural modes (see Appendix B). Despite the sensitivity of T4 being considerably lower than for R3, the resulting calibration factor from T4 modal frequency estimations of 1.47 can be rounded down to unity as a rough guideline for die redesign calculations. A value of r of approximately 3 is estimated from both mass addition and subtraction sensitivities of the R1 mode. However, for R1 and R0 the sensitivity estimations are poor because the anomalous nature of these two modes renders the simplification of geometry alterations to mass modifications invalid. In the case of the R0 mode, a mass subtraction by creating lobes is perceived as a combination of reduced mass and stiffness effects, such that the modal frequency is little affected by the physical modification, despite the fact that this mode is entirely antinodal. Although this leads to difficulties in anticipating the R0 modal frequency outcome of a die redesign, the significant advantage from this result is that most die geometry alterations will tend to maintain the R0 mode close to its original frequency and analysis can therefore concentrate on achieving the desired frequency shifts in the other close modes. This is particularly beneficial to the aluminium forming die redesign programme, where the sensitive R3 mode is to be separated from the insensitive R0 mode by a similar type of geometry alteration.

7.4 REDESIGN OF AN ALUMINIUM FORMING DIE

7.4.1 SDM Calculations for a Three-Lobed Die

The results provided by the previous sections on mass modification have led to the redesign approach for the aluminium forming die being directed towards

removal of mass from R3 mode antinodes, to create a three-lobed die geometry. It is anticipated from previous findings that the R0 and R1 modes will not be significantly affected by this alteration, other than to exhibit reduced modal coupling activity. The modification is aimed at achieving a considerable increase in the R3 modal frequency with the result of isolating the R0 mode.

Mass is removed from the die by creating three equispaced flats to include angles of 60°. The three lobes constitute 210 grams of mass removed, a loss of approximately 10% of the total mass of the die. The new die profile resulting from this modification is shown in Figure 7.18.

The R3 mode antinodes have already been identified as the most sensitive measurement DOFs to a mass modification. The calculated sensitivities of the T4 and R3 modes to a mass subtraction are presented in Figure 7.19. The R0 and R1 curves in the figure are obtained by adopting the estimated calibration factors for each of these two modes determined from the mass subtraction study of the steel die. The plotted data is therefore, the product of the mass value entered into the SDM calculations and the scale value appropriate to that mode, on the abscissa and the modal frequency calculated for the entered mass value, on the ordinate. The desired result is therefore to predict the four modal frequencies of the modified die directly from this graph.

By extracting the frequencies at a mass subtraction value of 210g from Figure 7.19, the following modal frequencies were predicted:

R1	16904 Hz	(+104 Hz)
T4	20082 Hz	(+347 Hz)
R0	20126 Hz	(+50 Hz)
R3	21556 Hz	(+731 Hz)

The achieved frequency increases are shown in brackets. By altering the die in this way, the SDM analysis predicts that the R3 mode will increase in frequency and separate from the R0 mode. In obtaining this improved vibration behaviour, the T4 and R0 modal frequencies have moved closer. Previous

experience of die operation has indicated that R0 and T4 modal coupling does not adversely affect the performance of the die and that the R0 mode will dominate the response under such conditions. The success of the SDM model and modified die operation must be judged in terms of accuracy before any conclusions can be drawn.

7.4.2 Validating the SDM Analysis

A modal test was performed on the three-lobed die to measure its natural frequencies and modes of vibration. In conjunction, measurement data was gathered using the ESPI technique to determine modal parameters. The results of these experiments are presented in Table 7.3. The classification of the modes in the table is consistent with all previous studies of thick cylinders in this thesis. However, with flats machined on the die, the mode shapes are no longer sinusoidally distributed displacement patterns described by this method of harmonic wave numbering. The cylinder mode nomenclature is retained in order to relate the effects of the design modification to modal frequency shifts. Typical mode shapes determined from FRFs at measurement DOFs around a modified die "circumference" are presented in Figure 7.20, to illustrate the departure from regular cylinder behaviour.

When it was verified that the SDM estimations appeared to be representative of the actual behaviour of the die, the two other measured modes, T1 and T3, were similarly analysed by mass subtraction. The T3 modal frequency was predicted by assuming a mass calibration factor of unity (in line with R3 behaviour), whereas the T1 modal frequency estimation adopted the R1 calibration factor to scale the sensitivity curve.

Finally, The FE model of the original die cylinder (see Chapter 6) was modified to calculate the vibration response of the three-lobed die. The modal frequencies predicted by the model are given in Table 7.3, along with the SDM estimations and measured frequencies.

Mode	Modal Frequencies (Hz)			
	SDM	EMA	ESPI	FEM
R2	14214	-	-	13922
T3	14355	14120	14060	14060
R1	16904	17030	17030	17386
T1	18893	18410	18600	19034
R0	20126	20125	20030	19989
T4	20082	-	20160	20238
R3	21556	21525	21590	22792
		21950	22000	

TABLE 7.3: MODAL FREQUENCY ESTIMATIONS FOR THREE-LOBED DIE

7.4.3 Discussion and Conclusions

Generally, the uncalibrated modal test data base can be used to predict the effects of a die design modification by employing the SDM algorithm. The calibration factor required to simulate the magnitude of the excitation force by a voltage signal, was found to be unity. The zero order and first order radial and torsional modes could not be adequately predicted by assuming that an alteration involving removal of material from the die circumference, could be simplified to a mass subtraction effect. The modal frequencies could however, be predicted by determining effective calibration factors, unique to the zero and first order modes.

On comparison of the SDM calculated modal frequencies and the EMA measured values, the method of adopting the unity mass calibration factor for all modes except the anomalous zero and first order mode and obtaining specific effective calibration terms for these two mode types, has resulted in a high degree of agreement between the sets of frequency values. The largest discrepancy is 2.5% for mode T1, with accuracy of 0% and 0.09% discrepancy for the R0 and R3 modes respectively. The T3 mode was predicted to be unaffected by the design modification, whereas measurement of the mode shows a slightly reduced frequency value. A possible explanation is that the T3 and R2 modes now occur at very close frequencies and exhibit coupled

behaviour. This was predicted by the SDM analysis but not confirmed by either EMA or ESPI studies, which could not detect the R2 mode in the measurement range.

The concern discussed earlier, that the modified die would continue to exhibit modal coupling of the R0 and T4 modes, has been shown to be true. The dominance of the response by the R0 mode has also been verified, by the inability to detect any T4 contribution in the modal test. The ESPI measurements could distinguish the two modes but found the T4 response to be weak and lightly damped. Frequency response function representation of the EMA and ESPI measurements are presented in Figures 7.21 and 7.22 respectively.

The finite element analysis predictions of modal frequencies of the 3-lobed die are within 4% discrepancy of the EMA estimations. Boundary plots of the calculated modes are presented in Figure 7.23. This further supports the FE modelling procedure outlined in Chapter 6. The validation of the FE model allows calculation of the effects of a design alteration on modal behaviour, before any physical modifications are instituted. Accuracy is paramount if the performance of a die is to rely on FE calculations of modal response.

The three-lobed die geometry successfully separates the problematic R3 mode from the R0 mode, whilst maintaining the R0 mode within the operating frequency band. The two lower frequency modes, R1 and T1, are not consequently frequency shifted too close to the operating frequency. Despite the proximity of the T4 mode, it has negligible influence on the R0 mode response. The main disadvantage of the 3-lobed design is the loss of amplitude uniformity around the die circumference. Figure 7.20(a) clearly illustrates the R0 mode shape distortion which results in an amplitude reduction at the die flats. This does not necessarily imply a reduced working amplitude at the forming surface, which is not predicted by the FE model (Figure 7.23(c)) but must be confirmed by trials.

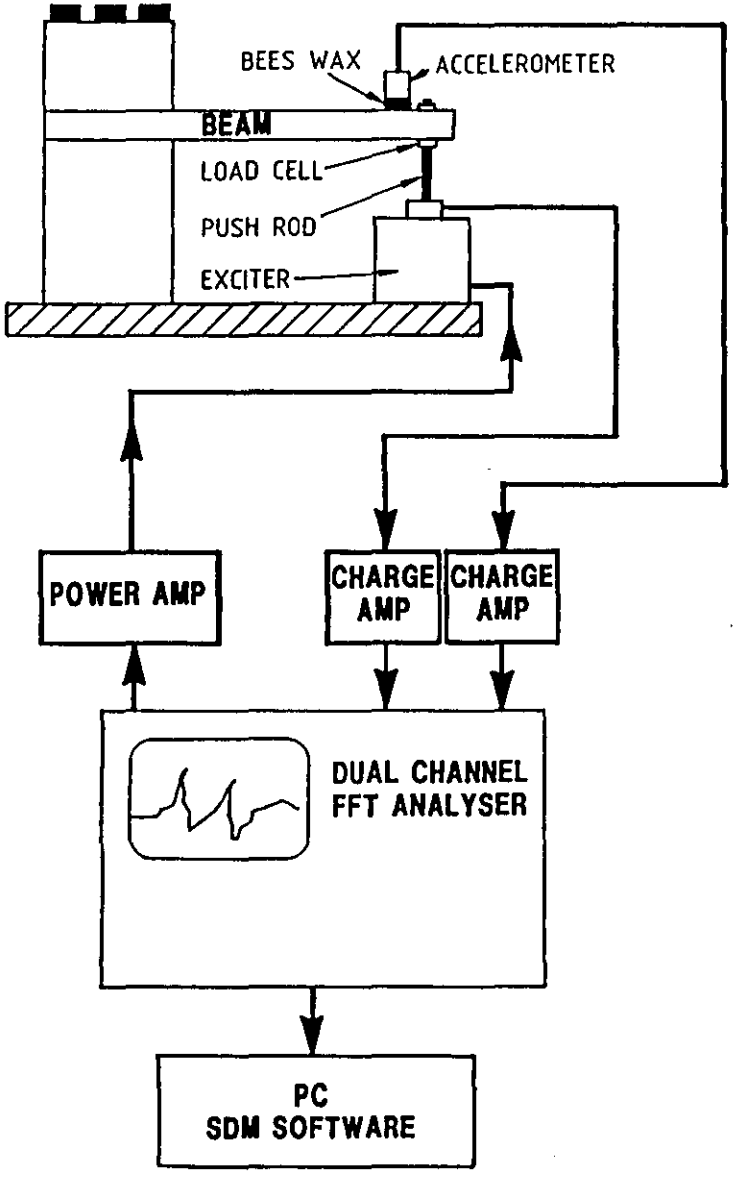

Figure 7.1 EXPERIMENTAL LAYOUT FOR EMA AND SDM OF CANTILEVER BEAM

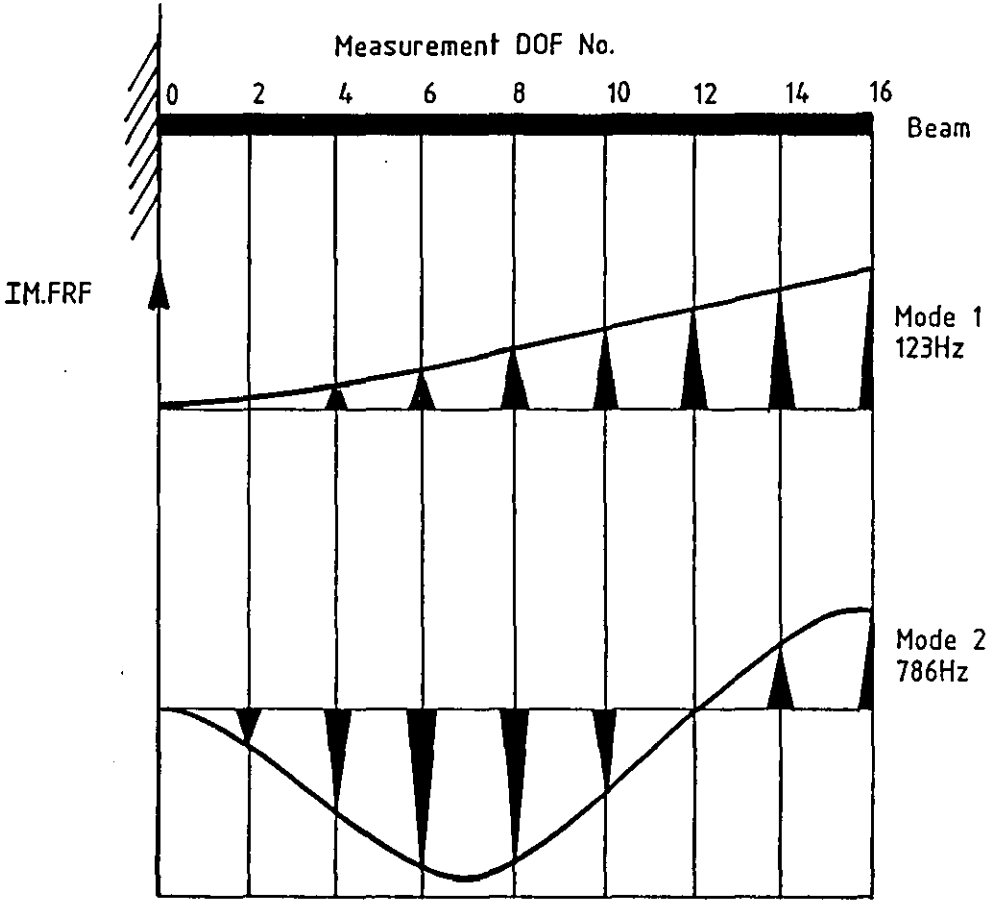

Figure 7.2 Beam modes of vibration by Quadrature Peak Picking from modal test.

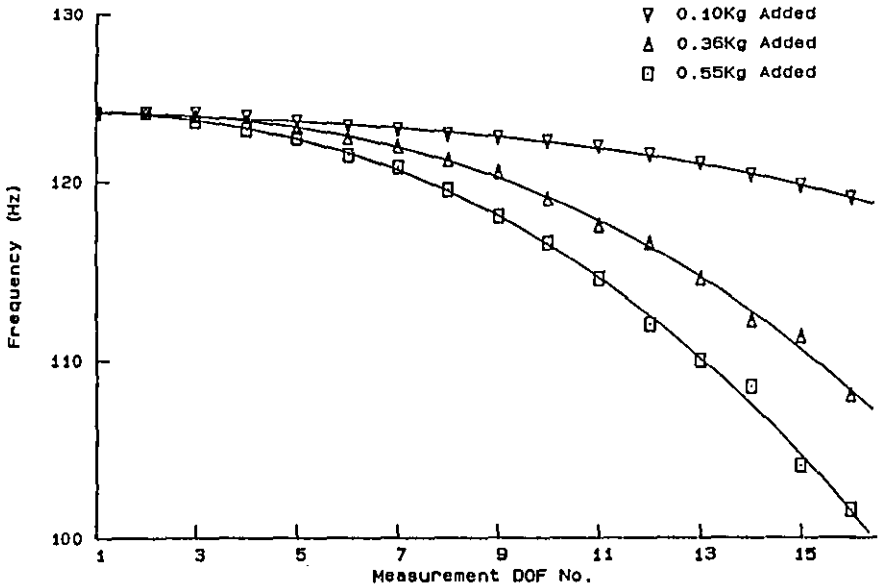

Figure 7.3 Measurement DOF Sensitivities for Mode 1

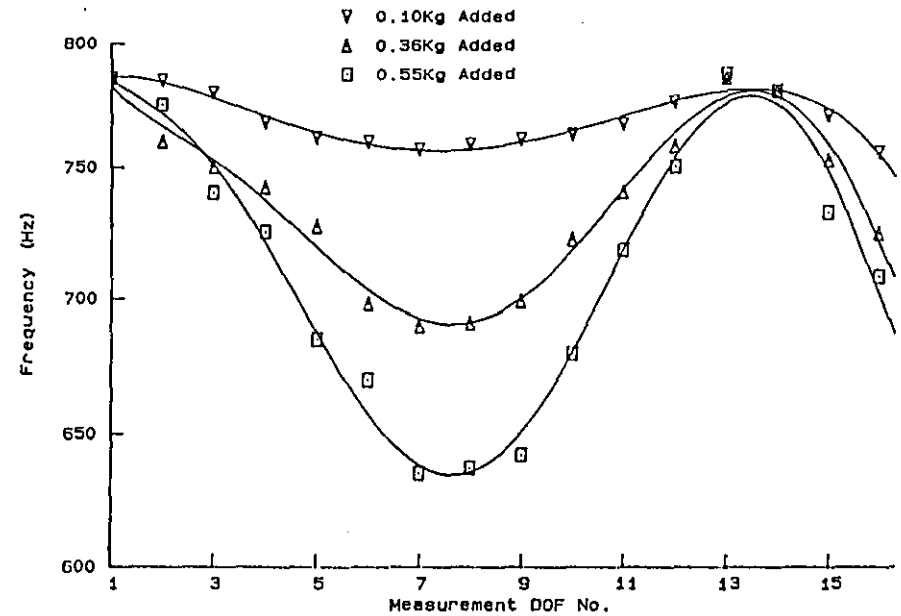

Figure 7.4 Measurement DOF Sensitivity for Mode 2

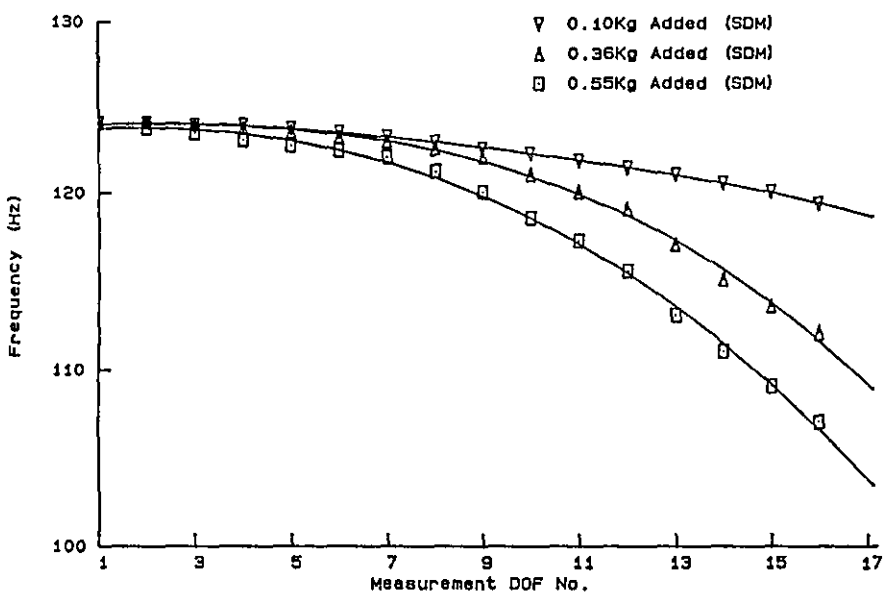

Figure 7.5 Sensitivities Calculated for Mode 1 by SDM

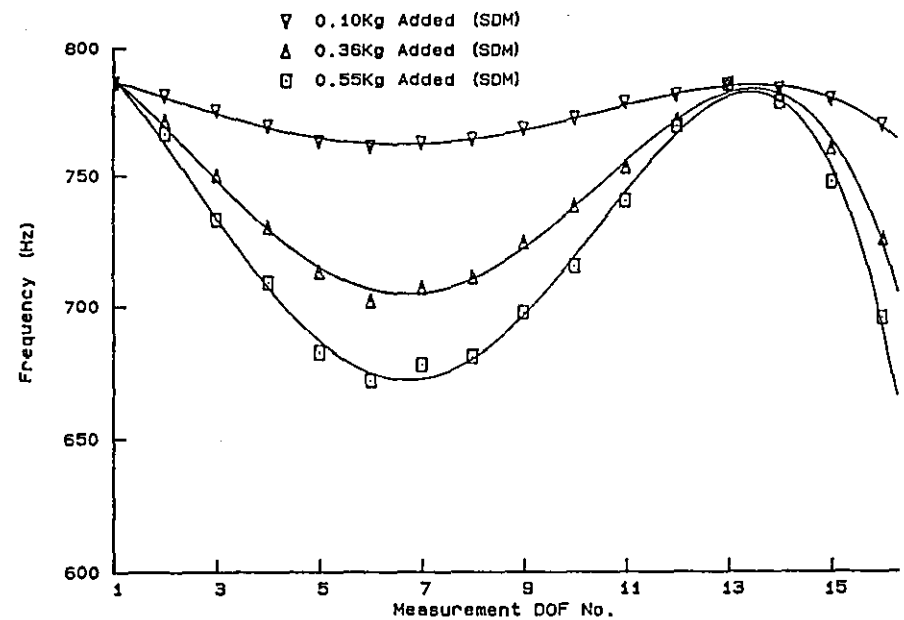

Figure 7.6 Sensitivities Calculated for Mode 2 by SDM

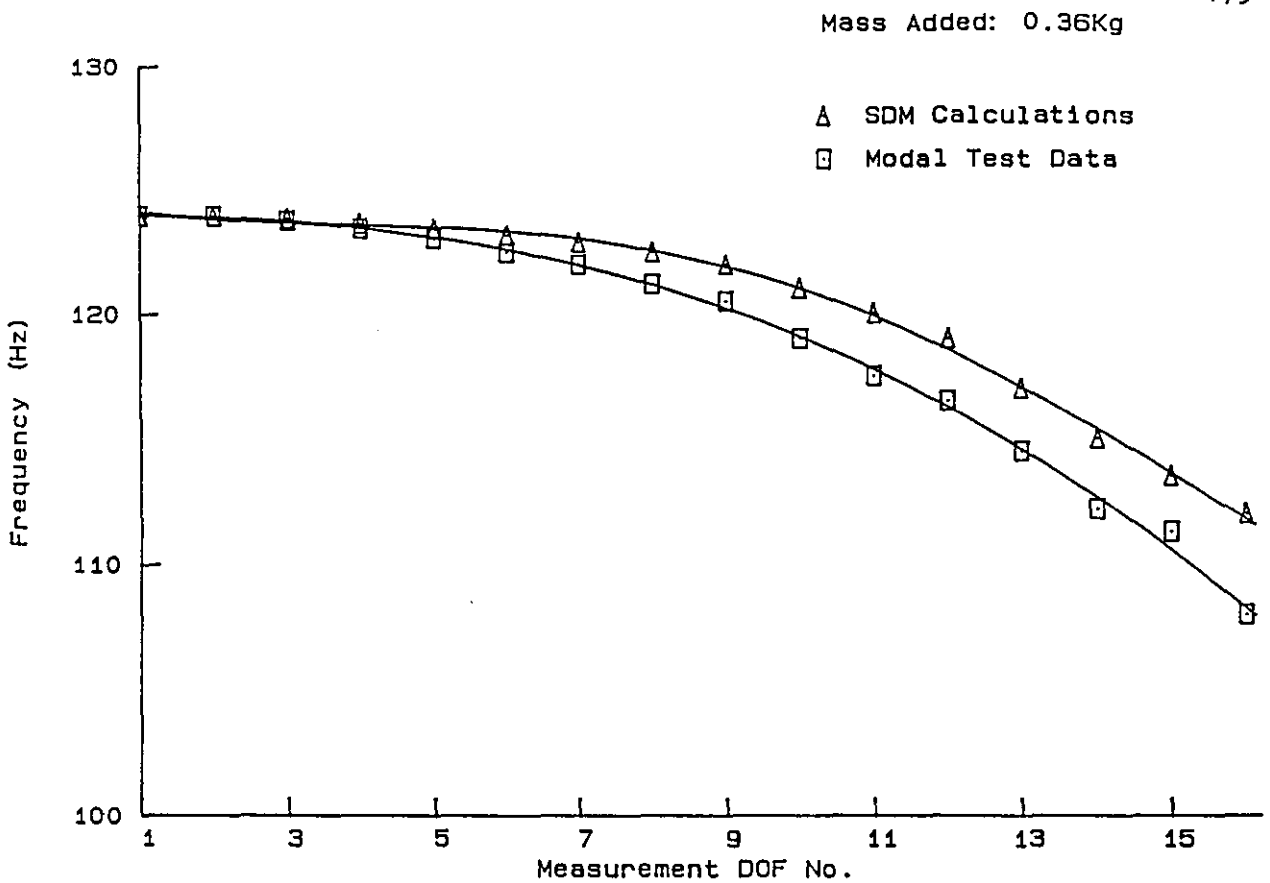

Figure 7.7 Comparing Modal Test and SDM Sensitivities for Mode 1

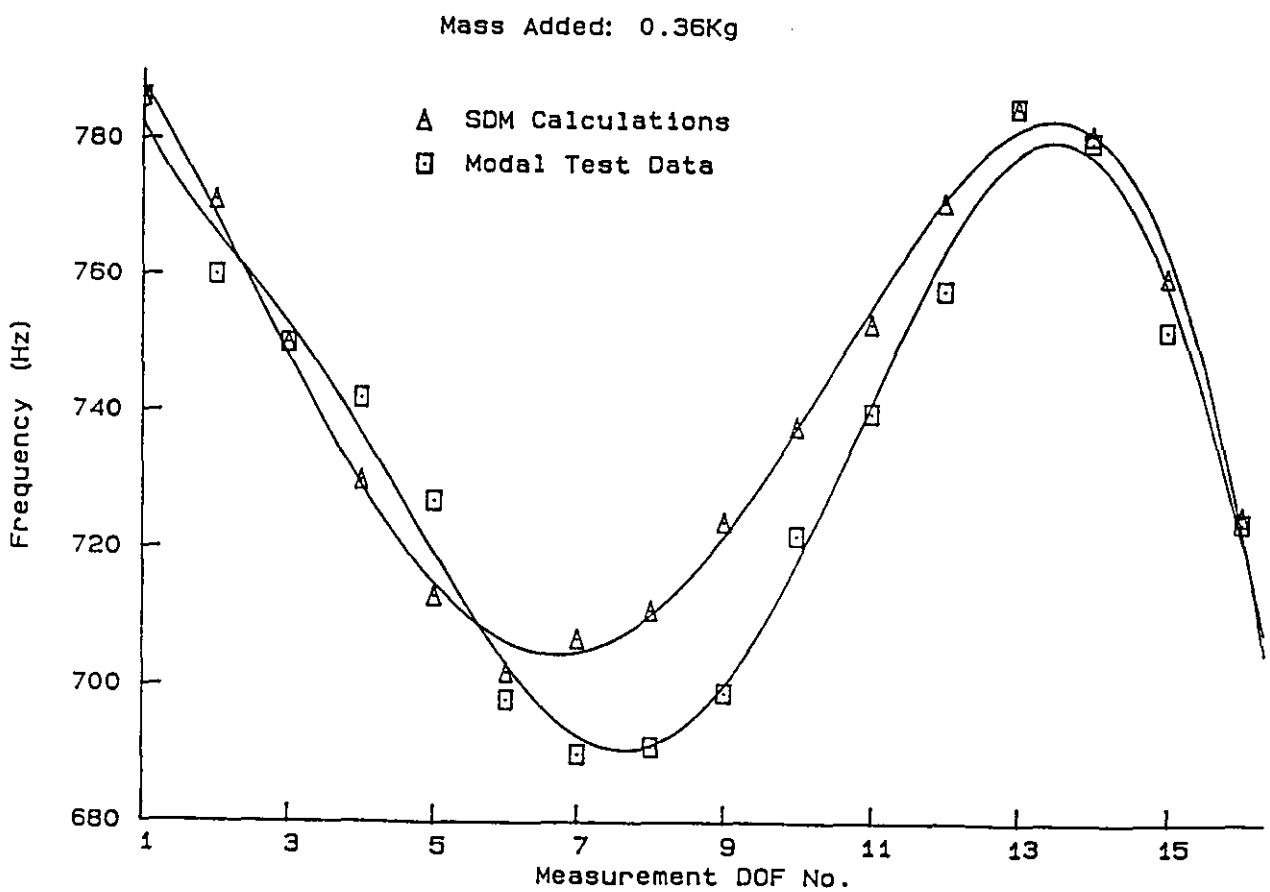

Figure 7.8 Comparing Modal Test and SDM Sensitivities for Mode 2

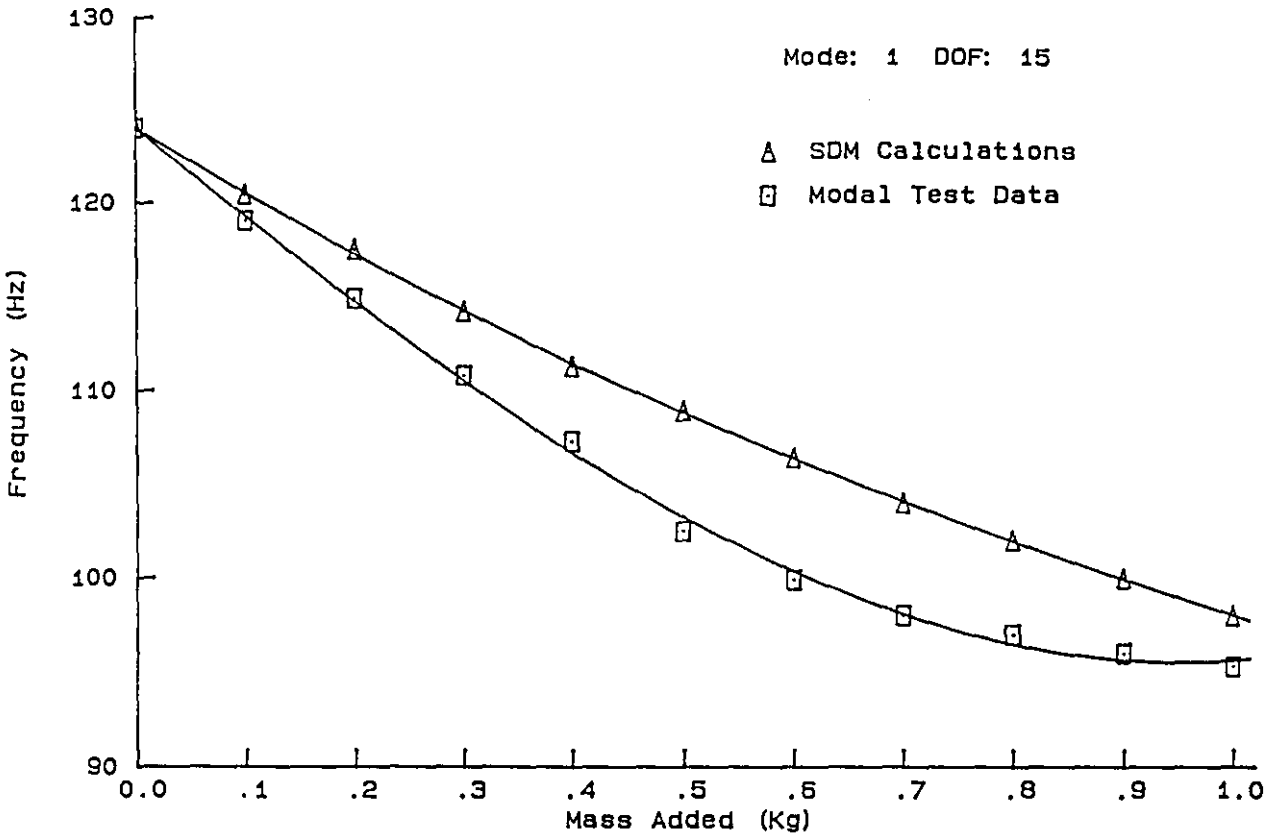

(a) Mass Sensitivity of Measurement DOF No.15

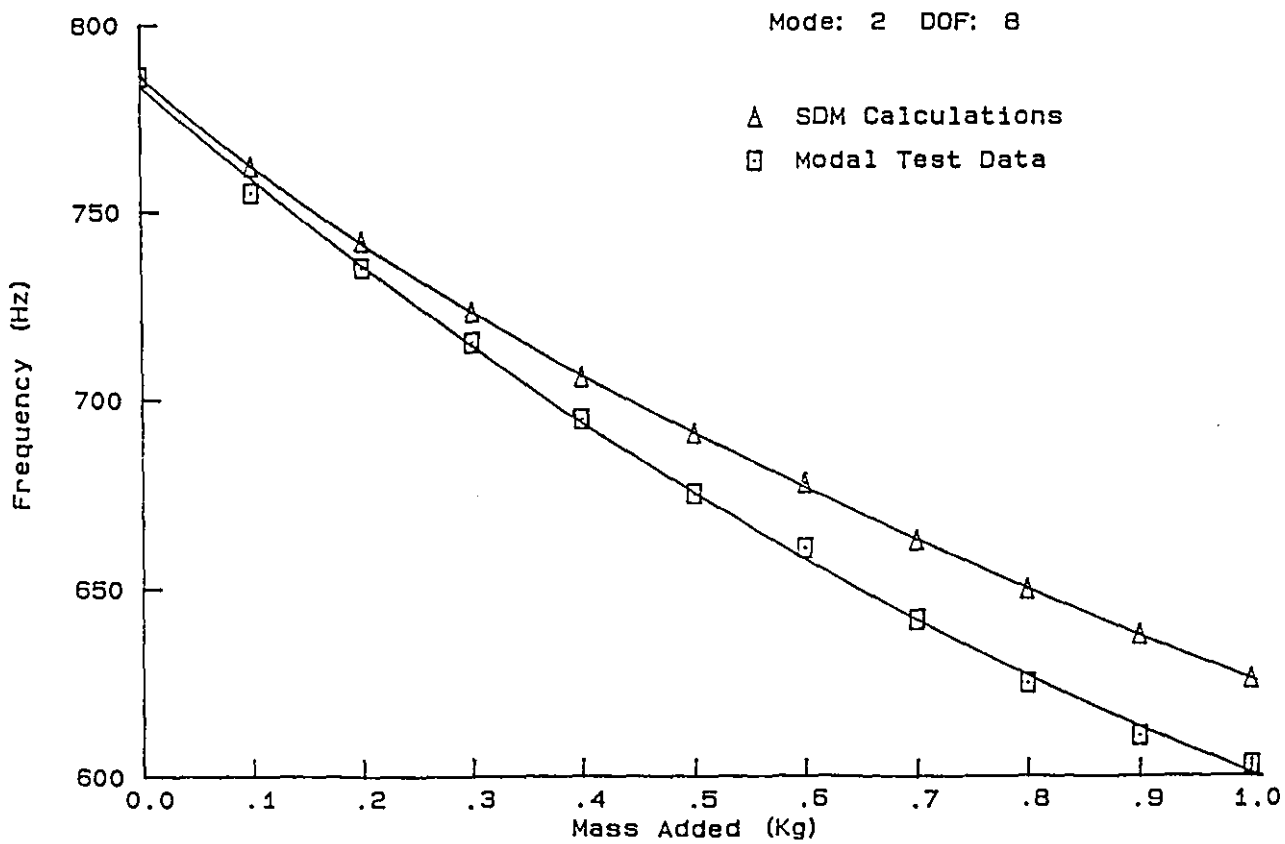

Figure 7.9 (b) Mass Sensitivity of Measurement DOF No.8

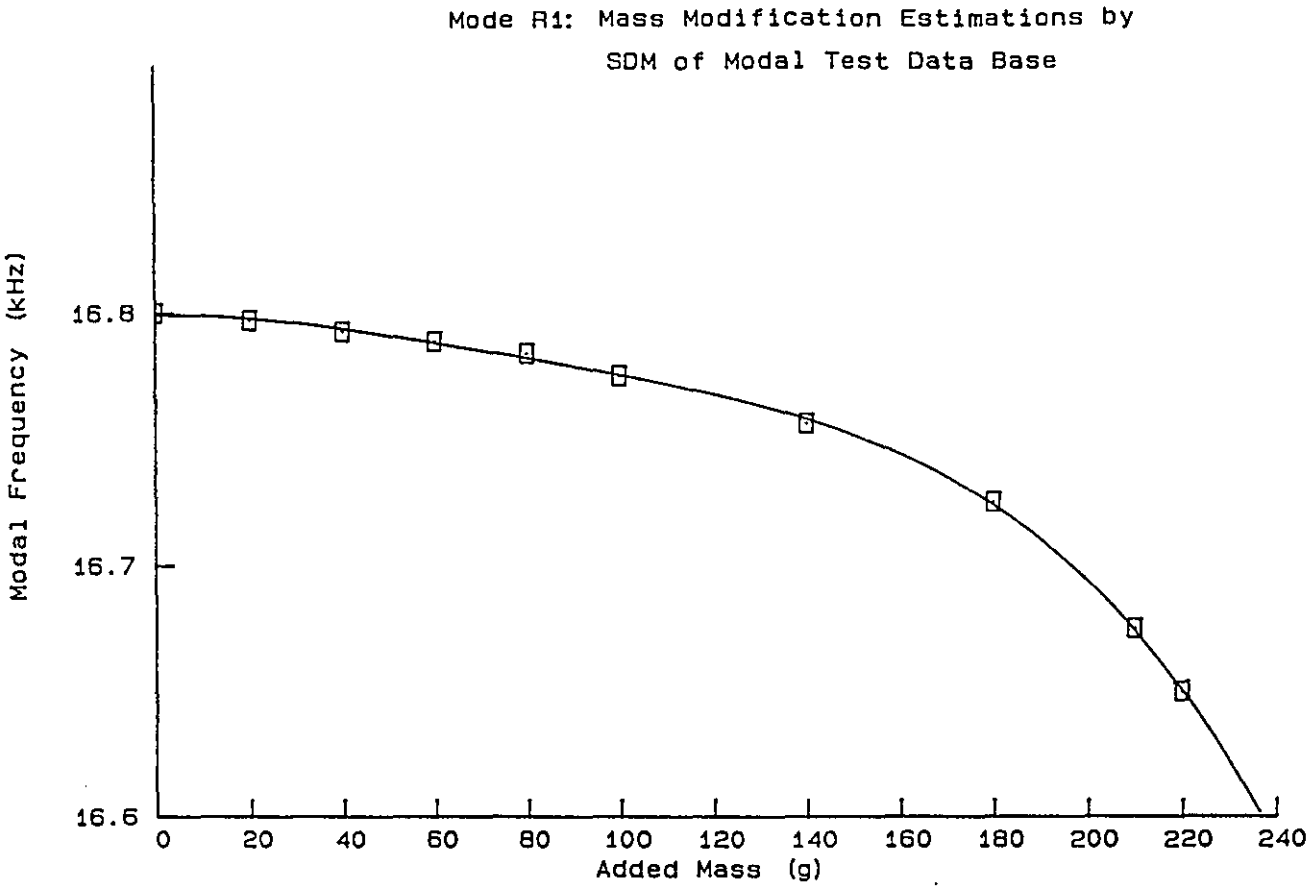

a) Identifying Linear Range for R1 Mode Calculations

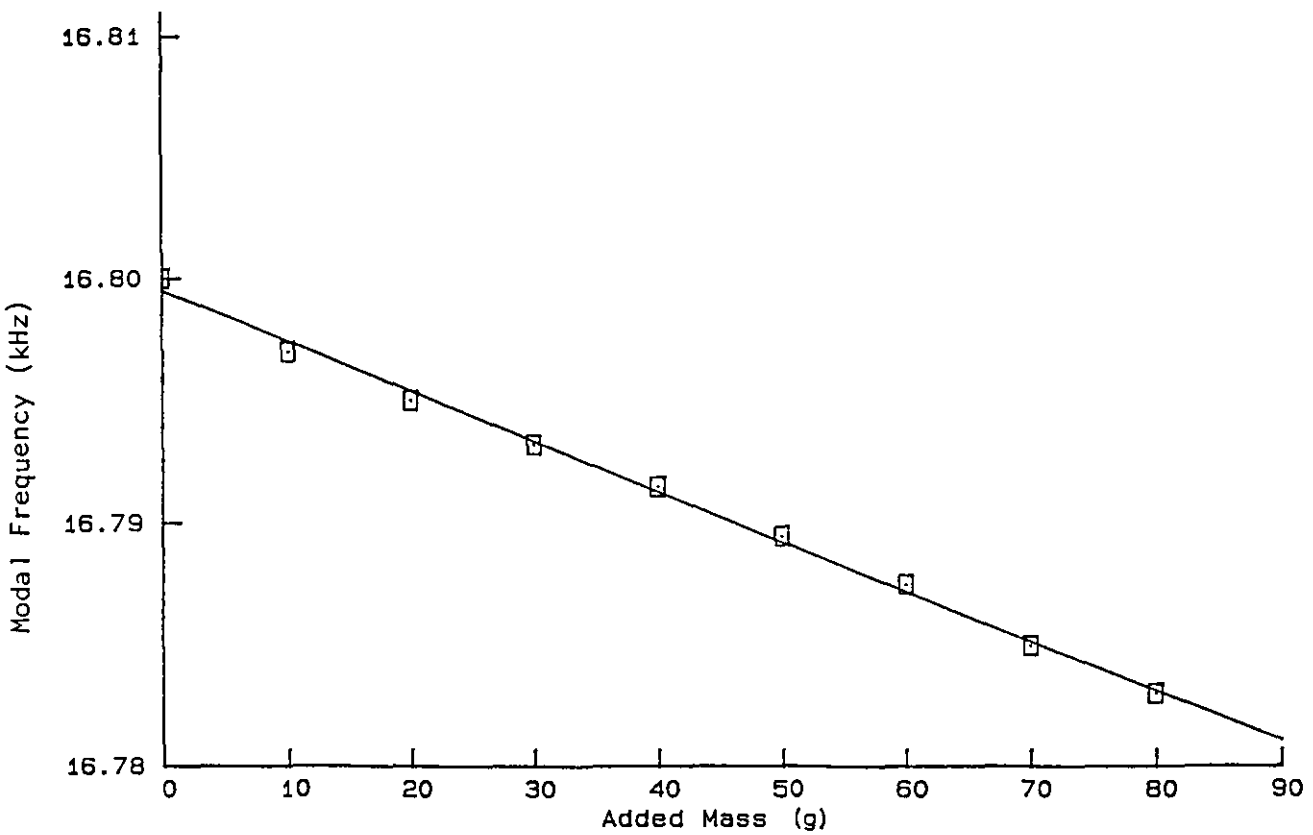

Figure 7.10 b) R1 Modal Frequencies due to Mass Additions

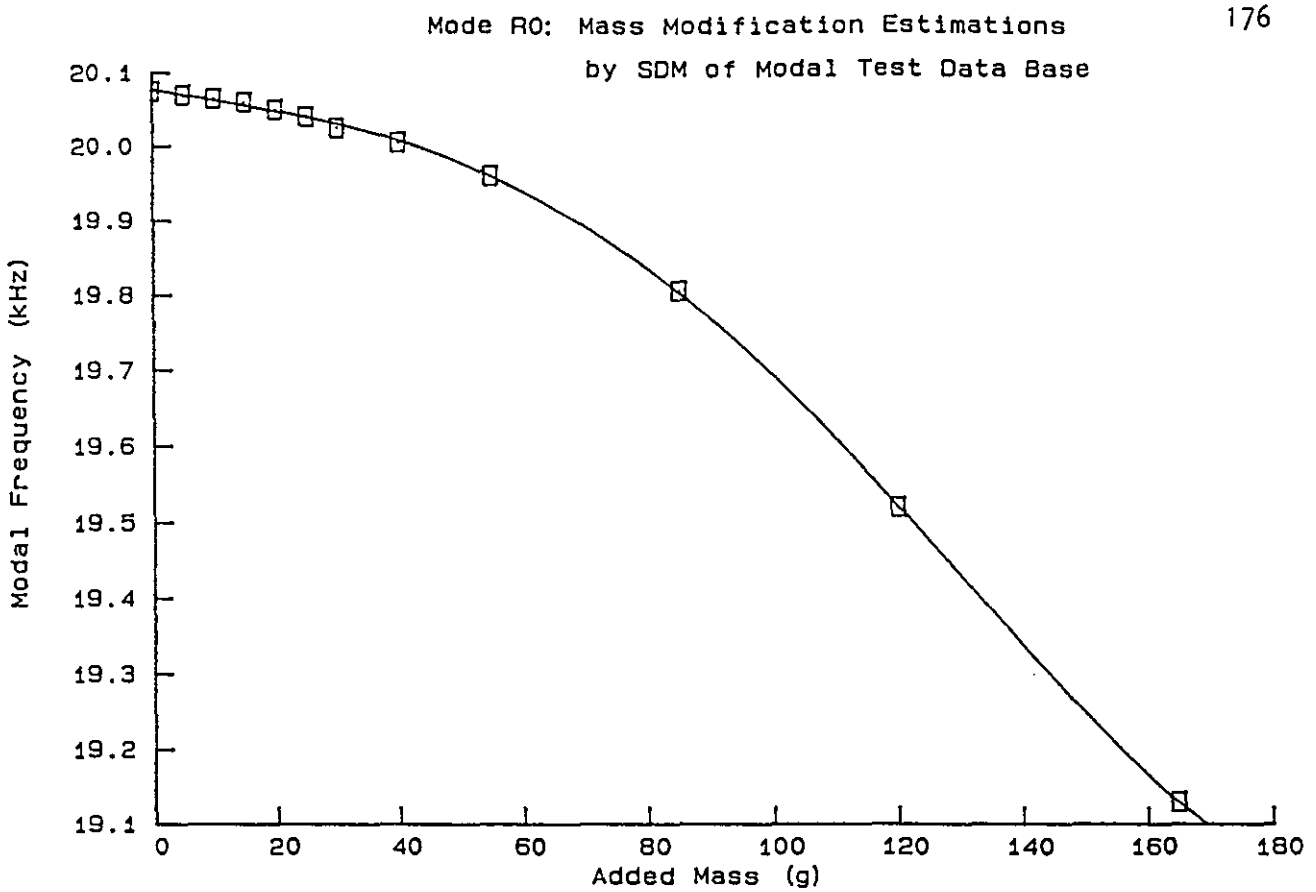

a) Identifying Linear Range for R0 Mode Calculations

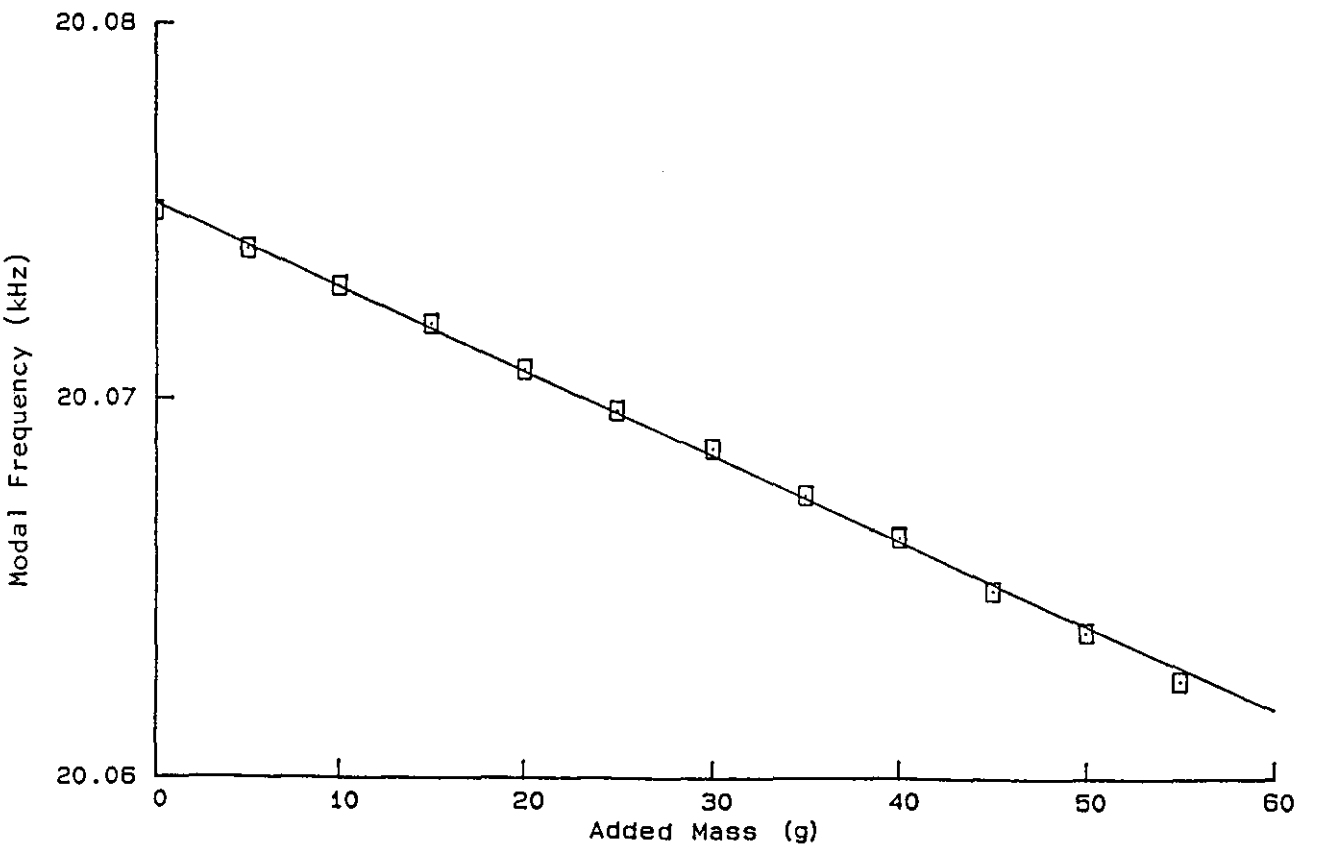

Figure 7.11 b) R0 Modal Frequencies due to Mass Additions

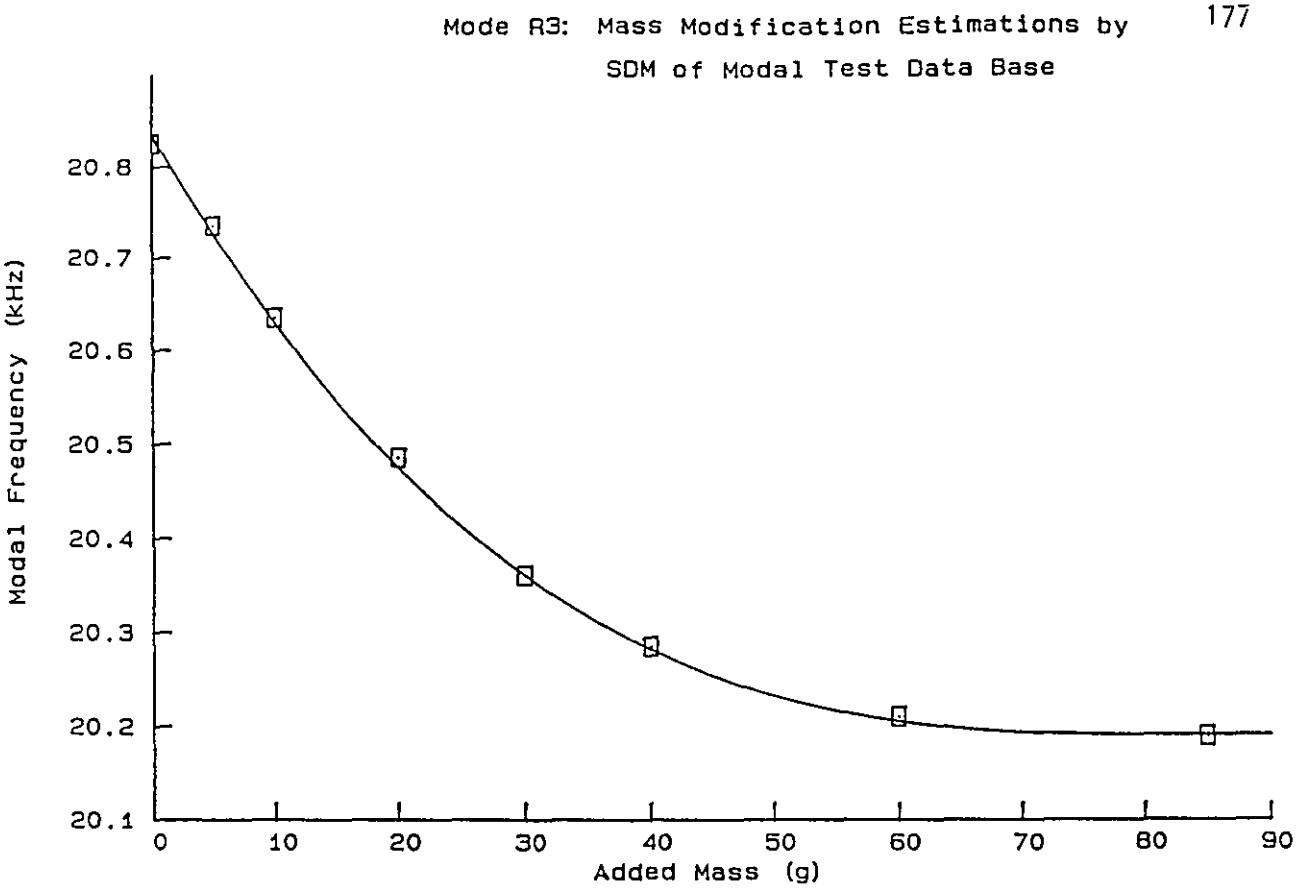

a) Identifying Linear Range for R3 Mode Calculations

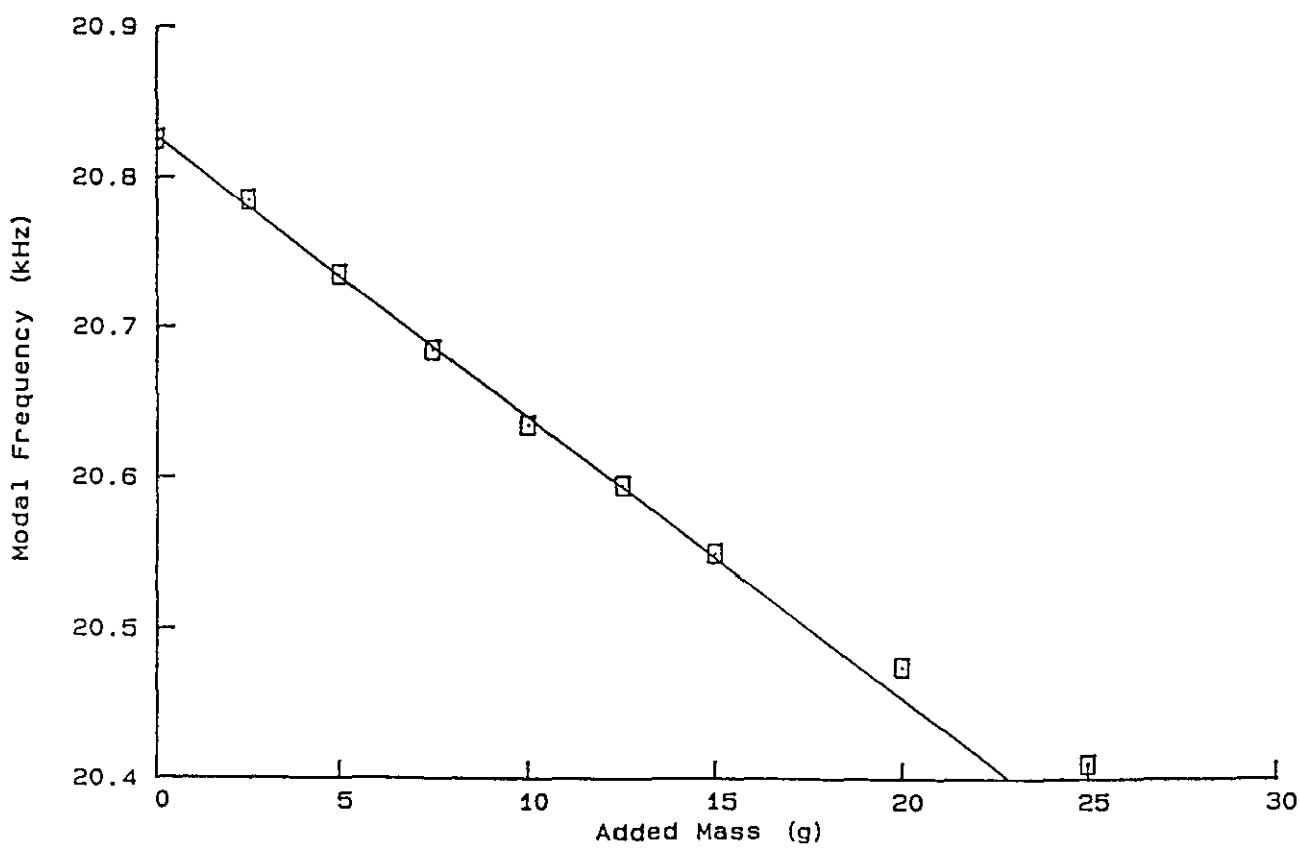

Figure 7.12 b) R3 Modal Frequencies due to Mass Additions

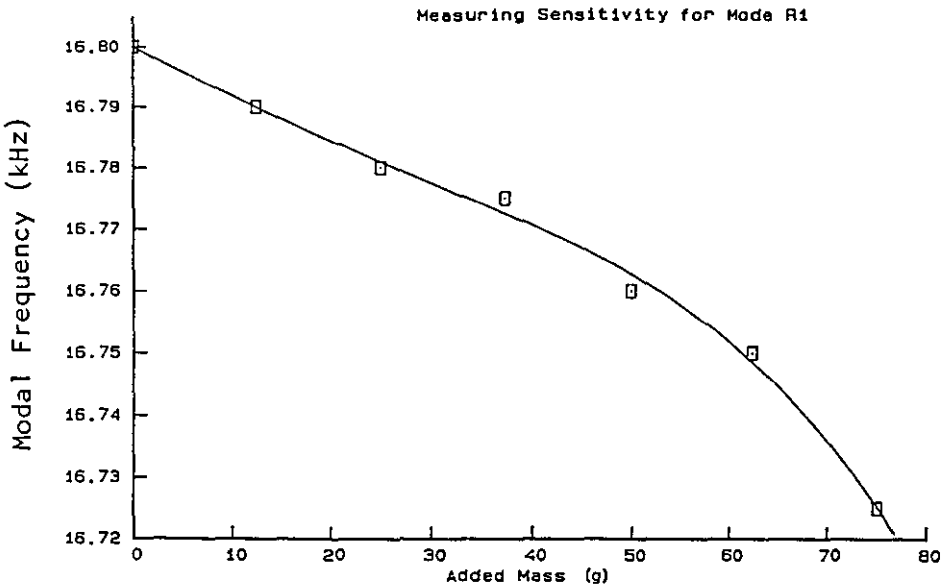

Figure 7.13 Experimental Modification of Die, Mode R1

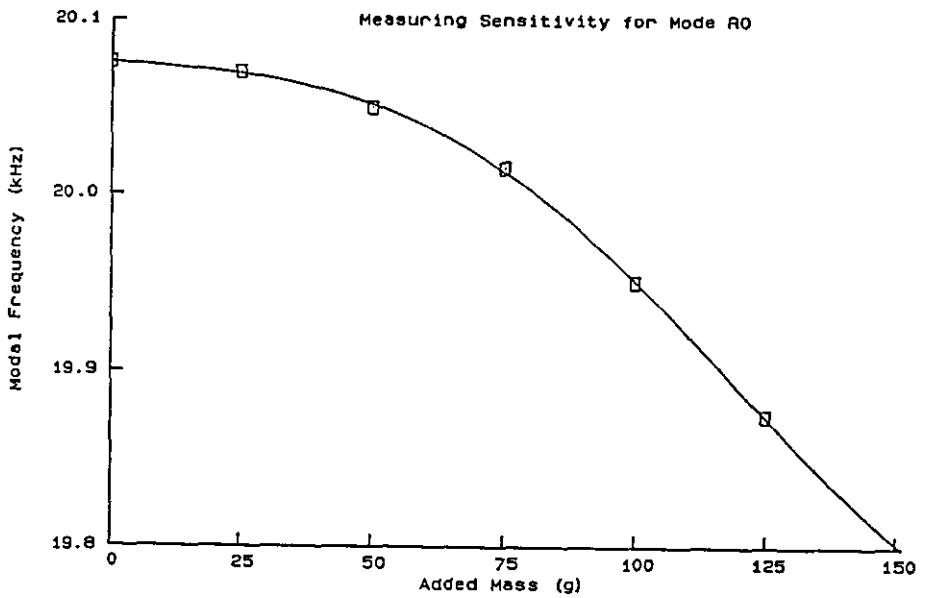

Figure 7.14 Experimental Modification of Die, Mode R0

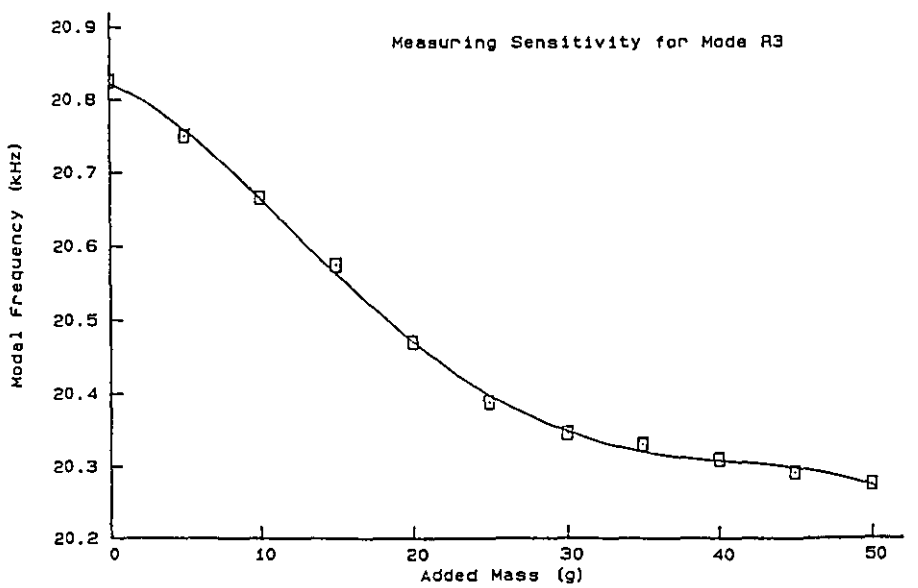

Figure 7.15 Experimental Modification of Die, Mode R3

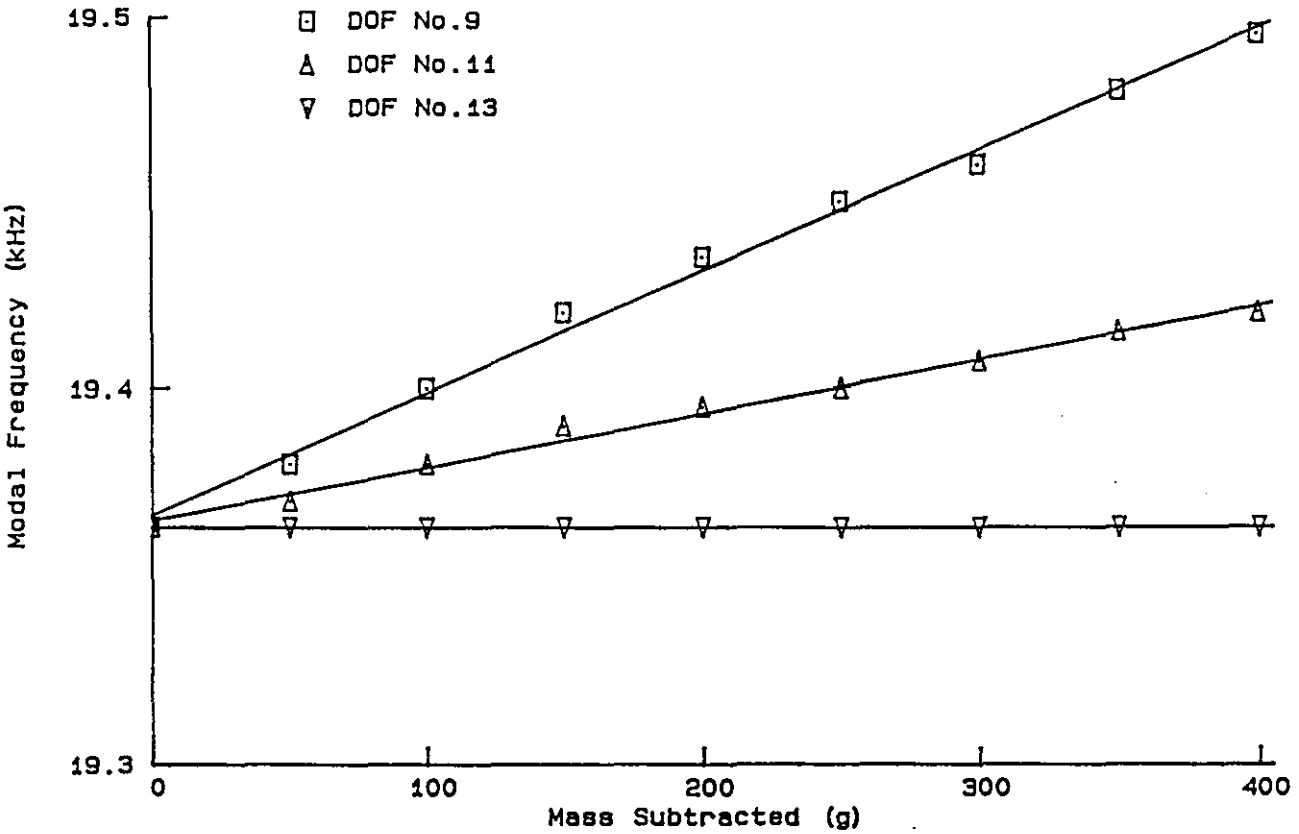

Figure 7.16(a) R1 Mode Sensitivities

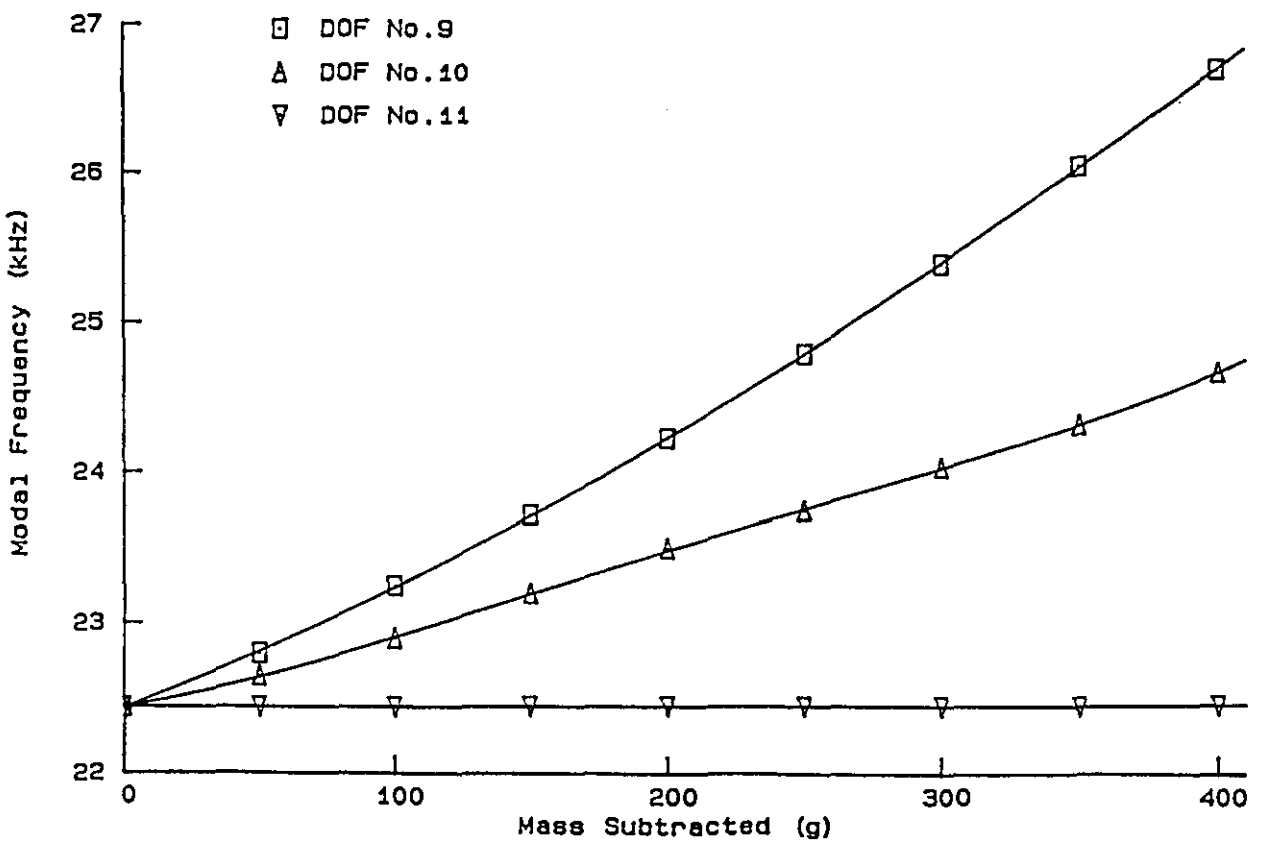

Figure 7.16(b) R3 Mode Sensitivities

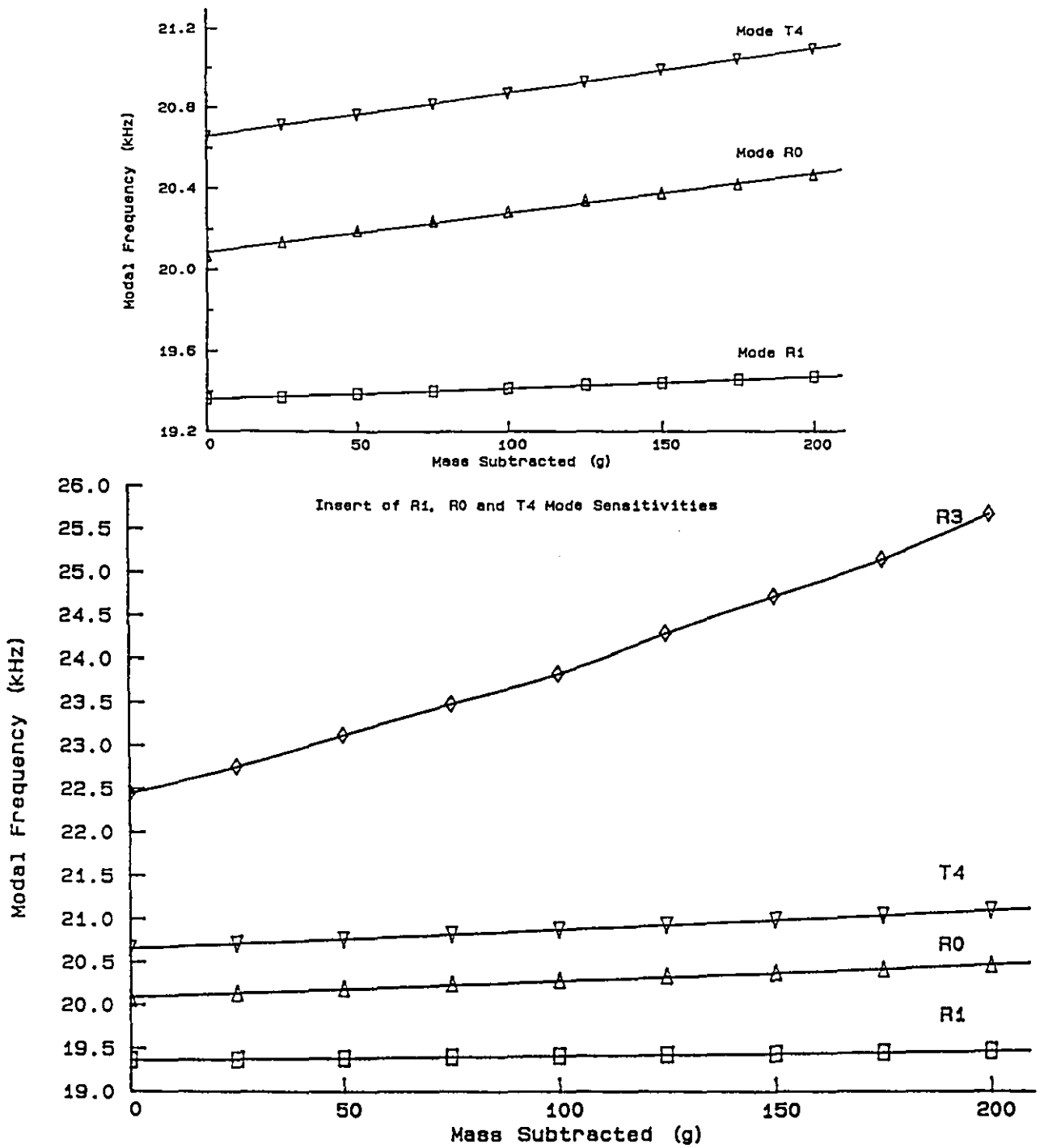

Figure 7.17 Mass Subtracted at 2-Lobed Die DOFs

Figure 7.18 Modified 3-Lobed Die

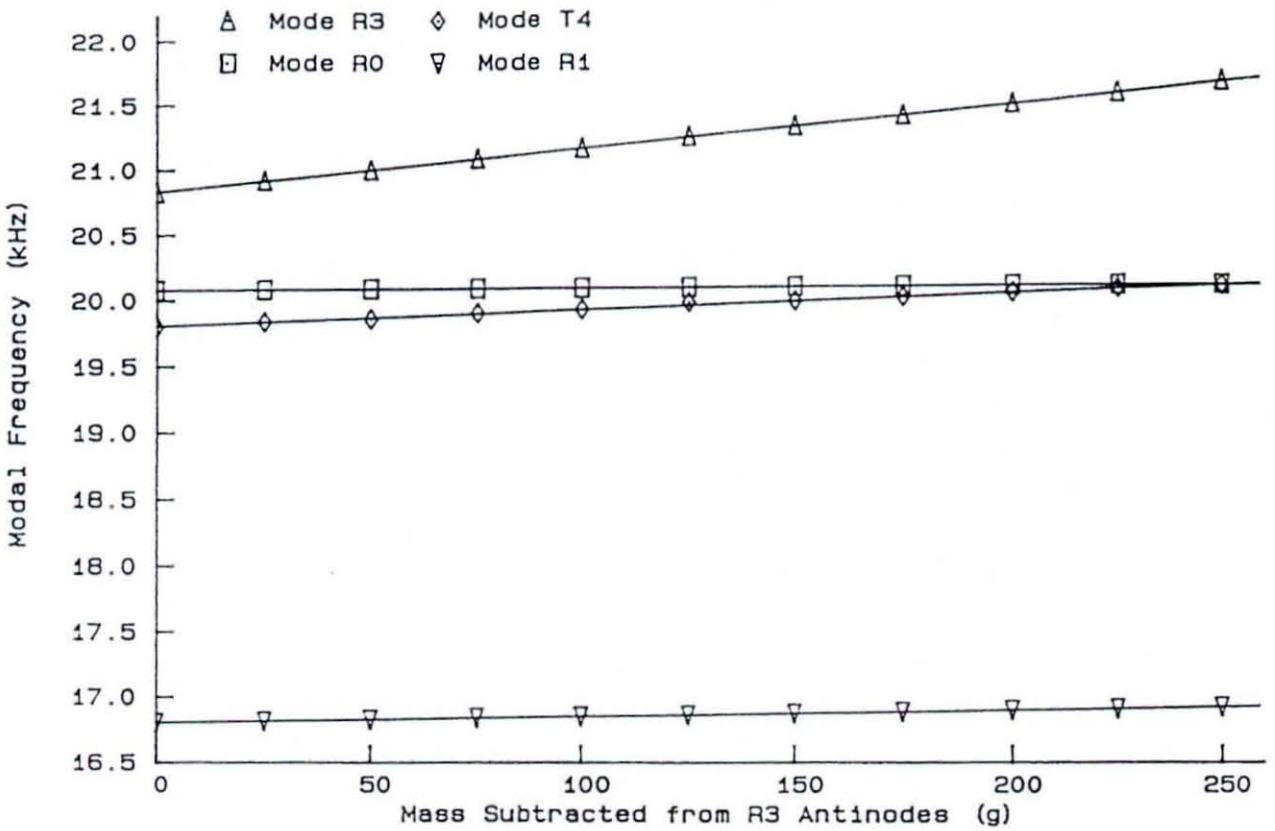

Figure 7.19 Predicting Modal Frequencies of a 3-Lobed Die

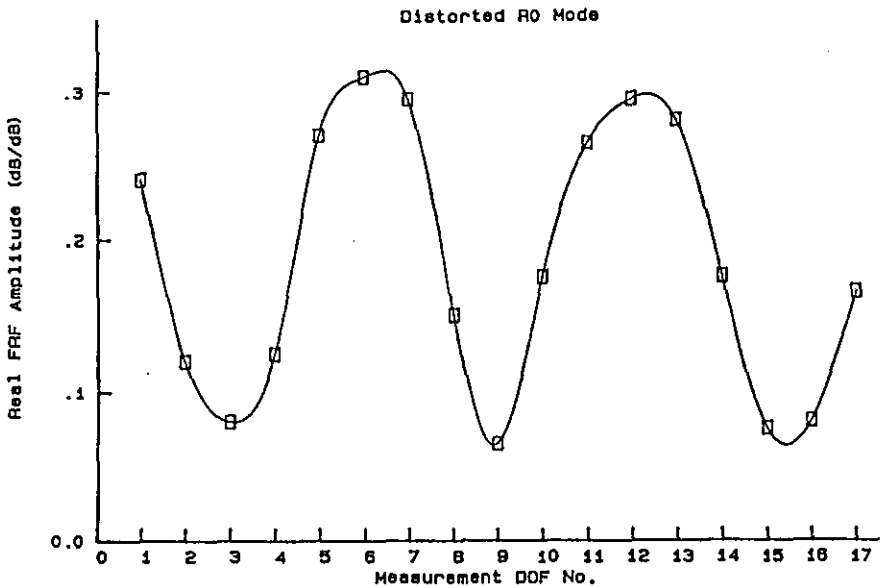

(a) Mode Shape of the R0 Mode of the 3-Lobed Die

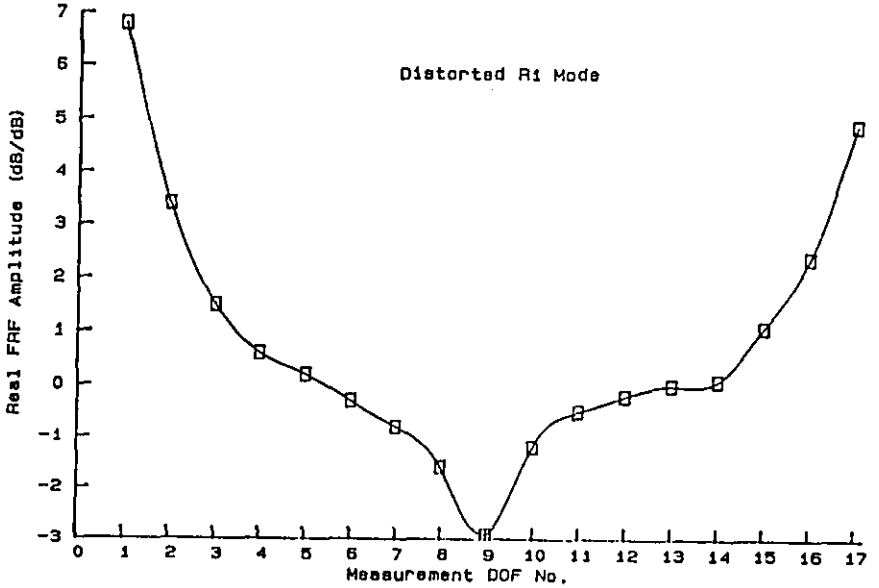

(b) Mode Shape of the R1 Mode of the 3-Lobed Die

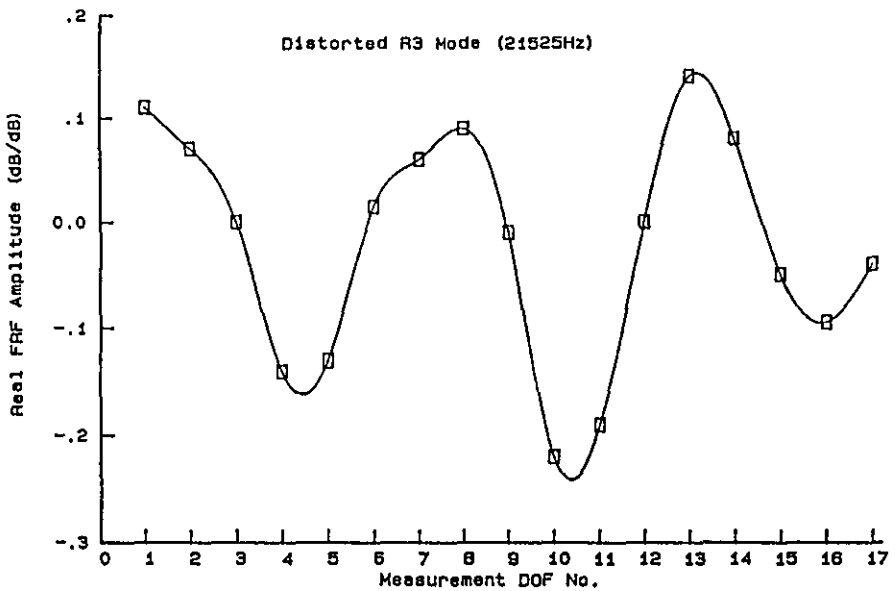

(c) Mode Shape of the R3 Mode of the 3-Lobed Die

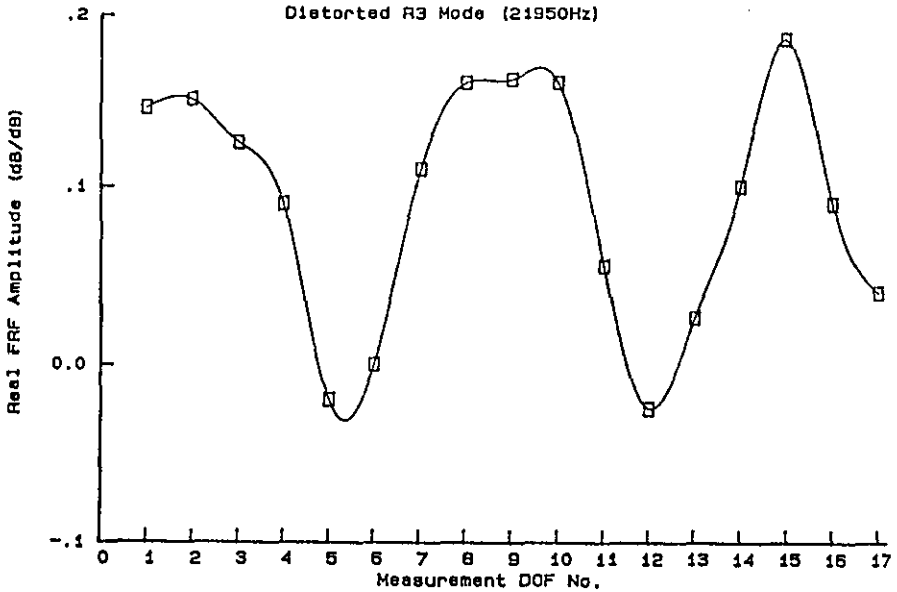

Figure 7.20 (d) Mode Shape of the R3 Mode of the 3-Lobed Die

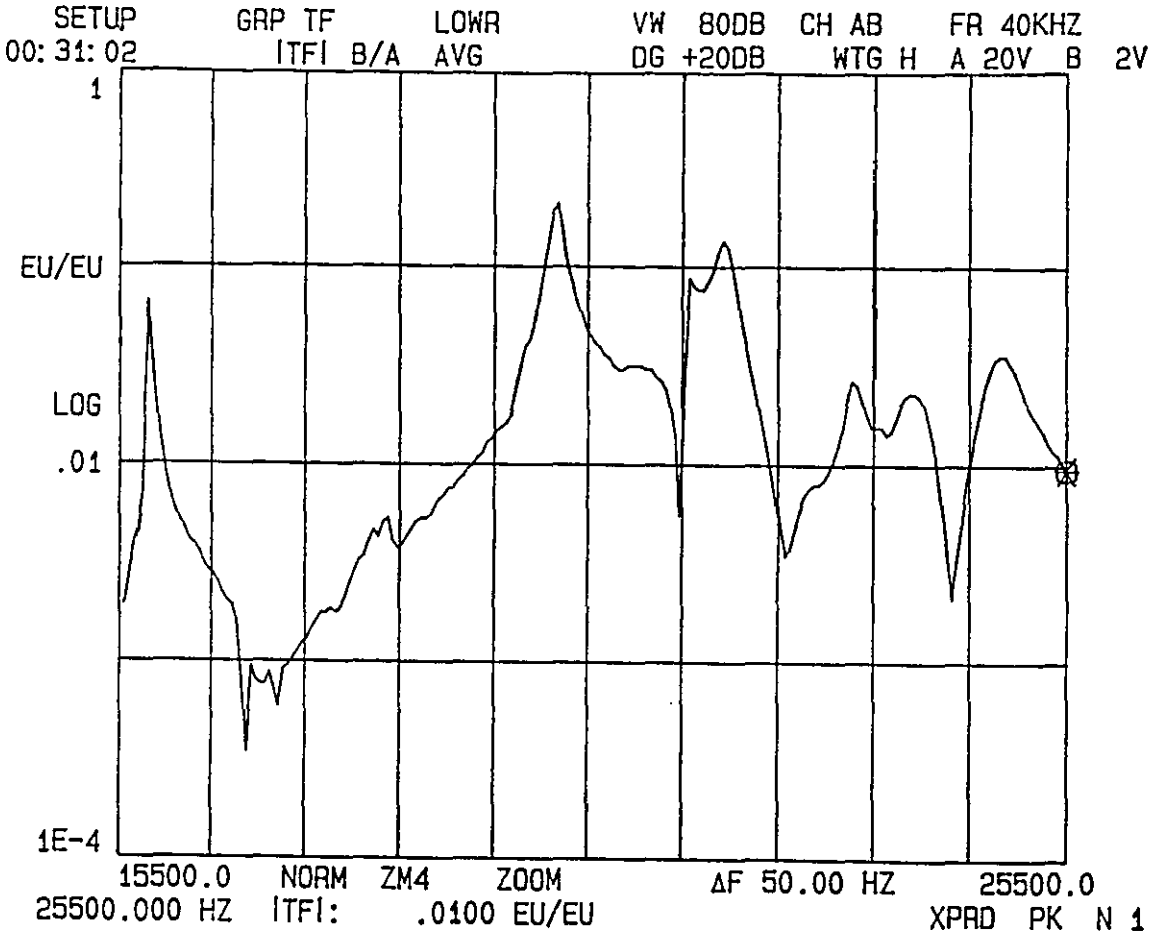

a) Wide Band Analysis

b) Narrow Band Analysis

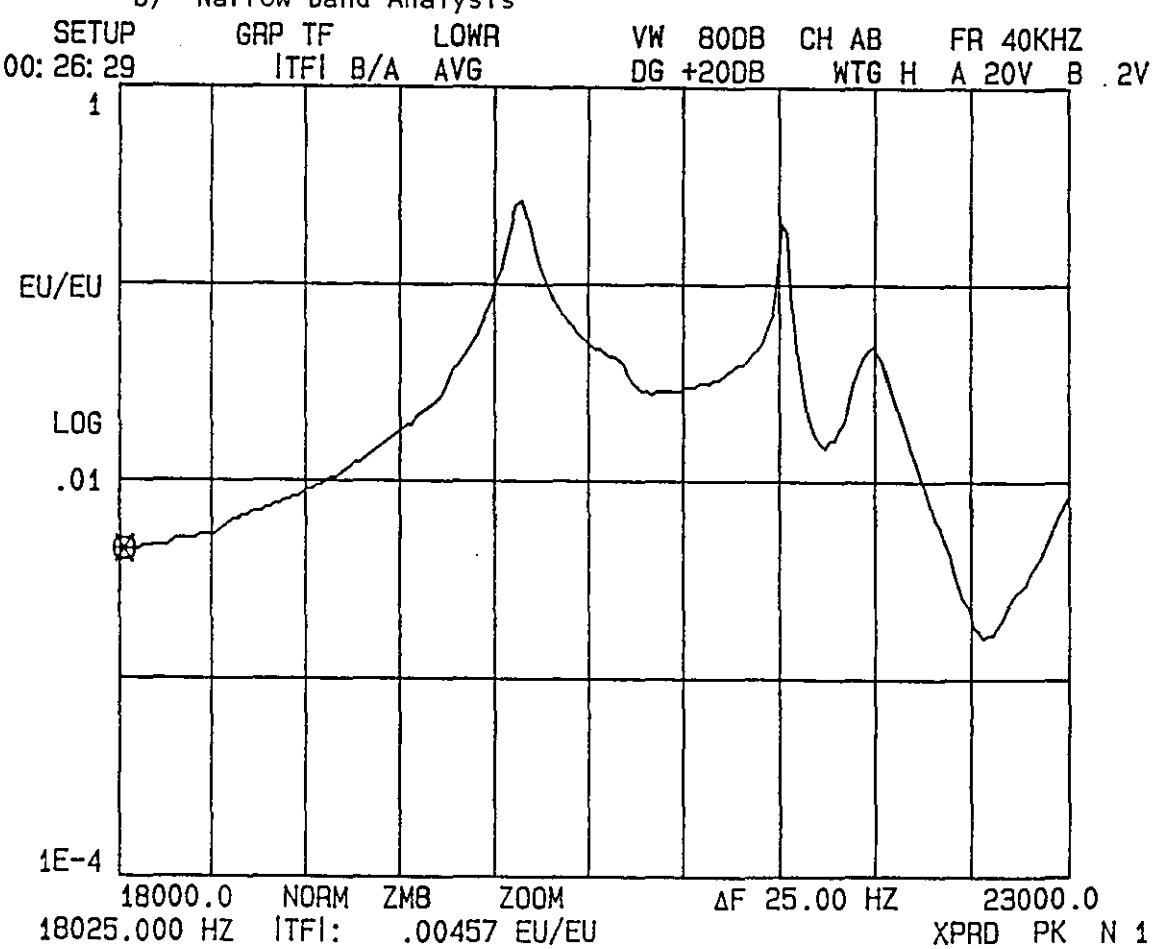

Figure 7.21 Radial Frequency Response Functions from Modified 3-Lobed Die

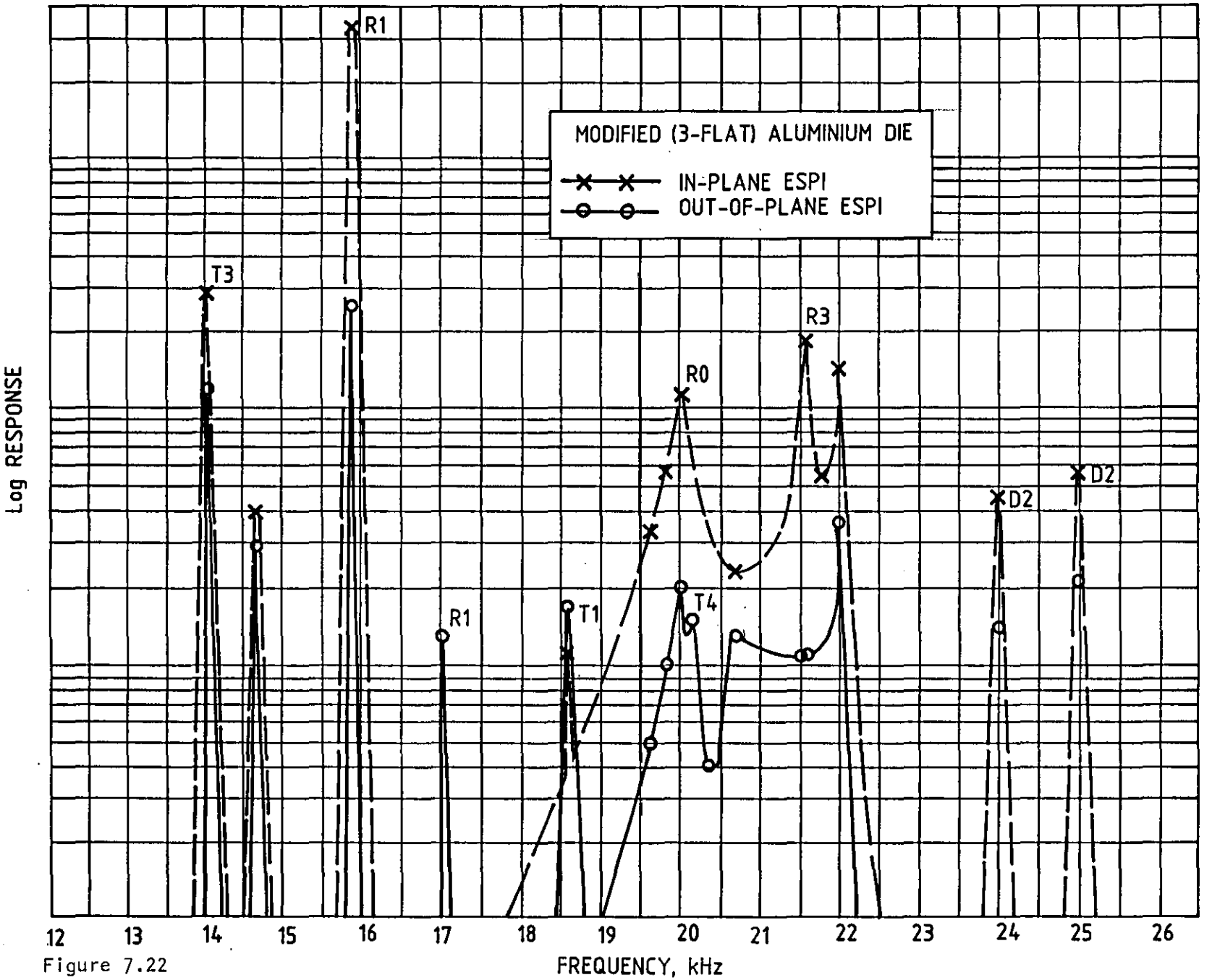
MODIFIED (3-FLAT) ALUMINIUM DIE
IN-PLANE ESPI
OUT-OF-PLANE ESPI
R1
T3
R3
R0
D2
D2
R1
T1
T4
Log RESPONSE
12
13
14
15
16
17
18
19
20
21
22
23
24
25
26
FREQUENCY, kHz

Figure 7.22

a) Mode R1: 17386 Hz

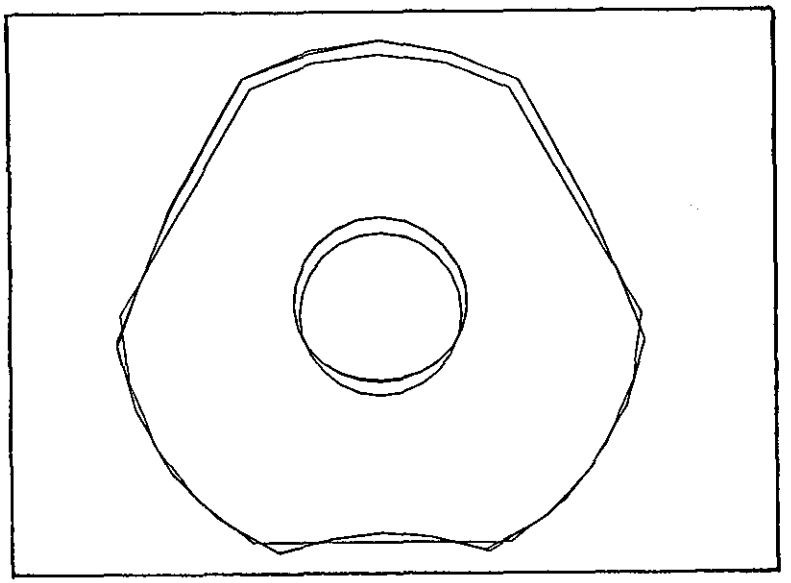

b) Mode T1: 19034 Hz

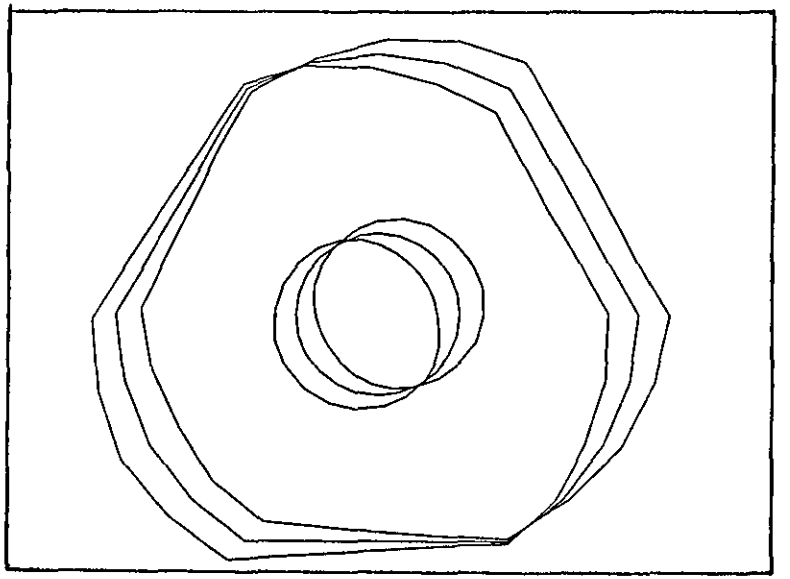

c) Mode R0: 19989 Hz

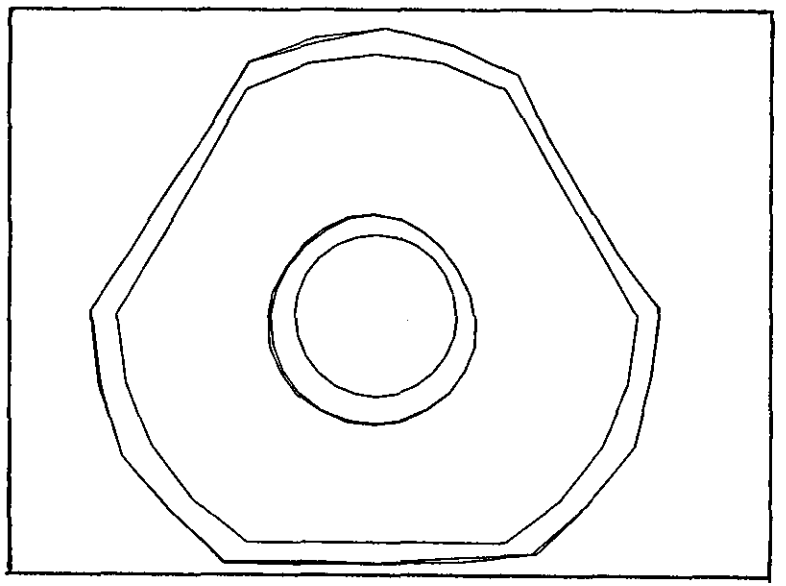

d) Mode T4: 20238 Hz

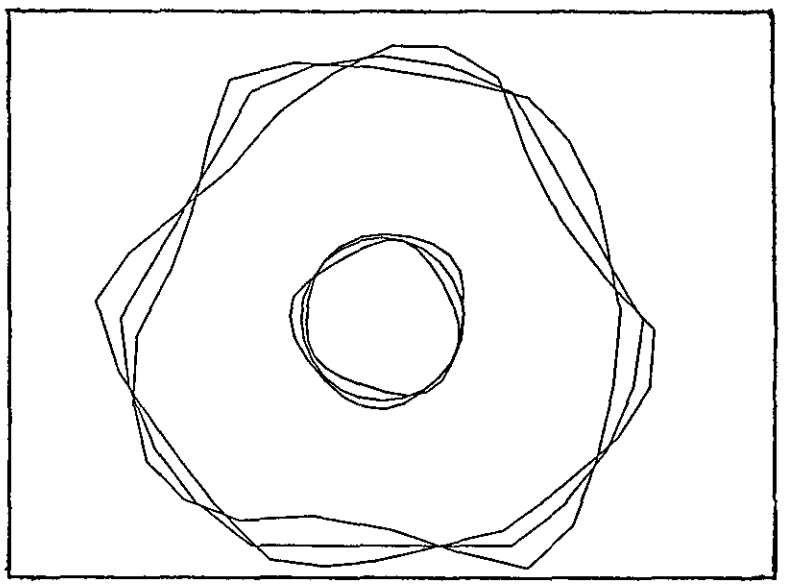

FIGURE 7.23: FINITE ELEMENT PREDICTIONS FOR MODIFIED THREE LOBED DIE

CHAPTER 8
CONCLUSIONS AND RECOMMENDATIONS FOR FURTHER WORK

8.1 CONCLUSIONS

1. Ultrasonics applied to metalworking processes has previously been directed at proposing the mechanisms of ultrasonic assistance. The work in this thesis has investigated the tuning of ultrasonic forming tools used in die necking of metal cans, by proposing a design strategy that improves process reliability by obtaining an understanding of the vibration characteristics of the tool. The design strategy involves a multiple estimation approach incorporating finite element modelling and experimental modal analysis to predict the tuned geometry of the die, its wider vibration behaviour and to produce a data base of experimental modal parameters from which redesigned die geometries can be estimated.

2. Initial measurements of process parameters during die necking trials allowed quantification of the die amplitude, power requirement and ram pressure through the time history of a complete necking operation. An analysis of the frequency content of the measurements provided indications of close modal activity and showed that the operating frequency changed value through the stages of the formation of the neck. The application of ultrasonics to a fully loaded die was simulated in order to compare the vibration characteristics of a fully loaded and unloaded die. A test rig was designed to load the die statically under realistic ram forces, with a preformed can. The results provided further evidence to support the idea that mode switching during forming was the cause of reliability problems which led to process failure in can necking trials. The uniform radial amplitude R0 mode was identified to be the

tuned operating mode of vibration, but a third radial harmonic (R3) mode was measured close to R0 in frequency and closely coupled to R0, especially under loaded conditions.

3. Measurement systems were developed to conduct vibration analysis of forming dies in the low ultrasonic frequency range. By using two accelerometers it was possible to extract some modal parameter information. The most dominant modes were identified but the technique did not produce data that could be post-processed to redesign the die. In order to progress it was necessary to find a signal that could be monitored to simulate the forcing function being applied to the die via the magnetostrictive transducer, so that an experimental modal analysis survey of the die could be instituted. It was established that the voltage supplied to the transducer coils from the ultrasonic generator simulated the forcing function in all but its phase relationship with the acceleration signal. In fact the resulting frequency response function exhibited the characteristics of an uncalibrated mobility measurement, which meant that the voltage signal could successfully be used to gather FRF data for modal parameter extraction.

4. The complexity of die behaviour was shown to require a rigorous approach to vibration analysis. A strategy was proposed for determining an accurate picture of die vibration that involved coincident peak picking, waterfall analysis and subsequently, FRF curve-fitting using SMS structural dynamics software. Careful investigation of coupled modes was performed, in particular by analysis of the FRF Nyquist circles, to aid and lend accuracy to the curve-fitting procedure. Rotational coordinate motion information was provided from a die study using electronic speckle pattern interferometry [74]. The data from the laser-based measurements was extracted in a frequency response function form to allow direct comparison with EMA results, thus providing further support to the vibration analysis. Application of the measurement strategy to alternative dies has similarly achieved accurate modal data.

5. Finite element modelling of ultrasonic dies further illustrated the desirability of adopting a vibration analysis strategy utilising multiple estimation techniques. The experimental results from EMA and ESPI analysis were used to validate FE models. Axiharmonic and cyclic symmetry modelling were investigated but a full three-dimensional analysis of the die was required to produce a model which could be adapted to incorporate structural modifications. Careful choice of master degrees-of-freedom, for eigenvalue economisation, and element mesh density, allowed optimisation of accuracy within the restrictions of solution time. Further accuracy could then be achieved by a process of selective model refinements that allowed the die FE model to be matched to experimentally determined mode estimations.

6. On the basis of an accurate EMA data base and realistic FE model, a die redesign procedure was proposed that involved physical modification of the outside circumference of the die. These alterations to the die profile were simulated by mass modifications. Since the EMA data base was uncalibrated, a scaling factor was determined to relate the monitored voltage signal amplitude to the amplitude of the excitation applied to the die during modal tests. Calibration was achieved by relating "effective" mass terms, input to the dynamics modification software, to real mass values that, in experiments, incur the same frequency shifts to the die modes. This method was found to be successful, but the scaling factor was mode shape dependent for those thick cylinder modes of vibration that exhibit anomalous frequency behaviour (i.e. the zero and first order radial and torsional modes). By analysis of mass addition and subtraction effects on two different dies, it was found that the scaling factor information was consistent and could lead to accurate prediction of redesign frequency data by structural modification calculations.

7. Structural dynamics modification and FE modelling were used to propose a die geometry for the aluminium forming die which isolated the tuned operating mode. Confirmation of the predictions was obtained from EMA of the manufactured redesigned die. Trials conducted at CMB using the modified die proved successful. The problems associated with mode switching were eliminated and necking process reliability improvements were achieved.

8. To some extent, the conclusion of the research project was overtaken by events. Political and economic upheavals in Eastern Europe (where the subsidised aluminium competitor of the tinplate can was manufactured) lessened the pressure at CMB to effect significant cost reductions in can manufacture. At the same time, pressure from the environmental lobby led to a departure from traditional aerosol can manufacture. However, the value of the research findings to alternative necking operations, such as beverage can production, is undisputed and the interest in ultrasonics applications is very much alive at CMB.

8.2 FURTHER WORK

The success of the die design strategy draws attention to the considerable scope for further work in alternative ultrasonic applications. In general, ultrasonic tools are prone to problematic modal behaviour. The identification of the tool vibration characteristics close to the operating frequency, allows design improvements to be instigated from modal sensitivity measurements. For example, the analysis techniques developed and utilised in this thesis could be adopted to improve performance reliability of plastic welding horns, ultrasonic machining tools, wire and tube drawing dies and many other common applications. Many of the ultrasonically assisted manufacturing operations that have not been fully exploited, may be found to be commercially viable if well designed and highly tuned tooling becomes available. Material joining and cutting would fall into this category. In these cases the joining staple or cutting

blade vibration response is as critical as the characteristics of the vibration transmission components and therefore tuning and mode isolation in the design procedure are the primary factors influencing reliability.

The benefits of employing several analysis techniques to produce accurate vibration information has been demonstrated in this thesis. The ability to produce a modal data base that includes rotational coordinate information, from the dynamic analysis of structures, would be advantageous to many vibration studies. The work would involve the development of software that could extract the frequency response function representations of ESPI measurements in a form compatible with frequency response function data obtained from a modal test using accelerometers. Data post-processing by curve-fitting would then result in all possible structural modes of vibration being identified. For well-calibrated test data, direct comparison with and refinement of FEM data could be achieved by employing techniques such as modal assurance criteria (MAC) estimation [48].

The literature review in Chapter 1 of this thesis highlighted some of the conflicting evidence gathered to explain the effects of ultrasonic excitation in metalworking processes. Since the early research was undertaken, there have been many advances in technology and systems are now in place to allow interfacial conditions to be studied further. For example: (a) normal to surface motion of the tool or workpiece can be measured remote from the operation using laser vibrometry, which detects the Doppler shift due to the motion of a point on the target, to produce a velocity signal, (b) advances in ESPI analysis which use a pulsed laser, are currently being developed at Loughborough University to view high frequency, large amplitude vibration response in a novel ultrasonic cutting process, (c) recent improvements in finite element software have provided the capability to model interfacial friction and plastic flow of materials.

The identification of novel applications of ultrasonic assistance in manufacturing processes could provide many benefits to industry. This would require work to

be carried out into the effects of ultrasonics on different groups of generic materials, to investigate for commonalities with metals and for alternative beneficial mechanisms.

APPENDIX A
ULTRASONIC EQUIPMENT AND PROCESS

A.1 INTRODUCTION

The initial trials of ultrasonic necking were conducted by CMB using a test rig developed at their research centre. This test rig was subsequently used for the investigation of forming parameters discussed in Chapter 3 of this study. The principles of the necking operation can be illustrated by referring to the forming rig, which encompasses all the necessary features required for one ultrasonic head of a can production machine. The other key feature is the excitation generation and transmission equipment. Throughout this study the experimental investigations have employed a variety of such ultrasonic equipment; the equipment used being dictated by the purpose of the particular analysis. This Appendix sets out to: a) describe the can forming process by referring to the CMB forming test rig, and b) clarify the uses and features of the associated ultrasonic generation and transmission equipment.

A.2 CAN FORMING TEST RIG

Figures A1 and A2 represent the ultrasonic die necking process. A hydraulically operated ram forces a thin cylindrical can into the die. The end of the ram is shaped to match the required neck profile and this acts as the blankholder and internal plug during forming. Once the cylinder diameter reduction is complete, the can is ejected from the die by an air-actuated spring return knockout. The ultrasonic vibratory energy is transmitted to the forming surface by the resonant excitation system consisting of a transducer, die cylinder and resonant mounting. The transducer is the electromechanical conversion unit, producing 20 kHz nominal frequency which is transformed by the horn to transmit vibration amplitude at the die/horn interface. This interface is achieved through a threaded mounting stud. The die is excited in a fundamental radial mode of vibration to attain maximum possible amplitude at

the die bore or forming surface. The die is constructed in two parts. The die pellet is manufactured from Ferro-titanit Nickro 292 which provides an extremely hard and wear resistant work surface. In order to minimise ultrasonic power input, the bulk of the die (the bolster) is made from aluminium alloy which is a low acoustic loss material. The die is completed by shrink-fitting the pellet into the bolster. Die mounting to the production machine is achieved by a tuned cylindrical tail which is essentially a rigid mounting but designed to be resonant at 20 kHz so that it becomes compliant during the ultrasonic forming operation. Thus tool alignment is safeguarded and die amplitude is largely unaffected. The forming rig is utilised extensively to test dies and ultrasonic equipment, primarily in terms of reliability of necked can production.

A.3 ULTRASONIC GENERATORS AND TRANSDUCERS

The ultrasonic can necking operation requires the generation and transmission of high power ultrasonic vibrations to the forming die. An ultrasonic generator converts mains electricity to 20 kHz nominal frequency and a transducer converts the high frequency electrical energy to mechanical vibrational energy.

The most utilised ultrasonic system in this study was supplied by Techno-Form Sonics. A general purpose ultrasonic frequency generator drives three magnetostrictive transducers brazed to a stainless steel concentrator (Figure A3). This type of transducer produces vibrations as the result of an applied magnetic field. Electromechanical conversion is maximised by designing the transducer to operate at resonance and therefore they have length equal to one half wavelength (the shortest length that will resonate at a fundamental frequency). The transducer is constructed from a stack of laminations whose cross-sectional area is dependent on the power requirements. The system in Figure A3 works at constant power which means that when the die is loaded, vibration amplitude is reduced. This, and the general low mechanical efficiency of magnetostrictive transducers (around 55%) makes this an unpopular system for modern engineering processes. However, the system has two advantages of concern to the experimentation in this study:

1. Although the generator is designed for high power use, it can also be used for low power applications and the output power can be set in the range 0-1600W. Since most of the experiments aim to determine the modal parameters of the die, it is not necessary to run the die at high power. In fact, the very large surface accelerations associated with high power, high frequency vibration would render vibration analysis of the die using contacting measurement devices impossible.

2. Ultrasonic transducers are tuned to excite vibration amplitude at the working frequency. However, magnetostrictive transducers are not as highly tuned as the piezoelectric type transducers and vibration transmission is still effective even when the system is detuned. This allows a magnetostrictive transducers to be used as an exciting system over a band of frequencies in the low ultrasonic range (for this system, approximately 13-28 kHz). This capability is essential for investigating die vibration behaviour around the operating frequency.

Two ultrasonic systems were employed in the experimental study of forming parameters (Chapter 3). Both systems consisted of a high power frequency generator and piezoelectric transducer and horn. These systems are more technologically advanced than the Techno-Form system described earlier. Such devices have smaller mechanical components and improved electromechanical conversion efficiency (around 95%).

The first of these systems was supplied by Kerry Ultrasonics. The frequency generator has a maximum power output of 1600W and drives a highly tuned piezoelectric transducer (Figure A4). The active element in this type of transducer is a lead-zirconate-titanate ceramic which produces vibrations as the result of an applied alternating electric field. The ceramic element, which has low tensile strength, is prestressed and clamped between two end masses under compression. The lengths of the masses are chosen so that the overall transducer length is one half wavelength. The ultrasonic transmission system that releases vibrational energy, is made up of two constituent parts; the

transducer as described above and the interstage horn (also known as the velocity transformer, booster or concentrator). The horn transmits vibratory energy to the transducer/tool interface transforming the amplitude delivered by the transducer to the amplitude required by the tool.

The Kerry system works at constant amplitude (rather than constant power). This means that under no-load conditions the die vibrates at a fixed amplitude requiring relatively low power while, under loaded conditions, vibration amplitude is maintained and the power input increases. The constant amplitude is preset up to a value of 27 μm pk/pk. This feature is essential in ultrasonic forming.

The second ultrasonic system was supplied by Telsonic (UK). The frequency generator uses modern switch-mode electronics for maximum efficiency and offers a power output up to 2 kW. The piezoelectric transducer (Figure A1) encloses electrical connections and exhibits high conversion efficiency. A preset amplitude is also a feature of this system.

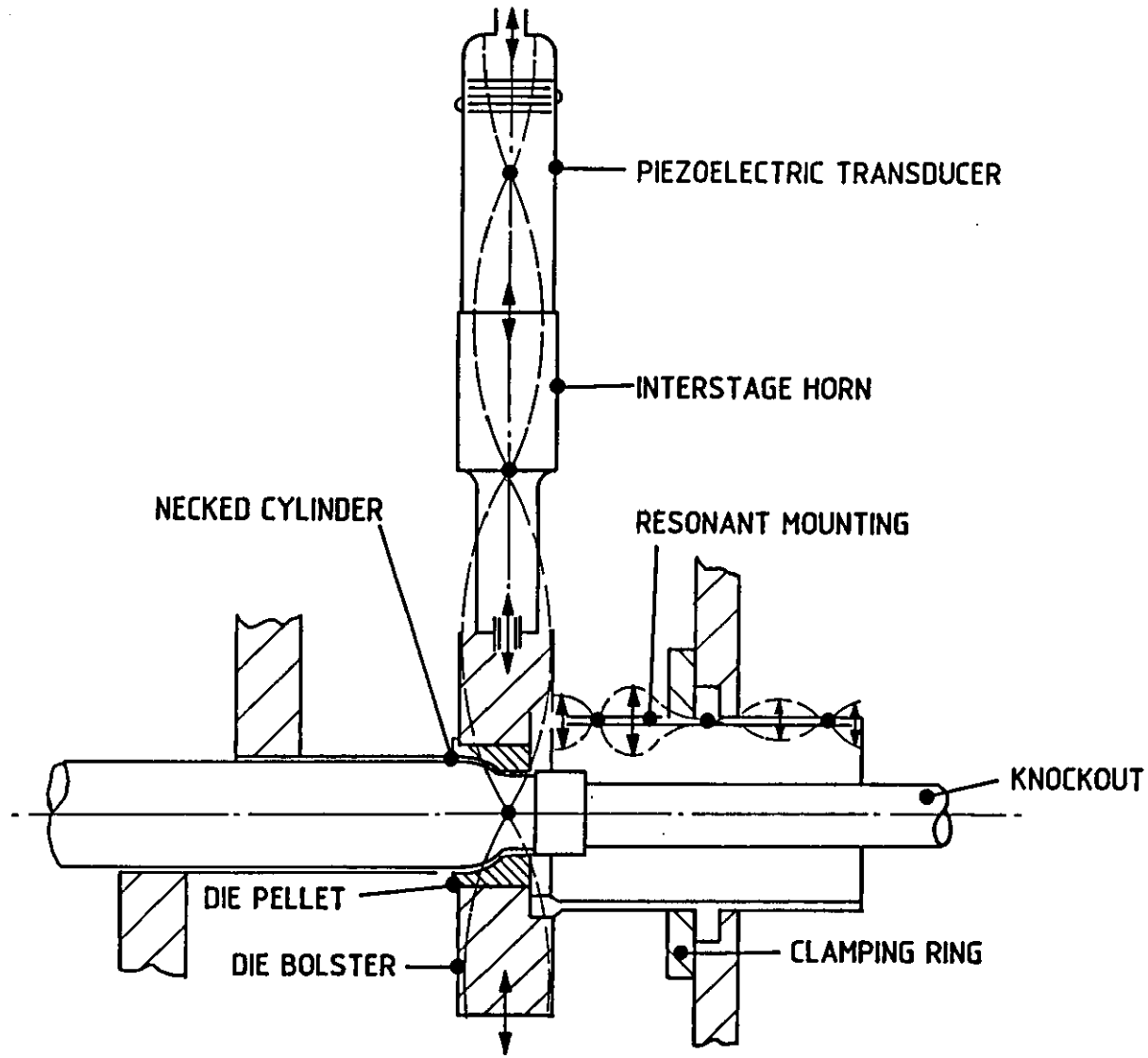

Figure A1 ULTRASONICALLY EXCITED DIE AND MOUNTING TAIL.
(mode shape indicated by dotted lines)

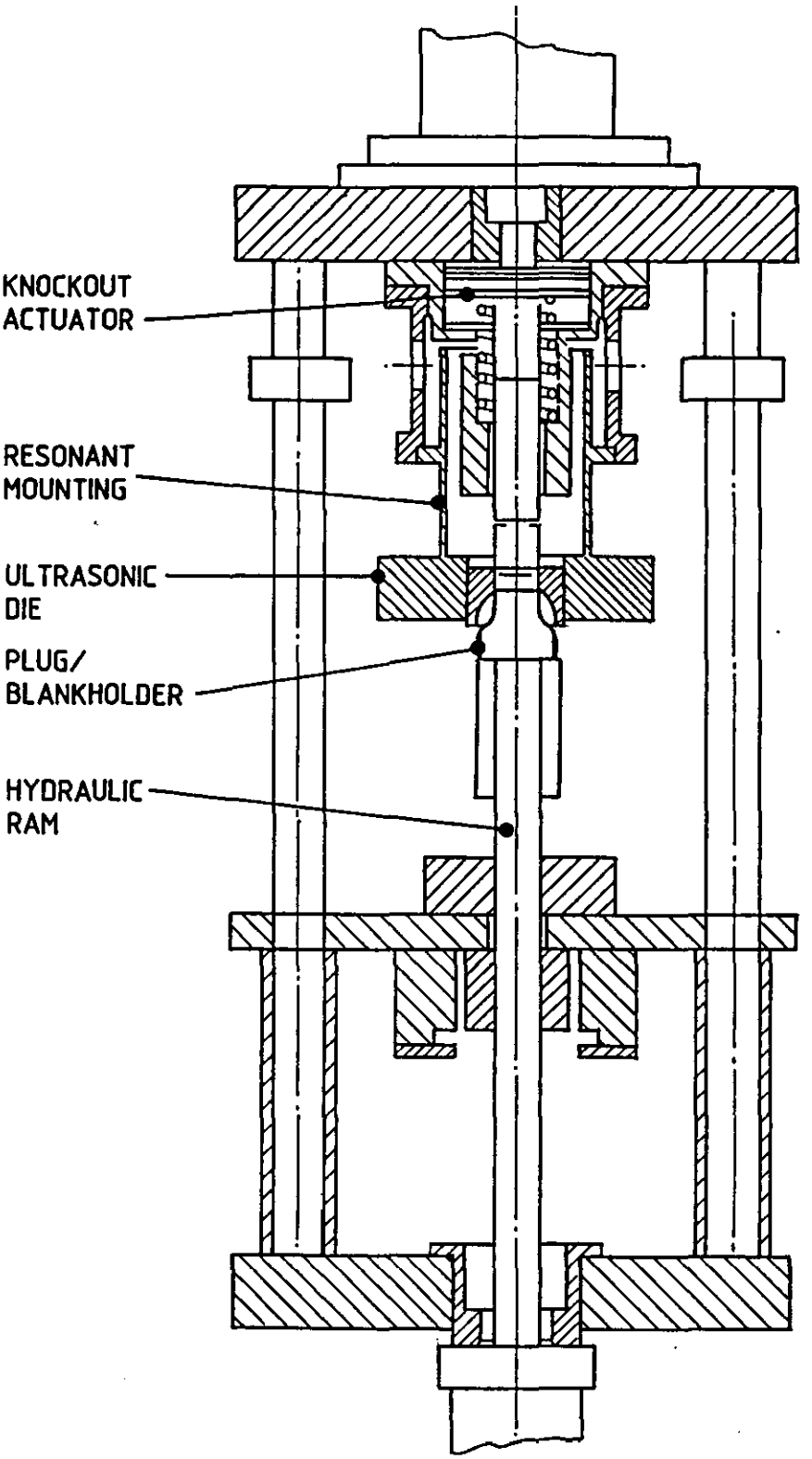

Figure A2: TEST RIG FOR ULTRASONIC NECKING

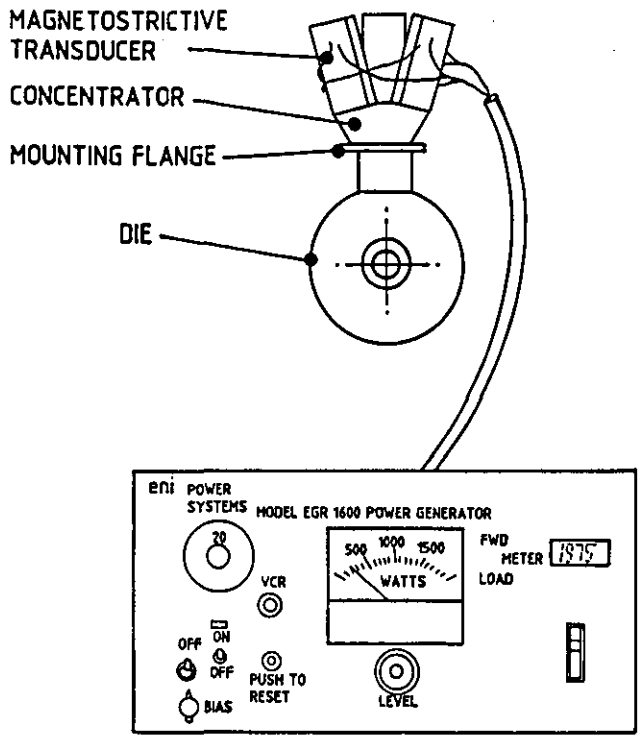

Figure A3. TECHNOFORM-SONICS ULTRASONIC EQUIPMENT

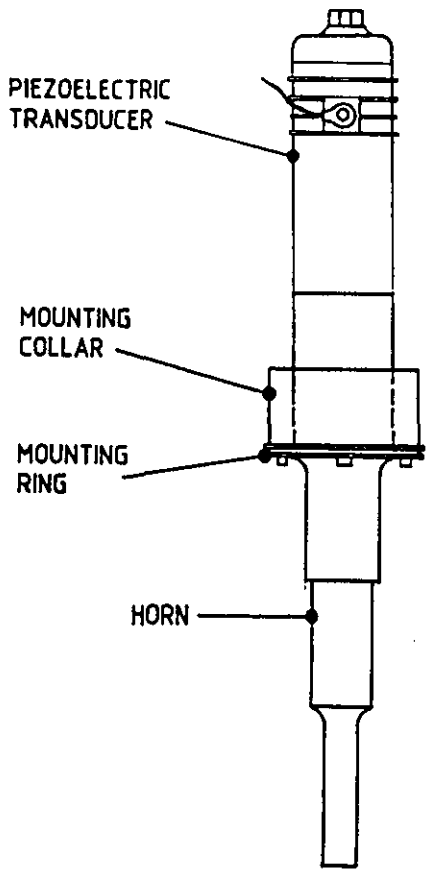

Figure A4. KERRY ULTRASONICS TRANSDUCER

APPENDIX B

THICK CYLINDER MODES OF VIBRATION

B.1 MODE CLASSIFICATION

The nomenclature adopted in this study to classify the modes of vibration is based on a system which uses two descriptors to define all possible thick cylinder modes. The descriptors denote the number of harmonic waves around the die and also identify each mode in terms of known generic deformation states.

First consider the classification of harmonic number. Three displacement directions are required in a cylindrical coordinate system:

1. Radial displacement, u_R
2. Axial displacement, u_A
3. Hoop (or tangential) displacement, u_H
   (Figure B1)

The deformation associated with all possible cylinder modes can therefore be described from these three displacements by the formulae:

$$u_R = f_1 \cos n\theta$$
$$u_A = f_2 \cos n\theta$$
$$u_H = f_3 \sin n\theta$$

(and the special case $u_R = u_A = 0$, $u_H = f_3$ when $n=0$)

where f_1, f_2, and f_3 are functions of position in cross-section,
n is the harmonic number
θ is the angular coordinate.

The value of n allows different mode shapes of the same order to be categorised as a related group.

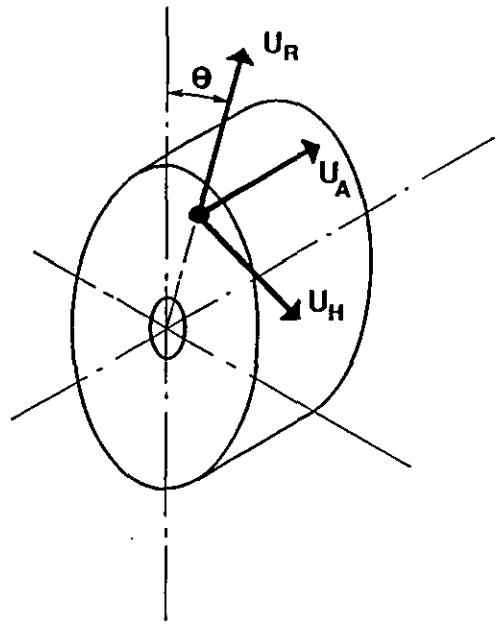

FIGURE B1

The other necessary component of the mode identifier describes the type of motion of the harmonic wave. In this study the mode is defined by the pattern of vibratory motion of the cylinder cross-section. The chosen nomenclature is illustrated in Figure B2.

As cylinder excitation using ultrasonics is commonly radially applied, the most prevalent cylinder modes are the Radial (R) and Torsional (T) modes. (These are sometimes also described as the symmetric and antisymmetric mode respectively of a particular harmonic number n, but this terminology is used to describe a mode and its phase shifted mode pair respectively in this study).

By this method of classification all cylinder vibratory motion can be labelled. Some of the mode shapes encountered may comprise a combination of these deformation categories, exhibiting both in-plane and out-of-plane cylinder response behaviour.

B.2 FREQUENCY BEHAVIOUR OF CYLINDER MODES

The vibration behaviour of a system is characterised by its natural frequencies and their associated mode shapes and modal damping values. For most simple systems, the fundamental mode is at the lowest natural frequency, the first harmonic occurs at a higher frequency and subsequent higher harmonic modes are excited at progressively higher frequencies. This means that for most lightly damped structures, the natural frequencies are well separated and easily identifiable. However for rings or cylinders this supposition does not hold for the families of radial (R) and torsional (T) harmonic modes. For such structures for example, the second harmonic (R2) has the lowest natural frequency. At significantly higher frequencies the fundamental, first and third harmonics (R0, R1, R3) may occur in any order. The fourth and higher harmonic modes then follow the rule of having progressively higher natural frequencies. For this reason, the R2 mode is sometimes referred to as the fundamental mode (ie. having the lowest natural frequency) in studies of rings and cylinders. In this study the fundamental natural frequency of any mode family is the mode with harmonic number zero.

The frequency behaviour of thick cylinder radial modes appears to follow the above rule with the exception of two anomalous modes; the fundamental and the first harmonic. These typically occur at frequencies close to the third harmonic. This feature of cylinder vibration is inherent in ultrasonic forming dies, which are essentially thick cylinders. The order in which R0, R1 and R3 appear in the frequency domain depends on the die material and geometry.

The anomalous frequency behaviour of the fundamental and first radial harmonic modes is due to the unique material straining of the cylinder deforming in these mode shapes. The radial harmonics of ring vibration are normally understood by likening the ring to a curved beam [83,77]. In beam vibration theory the frequency of a transverse (or bending) mode is determined by the effective length of the beam, which shortens with increased harmonic number. Therefore the higher the harmonic number, the higher the natural frequency of the mode. The same is true for cylinders with the exception of the

R0 and R1 modes which are not analogous to beam bending modes. The R2 and higher modes are well-balanced vibrating states; the mode shapes exhibiting equal amounts of tension and compression around the cylinder circumference throughout the vibration cycle. The R0 mode however, is either entirely compressive or entirely tensile at any point in the vibration cycle, and the R1 mode is entirely in shear. Therefore the fundamental induces large tensile strain in the cylinder and the first harmonic induces large shear strain. The extra straining has a stiffening effect on the cylinder which results in higher natural frequencies.

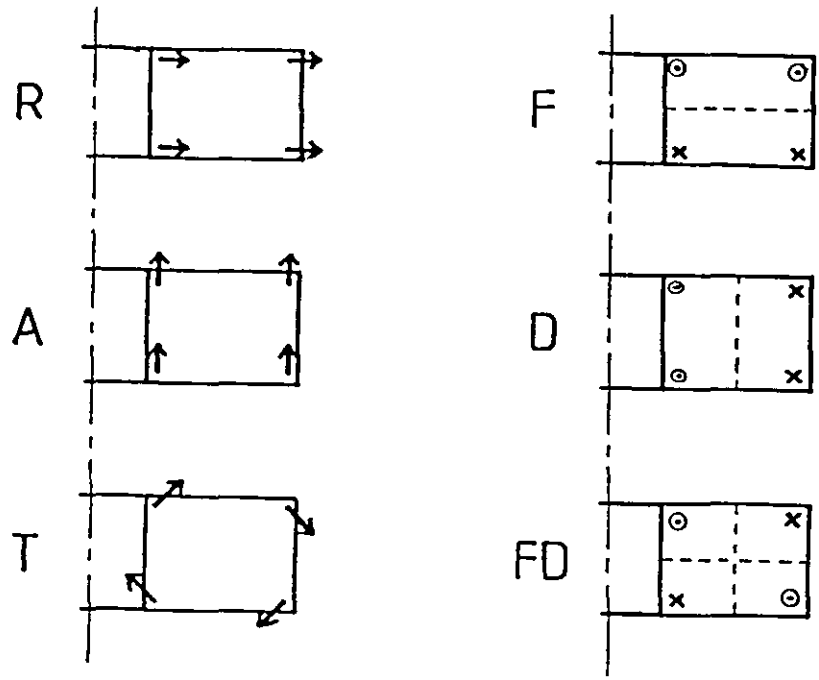

Radial (R): In-plane radial translation of cross-section

Axial (A): In-plane axial translation of cross-section

Torsional (T): In-plane rotation of cross-section

Face (F): Front and back faces rotate in opposition

Diameter (D): Inside and outside diameters rotate in opposition

FIGURE B2: CLASSIFICATION OF DIE VIBRATION MODES

APPENDIX C
SENSITIVITY TREND FOR MASS MODIFICATION

The sensitivity of the forming die's modes of vibration to mass modification is estimated in Chapter 7. The die's vibration response consists of many coupled modes but is assumed to exhibit single degree-of-freedom characteristics in the vicinity of resonance for the purposes of modal data extraction. This appendix looks at a simplified mass modification model in order to predict the form of the modal frequency versus mass modification curves that will result from the investigations in Chapter 7.

A mass modification effect on a structure's modal frequencies can be simplified by considering single degree-of-freedom mode sensitivity. If it is assumed that the modal response of a linear, lightly damped structure approximates SDOF behaviour in the vicinity of resonance, then the modal frequency ω_1 can be estimated from the modal stiffness and modal mass terms, k_m and m_m, from

$$\omega_1^2 = \frac{k_m}{m_m} \qquad (1)$$

If a small mass δ_m is added to the structure, such that the stiffness is unaltered, the new modal frequency ω_2 will be given by

$$\omega_2^2 = \frac{k_m}{m_m + \delta_m} \qquad (2)$$

By subtracting (2) from (1)

$$\omega_1^2 - \omega_2^2 = \frac{k_m \, \delta_m}{m_m + \delta_m}$$

For small δ_m, $m+\delta_m \approx m$. Let the frequency shift $\omega_1 - \omega_2 = \Delta\omega$.

Since k_m and m_m are constant, a relationship between added mass and frequency shift can be written as:

$$\Delta\omega \; \alpha \; \frac{\delta_m}{\omega_1 + \omega_2}$$

The resulting mode sensitivity curve for a mass modified structure is illustrated in Figure C1 below:

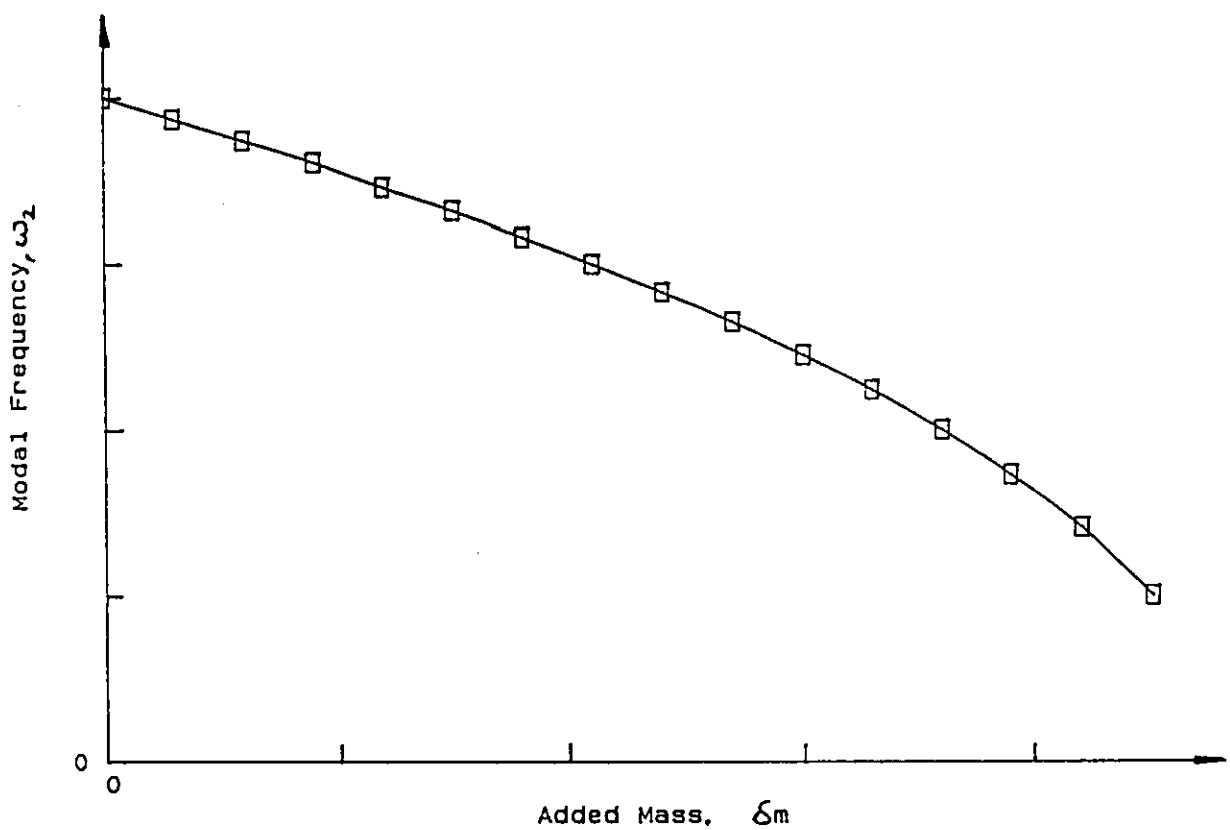

FIGURE C1: MODAL FREQUENCY BEHAVIOUR OF MASS MODIFIED STRUCTURE

The added mass versus modal frequency trend is approximated for an isolated, lightly damped mode of vibration simplified to a SDOF response. This indicates the nature of sensitivity curves for a mass addition.

APPENDIX D
PUBLICATIONS

The research presented in this thesis has generated the following publications:

1. Chapman, G.M. and Lucas M.
   "The Use of a Full Modal Analysis Package to Investigate Structural Modification in a Final Year Laboratory Class".
   Proceedings of the 6th Biennial Conference on the Teaching of Vibration and Noise, Sheffield, July 1988.

2. Chapman, G.M. and Lucas, M.
   "Frequency Analysis of an Ultrasonically Excited Thick Cylinder".
   Proceedings of the Conference on Modern Practice in Stress and Vibration Control, Liverpool, April 1989.

3. Lucas, M. and Chapman, G.M.
   "Vibration Analysis at Ultrasonic Frequencies".
   Proceedings of the 12th Biennial ASME Conference on Vibration and Noise, Montreal, September 1989.

4. Chapman, G.M. and Lucas, M.
   "Frequency Analysis of an Ultrasonically Excited Thick Cylinder".
   International Journal of Mechanical Sciences, Volume 32 (3), July 1990.

LOUGHBOROUGH UNIVERSITY OF TECHNOLOGY

THESIS ACCESS FORM Copy No. _____ Location _____

Author MARGARET LUCAS

Title THE APPLICATION OF VIBRATION ANALYSIS TECHNIQUES TO THE DEVELOPMENT OF AN ULTRASONICALLY ASSISTED DIE FORMING PROCESS

Status of access ~~OPEN~~ / ~~RESTRICTED~~ / ~~CONFIDENTIAL~~

Moratorium period : OPEN 3 years, ending 2 0 / 1 2 19 95

CONDITIONS of access approved by (Capitals) : TREVOR H. DAVIES

DIRECTOR OF RESEARCH (Signature) : T.H.Davies

DEPARTMENT OF MECHANICAL ENGINEERING

AUTHOR'S DECLARATION: **I AGREE THE FOLLOWING CONDITIONS :**

OPEN access work shall be made available (in the University and externally) and reproduced as necessary at the discretion of the University Librarian or Head of Department. It may also be copied by the British Library in microfilm or other form for supply to requesting libraries or individuals, subject to an indication of intended use for non-publishing purposes in the following form, placed on the copy and on any covering document or label. The statement itself shall apply to ALL copies. :

THIS COPY HAS BEEN SUPPLIED FOR NON-PUBLISHING PURPOSES ON THE UNDERSTANDING THAT IT IS COPYRIGHT MATERIAL AND THAT NO QUOTATION NOR ANY INFORMATION DERIVED FROM THE THESIS MAY APPEAR IN PUBLISHED FORM WITHOUT PRIOR WRITTEN CONSENT BY OR VIA THE UNIVERSITY LIBRARIAN.

RESTRICTED / CONFIDENTIAL WORK : All access and any photocopying shall be strictly subject to the written permission from the University Head of Department and any external sponsor if any.

Author's signature Margaret Lucas Date 16-12-92

USER'S DECLARATION for signature during any Moratorium period (Not Open work):
I UNDERTAKE TO UPHOLD THE ABOVE CONDITIONS :

Date	Name(Capitals)	Signature	Address

(Continue overleaf if necessary)

REFERENCES

1. Porucznik, P., "Investigation into the Necking of Welded Containers", Metal Box Technical Record No. TR0127, 1984.

2. Cheers, C.F., "Ultrasonically Assisted Die Necking", Metal Box Technical Record No. TR0814, 1985.

3. "Coneless Aerosol Status Report", Metal Box Technical Record No. TR1285, 1987.

4. Blaha, F., Langenecker, B., "Elongation of Zinc Monocrystals under Ultrasonic Action", Die Naturwissenschaften, 42(20), 1955.

5. Blaha, F., Langenecker, B., "Plasticity Test on Metal Crystals in an Ultrasonic Field", Acta Metallurgica, 7, 1959.

6. Nevill, G.E., Brotzen, F.R., "The Effect of Vibrations on the Static Yield Strength of Low-Carbon Steel", Proc. Am. Soc. for Testing Materials, 57, 1957.

7. Langenecker, B., "Effect of Ultrasound on the Deformation Characteristics of Metals", IEEE Trans. Sonics And Ultrasonics, SU-13(1), 1966.

8. Pohlman, R., Lehfeldt, E., "Influence of Ultrasonic Vibration on Metallic Friction", Ultrasonics, 4, 1966.

9. Aseff, G.V., Sproat, W.H., Kremheller, A., "High-Intensity Ultrasonics", IEEE Trans. Sonics and Ultrasonics, SU-17(1), 1970.

10. Kirchner, H.O.K., Kromp, W.K., Prinz, F.B., Trimmel, P., "Plastic Deformation under Simultaneous Cyclic and Unidirectional Loading at Low and Ultrasonic Frequencies", Materials Science and Engineering, 68, 1984-85.

11. Green, R.E., "Nonlinear Effects of High-Power Ultrasonics in Crystalline Solids", Ultrasonics, 13, 1975.

12. Schmid, E., "Basic Phenomena of the Influence of Ultrasound on Material Properties", Proc. 1st International Symposium on High-Power Ultrasonics, Austria, 1970.

13. Langenecker, B., Jones, V.O., Illiewich, J., "Metal Plasticity in Macrosonic Fields", Proc. 1st International Symposium on High-Power Ultrasonics, Austria, 1970.

14. Kristoffy, I., "Metal Forming With Vibrated Tools", Trans. ASME, J. Engineering for Industry, 91, 1969.

15. Atanasiu, N.E., "Intensification of Tube Drawing by Axial Ultrasonic Oscillation of the Plug", Ultrasonics, 18(6), 1980.

16. Winsper, C.E., Sansome, D.H., "The Influence of Oscillatory Energy on the Stresses During Plastic Deformation", J. Institute of Metals, 96, 1968.

17. Spiers, R.M., Winsper, C.E., Sansome, D.H., "Direct Extrusion of Metal with Applied Oscillatory Energy", Metal Forming, 36(10), 1969.

18. Winsper, C.E., Sansome, D.H., "Fundamentals of Ultrasonic Wire Drawing", J. Institute of Metals, 97, 1969.

19. Winsper, C.E., Dawson, G.R., Sansome, D.H., "An Introduction to the Mechanics of Oscillatory Metalworking", Metals and Materials and Metallurgical Reviews, 4, 1970.

20. Dawson, G.R., Winsper, C.E., Sansome, D.H., "Application of High and Low Frequency Oscillations to the Plastic Deformation of Metals", Metal Forming, 37, 1970.

21. Fridman, H.D., Levesque, P., "Reduction of Static Friction by Sonic Vibration", J. Applied Physics, 30, 1959.

22. Sansome, D.H., "Recent Developments in Oscillatory Metal Working", Engineering, April 1973.

23. Mitskevich, A.M., "Motion of a Body over a Vibrating Surface", Soviet Physics-Acoustics, 13(3), 1968.

24. Nosal, V.V., Rymsha, O.M., "Reducing the Drawing Forces by Ultrasonic Oscillations of the Drawplate and Determination of the Technological Parameters of Tube Drawing", Stal in English, 2, Feb. 1966.

25. Winsper, C.E., Sansome, D.H., "A Study of the Mechanics of Wire Drawing with Superimposed Ultrasonic Stress", Proc. 10th Machine Tool Design and Research Conf., Manchester, 1969.

26. Eaves, A.E., Smith, A.W., Waterhouse, W.J., Sansome, D.H., "Review of the Application of Ultrasonic Vibrations to Deforming Metals", Ultrasonics, 13, 1975.

27. Rees, T.W., Rippon, D.J., "The Application of Ultrasonic Vibrations in Tube Drawing", Proc. Conf. Developments in the Drawing of Metals, London, 1983.

28. Godfrey, D., "Vibration Reduces Metal to Metal Contact and an Apparent Reduction in Friction", ASLE Trans., 10(2), 1967.

29. Balamuth, L., "Sonic Press for Forming, Forging", American Machinist, 109(1), 1965.

30. Puskar, A., "The Use of High Intensity Ultrasonics", Materials Science Monographs, 13, Elsevier Scientific Publishing, 1982.

31. Dragan, O., Voinescu, H., Sirbu, A., Segal, E., Ciorica, D., Ivan, H., "Cold Drawing of Carbon Steel Tube with Ultrasonics", Proc. 1st Int. Symp. High-Power Ultrasonics, Austria, 1970.

32. Langenecker, B., Jones, V.O., "Macrosonic Wire Drawing and Tube Bending", Proc. 1st Int. Symp. High-Power Ultrasonics, Austria, 1970.

33. Smith, A.W., Young, M.J.R., Sansome, D.H., "Preliminary Results on the Effect of Ultrasonic Vibration on an Anologue of the Deep-Drawing Process", Proc. Ultrasonics International, London, 1973.

34. Dragan, O., "Cold Drawing of Tubes on an Ultrasonically Activated Plug", Proc. Ultrasonics International, London, 1973.

35. Jones, J.B., "Tube Drawing, Draw Ironing, Flare and Flange Forming...With an Ultrasonic Assist", Metal Progress, May 1968.

36. Shoh, A., "Industrial Applications of Ultrasound - A Review, 1.High-Power Ultrasound", IEEE Trans. Sonics and Ultrasonics, SU-22(2), 1975.

37. Kariyawasam, V.P., Young, M.J., Sansome, D.H., "An Experimental and Design Study of Fixed-Plug Tube-Drawing with Radial Ultrasonic Vibration of the Die", Wire Industry, Feb. 1979.

38. Young, M.J., Winsper, C.E., Sansome, D.H., "Radial Mode Vibrators for Oscillatory Metal Forming", Applied Acoustics, 3, 1970.

39. Young, M.J., Winsper, C.E., Sansome, D.H., "The Design of High-Intensity Radial Vibrators for Metal Working Applications", J.Phys.D: Applied Physics, 4, 1971.

40. Biddell, D.C., Sansome, D.H., "The Deep Drawing of Cans with Ultrasonic Radial Oscillations Applied to the Die", Proc. Ultrasonics International, London, 1973.

41. Biddell, D.C., Sansome, D.H., "The Development of Oscillatory Metal Drawing Equipment - an Engineer's View", Ultrasonics, Sept. 1974.

42. Cheers, C.F., "Finite Element Analysis of Tools for Ultrasonic Die Necking", Metal Box Technical Record, No. TR3005, 1988.

43. Parrack, H.O., "Effect of Airborne Ultrasound on Humans", International Audiology, 5, 1966.

44. Knight, J.J., "Effects of Airborne Ultrasound on Man", Ultrasonics, 6, 1968.

45. Daly, C., "Safety Considerations with High Power Ultrasonics", Proc. Ultrasonics International, London, 1973.

46. Proceedings of the International Modal Analysis Conference (IMAC), Union College, Schenectady, N.Y. 12308.

47. The International Journal of Analytical and Experimental Modal Analysis, Society for Experimental Mechanics Inc., Bethel, CT 06801.

48. Ewins, D.J., "Modal Testing: Theory and Practice", Research Studies Press Ltd., Letchworth, U.K., 1985.

49. "The Fundamentals of Modal Testing", Hewlett Packard, Application Note 243-3, 1986.

50. Dossing, O., "Structural Testing", Part 1 and 2, Bruel and Kjaer, Denmark.

51. Schmidtberg, R., Pal, T., "Solving Vibration Problems Using Modal Analysis", Solatron Instruments, N.Y.

52. Snoeys, R., Sas, P., Heylen, W., Van der Auweraer, H., "Trends in Experimental Modal Analysis", Mechanical Systems and Signal Processing, 1(1), 1987.

53. Randall, R.B., "Frequency Analysis", Bruel and Kjaer, Denmark, 1977.

54. Thrane, N., "Zoom-FFT", Bruel and Kjaer Technical Review, No.2, 1980.

55. "The STAR System Theory and Applications", SMS, 1990.

56. Pal, T., Schmidtberg, R., "Combining Analytical and Experimental Modal Analysis for Effective Structural Dynamic Modelling", Proc. IMAC-2, Vol. 2, Florida, 1984.

57. Wang, B.P., Clark, G., Chu, F.H., "Structural Dynamic Modification Using Modal Analysis Data", Proc. IMAC-3, Vol. 2, Florida, 1985.

58. Ramsey, K.A., Firmin, A., "Experimental Modal Analysis, Structural Modifications and FEM Analysis - Combining Forces on a Desktop Computer", Proc. IMAC-2, Vol. 2, Florida, 1984.

59. Deel, J.C., Luk, Y.W., "Modal Testing Considerations for Structural Modification Applications", Proc. IMAC-3, Vol. 2, Florida, 1985.

60. Davies, A.J., "The Finite Element Method: A First Approach", Oxford University Press, 1980.

61. Zienkiewicz, O.C., "The Finite Element Method in Structural and Continuum Mechanics", McGraw-Hill, 1967.

62. Rao, S.S., "The Finite Element Method in Engineering", Pergamon, 1982.

63. "PAFEC - Theory", PAFEC Ltd.

64. "PAFEC - Data Preparation", User Manual, PAFEC Ltd.

65. Chu, F.H. and Wang, B.P., "Experimental Determination of Damping in Materials and Structures", ASME - Damping Applications for Vibration Control, AMD-38, Nov. 1980.

66. Gladwell, G.M.L., "A Refined Estimate for the Damping Coefficient", J. Royal Aeronautical Society, Vol. 66, Feb. 1962.

67. Rasmussen, G., "Structural Dynamic Measurements Using Intensity Methods", Proc. IMAC-3, Vol. 2, Florida, 1985.

68. Grade, S., "Sound Intensity (Theory)", Bruel and Kjaer Technical Review, No.3, 1982.

69. Van der Burgt, C.M., "Motional Positive Feedback Systems for Ultrasonic Power Generators", IEEE Trans. UE-10, 2-19, July 1963.

70. Butterworth, S., Smith, F.D., "The Equivalent Circuit of the Magnetostriction Oscillator", Proc. Phys. Soc., Vol.43, 1931.

71. Kennedy, C.C., Pancu, C.D.P., "Use of Vectors in Vibration Measurement and Analysis", J. Aero. Sci., Vol.14, No.11, Nov. 1947.

72. Shellabear, M.C., Tyrer, J.R., "Three-Dimensional Vibration Analysis using Electronic Speckle Pattern Interferometry (ESPI)", Proc. SPIE, Vol.952, June 1988.

73. Shellabear, M.C., Tyrer, J.R., "Three-Dimensional Analysis of Volume Vibrations by Electronic Speckle Pattern Interferometry", Proc. SPIE, Vol.1084, March 1989.

74. Shellabear, M.C., "Application of Electronic Speckle Pattern Interferometry to the Study of Three-Dimensional Mechanical Vibrations", PhD Thesis, Loughborough University of Technology, March 1991.

75. Verma, S.P., Girgis, R.S., "Experimental Verification of Resonant Frequencies and Vibration Behaviour of Stators of Electrical Machines", Proc. IEE, Vol.128, Pt.B, No.1, Jan. 1981.

76. Lucas, M., "Vibratory Response of Stator Cores of Large Induction Motors Operating in an Offshore Installation", MPhil Thesis, RGIT Aberdeen, 1986.

77. Den Hartog, J.P., "Mechanical Vibrations", 4th Ed., McGraw Hill, 1956.

78. Cheers, C.F., "SERC Ultrasonic Necking Progress Report", CMB Packaging Technology, Wantage, UK, Sept. 1987.

79. Cheers, C.F., CMB Packaging Technology, Wantage, UK, Private Communication.

80. PAFEC Ltd., Private Communication.

81. Hitchings, D., "A Finite Element Dynamics Primer", NAFEMS, 1992.

82. Benson, P., "The Accuracy of Mass Modification", Final Year Project Report, Loughborough University, 1990.

83. Timoshenko, S., "Vibration Problems in Engineering", D. Van Nostrand, 3rd Ed., 1955.

GLOSSARY OF TERMS

DOF	Degree-of-Freedom
EMA	Experimental Modal Analysis
ESPI	Electronic Speckle Pattern Interferometry
FEA	Finite Element Analysis
FEM	Finite Element Method
FFT	Fast Fourier Transform
FRF	Frequency Response Function
FRM	Frequency Response Matrix
MDOF	Multiple Degree-of-Freedom
mDOF	Master Degree-of-Freedom
RFLS	Rational Fraction Least Squares
SDM	Structural Dynamics Modification
sDOF	Slave Degree-of-Freedom
SDOF	Single Degree-of-Freedom